UNIVERSITY OF SOUTHAMPTON

FACULTY OF ENGINEERING AND THE ENVIRONMENT

Institute of Sound and Vibration Research

Antenatal foetal monitoring through abdominal phonogram recordings: A single-channel independent component analysis approach

by

Aída **Jiménez González**

Thesis for the degree of Doctor of Philosophy

December 2010

UNIVERSITY OF SOUTHAMPTON

ABSTRACT

FACULTY OF ENGINEERING AND THE ENVIRONMENT
INSTITUTE OF SOUND AND VIBRATION RESEARCH

Doctor of Philosophy

ANTENATAL FOETAL MONITORING THROUGH ABDOMINAL PHONOGRAM RECORDINGS: A SINGLE-CHANNEL INDEPENDENT COMPONENT ANALYSIS APPROACH

by Aída **Jiménez González**

Today, it is generally accepted that current methods for biophysical antenatal surveillance do not facilitate a comprehensive and reliable assessment of foetal well-being. Alternatively, there is continuing development of existing technologies and research into new non-invasive methods that aim to improve antenatal examination procedures. To this end, these methods rely on the detection of information about the cardiac function and the overall foetal activity, which is done by using passive transducers that sense electric, magnetic or vibration signals. Here, attention has been paid to the vibrations that, recorded by a sensitive acoustic sensor positioned on the maternal womb, give rise to a signal referred to as the abdominal phonogram. Such a signal, recorded in a single-channel configuration, is rich in foetal information, but hidden by maternal and environmental interferences whose characteristics turn its extraction into a difficult and challenging task.

The research presented in this thesis studied Single-Channel Independent Component Analysis (SCICA) as a novel signal processing approach for retrieving information for antenatal foetal surveillance from the single-channel abdominal phonogram.

The study, conducted by developing three implementations of SCICA, gave rise to a methodology that successfully exploits the rich time-structure in the abdominal phonogram for decomposition purposes. Consequently, and especially outstanding for a Blind Source Separation approach, the current implementation of SCICA not only retrieves estimates of the sources underlying the abdominal phonogram, but also identifies their physiological origin (*i.e.* foetal cardiac, maternal cardiac, maternal breathing, and noise). Moreover, and significant to highlight in the aim of this research, is that a consistent extraction of foetal and maternal cardiac information in separate traces is reached even though their cardiac beats may temporary concur and completely hide the foetal activity. Clearly, these are exceptional achievements for such a single-channel methodology which, thoroughly tested on segments of abdominal phonograms,

not only performed better at separating foetal information than a rigid empirical filter, but also was more efficient at distinguishing foetal from maternal information than other methods reported in the literature.

In this way, when applied to 25 noisy single-channel abdominal phonograms (recorded at gestational ages ranging between 29 and 40 weeks) the current implementation of SCICA addressed the problem of separating out the signal into its underlying components, which were identified as the foetal phonocardiogram (PCG), the maternal PCG/pressure-wave, the maternal respirogram, and noise. Next, knowing that the foetal heart sounds (FHS) were consistently retrieved in the foetal PCG, this research explored the suitability of using such information for surveillance purposes. To this end, the foetal PCG was further processed to obtain the beat-to-beat foetal heart rate (FHR) and the average morphology of the FHS.

Results showed that the instantaneous FHR obtained from the foetal PCG constantly follows the trend given by a reference obtained from the abdominal ECG, which is especially significant when recalling that the PCG was retrieved from the noisy abdominal phonogram. Complementary, further processing of the maternal PCG/pressure-wave and the maternal respirogram showed that additional parameters such as the beat-to-beat maternal heart rate and the maternal breathing rate can be respectively obtained, which might be of interest for antenatal examination in future applications. This outcome, achieved by using semiautomatic algorithms, showed that the signals retrieved by SCICA from the abdominal phonogram are likely to provide useful information for foetal well-being surveillance.

Future work should focus on enhancing the quality of the estimated signals, developing better algorithms for obtaining meaningful parameters from such estimates, and increasing the dataset so that the suitability of using these estimates for foetal surveillance can be thoroughly tested.

LIST OF CONTENTS

LIST OF ACRONYMS

abdominal ECG	Abdominal Electrocardiography
ANS	Autonomic Nervous System
ApEn	Approximate Entropy
BPP	Biophysical Profile
BSS	Blind Source Separation
CMMR	Common-Mode Rejection Ratio
CNS	Central Nervous System
CST	Contraction Stress Test
CTG	Cardiotocography
DC	Direct Current
DUS	Doppler Ultrasonography
EEG	Electroencephalography
FAS	Foetal Acoustic Stimulation
FastICA	Fast Independent Component Analysis
FBM	Foetal Breathing Movement
FC	Foetal Cardiac activity

FECG	Foetal Electrocardiography
FHR	Foetal Heart Rate
FHS	Foetal Heart Sounds
FIR	Finite Impulse Response
FM	Foetal Movement
FMCG	Foetal Magnetocardiography
FFT	Fast Fourier Transform
HOS	Higher-Order Statistics
HRV	Heart Rate Variability
HS	Heart Sounds
IC	Independent Component
ICA	Independent Components Analysis
IG	Independent Group
LAPACK	Linear Algebra PACKage
MB	Maternal Breathing activity
MC	Maternal Cardiac activity
FMCG	Foetal Magnetocardiography
MBR	Maternal Breathing Rate
MD	Method of Delays
MECG	Maternal Electrocardiography
MEG	Magnetoencephalography
MEMG	Maternal Electromyography

MHR	Maternal Heart Rate
MICA	Multidimensional Independent Components Analysis
NST	Non-Stress Test
PCA	Principal Component Analysis
PCG	Phonocardiography
PSD	Power Spectral Density
SampEn	Sample Entropy
SCICA	Single-Channel Independent Component Analysis
SNR	Signal to Noise Ratio
SQUID	Superconducting Quantum Interference Device
SVD	Singular Value Decomposition
S1	First heart sound
S2	Second heart sound
TDSEP	Temporal Decorrelation source SEParation
UA	Umbilical Artery

LIST OF SYMBOLS

α = tolerance value to identify similar patterns in SampEn analysis

A = mixing matrix

$A_{(r,i)}$ = set of coefficients in the columns of matrix **A**

a_β = area under the curve given by the second half of s_β

$a_{\beta'}$ = area under the curve given by the first half of $s_{\beta'}$

$\mathbf{a}_i$ = set of vectors given by the columns of matrix **A** (vector representation of $a_i(n)$)

$a_i(n)$ = set of FIR filters given by the columns of matrix **A**

$\tilde{\mathbf{A}}_P$ = set of submatrices of **A**

aS_I = amplitude of $\hat{S}_x$ at S_I, *i.e.* $\max \hat{S}_x(f)$

c = index of the columns in **A** and **W**

cm = centimetres

$C^{m_s}(\alpha)$ = probability that any pattern $p_{m_s}(u)$ finds a match in the set P_{m_s}

$C^{m_s+1}(\alpha)$ = probability that any pattern $p_{m_s+1}(u)$ finds a match in the set P_{m_s+1}

$C_u^{m_s}(\alpha)$ = probability that a pattern $p_{m_s}(u)$ finds a match in the set P_{m_s}

D = number of degrees of freedom in a dynamical system

dB = decibels

$\hat{e}$ = Euclidean embedding dimension

$e(n)$ = envelope

$e_f(n)$ = filtered envelope

$\mathcal{E}_P$ = set of multidimensional subspaces

f = frequency

f_b = frequency bins

$f_i(n)$ = set of separation filters

f_l = lowest frequency of interest in $x(n)$

f_s = sampling frequency

γ = skewness

$h_P(n)$ = set of N_h-order FIR filters

$H[\cdot]$ = Hilbert Transform

$\mathbf{h}_P$ = vector representation of $h_P(n)$

$\mathbf{H}_P$ = set of Toeplitz matrices

hs_{val} = amplitude of a heart sound in $e_f(n)$

Hz = hertz

i = index of the components in a set of independent components (i= 1,…,m)

$\mathbf{I}$ = identity matrix

IC_p = Independent Component projected back to the measurement space

i_e = index of the peaks corresponding to heart sounds in $e_f(n)$

j = $\sqrt{-1}$

$\varphi(n)$ = phase

$\vartheta(n)$ = normalisation factor

k = sample index in a vector or pattern

K = number of multidimensional vectors that span **x** or
number of multicomponent sources that underlie $x(n)$

k_e, k_x, k_s, k_v, k_z = time-lag for the autocorrelation of $e(n)$, $x(n)$, **s**, **v**, and **z** respectively

kg = kilograms

kHz = kilohertz

kurt = kurtosis

$k_{\mathbf{v}max}$ = number of time-lags for $R^{\mathbf{v}}_{k_{\mathbf{v}}}$

l = number of overlapped windows in Welch's method

Λ = set of eigenvalues

ln = natural logarithm

log = logarithm with respect to base 10

λ_P = subsets of basis vectors $\mathbf{a}_i$

m = the embedding dimension

μ = mean

min = minutes

ml = millilitres

mm = millimetres

μm = micrometres

μPSD = mean value of a PSD

ms = milliseconds

m_s = number of samples in a pattern in SampEn analysis

mV = millivolts

μV = microvolts

n = sample index in a time-series or
block index in a sequence of vector observations

N = number of delay vectors in **v**

N = number of samples used in a *t*-test

N_A = number of samples in a "quasi-stationary" segment of $x(n)$

$N_{\mathcal{E}}$ = dimension of the subspace $\mathcal{E}_P$

N_{FFT} = number of samples in the PSD

N_h = order of the filter $h_P(n)$

$n_u^{m_s}(\alpha)$ = number of patterns in P_{m_s} that are similar to $p_{m_s}(u)$

$noise_L$ = amplitude of the noise on the left-hand side of a heart sound in $e_f(n)$

$noise_R$ = amplitude of the noise on the right-hand side of a heart sound in $e_f(n)$

$noise_{val}$ = average amplitude of the noise around a heart sound in $e_f(n)$

N_{ovl} = number of overlapped samples between adjacent segments

N_S = number of samples in a iteratively reconstructed time-series

N_T = number of samples in a time-series

ρ = number of sensors to record a set of observations

P = index of a multidimensional independent vector in a set of vectors or
index of a multicomponent group/source in a set of groups/sources

PCG' = PCG normalised to have variance one

PCG_{norm} = normalised PCG

P_f = Pearson's coefficient between a sinusoid oscillating at foetal heart rate and R_f^e

P_m = Pearson's coefficient between a sinusoid oscillating at maternal heart rate and R_f^e

P_{m_s} = set containing all the patterns $p_{m_s}(v)$ in $x(n)$

$p_{m_s}(u)$ = a pattern in $x(n)$ that begins at the u^{th} position of $x(n)$ and contains m_s samples

$p_{m_s}(v)$ = a pattern in $x(n)$ that begins at the v^{th} position of $x(n)$ and contains m_s samples

$\mathbf{psd}^i$ = set of vectors representing the PSDs of the IC_ps in *K*-means

$PSD^i_{f_b}$ = PSD values of the i^{th} IC

$\mathbf{psd}^P$ = set of vectors representing the centroids of the groups in *K*-means

Q = rotation transformation

θ_P^i = set of cosine angular separations

r = index of the rows in **A** and **W**

R = frequency of the rhythm in an IC_p, here referred to as rhythmicity

R' = frequency of the secondary rhythm in an IC_p

R_f^e = filtered autocorrelogram of $e(n)$

$R^e_{k_e=1,\ldots,N_A}$, $R^e_{k_e}$ = autocorrelogram of $e(n)$

$\mathbb{R}^m$ = m-dimensional Euclidean space

$R^{\mathbf{s}}_{k_{\mathbf{s}}}$ = time-lagged correlation matrices of **s**

$R^{\mathbf{v}}_{k_{\mathbf{v}}}$ = time-lagged correlation matrices of **v**

$R^{\mathbf{v}}_{k_{\mathbf{v}}=0}$, $R^{\mathbf{v}}_{k_{\mathbf{v}}=1}$ = time-lagged correlation matrix of **v** for $k_{\mathbf{v}}$= 0, 1

$R^{x}_{k_x=1,\ldots,N_T}$, $R^{x}_{k_x}$ = autocorrelogram of $x(n)$

$R^{\mathbf{z}}_{k_{\mathbf{z}}=1}$ = time-lagged correlation matrix of **z** for $k_{\mathbf{z}}$= 1

s = seconds

s = unobservable source signals

σ = standard deviation

$\hat{\mathbf{s}}(t)$, $\hat{\mathbf{s}}(n)$ = estimate of **s**, better known as the ICs

SampEn = sample entropy

s_β = segment of length N_A

$s_{\beta'}$ = adjacent segment to s_β

$\hat{s}_{\beta'}$ = scaled version of $s_{\beta'}$

Se = sensitivity

$\hat{S}_e(f)$, $\hat{S}_e$ = PSD of the envelope of an IC_p (*i.e.* autospectrum)

$\hat{S}_f(f)$, $\hat{S}_f$ = PSD of the filtered envelope of an IC_p (*i.e.* autospectrum)

s_i = set of coefficients in a superposition of vectors

$\mathbf{s}_i$ = set of ICs

S_I = central frequency of $\hat{S}_x$, *i.e.* $\arg_f \max \hat{S}_x(f)$

Sp = specificity

$s_P(n)$ = set of independent identically distributed random processes

$\mathbf{s}_P(n)$ = vector representation of $s_P(n)$

S_t = steadiness index

$\hat{S}_x(f)$, $\hat{S}_x$ = PSD of a signal (*i.e.* autospectrum)

t = time index

T = teslas

T = transpose

τ = time-lag when building **v** up

u, v = indexes of the samples in the patterns $p_{m_s}(u)$ and $p_{m_s}(v)$ respectively

$v_m(k)$ = k-delay segments of length m extracted from $x(n)$

V = volts

$\mathbf{v}(n)$, **v** = matrix of delays

$\mathbf{v}_m(k)$ = set of vectors of length m in **v**

W = unmixing matrix

$\mathcal{W}$ = whitening transformation

$W_{(i,c)}$ = set of coefficients in the rows of matrix **W**

$w(n)$ = weighting window to be used in Welch's method

$\mathbf{w}_i$ = set of vectors given by the columns of matrix **W** (vector representation of $w_i(n)$)

$w_i(n)$ = set of FIR filters given by the rows of matrix **W**

x = vector representation of observed data (*i.e.* multivariate data)

$x(n)$ = N_T-valued scalar time-series

$\mathbf{x}(n)$ = the n^{th} observation in $\mathbf{x}$

$x_a(n)$ = analytical signal

$x_s^{(i)}(n)$ = set of estimates of the sources projected back in the observational domain

$\mathbf{x}_s^{(i)}$ = vector representation of $x_s^{(i)}(n)$

$\mathbf{x}_P$ = set of multidimensional independent vectors

$x_P(n)$ = set of mutually independent random processes

$y(u), y(v)$ = amplitudes of $p_{m_s}(u)$ and $p_{m_s}(v)$ at the u^{th} and v^{th} samples respectively

$\mathbf{Y}^i$ = set of matrices of delays of the independent components

z = index of the elements in a Hankel matrix

$\mathbf{z}$ = whitened matrix

ζ = number of sources underlying a set of observations

LIST OF FIGURES

LIST OF TABLES

DECLARATION OF AUTHORSHIP

I, Aída **Jiménez González**, declare that the thesis entitled

Antenatal foetal monitoring through abdominal phonogram recordings: A single-channel independent component analysis approach

and the work presented in the thesis are both my own, and have been generated by me as the result of my own original research. I confirm that:

- this work was done wholly or mainly while in candidature for a research degree at this University;
- where any part of this thesis has previously been submitted for a degree or any other qualification at this University or any other institution, this has been clearly stated;
- where I have consulted the published work of others, this is always clearly attributed;
- where I have quoted from the work of others, the source is always given. With the exception of such quotations, this thesis is entirely my own work;
- I have acknowledged all main sources of help;
- where the thesis is based on work done by myself jointly with others, I have made clear exactly what was done by others and what I have contributed myself;
- parts of this work have been published as:
    - Jimenez-Gonzalez, A. and C. J. James (2008). Blind Source Separation to extract foetal heart sounds from noisy abdominal phonograms: a single channel method. 4th IET International Conference on Advances in Medical, Signal and Information Processing MEDSIP. Santa Margherita Ligure, Italy: Electrophysiology, 1.1.4.

- Jimenez-Gonzalez, A. and C. J. James (2008). Source separation of foetal heart sounds and maternal activity from single-channel phonograms: a temporal independent component analysis approach. 35th Annual Conference of Computers in Cardiology. Bologna, Italy. 35: 949-952.
- Jiménez-González, A. and C. J. James (2009). Extracting sources from noisy abdominal phonograms: a single-channel blind source separation method. Medical & Biological Engineering & Computing 47: 655-664.
- Jiménez-González, A. and C. J. James (2009). On the analysis of foetal heart sound morphology after de-noising the abdominal phonogram. The 5th UKRI PG Conference in Biomedical Engineering and Medical Physics. Oxford, UK: 7-8.
- Jiménez-González, A. and C. J. James (2010). On the measurement of physiological similarity between independent components: time-structure versus frequency-based methods. 37th Annual Conference of Computing in Cardiology. Belfast, North Ireland. 37: 477-480.
- Jiménez-González, A. and C. J. James (2010). Time-structure based reconstruction of physiological independent sources extracted from noisy abdominal phonograms. IEEE Transactions on Biomedical Engineering 57(9): 2322-2330.

Signed: ……..

Date: December 7th, 2011

ACKNOWLEDGEMENTS

I would like to express my sincerest gratitude to everyone who has helped me reach this stage in my life. First, to my sponsor, The Mexican Council for Science and Technology (Consejo Nacional de Ciencia y Tecnología, CONACYT), which supported my PhD studies. Second, to my family: to my grandparents –for the protection they always provided–, to my sisters and brother–for their support and caring–, and most importantly, to my mother, –for her devotion and unconditional love to the family–, her example of perseverance gave me the strength to keep going in times of difficulty and frustration. Third, to my friends and colleagues from work at Universidad Autónoma Metropolitana-Iztapalapa in México City, especially to Dr. Ortiz-Pedroza, who took care of my academic businesses in México. She also provided the dataset used in this research and gave me valuable comments about the first four chapters in this thesis. Fourth, to my supervisor, Prof. Christopher J. James, for his example of commitment towards his students and his opportune advice. Finally, to my friends at ISVR and at the Mexican Society in Southampton, for a wonderful friendship that lighted up my way through tough and confusing times during my PhD.

Thank you all,

Aída

1 INTRODUCTION

1.1. Motivation

Antenatal foetal surveillance is an essential part of foetal care that aims to identify those foetuses whose physiological defence mechanisms against hypoxemia are compromised. In this way, obstetricians can (1) classify pregnancy as in low-risk or high-risk status and, whenever necessary, (2) act before decompensation and severe/irreversible damage appear (Clerici *et al.* 2001; Gribbin and James 2004; Martin 2008). This is performed by keeping attention on a set of unique physiological responses (*i.e.* adaptations) that the foetus puts into action against the stress of hypoxemia (Clerici *et al.* 2001; Davies 2000; Rychik 2004; Tucker 2007). Such adaptations, given by changes in the foetal heart rate (FHR), the foetal movements (FMs), the foetal breathing movements (FBM), the blood flow distribution, and the behavioural states, are proof of a mature and healthy autonomic nervous system (Clerici *et al.* 2001; Martin 2008; Rychik 2004).

At present, clinical observation of these adaptations strongly relies on ultrasonography, a screening tool that makes it possible the biophysical assessment of foetal well-being and thus, the classification of pregnancy as in low-risk or high-risk status. Unfortunately, even though this technological option has been used since the end of the 60s, the rate of foetal loss in the UK over the last 40 years has not shown a significant reduction (Gribbin and James 2004). Most importantly, it has been reported that the majority of stillbirths have happened in the low-risk group (Gribbin and James 2004). Thus, when foetal surveillance is performed, there might be some unidentified factors that result in the wrong identification of foetal risk and, consequently, in the incorrect assignment of some women to the low-risk group (Gribbin and James 2004). This poor outcome could be associated to human error, lack of a complete understanding of how the foetus responds to prolonged hypoxemia or perhaps lack of sensitivity in the screening tools currently available (Ansourian *et al.* 1993; Bocking 2003; Gribbin and James 2004; Heazell and

Froen 2008; Jansen and Chernick 1991; Menihan and Kopel 2008). In any case, it is clear that there is a need of methods that effectively identify foetuses at risk in apparently low-risk pregnancies (Gribbin and James 2004).

In an attempt to increase the screening efficiency, it has been taken into account that a normally oxygenated foetus can become abnormally hypoxemic (*i.e.* at risk) at any time during pregnancy. Consequently, attention has been paid to *long-term monitoring* of foetal responses such as FHR, FMs, and FBM to increase the possibilities of detecting dangerous hypoxemic events as soon as they appear. Clearly, since long exposure to ultrasound might harm the foetus, this screening tool becomes an unsuitable option for long-term monitoring and foetal distress prediction (Barnett 2001; Holburn and Rowsell 1989). Alternatively, there has been continuing development of existing technologies as well as research into new non-invasive methods that aim to improve antenatal monitoring procedures. These non-invasive methods rely on the detection of information regarding the cardiac function along with foetal activity, which is done by using passive transducers that sense electric (abdominal ECG), magnetic (foetal MCG) or vibration signals (abdominal phonography).

This work has paid attention to the vibrations recorded by positioning a sensitive acoustic sensor on the maternal womb, *i.e.* the abdominal phonogram (Colley *et al.* 1986; Goovaerts *et al.* 1989; Holburn and Rowsell 1989; Talbert *et al.* 1986; Zuckerwar *et al.* 1993). The signal, usually recorded in a single-channel configuration, is rich in information about foetal activity such as heart sounds (FHS), heart rate, and breathing/body movements (Colley *et al.* 1986; Goovaerts *et al.* 1989; Talbert *et al.* 1986; Zuckerwar *et al.* 1993). Additionally, the spectral overlapping of foetal and maternal cardiac activities in the abdominal phonogram is not as significant as in the abdominal ECG and foetal MCG, which is an important characteristic. Unfortunately, the acoustic energy of the foetal components in the abdominal phonogram is so low that they are easily hidden by environmental, maternal, and artifactual (*i.e.* slow motion) sources (Varady *et al.* 2003), which turns the extraction of foetal information into a challenging task.

To date, in the quest of recovering foetal information from abdominal recordings, most signal processing methods in the literature have followed the approach of using rigid and empirical criteria to extract pre-selected components (*e.g.* FHS or FBM) and irreversibly discarding other physiological information (*e.g.* maternal cardiac activity) (Goovaerts *et al.* 1989; Holburn and Rowsell 1989; Zuckerwar *et al.* 1993). As a result, methods with different types of sensors (Colley *et al.* 1986; Goovaerts *et al.* 1989; Holburn and Rowsell 1989; Talbert *et al.* 1986; Zuckerwar *et al.* 1993), number of channels (Moghavvemi *et al.* 2003; Varady *et al.* 2003), and signal processing schemes (Akay and Szeto 1995; Jimenez *et al.* 2001; Kovacs *et al.* 2000) have been proposed. However, even though high quality technology and powerful

processing schemes have been combined to enhance the signal to noise ratio (SNR), the effective extraction of foetal information for well-being surveillance may be still difficult.

The main problem, from the point of view of this research, is that a rigid approach does not give any chance for a method to adapt to the natural variations that physiological phenomena (*i.e.* the foetal adaptations) may present over time and between subjects. Besides, since some information is discarded during the process, the richness of information in the abdominal phonogram is being ignored, which might turn into loss of valuable observations about foetal status or even maternal condition. As an alternative, this work has proposed that information of interest can be better recovered by means of a data-dependent signal processing approach that, by exploiting the wealthy temporal information in a single-channel recording, freely retrieves the components underlying the abdominal phonogram as entire traces from where the beat-to-beat heart rate can be monitored to determine foetal well-being (which is a valuable observation since it changes in the stress of hypoxemia and rapidly reflects the foetal oxygenation status). Such a signal processing perspective, referred to and studied as Single-Channel Independent Component Analysis (SCICA) by Davies and James (2007), has been successfully applied to biomedical signals such as EEG (James *et al.* 2006; James and Lowe 2000) and MEG (James and Lowe 2001; Woon and Lowe 2004), but never to the abdominal phonogram.

The aim of the research presented in this thesis has been to study, for the first time, Single-Channel Independent Component Analysis as an alternative signal processing approach to retrieve information for antenatal foetal surveillance from the single-channel abdominal phonogram.

The study, conducted through the development of three implementations of SCICA, has produced a methodology that successfully exploits the rich time-structure in the abdominal phonogram for decomposition purposes (Jimenez-Gonzalez and James 2008; Jiménez-González and James 2009; Jiménez-González and James 2010b). Such a methodology is performed by following three steps:

1. The single-channel abdominal phonogram is projected into a higher-dimensional space by using the Method of Delays (MD) (Broomhead and King 1986). This produces a matrix of delays, which is a rich representation of the states of the dynamical system that generated the phonogram.

2. The matrix of delays is transformed by using Temporal Decorrelation source SEParation (TDSEP) (Ziehe and Muller 1998), which is an ICA implementation that exploits the time-structure of the sources to minimise the dependence of the output components (*i.e.* Independent Components, ICs). This produces a set of spectrally

disjoint components (Davies and James 2007) corresponding to the physiological activities underlying the abdominal phonogram.

3. Similar ICs are grouped by using rhythmicity-based analysis, which is a method developed in this research to disclose the rhythmic patterns in the ICs and thus, to automatically identify the physiological processes underlying them. This produces groups whose constituent ICs are used to consistently retrieve the estimates of the physiological sources underlying the abdominal phonogram.

In this way, the methodology implemented in this work not only freely retrieves estimates of the sources underlying the single-channel abdominal phonogram, but also automatically identifies their physiological origin, which are two essential contributions of this research (Jiménez-González and James 2010a; Jiménez-González and James 2010b). Indeed, as results from 25 noisy single-channel abdominal phonograms showed, the current implementation of *SCICA consistently managed to retrieve entire estimates of the sources corresponding to the foetal phonocardiogram (PCG), the maternal PCG/pressure-wave, the maternal respirogram, and the noise* (Jiménez-González and James 2010b). Such estimates, further analysed to successfully collect information of interest such as foetal/maternal heart rate and breathing rate, have turned into *promising sources of information for foetal well-being surveillance.*

The next sections will give details on the organisation of this document, the specific contributions of this research, and finally, the publications arisen from this work.

1.2. Thesis organisation

This thesis starts by presenting the literature review performed in this research, which is contained in Chapter 2, Chapter 3, and Chapter 4. In Chapter 2, fundamentals of the adaptations developed by the foetus in response to hypoxemia are introduced, which provide the background needed to understand the significance of their observation for assessing foetal well-being. Next, Chapter 3 discusses the methods used to observe such adaptations for antenatal examination by means of subjective perception, ultrasound biophysical measurements and, alternatively, non-invasive long-term recordings (*i.e.* the abdominal ECG, the foetal MCG, and the abdominal phonogram). After that, Chapter 4 discusses some approaches reported in the literature to process such non-invasive but noisy recordings in order to retrieve the foetal information. Finally, this chapter focuses on the potential of using abdominal phonogram recordings for foetal surveillance and proposes the idea of studying SCICA as an alternative signal processing approach to do that.

Chapter 5 describes the recording setup and the characteristics of the dataset available for this research. Additionally, to illustrate how challenging the extraction of foetal information from these signals is, some examples of abdominal phonograms are shown.

Chapter 6, Chapter 7, and Chapter 8 describe the development of SCICA necessary to recover foetal information from the abdominal phonogram. Chapter 6 introduces the fundamentals of source separation by SCICA and describes the former two implementations developed in this research (based on MD, FastICA/TDSEP, and *K*-means), which made it possible to enhance the separation step and discuss the requirements for SCICA (*i.e.* based on TDSEP) to truly become a robust signal processing alternative for antenatal surveillance. Next, Chapter 7 details a comprehensive study designed in this work to gain knowledge about the components separated by TDSEP. The study, based on descriptive, spectral, entropy, and rhythmicity analyses, disclosed essential characteristics of the ICs and TDSEP that provided the bases needed for improving the performance of SCICA. One of such improvements is described in Chapter 8, where a novel scheme for classification purposes is presented. Such a scheme, referred to in this thesis as rhythmicity-based analysis, not only groups similar ICs, but also associates the groups to physiological phenomena, which is a desire quality in a blind source separation approach. Thus, the method manages to successfully classify ICs into groups corresponding to maternal respiratory activity, maternal cardiac activity, foetal cardiac activity, and noise activity. Additionally, tests on segments of abdominal phonograms show that this scheme performs faster than a classifier based on entropy and, additionally, that it is more consistent than *K*-means.

Chapter 9 presents the evolution of SCICA through this research, both at the separation and the grouping steps. To this end, the separate components and the resulting sources –of each implementation– are illustrated and carefully discussed by focusing on their relevance for antenatal surveillance purposes. Hence, it is possible to see how SCICA evolves into an implementation that, working on segmented data, reliably retrieves traces of the physiological sources underlying the abdominal phonogram (*i.e.* the foetal PCG, the maternal PCG/pressure-wave, the maternal respirogram, and noise). Also, for comparison purposes, the foetal PCG recovered by means of a rigid filter is included.

Chapter 10 presents the last stage of this research, which consist of (a) the reconstruction of entire time-series of the sources underlying the abdominal phonogram and then, (b) the recovery of information for performing foetal well-being surveillance. In (a), to perform the last improvement for SCICA, the segmented traces retrieved by SCICA were concatenated to build up entire time-series corresponding to the foetal PCG, the maternal PCC/pressure-wave, the maternal respirogram, and noise. In (b), the signals were semiautomatically processed to obtain the beat-to-beat FHR, the average morphology of the FHS, the beat-to-beat maternal heart rate

(MHR), and the maternal breathing rate (MBR). The analysis of such parameters has shown that the beat-to-beat FHR obtained from the foetal PCG consistently follows the trend given by the reference FHR calculated from the abdominal ECG, which is especially significant since the PCG comes from the noisy abdominal phonogram. Also, it has been seen that additional parameters such as the beat-to-beat MHR and the MBR can be collected respectively from the maternal PCG/pressure-wave and the maternal respirogram. These results, obtained from 25 recordings, indicate that the signals estimated by SCICA from the abdominal phonogram are promising sources of information for foetal well-being surveillance.

Finally, Chapter 11 draws the conclusions of this work and outlines some physiological and technological challenges that should be considered for future research.

1.3. Contributions

The contributions of this research have been categorised in terms of the development of SCICA as a methodology to retrieve the sources underlying the abdominal phonogram and the findings from the studies performed on the components/sources separated by this methodology. Thus:

1. *Implementation and novel application of SCICA to the noisy abdominal phonogram for adaptive separation into its underlying sources* (Jimenez-Gonzalez and James 2008). As discussed in Chapter 7 and Chapter 9, such a separation is actually performing as a spectral decomposition that depends on the temporal-structure of the signals rather than on rigid pre-defined frequency bands. The decomposition is sensitive enough to retrieve the traces of the physiological sources corresponding to the foetal PCG, the maternal PCG/pressure-wave, the maternal respirogram, and noise, all from a noisy single-channel recording.

2. *Development of a new methodology for automatic identification and classification of similar ICs.* As discussed in Chapter 8, this is done by disclosing the rhythmic patterns in the ICs, which makes it possible to identify the physiological processes driving the components and, consequently, to classify ICs into physiological groups corresponding to foetal cardiac activity, maternal cardiovascular activity, maternal breathing activity, and noisy activity (Jiménez-González and James 2010b).

3. *Design of an extensive study of the ICs to disclose, for the first time, essential characteristics of the components underlying the abdominal phonogram.* As discussed in Chapter 7, this is performed by combining four different methods for time-series analysis that (i) revealed meaningful features of the components separated by TDSEP and (ii) provided the bases needed to enhance the performance of SCICA: (1) the ICs are spectrally disjoint, (2) the ICs are sorted according to their frequency content, (3)

the slowest ICs are more likely to present strong regular patterns, and (4) the regular patterns in the ICs are driven by well-known physiological processes, *i.e.* the maternal breathing rate, the maternal heart rate, and the foetal heart rate.

4. *Implementation of a study of the sources estimated by SCICA to explore their appropriateness for antenatal surveillance purposes.* As discussed in Chapter 10, this **was** done by creating semiautomatic algorithms that further process the SCICA estimates in order to obtain the beat-to-beat FHR, the average morphology of the FHS, the beat-to-beat maternal heart rate (MHR), and the maternal breathing rate (MBR). Preliminary results show that the FHR, the MHR, and the MBR collected from the SCICA signals are likely to follow the trends given by reference signals. This means that such estimates, identified as the foetal PCG, the maternal PCG/pressure-wave, and the maternal respirogram, are promising sources of information for antenatal surveillance of foetal well-being.

1.4. Publications arisen from this research

1.4.1. Refereed journal articles

1. A. Jiménez-González, C. J. James. "Extracting sources from noisy abdominal phonograms: a single-channel blind source separation method". *Medical & Biological Engineering & Computing*, 47(6), pp. 655-664, 2009. DOI: 10.1007/s11517-009-0474-8.

2. A. Jiménez-González, C. J. James. "Time-Structure Based Reconstruction of Physiological Independent Sources Extracted from Noisy Abdominal Phonograms". *Transactions on Biomedical Engineering*, 57(9), pp. 2322-2330, 2010. DOI: 10.1109/TBME.2010.2051226.

1.4.2. Refereed conference papers

1. A. Jiménez-González, C. J. James. "Blind Source Separation to extract foetal heart sounds from noisy abdominal phonograms: a single channel method". In: *Proceedings of The 4th IET International Conference on Advances in Medical, Signal and Information Processing MEDSIP* (Electrophysiology, 1.1.4.), 2008.

2. A Jimenez-Gonzalez, CJ James. "Source separation of foetal heart sounds and maternal activity from single-channel phonograms: a temporal independent component analysis approach". In: *Proceedings of The 35th Annual Conference of Computers in Cardiology*, pp. 949-952, 2008.

3. A Jiménez-González, C J James. “On the analysis of foetal heart sound morphology after de-noising the abdominal phonogram”. In: *Proceedings of The 5th UK & RI postgraduate conference in Biomedical Engineering & Medical Physics*, pp. 7-8, 2009.

4. A Jimenez-Gonzalez, CJ James. “On the measurement of physiological similarity between independent components: time-structure versus frequency-based methods”. In: *Proceedings of The 37th Annual Conference of Computing in Cardiology*, pp. 477-480, 2010.

1.4.3. Oral presentations

1. Aida Jimenez Gonzalez. “Extracting sources from noisy abdominal phonograms: a single-channel Blind Source Separation approach”. The 6th Symposium of Mexican Students and Studies, Imperial College, London, United Kingdom, 28-29 June, 2008.

2. Aída Jiménez González. “Single-channel Blind Source Separation of the abdominal phonogram: foetal heart sounds, maternal activity and something else”. Electrical Engineering Department, UAM-Iztapalapa, Mexico City, Mexico, August 13th, 2008.

3. A Jiménez-González. “On the analysis of foetal heart sound morphology after de-noising the abdominal phonogram”. 7th Symposium of Mexican Students and Studies, Cambridge University, Cambridge, United Kingdom, July 4th, 2009.

4. A Jiménez-González. “Time-structure based reconstruction of physiological independent sources extracted from noisy abdominal phonograms”. 8th Symposium of Mexican Students and Studies, Manchester University, Manchester, United Kingdom, July 2nd, 2010.

2 FUNDAMENTALS OF FOETAL PHYSIOLOGY

Antenatal foetal surveillance is an essential part of foetal care that aims to identify those foetuses whose physiological defence mechanisms against hypoxemia are compromised. In this way, obstetricians can (1) classify pregnancy as in low-risk or high-risk status and, whenever necessary, (2) act before decompensation and severe/irreversible damage appear (Clerici *et al.* 2001; Gribbin and James 2004; Martin 2008). This is performed by keeping attention on the set of unique physiological responses (*i.e.* adaptations) that the cardiovascular and neurological foetal systems put into action to favour foetal survival when hypoxemic stress is present (Clerici *et al.* 2001; Davies 2000; Rychik 2004; Tucker 2007). Such adaptations, given by variations in the FHR, the FMs, the FBM, the blood flow distribution, and the behavioural states, have become a key point in antenatal surveillance for foetal well-being assessing (Clerici *et al.* 2001; Martin 2008).

This chapter presents the fundamentals necessary to understand how the cardiovascular and nervous systems in the foetus respond to hypoxemia and thus, makes it clearer the importance of paying attention to their adaptations during the antenatal assessment of foetal well-being.

2.1. The foetal cardiovascular system

Over the last 30 years, due to intensive research and new technologies development, comprehension of the foetal cardiovascular physiology has advanced significantly (Hanson 1997; Rychik 2004). In its former stages, mainly performed on sheep and goats, such research gave rise to significant information about the mammalian foetal circulation (Rychik 2004), which formed the bases for understanding the human foetal cardiovascular physiology (Rudolph and Heymann 1967). Later on, with the arrival of ultrasonic imaging and foetal echocardiography, it was possible to observe the phenomena occurring during gestation in both healthy and diseased foetuses, which expanded the knowledge of the cardiovascular system (Blaas and Eik-Nes 2008; Cook *et al.* 2004; Rychik 2004). However, even though important

structural and functional features about the foetal cardiovascular system have been elucidated, there are still gaps to fill in before reaching a complete understanding of: (i) its function in response to the stress of hypoxemia and then, (ii) the circumstances that make it fails and lead to foetal damage or death.

The problem is neither easy to explain nor easy to solve and, as a first step, some bases about the structure, function, and regulation of the foetal cardiovascular system must be understood.

2.1.1. Structural characteristics

The cardiovascular system, by definition, is composed of *the heart* and *the blood vessels* (Tucker 2007). In this section, due to their importance for supporting foetal life, *the placenta* and *the umbilical cord* are mentioned as well:

a) The foetal heart: Shown in Figure 2.1, the foetal heart can be simply described as an organ composed of four discrete chambers (the right and left atria, as well as the right and left ventricles) and two arterial trunks (the aorta and the pulmonary artery). This organ starts functioning between the fourth (Bahtiyar and Copel 2008) and fifth (Blaas and Eik-Nes 2008) weeks of gestation, and completes its formation by the sixth (Bahtiyar and Copel 2008) or eighth gestational weeks (Cook *et al.* 2004). By this time, some structures such as the venous connections, the atrial and ventricular chambers, the arterial roots, and the intrapericardial arterial trunks, have been completely formed. However, it is not until the twelfth week that the atrioventricular and arterial valves have sufficiently developed to produce a miniaturised version of the adult heart, although it is still difficult to visualise (Cook *et al.* 2004).

The main foetal heart structures such as the myocardium, the heart valves, the foramen ovale, and the crista dividens (shown in Figure 2.1), are described next:

1. *The myocardium*, which is the muscular wall of the heart, contracts to pump blood out of the heart and then relaxes to allow the heart to refill with returning blood.

2. *The heart valves* ensure that blood flow goes from atria to ventricles and next out to the great arteries, this by opening and closing in response to differences in blood pressure on their two sides (Marieb 2004).

   There are four heart valves, two atrioventricular and two semilunar valves. The atrioventricular valves are located at each atrial-ventricular junction, and prevent backflow into the atria when the ventricles are contracting. The valve at the right atrial-ventricular junction is called *the tricuspid valve*, and the valve at the left atrial-ventricular junction is called *the mitral valve*. On the other hand, the semilunar valves,

which guard the bases of the large arteries issuing from the ventricles (the aorta and the pulmonary trunk), prevent backflow into the left and right ventricles respectively. These valves are named based on their anatomical position so that the valve at the base of the aorta is called *the aortic valve*, whereas the one at the base of the pulmonary trunk is called *the pulmonary valve* (Marieb 2004).

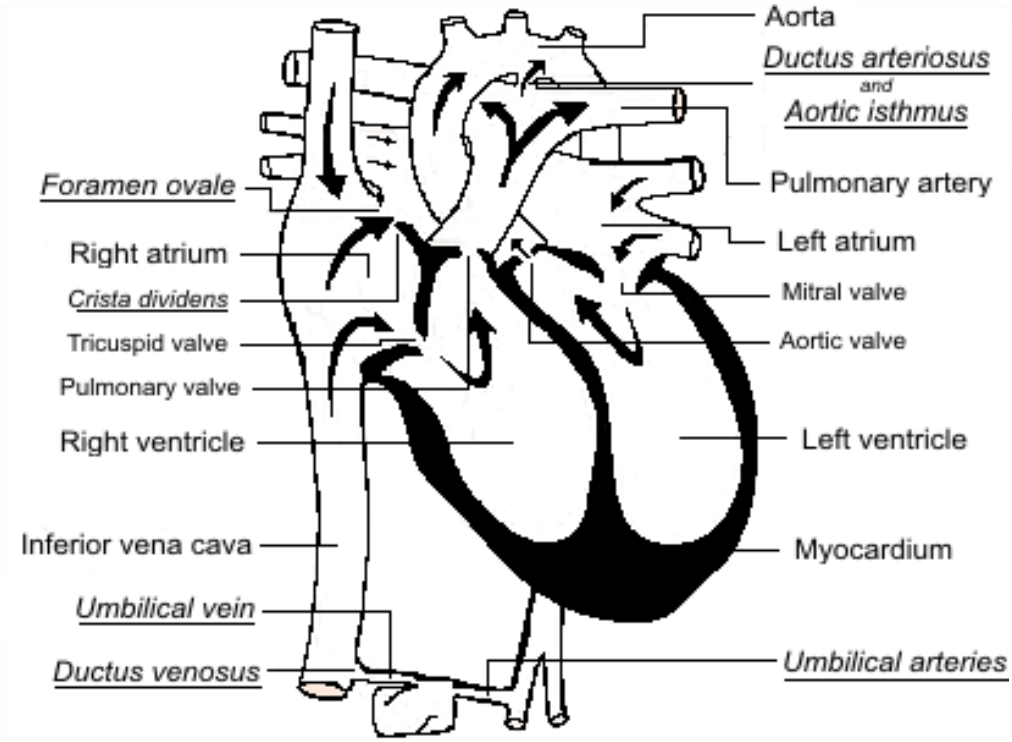

Figure 2.1. The foetal heart and its main structures: the blood vessels (arteries –aorta and pulmonary artery–, veins –vena cava and pulmonary vein–), the atrial and ventricular chambers (right and left), the heart valves (right side –tricuspid and pulmonary–, left side –mitral and aortic–), and the two major connections between the right and left sites of the foetal circulation (*the foramen ovale* and *the ductus arteriosus*) along with *the crista dividens* and the *aortic isthmus*. Other components of the cardiovascular system are shown as well (*umbilical vein/arteries* and *the ductus venosus*), and those present only during the foetal stage are indicated in both italic and underlined font. Modified from Stumper (2009).

3. *The foramen ovale*, which is present only during the foetal stage, is formed by the overlap of the septum secundum over the septum primum and constitutes a straight connection between the right and left atria. *The crista dividens*, which is the free edge of the atrial septum (Creasy and Resnik 2004; Macdonald and Johnstone 1995), separates out the oxygenated blood coming from the inferior vena cava into two streams, one for the left atrium and another for the right atrium.

b) The blood vessels: Composed of *the aorta*, *the pulmonary artery*, and *the vena cava* (inferior and superior branches), the blood vessels transport the foetal blood outside the

foetal heart and back to it (as described in the next section). Additionally, and present only during foetal life, *the ductus arteriosus* connects the main pulmonary artery to the descending aorta (as shown in Figure 2.1), which transports the majority of blood flow towards the foetal lower body and the placenta (Rychik 2004).

c) The placenta: Shown in Figure 2.2, the placenta is an organ that carries out three important functions in the foetal cardiovascular system such as (1) interface between the foetal and maternal systems, (2) execution of many of the functions for the foetus that the lungs will later assume in extrauterine life, and (3) metabolic exchange (Clerici *et al.* 2001; Menihan and Kopel 2008; Rychik 2004). In other words, the placenta is fundamental for the foetus since it brings in oxygen and nutrients whilst removes waste products (Menihan and Kopel 2008).

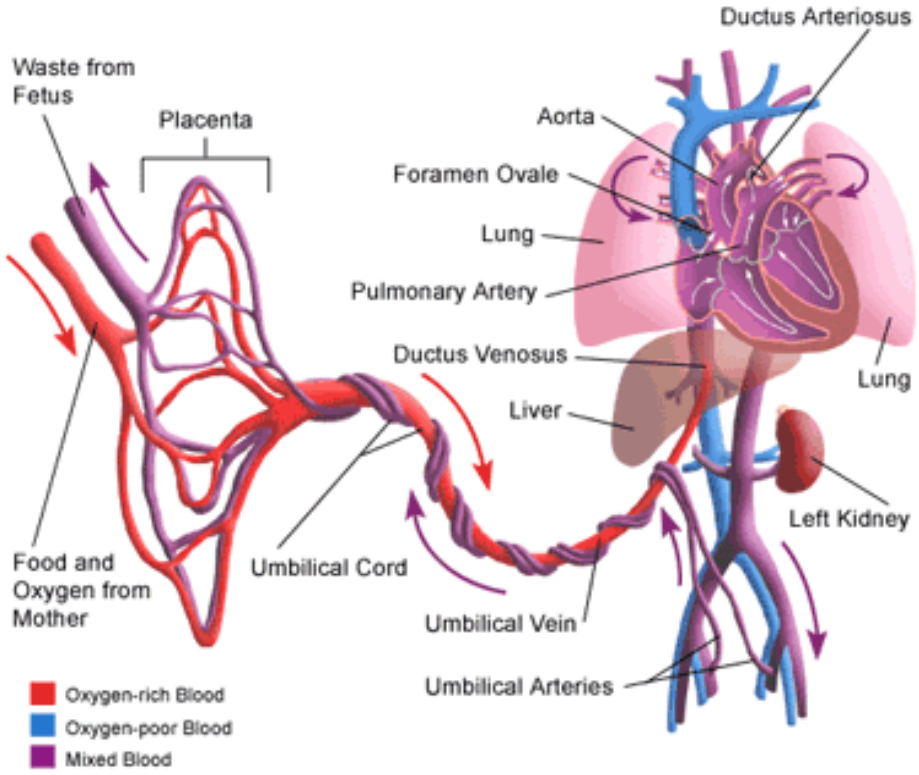

Figure 2.2. Anatomical structure of the foetal cardiovascular system. Changes in colour show oxygen levels in the blood circulating through each structure. Taken from Driscoll-Children's-Hospital (2010).

d) The umbilical cord: Shown in Figure 2.2 as well, the umbilical cord is composed of *the umbilical vein* and *two umbilical arteries*. The former transports oxygen-rich blood from the placenta to the foetus whilst the latter transport deoxygenated blood from the foetus to the placenta (Menihan and Kopel 2008; Rychik 2004). In addition, and present only during foetal life, *the ductus venosus* connects the umbilical vein (after it enters into the foetal

abdomen) with the inferior vena cava just as it enters the right atrium (as shown in Figure 2.2) (Rychik 2004).

2.1.2. Functional characteristics

Once the main structural components of the foetal cardiovascular system have been depicted, it is possible to go further into the description of how they contribute to keep the foetal tissues well oxygenated for foetal development. As this section explains, such good oxygenation is possible due to (a) the paths followed by the blood throughout the foetal circulation and (b) the adaptive mechanisms that provide high oxygen-carrying capacity during foetal life.

a) Foetal circulation: First of all, it is important to highlight that the foetal circulatory patterns differ markedly from those of extrauterine life (Rudolph and Heymann 1967; Rychik 2004; Tucker 2007). This is due to the presence of unique intracardiac and vascular passages (*i.e.* shunts) that allow for blood streaming patterns that exist exclusively during foetal life (see Figure 2.3). Thus, during the prenatal period, it is possible to distinguish two fundamental features of the foetal circulation (Bahtiyar and Copel 2008; Rudolph and Heymann 1967): (i) it works in parallel (see Figure 2.3), which means that left and right ventricles work simultaneously instead of consecutively (as in the adult case) and (ii) it possesses two major connections between its right and left sites, which are given by the foramen ovale and the ductus arteriosus (see Figure 2.2).

The parallel function of the right and left ventricles is fundamental to keep the foetal body and the placenta (a richly vascularised and low-resistance circuit that receives 50% of the combined cardiac output of the foetal heart) perfused (Rychik 2004). To do this, once *the placenta* performs the metabolic exchange necessary to sustain foetal life, highly oxygenated blood is delivered back to the foetus through *the umbilical vein* (see Figure 2.4). Next, one part of such rich blood passes through the *ductus venosus* directly into *the inferior vena cava*, whilst the remaining goes first throughout the foetal liver and then enters into the inferior vena cava as well[1] (Bahtiyar and Copel 2008; Tucker 2007). After that, the blood from the inferior vena cava enters *the right atrium* where the eustachian valve, a tissue flap at the junction of the right atrium and the inferior vena cava, directs the blood from the dorsal portion of the vein (where the more highly oxygenated blood flows)

[1] Blood entering into the inferior vena cava via the ductus venosus joins with that returning from the lower part of the foetal body. Once in the inferior vena cava, since the blood from the umbilical vein has not only a greater content of oxygen, but also a higher kinetic energy, it stays in a stream separated of the blood returning from the lower body. As a result of this preferential streaming, the ductus venosus blood is found along the left dorsal wall of the inferior vena cava.

towards *the foramen ovale* (Tucker 2007). There, the crista dividens (Creasy and Resnik 2004; Macdonald and Johnstone 1995) splits this highly oxygenated flow into two streams, with 50 to 60% being diverted into *the left atrium* and the rest into *the right atrium* (Tucker 2007).

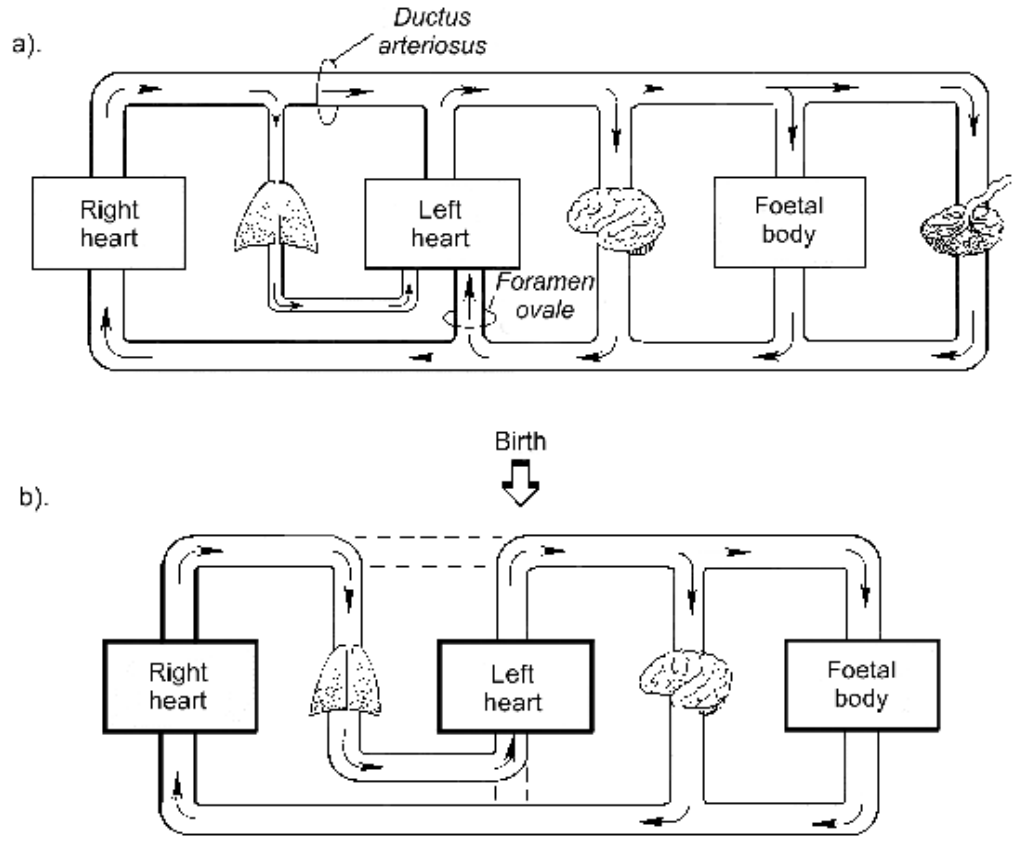

Figure 2.3. Circulatory system of (a) the foetus (parallel), and (b) the adult (serial). © 2007 SAUNDERS Elsevier. Reprinted, with permission of the publisher[2].

Once in the atria, right and left respectively, oxygenated blood mixes with deoxygenated blood that returns through (1) the superior vena cava from the foetal brain, the coronary sinus and the right dorsal side of the inferior vena cava, and (2) the (minimal) pulmonary venous return (Tucker 2007). Next, this blood (still highly oxygenated) passes through the atrioventricular valves to the corresponding ventricles where, upon contraction of the heart,

[2] This figure was published in Maternal, fetal, & neonatal physiology: a clinical perspective, Third edition, Susan Tucker Blackburn, figure 9-13, pp. 294, SAUNDERS Elsevier 2007.

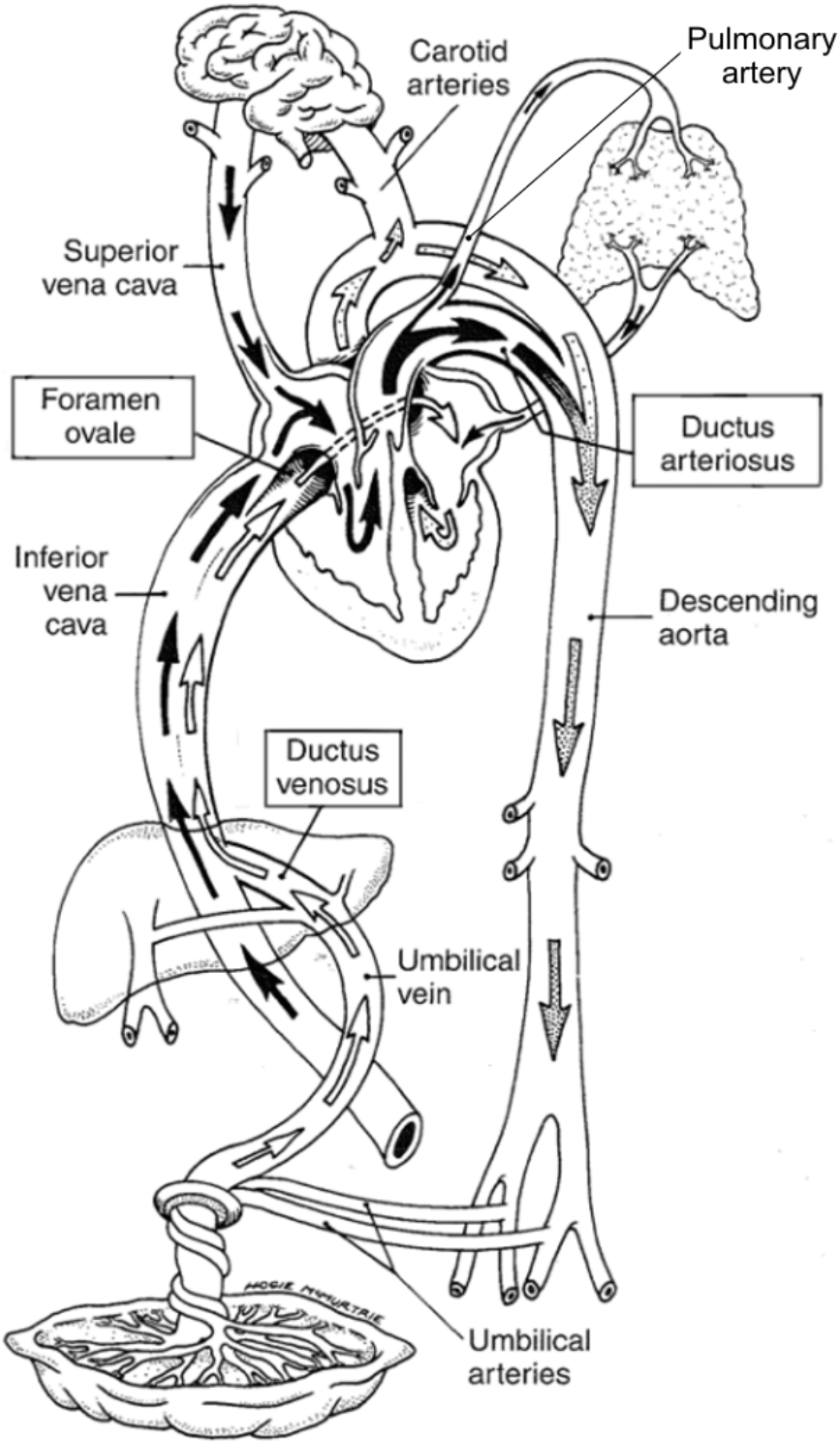

Figure 2.4. Foetal circulation. © 2007 SAUNDERS Elsevier. Reprinted, with permission of the publisher[3].

[3] This figure was published in Maternal, fetal, & neonatal physiology: a clinical perspective, Third edition, Susan Tucker Blackburn, figure 9-14, pp. 295, SAUNDERS Elsevier 2007.

is ejected. In this way, *the right ventricle output* flows directly into *the main pulmonary artery* and *the ductus arteriosus*, with a small portion going to the vasoconstricted vascular bed in *the foetal lungs* and the rest to *the aorta* respectively. Thus, *the descending aorta*, *the lower part of the body* (the systemic circulation), and *the placental circulations* are perfused by the right ventricle. On the other side, *the left ventricle* output is directed towards the coronary and cerebral circulations, with a small portion crossing *the aortic isthmus* to perfuse *the lower body*. Finally, the blood from the systemic circulation returns through the iliac arteries and *the umbilical arteries* to *the placenta*, where the cycle starts again (Rudolph and Heymann 1967; Rychik 2004).

b) Foetal oxygenation: The cardiovascular system is the first system in the foetus to function (it begins as early as the end of the third week) (Bahtiyar and Copel 2008; Blaas and Eik-Nes 2008; Tucker 2007). This is in response to the need for substrates to support the exponential growth and rapid development of the foetus, which necessitates the early development of a system that transports both nutritional elements and metabolic products to and from the cells of the body (Tucker 2007). For this purpose, the parallel arrangement of the system becomes fundamental since it provides the foetus with a continuous and large flow of oxygenated blood. However, as this arrangement allows for mixing of oxygenated and deoxygenated blood at the atria and great vessels (Tucker 2007), the partial pressure[4] of oxygen in the foetal blood is much lower than in the adult blood (Clerici *et al.* 2001; Martin 2008). To override this situation, the foetal circulatory system develops adaptive mechanisms that permit the foetus to maintain a level of oxygen supply similar to that in extrauterine life (Clerici *et al.* 2001; Jensen *et al.* 1999; Martin 2008; Tucker 2007). Such mechanisms, efficient enough to deliver levels of oxygen that exceed the metabolic needs of foetal tissues, are given by (1) high levels of cardiac output and (2) high concentrations of foetal haemoglobin (along with the oxygen dissociation curve of foetal erythrocytes) (Clerici *et al.* 2001; Martin 2008; Tucker 2007):

1. *The cardiac output* is defined as the volume of blood pumped by the heart per minute. In the foetal case, under normal conditions, the resting cardiac output is the highest of

[4] There is an important reason based on the structural and functional characteristics of the placenta for the foetal partial pressure of oxygen to be lower than the maternal partial pressure, which is that the oxygen diffuses from the mother to the foetus by following the gradient of pressure (Rudolph and Heyman, 1967). Another reason for such a foetal partial pressure is that lower PO_2 levels are necessary to keep the lungs collapsed.

any time of life with a combined value of 450 to 500 ml/min/kg[5] at term, compared with approximately 75 ml/min/kg in a resting adult (Jensen *et al.* 1999; Martin 2008; Mielke and Benda 2001; Tucker 2007). By maintaining these high values of cardiac output the foetus meets its high oxygen consumption demands (1.5 to 2 times the adult case) in spite of the low oxygen tension in the foetal blood (Martin 2008; Tucker 2007). This ability to maintain such a high output is due to the elevated foetal heart rate and the cardiac shunts (given by the foramen ovale and the ductus arteriosus) (Tucker 2007).

The heart rate is the most effective mechanism that the foetus has to control ventricular function and cardiac output (Rychik 2004; Tucker 2007). In fact, there is a direct relationship between heart rate and cardiac output so that a 10% increase in foetal heart rate, above the resting level, is immediately followed by an increase in the combined ventricular output, whereas a decrease in foetal heart rate decreases the cardiac output (Tucker 2007).

The cardiac shunts, given by the foramen ovale and the ductus arteriosus (see Figure 2.4), make it possible for the ventricles to work largely in parallel rather than in series to perfuse different parts of the body (Martin 2008; Rychik 2004). As a result, the highest oxygenated foetal blood passes directly from the inferior vein cava (from its left dorsal wall through the foramen ovale) to the left heart for preferential distribution to the brain and myocardium (Martin 2008). At the same time, less oxygenated blood from the right heart passes (through the ductus arteriosus) to the aortic artery, the lower body, and finally, the placenta. In other words, blood from the right heart (after perfusing the lower body) is preferentially returned to the placenta for reoxygenation (Creasy and Resnik 2004).

2. *The foetal haemoglobin* in red blood cells has high affinity for oxygen even at low oxygen concentrations that, in consequence, improves oxygen saturation as well as facilitates transport of oxygen to the foetal tissues (Tucker 2007). This affinity property is fundamental for red cells to become highly saturated with oxygen whilst they circulate through the placenta (Creasy and Resnik 2004), and to easily release

[5] The reason to express the cardiac output in ml/min/kg rather than in ml/min (as its definition implies) is for comparison purposes, which requires to take into account that the foetal volume of blood depends on its weight (i.e. the foetal volume of blood is considerably lower than the adult volume of blood because of the weight). In fact, during foetal life, the volume of blood significantly increases as the foetus gains more and more weight. Conversely, in adult life, where the weight remains “steady”, the volume of blood does not increase anymore. Thus, to properly compare foetal and adult cardiac outputs, the values in the former are expressed per kg of weight.

oxygen whilst they circulate through foetal tissues (Martin 2008; Tucker 2007). Supplementary to such a higher affinity for oxygen, the foetus also has an increased number of red blood cells, more haemoglobin, and more capillaries per unit of tissue. As a result, the foetal oxygen-carrying capacity is even higher than the maternal one (Tucker 2007).

2.2. Control of foetal circulation

At this stage, the main structural and functional features of the foetal cardiovascular system have been described. This description, focused on its main components and mutual interactions, depicted the path followed by the blood in the foetal circulation and the mechanisms developed by the foetus to achieve a high oxygen-carrying capacity that satisfies its own consumption needs. However, this description is not enough to understand the foetal circulation, which is a complex and non steady-state phenomenon under continuous regulation. This regulation, also referred to as control of foetal circulation (Tucker 2007), is performed by the foetal nervous system and aims to favour foetal survival during the stress of hypoxemia, a task achieved by regulating the blood flow throughout the cardiovascular system (*i.e.* the hemodynamic adaptation to hypoxemia). This section describes how the foetal nervous system, both structurally and physiologically, performs such a control of the foetal circulation.

First of all, it is important to notice that the control of foetal circulation requires (a) continuous monitoring of changes in oxygen/carbon dioxide and arterial pressure levels, and (b) fast mechanisms to restore significant changes in those parameters to normal conditions. These tasks are performed by neural inputs and humoral factors such as catecholamines, vasopressin, angiotensin II, and prostaglandins (Tucker 2007). In particular, this chapter focuses on the neural inputs since they are related to both monitor and control tasks, the former by biological sensors referred to as chemoreceptors and baroreceptors, and the latter by the Central Nervous System (CNS) –via its sympathetic and parasympathetic branches–.

2.2.1. Biological sensors

The chemoreceptors are sensory nerves that monitor the chemical makeup of the environment surrounding the foetus (Menihan and Kopel 2008). These receptors (present in the carotid artery, carotid sinus, and aorta), become activated by pH changes due to either decreased levels of circulating oxygen (*i.e.* hypoxemia) or increased levels of circulating carbon dioxide (*i.e.* hypercapnia) (Tucker 2007). In response to these changes, the foetal brain sends nerve impulses towards the heart to either speed up or slow down the heart rate (*i.e.* tachycardia or bradycardia respectively) (Creasy and Resnik 2004; Menihan and Kopel 2008). The specific response depends on which chemoreceptor is stimulated such that, stimulation of central or carotid

chemoreceptors causes mild increasing of heart rate and rising up of arterial blood pressure (*i.e.* hypertension). On the other hand, stimulation of aortic chemoreceptors causes bradycardia and modest increasing of arterial blood pressure (Creasy and Resnik 2004).

The baroreceptors, present in arterial and venous vessels, are sensory nerves highly sensitive to changes in the pressure of the blood against vessel walls. Arterial baroreceptors are located in the walls of the aortic arch and the carotid bodies, whereas venous baroreceptors are in the wall of the terminal portions of the vena cava and the right atrium (Tucker 2007). Thus, when the arterial pressure rises above normal levels, the baroreceptors stimulate the vasomotor centre and the vagus nerve, which results in reflex responses that produce vasodilatation of the arterial vessels, bradycardia and, consequently, reduces the blood pressure. On the contrary, when the arterial pressure falls below normal levels, the stimulation is reduced, the reflex responses produce tachycardia and vasoconstrict the peripheral blood vessels so that the arterial blood pressure rises up (Menihan and Kopel 2008; Tucker 2007). Finally, with regards to the baroreceptors in the veins, they become activated by high venous blood pressure, which causes the heart rate to increase.

In summary, activation of chemoreceptors and baroreceptors produces reflex responses of the CNS that modify the blood flow in an attempt to promptly restore the foetal environment.

2.2.2. The central nervous system

Like the cardiovascular system, the CNS can be described according to its structure (anatomically) and function (physiologically). The anatomic portion is composed of the brain and the spinal cord, whereas the physiological part includes the somatic nervous system (which is voluntary, SNS) and the autonomic nervous system (which is involuntary, ANS) (Menihan and Kopel 2008). Both systems, SNS and ANS, consist of nerve fibres that connect the CNS with structures of the body, the SNS with skeletal muscle and skin, and the ANS with smooth muscle, glands, and cardiac muscle (Menihan and Kopel 2008). Here, as the interest is only on the cardiac structure, the rest of this chapter will focus on the ANS and its control of the blood flow distribution.

The ANS (as shown in Figure 2.5) is both structurally and functionally divided into the parasympathetic and sympathetic branches, whose description is especially important as they are responsible for the changes in the foetal heart rate and arterial pressure, *i.e.* in the control of blood flow (Menihan and Kopel 2008).

The parasympathetic nervous system coordinates activities related to the restoration and conservation of body energy, and the elimination of body waste. Its major component is the vagus nerve, which connects the cardioinhibitory centre in the brain and the heart (Menihan and Kopel 2008). Thus, when the parasympathetic branch becomes activated, the vagus nerve

carries a message from the brain to the heart telling it to slow down the heart rate (*i.e.* bradycardia) (Menihan and Kopel 2008). This communication commonly happens when the foetal head is compressed, for example, during uterine contractions, foetal descent, or forceps application (Menihan and Kopel 2008).

The sympathetic nervous system prepares the body for any intense muscular activity that might be involved in meeting the challenges of a stressful situation. It connects the cardioaccelerator centre in the brain to the heart (Menihan and Kopel 2008). Consequently, when the sympathetic branch becomes activated, the brain tells the heart to accelerate the heart rate (*i.e.* tachycardia) in order to shunt more blood to the vital organs. In the foetal case, this response is evoked by loud noise, vibrations, maternal abdominal palpation, scalp stimulation, or application of the spiral electrode (for recording intrapartum ECG) (Menihan and Kopel 2008).

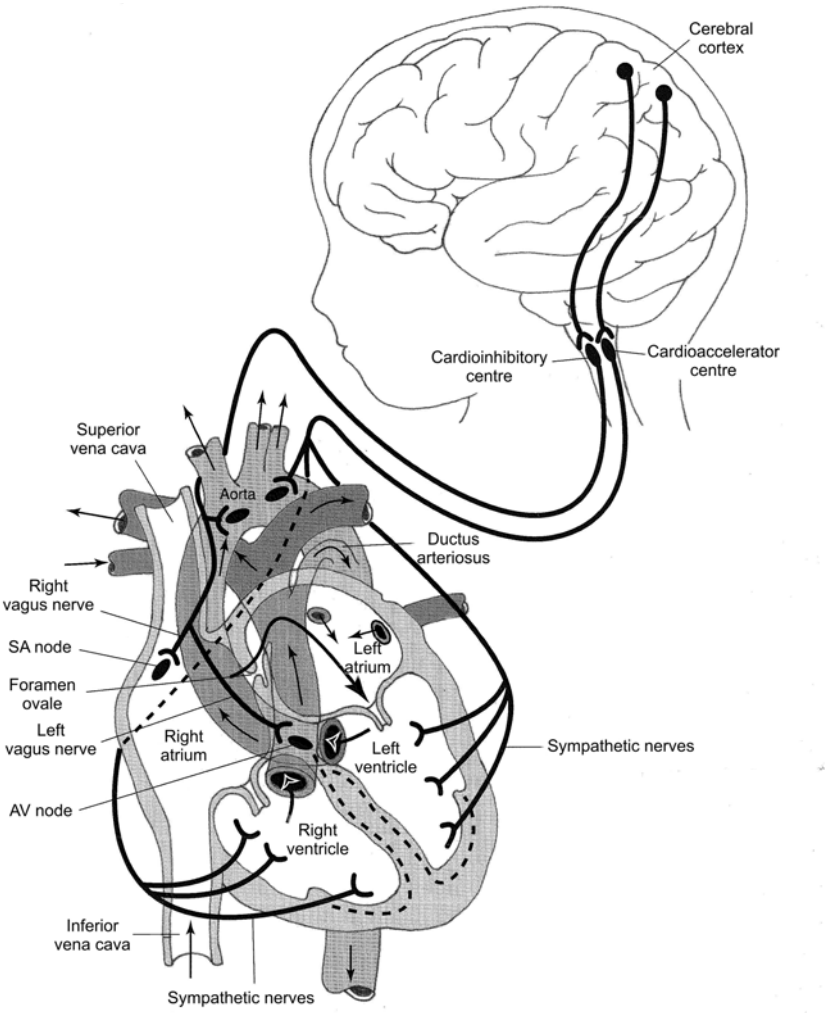

Figure 2.5. Foetal nervous system and foetal heart innervations. © 2008 Lippincott Williams & Wilkins, a Wolters Kluwer business. Reprinted, from Electronic Fetal Monitoring: concepts and applications. Second edition, Menihan & Kopel, figure 1-2, pp. 8, Lippincott Williams & Wilkins 2008.

Thus, on the subject of the variations in the heart rate, the actions and effects of the sympathetic and parasympathetic nervous systems counterbalance each other. Also, these systems do not function independently but collaboratively in order to maintain a balance (unless one is sufficiently stimulated to override the other). Such a balance, proof of a mature and healthy ANS[6], is evident by the presence of variations in the duration of each cardiac cycle (also referred to as heart rate variability, HRV) (Clerici *et al.* 2001; Creasy and Resnik 2004; Martin 2008; Menihan and Kopel 2008; Tucker 2007). Hence, since HRV reflects the synergic work of the sympathetic and parasympathetic nervous systems, and recalling that they become activated by the CNS in response to changes in oxygen/carbon dioxide levels, the *HRV becomes one indicator of foetal oxygen autoregulation capability and, consequently, of neurological development* (Clerici *et al.* 2001; Creasy and Resnik 2004; Martin 2008; Menihan and Kopel 2008; Tucker 2007). The next section will describe in more detail how the HRV changes in conditions of normal and abnormal oxygenation along with its association to the foetal behaviour.

2.3. Oxygenation and foetal behaviour

Normally oxygenated foetuses are so active that, depending on the gestational age, they spend two to three times as much time in activity than in rest. When the foetus is at rest, the rest periods generally last less than 6 minutes before 20 weeks of gestation, and up to 37 minutes after 32 weeks of gestation (Martin 2008). When the foetus is active, it performs body, eye, and breathing movements, not independent but linked, *e.g.* simultaneous body and eye movements. This linkage increases as the gestational age increases (especially after 36 weeks) and results in a "reactive" HRV trace that shows increased variability and accelerations during these episodes. Also, such movements become even more tightly linked as soon as the foetal behavioural states emerge (*i.e.* foetus is asleep or awake) (Martin 2008). Conversely, in abnormally oxygenated situations (referred to as long-lasting hypoxemia), the foetus adapts itself not only with hemodynamic changes, but also with decreased growth and altered behaviour (*e.g.* reduced episodes of body movements) (Clerici *et al.* 2001; Jensen *et al.* 1999; Martin 2008).

The hemodynamic adaptations (previously referred to as changes in the foetal circulation), are the earliest foetal reaction to hypoxemia and are accomplished by changing the foetal heart rate and redistributing the foetal cardiac output (*i.e.* the blood flow). Thus, in an intact foetus,

[6] The ANS is expected to be fully developed by approximately 32 weeks of gestation, although many foetuses accomplish such development at earlier gestational ages. By this time, the ANS is capable of effecting predictable responses to various stimuli as demonstrated by changes in the heart rate (Rychik, 2004).

the initial response to sudden hypoxemia is performed by (1) temporary slowing the foetal heart rate and increasing its variability (a chemoreceptor response mediated by the vagus nerve) (Hanson 1997), and (2) redistributing the blood flow in favour of the most important organs (brain, heart, and adrenals) and away from others (lungs, intestines, kidneys, and skeletal muscles). This initial response is referred to as the "centralisation of circulation", which is a complex task that combines reflex, local, and humoral mechanisms (Clerici *et al.* 2001; Hanson 1997; Jensen *et al.* 1999; Martin 2008; Rychik 2004).

In those cases where this initial foetal response does not manage to compensate the hypoxemic condition after some time (which is mostly due to placental vascular insufficiency), the impedance to blood flow in the umbilical artery, renal artery, and aorta is further increased. As a result, the hypoxemic foetal status is further increased, which produces more pronounced blood flow redistribution. This affects the cardiac hemodynamics in such a way that the left ventricle afterload is decreased and the right ventricle afterload is increased. In very long lasting cases, this pronounced blood redistribution may lead to a decompensatory phase where the CNS becomes affected, the sympatho-vagal balance fails, and the foetal cardiac function responds weakly to prolonged hypoxemia (Clerici *et al.* 2001; Hanson 1997; Jensen *et al.* 1999; Menihan and Kopel 2008; Rychik 2004). In those cases, unless the sympatho-vagal balance is restored quickly (*i.e.* oxygenation), excessive amounts of lactic acid are produced by the anaerobic foetal metabolism. Consequently, the activity in muscle cells becomes depressed, the muscle responsiveness decreases, and the foetal behaviour is affected (Menihan and Kopel 2008). In addition, the foetal heart rate shows changes in variability, amount of accelerations, tachycardia and, ultimately, derives in terminal bradycardia (Menihan and Kopel 2008; Rychik 2004). Finally, when the hypoxemic condition persists long enough to affect foetal tissues (*i.e.* turns into chronic hypoxia), the foetus becomes in large risk of suffering permanent damage to organs and progressing into a fatal condition (Clerici *et al.* 2001; Hanson 1997; Jensen *et al.* 1999; Menihan and Kopel 2008; Rychik 2004).

Thus, once the dangerous effects of long-lasting hypoxemia on foetal well-being have been depicted, it is easier to understand the principal aim of antenatal surveillance, which is the identification of those foetuses whose physiological defence mechanisms against hypoxemia are compromised (*i.e.* improperly oxygenated foetuses). Furthermore, since foetal responses to hypoxemia can be clinically detected (through changes in foetal heart rate, distribution of blood flow, and foetal motility/behaviour), it is clearer why their observation is a key point for obstetricians to perform antenatal foetal surveillance (Martin 2008). This will be further discussed in Chapter 3, where techniques used to observe foetal adaptations to hypoxemia will be described.

2.4. Summary

This chapter described how the foetal cardiovascular and nervous systems adapt to hypoxemia in order to provide levels of oxygen that are appropriate for foetal development and survival. During examination, antenatal surveillance observes the foetal heart rate, blood flow distribution, foetal motility, and foetal behavioural states because their variations indicate the maturity and health of the autonomic nervous system. Thus, their observation has become a key mechanism for antenatal surveillance from where obstetricians aim to assess well-being and detect compromised foetuses before they suffer permanent damage or death due to long-lasting hypoxemic conditions. Chapter 3 will discuss techniques used for detecting these adaptations in antenatal foetal surveillance.

3 ANTENATAL FOETAL SURVEILLANCE

Chapter 2 described how the foetus exhibits a unique set of physiological responses to the stress of hypoxemia. These responses, also referred to as adaptations –and observed through changes in the foetal heart rate (FHR), the distribution of blood flow, and the foetal motility/behavioural states– can be clinically detected and provide useful information for antenatal assessment of foetal well-being (ACOG 2000; Clerici *et al.* 2001; Davies 2000; Menihan and Kopel 2008; Rychik 2004; Tucker 2007). This chapter discusses the techniques used to observe such adaptations for antenatal foetal surveillance.

3.1. Aims of foetal surveillance

The challenge of obstetric surveillance is to identify those foetuses whose physiological defence mechanisms against hypoxemia are compromised so that obstetricians can: (1) classify pregnancy as low-risk or high-risk status and, whenever necessary, (2) act before decompensation and severe damage has occurred (ACOG 2000; Clerici *et al.* 2001; Davies 2000; Menihan and Kopel 2008; Rychik 2004; Tucker 2007). Also, according to (Gribbin and James 2004), obstetricians can (3) optimise the timing of delivery, (4) avoid unnecessary intervention in high-risk pregnancies, and (5) improve the understanding of foetal pathophysiology.

According to Gribbin and James (2004), although neonatal mortality in the UK had fallen from around 15 per 1000 live births in the 60's to about 7 per 1000 in 2004, foetal death rates had not followed the same trend. Indeed, by the time that such a study was reported, foetal loss rates (in the same 40-year period) not only failed to show significant decline, but also accounted for 50% of deaths between 20 weeks of pregnancy and one year of age. Moreover, since the majority of stillbirths had occurred in the low-risk group, it was clear that the techniques used for surveillance and assessing foetal well-being still present fundamental gaps that must be filled. Such gaps are discussed in the next sections, where the techniques used for antenatal

surveillance will be further described in blocks categorised as perceptual, biophysical, and alternative.

3.2. Perceptual assessment of foetal well-being

The FHR and general foetal activity are particularly sensitive to hypoxemia/acidemia and relatively easy to detect in the clinical environment (ACOG 2000; Davies 2000; Gribbin and James 2004; Menihan and Kopel 2008; Tucker 2007). For these reasons, the observation of these adaptations has become the basis of clinical techniques to detect hypoxemia.

3.2.1. Foetal movements

Maternal perception of foetal movements (FMs) is the oldest and most common tool used for assessing foetal well-being (Govindan *et al.* 2007; Heazell and Froen 2008; Olesen and Svare 2004; Rolfe *et al.* 2006). Considered as one of the first signs of foetal life, FMs provide an indirect measure of the functionality and integrity of the CNS (Berbey *et al.* 2001; Olesen and Svare 2004). Thus, since the foetus adapts to prolonged hypoxemia by saving energy (*i.e.* by reducing FMs) (Olesen and Svare 2004), the presence of regular FMs is considered an expression of foetal well-being. Consequently, their observation is recommended as a way that may prevent adverse events in the foetus and newborn (Berbey *et al.* 2001; Govindan *et al.* 2007).

Unfortunately, as the observation of FMs is based on the subjective perception of pregnant women, the counting results and the time required for counting vary widely amongst individuals (Davies 2000; Govindan *et al.* 2007; Heazell and Froen 2008; Olesen and Svare 2004). Moreover, because of several counting protocols have been developed, neither the optimal number of movements nor the ideal interval of time for counting have been defined (ACOG 2000; Mangesi and Hofmeyr 2007; Olesen and Svare 2004). In practice, when any reduction in the number of FMs is perceived, further assessment is always required because such a reduction might show either foetal distress or a merely maternal mistake (ACOG 2000; Berbey *et al.* 2001).

3.2.2. Foetal heart sounds

Foetal heart sounds (FHS) have been traditionally perceived with the foetal stethoscope since 1816, and from these the FHR can be estimated (Ansourian *et al.* 1993; Rolfe *et al.* 2006). In this way, alterations in the FHR baseline such as tachycardia or bradycardia have been used over time decades for intermittent assessment of foetal health in the antenatal period (ACOG 2000; Bocking 2003; Davies 2000; Gribbin and James 2004). However, since this FHR auscultation is intermittently performed, it does not detect abnormal variations in the FHR,

which is fundamental for detecting a suboptimally oxygenated foetus (ACOG 2000; Bocking 2003; Davies 2000; Gribbin and James 2004; Steer 2008). Alternatively, long-term monitoring has been proven to be the core of foetal surveillance –before and during labour– as it ensures that any FHR abnormality can be detected whenever it happens (*i.e.* at any time during pregnancy) (Najafabadi *et al.* 2006).

3.3. Biophysical assessment of foetal well-being

Biophysical assessment of foetal well-being is also based on the observation of adaptations such as general activity, muscle tone, and FHR, which is done by taking advantage of technological development and signal processing schemes (Guimaraes-Filho *et al.* 2008; Menihan and Kopel 2008; Pattison and McCowan 1999). As a result, it has been possible not only to gain access to better quality observations of such adaptations, but also to include the observation of blood flow distribution. Thus, it has been possible to confirm results by (1) performing combined observations of adaptations (*e.g.* FMs and FHR) and (2) including information like uterine activity and foetal images (Guimaraes-Filho *et al.* 2008).

3.3.1. Cardiotocography

Antenatal cardiotocography (antenatal-CTG) is a form of foetal assessment that looks for signs of hypoxia by performing simultaneous recording of FHR, FMs, and uterine contractions (Pattison and McCowan 1999). The former two are measured by Doppler ultrasonography (DUS), whereas the latter is measured by tocography (Menihan and Kopel 2008).

At present, antenatal-CTG is considered the primary method for antenatal monitoring and is applied to pregnancies where foetal well-being is questioned, for example, in presence of reduced FMs, post-term pregnancy or growth restriction (ACOG 2000; Bocking 2003; Davies 2000; Gribbin and James 2004; Olesen and Svare 2004; Pattison and McCowan 1999). In more detail, the antenatal-CTG consists of a continuous record of the FHR that is obtained via an ultrasound transducer placed on the maternal abdomen (Menihan and Kopel 2008; Pattison and McCowan 1999). In this way, the FHR baseline, its variability, heart rate rising (*i.e.* accelerations), and heart rate dropping (*i.e.* decelerations), whenever present, are electronically recorded on a paper trace (Menihan and Kopel 2008; Pattison and McCowan 1999). Next, in those cases where reduced variability and decelerations are present (*i.e.* abnormal traces that could be associated to foetal distress and placental dysfunction), further tests are performed by taking into account concurrent FMs and uterine activity (ACOG 2000; Menihan and Kopel 2008; Olesen and Svare 2004; Pattison and McCowan 1999). These tests are classified as:

a) Contraction Stress Test (CST): This test is based on simultaneous recording of FHR and uterine contractions (ACOG 2000; Devoe 2008; Olesen and Svare 2004). This antenatal-CTG test relies on the premise that foetal oxygenation will be momentarily reduced by uterine contractions. Accordingly, if the foetus is suboptimally oxygenated, then the resultant intermittent reduction in oxygenation due to uterine contractions would lead to late decelerations[1] in the FHR pattern (ACOG 2000; Davies 2000; Menihan and Kopel 2008; Olesen and Svare 2004; Tucker 2007).

The CST is supposed to last 10 minutes but, as it requires the appearance of at least three spontaneous contractions that last more than 40 seconds each, it becomes time-consuming in practical terms. Furthermore, in those cases where less than three contractions occur, it is necessary to induce them by either administration of oxytocin or nipple stimulation (ACOG 2000; Davies 2000). Consequently, this test becomes invasive and contraindicated in cases associated with increased risk of preterm labour and delivery, uterine rupture or uterine bleeding (ACOG 2000; Barsoom *et al.* 2001).

b) Non-Stress Test (NST): This is a non-invasive test based on simultaneously recording the FHR and FMs (ACOG 2000; Barsoom *et al.* 2001; Bocking 2003; Devoe 2008; Olesen and Svare 2004). This antenatal-CTG test relies on the premise that a well-oxygenated and neurologically healthy foetus will temporarily accelerate its FHR in presence of FMs. Thus, an increase in the FHR baseline during FMs shows good oxygenation and satisfactory coordination between the CNS and the heart (Alus *et al.* 2007). This behaviour, also referred to as HR "reactivity", is considered a good indicator of normal autonomic function in the foetus (ACOG 2000; Bocking 2003; Davies 2000; Olesen and Svare 2004; Tucker 2007). However, loss of reactivity (given by either absence of accelerations or appearance of decelerations associated with FMs) cannot be straightforward interpreted as it may be due to either the beginning of hypoxemia, normal foetus/mother conditions (*e.g.* foetal sleep cycles (ACOG 2000; Guimaraes-Filho *et al.* 2008; Olesen and Svare 2004), maternal position (Alus *et al.* 2007; Cito *et al.* 2005; Tamas *et al.* 2007)) or even mistakes at counting FMs. Thus, reliable classification of the non-reactivity NST becomes a big issue that makes the method highly inconsistent and plenty of variations inter and intra observer (Black and Campbell 1997; Devoe 2008; Heazell and Froen 2008). Additionally, it has been reported that in those cases where the test lasts more than 20 minutes the mothers experience back pain, which complicates the study (Alus *et al.* 2007).

[1] Late decelerations are defined as reductions of the FHR baseline that reach their maximum value after the peak of the uterine contraction and that usually persist beyond the end of the contraction.

An alternative option, although only for some non-reactive tests, is reached by using foetal acoustic stimulation (FAS), which elicits FHR accelerations during periods of low-FHR reactivity caused by sleep cycles (Devoe 2008; Pinette *et al.* 2005). As a result, the time needed for testing well-being may be safely reduced (by reducing the number of non-reactive CTGs traces due to foetal sleep states) without compromising the detection of acidosis[2] (ACOG 2000; Olesen and Svare 2004; Pinette *et al.* 2005).

c) Real time ultrasonography: Sonography allows visual examination of foetal development in uterus. In particular, real time ultrasonography (B-mode US) has made it possible to further study foetal behavioural and physiological variables such as breathing/body movements, foetal tone[3], and amniotic fluid volume (Banks and Miller 1999; Gribbin and James 2004; Magann *et al.* 1999; Olesen and Svare 2004; Sener *et al.* 1996).

Up to date, systematic observation of the foetus by B-mode US has provided plenty of knowledge about the development of foetal behaviour. It has made it possible to study foetal general body movements and to identify parameters such as onset, incidence, rest-activity cycles, and diurnal rhythms (Luchinger *et al.* 2008; ten Hof *et al.* 1999). Consequently, different patterns of foetal movements have been identified and categorised as gross body movements (previously referred to as FMs), sucking/swallowing movements, and breathing movements (FBMs) (Cosmi *et al.* 2003; Levy *et al.* 2005; Luchinger *et al.* 2008; ten Hof *et al.* 1999). A description of these movements is presented in the next paragraphs.

1. *FMs* comprises complex and variable patterns that involve random movements of trunk, limbs, and head (ten Hof *et al.* 1999). According to (Luchinger *et al.* 2008), these movements evolve from "just discernible" to more complex movements as the spinal and brainstem mature, which happens after the ninth week of gestation. Then, as the third trimester progresses, FMs become naturally reduced (ten Hof *et al.* 1999).

2. *Swallowing and sucking movements* allow the development of the mechanisms necessary for the baby to suck on the breast in neonatal life (Levy *et al.* 2005). Swallowing movements appear about at week 11th and contribute to regulation and homeostasis of amniotic fluid volume, intrauterine fluids, and foetal growth. Sucking

[2] Acidosis is a blood condition in which the bicarbonate concentration is below normal values and results from anaerobic processes during long-lasting hypoxemia.

[3] Foetal tone makes reference to the extension of a foetal extremity with return to flexion or opening/closing a hand.

movements appear about at week 15th, increase their rhythm in late pregnancy, and change both rhythm and frequency in response to flavours.

3. *FBMs* in uterus are not associated with alveolar expansion or gas exchanging, but with developing of diaphragmatic muscles and lungs, which prepares the respiratory system to maintain breathing after birth (Ansourian *et al.* 1993; Cosmi *et al.* 2003). These movements are described depending on (i) their regularity and frequency, which ranges from 30 to 90 breaths per minute (Ansourian *et al.* 1993), and (ii) their links with FMs and FHR (Cosmi *et al.* 2003). Thus, three patterns of FBMs have been identified during pregnancy (Cosmi *et al.* 2003):

   Rapid and regular movements: they are the most common FBMs and are characterised by an average rate of 60/min and small amplitude. In addition, whenever present, FBMs are accompanied by increased FMs and more variability in the FHR.

   Rapid and irregular movements: they are low amplitude movements that appear amongst slower movements of larger amplitude.

   Abrupt and isolated movements: these movements are characterised by large-amplitude excursions whose frequency ranges from 10 to 15 movements per minute. These movements are usually recognised as hiccups and do not have any association with FMs.

Ultrasound observation for foetal surveillance can take up to 30 minutes, and current techniques for monitoring foetal well-being heavily rely on this technique (Sener *et al.* 1996). For example, in high-risk pregnancies, measurements of abdominal circumference and estimations of foetal weight by US are considered as the most accurate way to predict growth-restricted foetuses (Gribbin and James 2004). However, in terms of monitoring foetal well-being, US has two disadvantages: (i) there is concern that long-term exposure to ultrasound may be harmful to the foetus (Barnett 2001; Holburn and Rowsell 1989) and, (ii) the US machine and its trained operator are an expensive resource. Consequently, US observation cannot be applied for long periods of time in order to anticipate foetal distress (Holburn and Rowsell 1989).

d) Biophysical profile (BPP): This considers that the accuracy of foetal well-being assessment is increased by the combined used of five physiological variables (Devoe 2008; Guimaraes-Filho *et al.* 2008; Olesen and Svare 2004). Thus, the BPP combines the CTG (NST) along with four observations made by B-mode US, *i.e.* the FBMs, the FMs, the foetal tone, and the amniotic liquid volume (ACOG 2000; Olesen and Svare 2004; Sener *et al.* 1996).

During the BPP study, each component is scored according to the perception of the examiner and the total sum is used to qualify the foetal well-being (ACOG 2000; Davies 2000). The main problem with BPP is that correct interpretation of the results requires proper understanding about not only foetal adaptations to hypoxemia, but also intrinsic/extrinsic factors that may affect the result (*e.g.* the gestational age and sleep cycles) (Guimaraes-Filho *et al.* 2008; Manning 2002). Thus, although the test should last up to 50 minutes (*i.e.* 30 min for the ultrasonographic observation and 20 min for the NST), in those cases where the foetus shows diminished biophysical activities and a non-reactive NST, the test must be repeated and, consequently, the study lasts longer (Sener *et al.* 1996).

3.3.2. Umbilical artery Doppler velocimetry

Doppler velocimetry is a technique used to assess the hemodynamic components of vascular impedance, *i.e.* the distribution of blood flow throughout the circulatory system (ACOG 2000). In obstetrics, umbilical artery (UA) Doppler velocimetry has been applied to foetal surveillance since 1977 (Korszun *et al.* 2002; Olesen and Svare 2004) and, amongst the set of Doppler velocimetry studies, it has become the favourite option to be performed (Abramowicz and Sheiner 2008; Korszun *et al.* 2002).

UA Doppler velocimetry is based on the observation of waveform patterns in the UA, which show noticeable differences between normally-growing and growth-restricted foetuses (ACOG 2000; Davies 2000; Olesen and Svare 2004). As a result, UA Doppler assessment of high-risk pregnancies has been found to improve outcome and reduce hospital admissions (Abramowicz and Sheiner 2008; Davies 2000; Seyam *et al.* 2002; Turan *et al.* 2007). On the contrary, routine Doppler velocimetry in low-risk populations has not shown to benefit the outcome, which means it is an unnecessary tool for screening the general population (Abramowicz and Sheiner 2008; ACOG 2000; Davies 2000; Gribbin and James 2004; Seyam *et al.* 2002).

So far this chapter has described the most important characteristics of the techniques used by obstetricians to perform antenatal foetal surveillance. This information, necessary to understand the gaps in such techniques (and why stillbirths may occur in the low-risk group), can be summarised as follows:

(1) Reduction of perinatal mortality in the last decades confirms that observations of foetal adaptations such as FHR and FMs are valuable to perform antenatal foetal surveillance (Bocking 2003; Heazell and Froen 2008).

(2) Antenatal surveillance by CTG is the most popular test in the clinical environment. However:

- Reliable interpretation of non-reactive tests remains a big problem (Black and Campbell 1997; Heazell and Froen 2008). Most importantly, although better identification is desirable, it will not necessary improve the outcome as an abnormal NST is a late indicator of foetal hypoxemia (Korszun *et al.* 2002).

- Monitoring FHR by DUS is a reliable technique to detect the FHR baseline, but it shows higher FHR variability in comparison to the variability recovered by using direct ECG (Peters *et al.* 2004). Besides, since DUS is very sensitive to noise, it produces FHR traces containing spurious data that may lead to wrong interpretations and unnecessary interventions (Kahler *et al.* 2002; Menihan and Kopel 2008). Most importantly, interpretation of FHR patterns shows large variations inter and intra observer (Parer and King 2000).

(3) US techniques have provided plenty of knowledge about foetal behaviour development, but it is unsuitable for long-term monitoring of foetal well-being (Holburn and Rowsell 1989). Besides, DUS techniques generate a FHR signal with low temporal resolution, which makes it impossible to obtain beat-to-beat information (Kahler *et al.* 2002; van Leeuwen 2004).

In summary, since stillbirths occur in the low-risk group (either by human error, lack of a complete understanding of how the foetus responds to prolonged hypoxemia or perhaps lack of sensitivity in the screening tools), it is clear that the problem of effective and non-invasive monitoring of foetal well-being remains a challenge in the field of antenatal foetal surveillance (Ansourian *et al.* 1993; Jansen and Chernick 1991; Lewis 2003; Rolfe *et al.* 2006). To overcome the problem, and taking advantage of technological development of sensors (Rolfe *et al.* 2006), data acquisition systems, and signal processing schemes, alternative methods have been explored (Lewis 2003). These methods are discussed in the next section and, as the reader will see, they aim to a long-term and non-invasive observation not only of foetal adaptations, but also of further cardio-respiratory information that objectively reinforces the assessment of foetal well-being (Lewis 2003).

3.4. Alternative assessment of foetal well-being

As previously mentioned, foetal well-being assessment is routinely performed based on FHR calculation by means of DUS techniques that generate a FHR signal with low temporal resolution (Kahler *et al.* 2002; van Leeuwen 2004). Alternatively, research has shown that the study of morphological and temporal features of the signals produced by the foetal heart function (*e.g.* electric, magnetic, and vibration) provide additional information about foetal well-being (Kahler *et al.* 2002; Lewis 2003; Martens *et al.* 2007). Such extra information, along with FHR calculation, may be extracted from non-invasive recordings referred to as foetal

electrocardiogram (Al-Zaben and Al-Smadi 2006; Lewis 2003; Martens *et al.* 2007; Matonia *et al.* 2006; Pieri *et al.* 2001; Puthusserypady 2007; Zarzoso and Nandi 2001), foetal magnetocardiogram (Comani *et al.* 2005a; Comani *et al.* 2004b; Comani *et al.* 2004c; Kahler *et al.* 2002; Lewis 2003; van Leeuwen 2004), and abdominal phonogram (Ansourian *et al.* 1993; Colley *et al.* 1986; Goovaerts *et al.* 1989a; Goovaerts *et al.* 1989b; Holburn and Rowsell 1989; Moghavvemi *et al.* 2003; Rolfe *et al.* 2006; Varady *et al.* 2003; Zuckerwar *et al.* 1993). The main characteristics of such recordings will be described in the next sections. Later on, in Chapter 4, details about some typical signal processing methodologies for extracting information of interest will be discussed.

3.4.1. Foetal electrocardiography

The foetal electrocardiogram (FECG) represents the summation of electrical activities of the foetal heart seen from the surface of the maternal womb (Al-Zaben and Al-Smadi 2006). In a general description, the FECG is a signal composed of the P, QRS, and T waves, which are separated by the PR, and ST intervals (see Figure 3.1) (Al-Zaben and Al-Smadi 2006; Martens *et al.* 2007). Also, the amplitude of the FECG ranges from 10 to 100 μV (Puthusserypady 2007), whereas its frequency content (*i.e.* bandwidth) ranges from 20 to 40 Hz (Matonia *et al.* 2006).

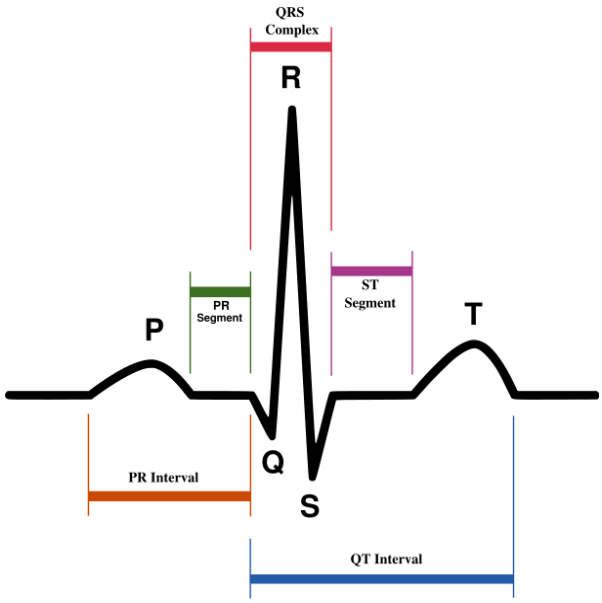

Figure 3.1. The electrocardiogram and its components (P, QRS, and T waves). Taken from WIKIMEDIA-project (2011).

The FECG records information about the conduction system of the foetal heart, consequently, it provides valuable information about maturity of the foetal nervous system and thus, about well-being (Puthusserypady 2007). This information is obtained by measuring the

R-R interval, which makes it feasible to calculate the FHR and thus, to further analyse its baseline, variability, and accelerations/decelerations (Al-Zaben and Al-Smadi 2006). Also, by analysing changes on the PR- and PQ- intervals, the width of the QRS complex, the P wave, the T wave, and the ST segment during labour, it has been attempted to find correlations between these temporal characteristics and the level of foetal oxygenation (Lewis 2003; Martens *et al.* 2007; Matonia *et al.* 2006; Sato *et al.* 2007). As a result, it has been reported that the duration of the P wave and the QRS complex linearly increases as the gestational age increases, which could be used to evaluate foetal growth and status (Lewis 2003). Additionally, it has been found that changes in the HRV in relation to a significant rising in the ST segment are more pronounced in acidotic foetuses (*i.e.* under acute hypoxia) than in normally oxygenated foetuses (Siira *et al.* 2007) and that the correlation between the PR and RR intervals changes from positive to negative when occlusions of the umbilical (*i.e.* progressive asphyxia) are present (Keunen *et al.* 1999; Westgate *et al.* 1998).

During pregnancy, the FECG can be transabdominally recorded by placing ordinary electrodes on the maternal abdomen (Al-Zaben and Al-Smadi 2006; Martens *et al.* 2007; Matonia *et al.* 2006). The method, referred to as abdominal electrocardiography (abdominal ECG), is passive and non-invasive, which makes it possible to use it for long-term ambulatory recording (Martens *et al.* 2007; Matonia *et al.* 2006; Pieri *et al.* 2001; Puthusserypady 2007). Unfortunately, when the abdominal ECG is recorded, it contains not only the FECG, but also large artefacts such as the maternal ECG (MECG), maternal electromyogram (MEMG), power-line interference, and artefacts due to electrode motion (Al-Zaben and Al-Smadi 2006; Martens *et al.* 2007; Matonia *et al.* 2006; Pieri *et al.* 2001; Puthusserypady 2007). Besides, because of its small amplitude, the FECG is easily swamped by the maternal ECG and, because of their frequency bands similarity, it is impossible to separate them by using simple filtering methods (Matonia *et al.* 2006). This problem is accentuated between 24 and 32 weeks of gestation, when the SNR becomes severely degraded due to the insulating effect of the vernix caseosa[4] (Kahler *et al.* 2002; Lewis 2003; Sato *et al.* 2007; Stinstra and Peters 2002).

To deal with such a contamination problem, several signal processing techniques have been proposed to recover the FECG from the abdominal ECG, *e.g.* coherent time-averaging, matched filtering, subtraction, blanking, noise cancelling (Assaleh 2007; Khamene and Negahdaripour 2000; Matonia *et al.* 2006; Pieri *et al.* 2001), and more recently, approaches based on blind source separation methods, singular value decomposition, and H-infinity analysis (Al-Zaben and Al-Smadi 2006; Martens *et al.* 2007; Najafabadi *et al.* 2006; Puthusserypady 2007; Sato *et*

[4] This is a waxy white substance that coats the foetal skin to keep it moisturised and protected against environmental stress (*e.g.* the passage of bacteria).

al. 2007; Zarzoso and Nandi 2001). Results have shown FECGs traces with only 65% of detectable QRS complexes that have been used to estimate only average FHR values (Matonia *et al.* 2006; Pieri *et al.* 2001). Thus, since the FECG is a weak signal (highly dependent on uncontrolled factors such as gestational age and foetal orientation in the maternal abdomen), it has been impossible to reconstruct accurate and complete traces of the whole FECG. Consequently, reliable recovery of shapes/intervals of the FECG component waves –P, QRS, and T– is still an unsolved problem.

In summary, although the FECG contains plenty of information about foetal well-being, a huge part of such information (*i.e.* the R-R, PR- and PQ- intervals, the width of the QRS complex, and changes in the P wave, the T wave, and the ST segment) becomes hardly accessible as soon as the signal is transabdominally recorded (Comani *et al.* 2004b). Moreover, although different signal processing schemes have been already applied, they only have achieved a partial recovery of such information, which means that further research is still needed. These will be further discussed in Chapter 4.

3.4.2. Foetal magnetocardiography

Magnetocardiography (MCG) is a non-invasive technique used to record the spontaneous activity of the heart, which is done by measuring the weak magnetic field variations produced by ionic currents that flow through the myocardium during the cardiac cycle (Comani *et al.* 2004a). This recording is performed by using superconducting systems called SQUIDs, which detect the cardiac magnetic field without making any contact with the body and, most importantly, with high sensitivity from a number of precise positions over the region of interest (Comani *et al.* 2004a; Lewis 2003).

In the foetal case, the foetal magnetocardiogram (FMCG) non-invasively records, as early as the 13^{th} week of gestation (van Leeuwen 2004), the electrical activity of the foetal heart by measuring the associated magnetic field variations on the maternal abdomen surface (Comani *et al.* 2005a; Comani *et al.* 2004a; Lewis 2003; Stinstra *et al.* 2002). Additionally, the FMCG contains some maternal cardiac and muscle activity, uterine activity and, when present, FMs, and foetal diaphragmatic activity due to sucking, swallowing, and hiccups (Popescu *et al.* 2007; Popescu *et al.* 2008; Zhao and Wakai 2002).

The FMCG shows morphological and temporal similarities with the FECG and, because there is no direct contact between the magnetometer and the maternal abdomen, interference due to poor electrode contact or DC contact potentials is completely eliminated (Comani *et al.* 2005a; Comani *et al.* 2004a; Lewis 2003; van Leeuwen 2004). In addition, and contrary to the abdominal ECG recording, it has been reported that the SNR increases as the pregnancy progresses (Stinstra and Peters 2002). Consequently, the rate of extraction of the entire PQRST

waveform patterns from the FMCG has been reported to be higher than the rate from the abdominal ECG (100% and 70% respectively according to (Kahler *et al.* 2002)) and, most importantly, less dependent on the gestational age and presence of the vernix caseosa (Comani *et al.* 2005a; Lewis 2003; Popescu *et al.* 2008). Thus, after some signal processing stages (*e.g.* components separation, reconstruction, and smoothing), it has been possible to identify the onset and offset of the P, QRS, and T waves, foetal cardiac time intervals such as FHR (Comani *et al.* 2005a; Comani *et al.* 2005b; Kahler *et al.* 2002; Mantini *et al.* 2005; Sreeman and Brockmeier 2004; van Leeuwen 2004), and some patterns of diaphragmatic activity (Parer and King 2000; Popescu *et al.* 2007; Popescu *et al.* 2008).

For practical applications, however, it is important to consider that the magnetometer is a very high-tech and expensive system that must have not only high sensitivity to the smaller-amplitude foetal signal (10^{-12} T), but also high rejection levels to the larger-amplitude magnetic signals from the earth ($\sim 10^{-4}$ T), large nearby metallic objects ($\sim 10^{-7}$ T), and even metallic objects worn by the patient (Lewis 2003). Thus, preparation of such a high-tech system for a study requires considerable technical skills to successfully set it up and guarantee its correct function. Also, ongoing costs must consider not only payment of trained personal, but also purchasing of consumables (*e.g.* liquid helium) and outfitting of shielded facilities, which results in a prohibitively expensive system for clinical applications (Lewis 2003; Sreeman and Brockmeier 2004).

3.4.3. Abdominal phonography

Phonography is one of the oldest methods for detecting biophysical activities in the body and, although its use lost popularity with the arrival of DUS during the 70s, the concern of possibly harming the foetus by long-exposure to US along with the development of new sensors have renewed interest in this method for foetal surveillance purposes (Ansourian *et al.* 1993; Moghavvemi *et al.* 2003; Rolfe *et al.* 2006; Varady *et al.* 2003).

Phonography takes advantage of the fact that sounds generated in the human body can be detected by using an acoustic transducer placed on the skin surface. Thus, monitoring of foetal activity can be implemented with a sensitive transducer positioned on the maternal abdomen (Ansourian *et al.* 1993; Colley *et al.* 1986; Goovaerts *et al.* 1989a; Goovaerts *et al.* 1989b; Holburn and Rowsell 1989; Rolfe *et al.* 2006; Zuckerwar *et al.* 1993). The technique is passive, non-invasive, and low-cost, consequently, can be used for long-term monitoring (Ansourian *et al.* 1993; Holburn and Rowsell 1989; Moghavvemi *et al.* 2003; Varady *et al.* 2003). The resulting recorded signal, referred to as the abdominal phonogram, carries valuable information about physiological parameters such as FHS (mainly composed of S1 and S2, which are better known as the first and the second heart sounds respectively), FMs, FBMs, and cardiac cycle

timing (*i.e.* FHR, systolic and diastolic intervals). Together, these are considered to provide an assessment of foetal well-being (Colley *et al.* 1986; Goovaerts *et al.* 1989a; Goovaerts *et al.* 1989b; Holburn and Rowsell 1989; Moghavvemi *et al.* 2003).

Unfortunately, because of the acoustic damping in the maternal tissues, the foetal acoustic energy in the abdominal phonogram is considerably low (Ansourian *et al.* 1993; Holburn and Rowsell 1989; Zuckerwar *et al.* 1993). As a result, the foetal information is easily hidden by external sources from the environment (*e.g.* speech), biological sources from the mother (*e.g.* placental blood flow, digestive activity, aortic pressure wave[5], heart sounds, and respiratory sounds), and artifactual sources produced by small movements of the transducer (Holburn and Rowsell 1989; Varady *et al.* 2003; Zuckerwar *et al.* 1993). Furthermore, since the characteristics of such noises make it possible for them to completely bury the foetal information, they make it difficult to extract reliable information about foetal activity. For example, because of the lower energy (60 dB below the magnitude of some maternal signals (Zuckerwar *et al.* 1993)) and wider spectral range of the FHS (20-150 Hz) (Holburn and Rowsell 1989; Moghavvemi *et al.* 2003; Varady *et al.* 2003), they may be affected by almost any source. On the other hand, the FBMs, which tend to be one order of magnitude larger than the FHS (Ansourian *et al.* 1993; Holburn and Rowsell 1989) and with a lower bandwidth (0.5-2 Hz) (Ansourian *et al.* 1993; Goovaerts *et al.* 1989a; Holburn and Rowsell 1989), may be mainly contaminated by the maternal breathing and artifactual sources. As a result, it may be virtually impossible to distinguish foetal information in the abdominal phonogram so that its extraction has become a challenging task.

At present, there have been significant efforts to develop long-term monitoring methods for foetal well-being, some based on the detection of FHS (*i.e.* phonocardiography, PCG) or FBMs. Indeed, FHS and FBMs have been long researched giving rise to methods with different types of sensors (Ansourian *et al.* 1993; Colley *et al.* 1986; Goovaerts *et al.* 1989a; Goovaerts *et al.* 1989b; Holburn and Rowsell 1989; Talbert *et al.* 1986; Zuckerwar *et al.* 1993), number of channels (Moghavvemi *et al.* 2003; Najafabadi *et al.* 2006), and signal processing schemes such as digital filters, noise cancelling, and time-frequency analysis (Ansourian *et al.* 1993; Bassil

[5] The pressure wave is a transient increase in blood pressure that spreads like a pulse wave through the arteries, starting in the aorta and pulmonary trunk. This wave follows the pumping action of the heart and, consequently, reaches a peak when ventricles contract, and falls to a minimum when the ventricles relax before it begins to rise and fall again in the next cardiac cycle. The intensity of this wave depends on the artery where it is detected, happening to generally increase as the artery becomes closer to the heart (Northrop 2001). Clearly, the closer the sensor position to the maternal aorta, the higher the possibilities that the aortic pressure wave, referred to in the future as the maternal pressure wave, affects the foetal components in the abdominal phonogram.

and Dripps 1989; Goovaerts *et al.* 1989a; Goovaerts *et al.* 1989b; Holburn and Rowsell 1989; Talbert *et al.* 1986; Zuckerwar *et al.* 1993). However, although some studies have shown some improvement in the SNR of the signals (Goovaerts *et al.* 1989a; Jimenez *et al.* 1999; Kovacs *et al.* 2000; Varady *et al.* 2003), the detection of FHS and FBMs may still be difficult. Thus, even though high quality technology and processing schemes have been combined, the extraction of reliable information from the abdominal phonogram remains a challenging task.

3.5. Summary

This chapter discussed methods used to observe foetal adaptations for antenatal surveillance. As mentioned, it is generally accepted that current methods for biophysical antenatal monitoring do not facilitate a comprehensive and reliable assessment of foetal well-being. Alternatively, there is continuing development of existing technologies along with research into possible new and non-invasive methods that aim to improve current antenatal monitoring procedures. These non-invasive methods rely on the detection of information regarding the cardiac function along with foetal activity, which is done by using passive transducers that sense electric, magnetic or vibration signals. The resulting signals, recorded on the surface of the maternal womb and referred to as abdominal ECG, FMCG, and abdominal phonogram, are plenty of information about foetal condition. However, as described in this chapter, every measuring technique records not only foetal information, but also additional interference signals from the mother and the environment. Moreover, since the foetal information is completely buried by some of these interferences, the recorded signals require further signal processing analyses to recover information of interest. Chapter 4 will discuss signal processing methods used in the literature to recover such foetal information from the abdominal ECG, the FMCG, and the abdominal phonogram.

4 SIGNAL PROCESSING METHODS FOR ANTENATAL SURVEILLANCE

Chapter 3 discussed methods used for antenatal monitoring and assessment of foetal well-being. Some of these methods, resulting from continuous development of technologies and research, provide new and non-invasive alternatives that might improve current antenatal monitoring procedures. Such methods rely on the detection of information regarding the cardiac function along with foetal activity using passive transducers that sense electric, magnetic or vibration signals. The resulting signals, referred to as abdominal ECG, FMCG, and abdominal phonogram respectively, are rich in information about both foetal cardiac function and activity. However, because of their lower amplitude, foetal signals are deeply immersed in maternal and environmental sources. Furthermore, all these sources may overlap foetal components in both time and frequency making it difficult to extract reliable information about foetal activity. Consequently, the extraction of foetal information from the abdominal ECG, FMCG, and abdominal phonogram must be performed by using signal processing strategies.

This chapter discusses some of the approaches reported in the literature to process the abdominal ECG, the FMCG, and the abdominal phonogram in order to extract foetal information. Next, it introduces the approach that has been studied in this research for antenatal surveillance purposes.

4.1. Processing the abdominal electrocardiogram

The FECG can be recorded during pregnancy by placing ordinary electrodes on the maternal abdomen (Al-Zaben and Al-Smadi 2006; Martens *et al.* 2007; Matonia *et al.* 2006). However, the signal recorded in this way, called abdominal ECG, encompasses not only the foetal FECG (an electric signal from the foetal heart whose amplitude ranges between 5 and 100 μV depending on electrode location, foetal position, and gestational age (Oldenburg and Macklin 1977; Puthusserypady 2007)), but also the MECG, some MEMG, power-line interference, and artefacts due to electrodes motion (Al-Zaben and Al-Smadi 2006; Martens *et al.* 2007; Matonia

et al. 2006; Pieri *et al.* 2001; Puthusserypady 2007). Amongst these interference signals, there is one whose characteristics make the extraction of the FECG a task that cannot be performed by using simple filtration methods, the MECG. The reason behind this is that the MECG possesses not only a higher energy than the FECG (5-1000 times) (Adam and Shavit 1990), but also a similar frequency content, which makes it possible for the MECG to completely overlap the FECG in time and frequency domains (Matonia *et al.* 2006).

At present, different methods have been implemented to separate the FECG from the MECG in the abdominal ECG. In general, two approaches can be identified, one strongly based on the number and location of the electrodes, and another based mainly on the characteristics of the signals underlying the abdominal ECG (*i.e.* statistics, amplitude, timing, frequency, or a combination of them all). In the former approach, referred to as "weighted addition" or "spatial filtering", a linear (sometimes nonlinear) combination of signals from several electrodes is calculated to remove the MECG from the electrodes measuring the abdominal ECG (Adam and Shavit 1990; Bergveld *et al.* 1986; Bergveld and Meijer 1981). In the latter, or straightforward approach, diverse signal processing techniques such as template subtraction (Azevedo and Longini 1980; Horner *et al.* 1995; Oldenburg and Macklin 1977), noise cancelling (Adam and Shavit 1990; Al-Zaben and Al-Smadi 2006; Assaleh 2007; Ferrara and Widrow 1982; Khamene and Negahdaripour 2000; Puthusserypady 2007; Widrow *et al.* 1975), and blind source separation (BSS) methods have been applied (Martens *et al.* 2007; Najafabadi *et al.* 2006; Zarzoso and Nandi 2001).

4.1.1. Weighted addition for spatial filtering

This method relies on the idea that a special arrangement of surface electrodes can be used to create a "virtual" electrode that contains a good-quality version of the MECG in the abdominal ECG. This virtual MECG, estimated using a weighted combination of signals from some electrodes, is then subtracted from the abdominal ECG to enhance the FECG (Bergveld and Meijer 1981). Several variations of this perspective have been developed and, depending on the method used to calculate the weighting factors and the virtual MECG, they can be classified as manual and automatic (Adam and Shavit 1990; Bergveld and Meijer 1981; Vanderschoot *et al.* 1987).

In their work, Bergveld *et al.* (1981) mention that in the manual method, the virtual MECG can be created by using a resistor/potentiometer network to combine some leads, by looking for a separate and pure MECG (elsewhere on the mother and similar to the one in the abdominal ECG), or by using the MECG in the abdominal ECG (detected using threshold levels and timing). Conversely, in the automatic method, the "optimal" linear combination is computed according to some criteria such as independence and orthogonality of the measurements, sign,

and number of leads to record the foetal component on the maternal abdomen (Bergveld *et al.* 1986; Bergveld and Meijer 1981). In both cases, however, although the FECG has been enhanced, the methods have failed to completely remove the MECG.

This failure can be explained by considering that the subtraction process assumes that (a) there is a perfect match between the virtual MECG and the MECG in the abdominal ECG and (b) there is a single and fixed linear combination that properly deals with changes in the MECG shape, which is not the case since (a) the morphology of the MECG highly depends on the electrode position and, (b) the signal changes beat-to-beat due to maternal breathing and other movements. In addition, in the absence of a standard electrode configuration, the methods remain highly dependent on the number and location of electrodes (some of them on the abdomen and some on the chest). For example, whilst some authors have proposed that at least four leads might be enough (using only one lead on the abdomen) (Bergveld *et al.* 1986; Bergveld and Meijer 1981), others have suggested that a better separation could be reached using more leads, especially on the maternal abdomen (Vanderschoot *et al.* 1987). In the end, there is a need of having an expert to appropriately place the electrodes and look for good quality signals, which complicates the application in the clinical environment (Adam and Shavit 1990; Bergveld and Meijer 1981).

4.1.2. Template subtraction

This method (Hon 1965), based on signal averaging, was first suggested for FECG enhancement. To work, the method assumes that the two main signals contaminating the FECG in the abdominal ECG, *i.e.* the MECG and the MEMG, can be considered as periodic and random noise sources respectively (Oldenburg and Macklin 1977). Thus, the periodic MECG can be removed from each lead by creating an average maternal waveform (a template), which is subtracted every time the maternal component occurs in the recording. Next, the random MEMG signal is reduced by averaging foetal waveforms and, as a result, the ratio of signal to random noise is increased. However, although the idea seems very simple, all implementations present the same problems (Oldenburg and Macklin 1977): (1) the timing process, used to detect and remove/subtract the MECG, either removes foetal components or keeps maternal information that affects the FECG average; (2) the averaging process, used to reduce the MEMG in the FECG, requires a signal to be triggered (which is usually chosen by visual inspection of the abdominal channel with the highest SNR) and; (3) results are highly dependent on changes of foetal position which, as a result, not only demands continuous examination of the recording, but also limits the SNR improvement by restricting the number of foetal cycles to be averaged.

Variations of the template subtraction method include synchronisation (for detecting and aligning QRS complexes), scaling (for increasing the amount of the MECG suppressed), and matched filtering (for tracking the FECG). The former, implemented by using correlation, improves the maternal QRS detection, but makes the method easily corrupted by high-frequency spikes and high-amplitude noise (Horner *et al.* 1995). Also, as the correlation does not make any difference between a pure maternal QRS and an overlapped foetal-maternal QRS, it is common for the method to cancel the foetal signal as well, causing loss of information that leads to wrong interpretations (Horner *et al.* 1995). The scaling, implemented to adjust the weights for the maternal components to be averaged and create the template (either for the whole MECG (Martens *et al.* 2007) or for each wave component (Vullings *et al.* 2009)), although improving the MECG suppression, still shows difficulties to deal with the variability of the MECG morphology. Finally, the matched filtering method, implemented to recover the FECG, works by creating a filter whose impulse response is the time inverse of the waveform to be detected, *i.e.* the FECG (Azevedo and Longini 1980). However, as the FECG signal shape remains unknown and variable from subject to subject, the generation of a foetal template faces the problems of tracking and matching a signal that is immersed in extremely noisy signals that are also time varying (Azevedo and Longini 1980).

4.1.3. Noise cancelling

Looking for an alternative method for tracking the time varying noise given by the MECG, attention has been paid to noise cancelling, a variation of adaptive filtering that has been considered to be advantageous for removing the MECG from the abdominal ECG. The method, as shown in Figure 4.1, uses two inputs to work, one containing the signal of interest –corrupted by additive noise (*i.e.* the abdominal ECG)–, and another containing a "reference" signal –correlated with the noise that corrupts the signal of interest (*i.e.* a recording of thoracic ECG). Then, the reference signal is adaptively filtered and subtracted from the abdominal ECG to enhance the FECG.

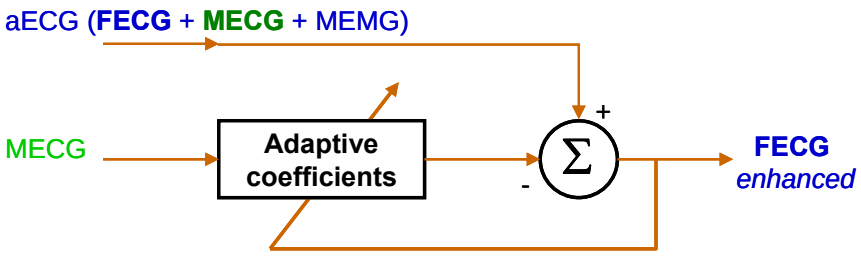

Figure 4.1. Noise cancellation of the MECG in the abdominal ECG for enhancing the FECG.

The scheme, first proposed by Widrow *et al.* (1975), is considered to allow the treatment of signals that are deterministic or stochastic, stationary or time-variable, and shows good performance to remove the MECG from the abdominal ECG to enhance the FECG. However, in the next step, when applied to removing the MEMG, the resulting FECG was considerably distorted by the effects of the LMS adaptive filter (Ferrara and Widrow 1982). These results showed the difficulty of an LMS adaptive filter to track the FECG, a signal that, composed of rapid and recurrent pulses in noise, possesses a high time-varying statistical character (nonstationary) (Adam and Shavit 1990; Ferrara and Widrow 1982).

As an alternative, it was proposed that an adaptive filter that exhibited a rapid and varying impulse response would be suitable for these applications. Such a filter, referred to as a time-sequenced adaptive filter, is an extension of the LMS method and uses multiple sets of adjustable weights to achieve the required impulse response (Adam and Shavit 1990; Ferrara and Widrow 1982). To work, the method considers that, even though the FECG pulse changes its morphology from beat-to-beat, it maintains similar statistical properties. Thus, if the FECG is modelled as a stochastic process, then the pulses could be aligned in time to form an ensemble whose statistical properties can be calculated and, consequently, each set of weights may filter a particular pulse (Ferrara and Widrow 1982). As a result, the method performs better than any time-invariant filter and beat-to-beat "averager". It not only shows a sharper and more accurate estimation of the underlying FECG, but also retains individual variations in pulse shape (Ferrara and Widrow 1982). Its main problem, however, is that it needs good estimates of the foetal pulse locations to synchronise the filter with the foetal heart cycle (Adam and Shavit 1990; Ferrara and Widrow 1982).

Modern versions of the noise cancelling scheme include combinations of singular value decomposition (SVD), H-infinity analysis, and inference systems (for improving the weights adjustment), or time-frequency methods (for reaching a better detection of pulses) (Al-Zaben and Al-Smadi 2006; Assaleh 2007; Callaerts *et al.* 1990; Khamene and Negahdaripour 2000; Puthusserypady 2007). However, although this adaptive scheme has shown enough enhancement of the FECG to measure an average FHR (Pieri *et al.* 2001), the assumption of correlation between signals is not totally correct. As a result, the problem of extracting a good quality FECG (*i.e.* a complete trace suitable for morphological analysis and study of the conduction system in the foetal heart) has not been tackled. In response, some authors have recently proposed that a reliable FECG extraction calls for a complete reformulation of the problem, this by considering an approach that takes into account the fundamental aspects behind the biological problem (Zarzoso and Nandi 2001).

4.1.4. Blind source separation

Recently, it has been proposed that the problem of extracting the FECG can be better formulated by considering the bioelectrical phenomena that controls the heart activity along with the propagation of heartbeat signals across the body (Callaerts *et al.* 1990). In this approach, it is considered that each of the ρ electrodes located on the maternal body, say $\mathbf{x}(t)= [x_1(t), x_2(t),\ldots, x_\rho(t)]^T \in \mathbb{R}^\rho$, records an instantaneous linear mixture of the bioelectric current sources of interest. Assuming that the activity of such bioelectric sources can be modelled by means of ζ unobservable independent source signals, $\mathbf{s}(t)= [s_1(t),s_2(t),\ldots,s_\zeta(t)]^T \in \mathbb{R}^\zeta$, then the measurements from the electrodes can be expressed as

$$\mathbf{x}(t) = \mathbf{A}\ \mathbf{s}(t), \tag{4.1}$$

where **A** is referred to as the *mixing matrix*, whose constant coefficients (1) give the mixing weights and (2) are determined by the body geometry, the electrode/source positions, and the conductivity of the body tissues (Vanderschoot *et al.* 1987). These coefficients are assumed unknown since it is impossible to know the values in **A** without knowing all the properties of the physical mixing system, which can be extremely difficult in general. In addition, since the problem is that it is impossible to record them directly, the source signals are unknown as well, which is what gives the name of blind source separation (BSS) to the problem, the need of finding $\mathbf{s}(t)$ from $\mathbf{x}(t)$, and blind means that very little is known, if anything, about the original sources (Hyvarinen *et al.* 2001; Stone 2004).

The BSS problem is solved by assuming that the mixing matrix is invertible and, consequently, that exists an *unmixing* matrix (**W**) that makes it possible to estimate the sources, $\hat{\mathbf{s}}(t)$, as

$$\hat{\mathbf{s}}(t) = \mathbf{W}\ \mathbf{x}(t). \tag{4.2}$$

Figure 4.2 depicts a schematic representation of the BSS problem. There, the only information available is given by the multivariate data, $\mathbf{x}(t)$, and, from this, the unmixing matrix **W** must be found to make it possible the representation of the sources, $\hat{\mathbf{s}}(t)$. To do this, according to Hyvarinen *et al.* (2001), it is suitable to consider each signal in $\mathbf{x}(t)$ as a sample of a random variable, and use very general statistical properties to find **W** (*i.e.* second-order or higher-order statistics) and, consequently, to estimate the sources underlying $\mathbf{x}(t)$.

Considering the problem of processing the abdominal ECG for foetal surveillance, some authors have proposed that BSS techniques are suitable to tackle the FECG extraction problem by decomposing the abdominal ECG into its underlying sources. Thus, two variations of BSS have been explored by different authors: principal component analysis (PCA) and independent

component analysis (ICA). The former, explored by Vanderschoot *et al.* (1987) and Callaerts *et al.* (1990), relies on the second-order statistics of the data and looks to remove second-order dependencies amongst the observations **x**(*t*). Unfortunately, as the authors pointed at, the main problem of the PCA method is that the quality of the separation strongly depends on the electrode positions, *i.e.* for each subject, the most ideal electrode positions must be found to guarantee that the foetal signals are sufficiently strong in comparison to all other unwanted signals present in the recordings (Callaerts *et al.* 1990; Vanderschoot *et al.* 1987; Zarzoso and Nandi 2001). In contrast, as shown by Zarzoso and Nandi (2001), since ICA exploits higher-order statistics and looks for higher-order independence to estimate the sources (Hyvarinen *et al.* 2001), the outcome is less dependent on the electrode location (Zarzoso and Nandi 2001).

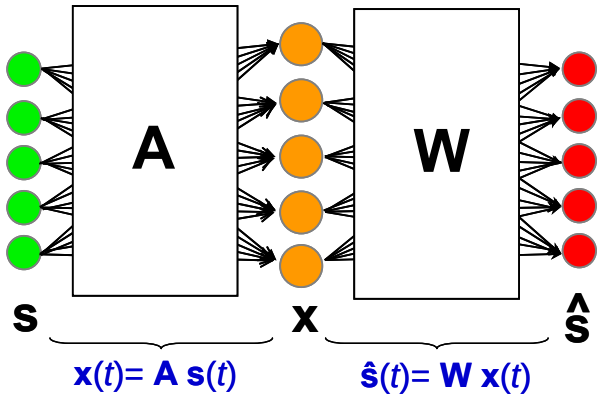

Figure 4.2. Schematic representation of the BSS problem. The measurements at the sensors, **x**(*t*), are assumed to be composed of a linear mixture of the sources, **s**(*t*). **A** represents the unknown mixing matrix and **W** represents the unmixing matrix that must be found in order to estimate the sources **ŝ**(*t*).

Results on real and semi-synthetic data have shown that ICA is suitable for extracting the FECG from the abdominal ECG (Najafabadi *et al.* 2006; Zarzoso and Nandi 2001). Furthermore, Zarzoso and Nandi (2001) showed that ICA performs better than existing non-blind separation methods, and described the quality of the reconstructed FECGs as "notably superior" and less noisy. In addition, this work showed that (1) ICA is robust with respect to electrode position and (2) ICA does not need a thoracic lead (reference) to work since the abdominal signals are enough (Zarzoso and Nandi 2001). However, the authors also reported that (1) ICA computing is time-consuming and therefore hardly suitable for on-line applications (due to the large sample sizes required for higher-order statistical analysis), (2) further research is still necessary to explore the relationship between physiological sources of cardiac activity and the statistically-independent sources that ICA estimates and, according to (Martens *et al.* 2007), (3) under lower SNR conditions, produced between 24 and 32 weeks of gestation, ICA performance experiences a considerable reduction.

In general, it might be said that the main problem with the signal processing methods applied to the abdominal ECG is that they usually impose rigorous requirements such as: a relatively large number of abdominal signals and some form of maternal chest leads as a reference (except in ICA analysis) (Assaleh 2007; Martens *et al.* 2007; Pieri *et al.* 2001; Puthusserypady 2007), a strict and non-standard configuration of electrodes or large time-consuming algorithms (Matonia *et al.* 2006). Also, although different methods have been proposed to improve the SNR, they have met with limited degrees of success that, consequently, make it impossible to reconstruct a reliable and complete FECG trace. Moreover, it has been reported that, from the FECG extracted, the percentage of foetal QRS complexes detected remains lower than 70% (especially between 24 and 32 weeks of gestation, when the SNR is severely degraded because of the insulating effect of the vernix caseosa) (Kahler *et al.* 2002; Lewis 2003; Sato *et al.* 2007; Stinstra and Peters 2002). As a result, valuable foetal well-being information in the abdominal ECG (*e.g.* shape and duration of the P-QRS-T waves, the beat-to-beat heart rate and the presence of arrhythmias) remains unreachable and keeps the technique far away from acceptance into routine clinical practice (Pieri *et al.* 2001).

4.2. Processing the foetal magnetocardiogram

The FMCG records the magnetic field variations occurring over the abdomen of a pregnant woman. The data obtained contain a combination of signals that are mainly due to the electromagnetic activity of both the foetal and the maternal hearts along with uterine activity and, when present, FMs and foetal diaphragmatic activity (Comani *et al.* 2004b; Popescu *et al.* 2007; Popescu *et al.* 2008; Stinstra *et al.* 2002; Zhao and Wakai 2002). Moreover, as the magnetic fields variations remain almost unaffected by the vernix caseosa, the quality of the FMCG between 24 and 32 weeks of gestation is better than the quality of the abdominal ECG during the same period (Stinstra *et al.* 2002). Consequently, the FMCG has made it possible to reconstruct useful foetal traces from where a normal rhythm and conduction abnormalities have been identified (van Leeuwen *et al.* 1999).

The FMCG shows not only morphological and temporal similarities with the FECG, but also the inconvenience that foetal beats may be mainly hidden by the more intense maternal beats. Also, although the quality of the FMCG is better than the quality of the abdominal ECG, the FMCG data may still have a variable SNR, which is a function of the characteristics of the acquisition system (whether it works in a shielded room or not), foetal age, position, and the amount of noise and residual magnetic contamination (Comani *et al.* 2004a). Therefore, as in the abdominal ECG case, the reconstruction of a reliable foetal trace, this time from the FMCG, requires signal processing techniques that safely remove its main noise component, the maternal signal (Comani *et al.* 2004a).

As far as this literature review has gone, and contrary to all expectations, only two signal processing methods to reconstruct the foetal trace from the FMCG were found: template subtraction and ICA. The former, as mentioned in Section 4.1.2, first produces average templates to subtract the MECG and then calculates average foetal beats to reduce the MEMG. The latter, uses higher-order statistics to decompose the FMCG into its underlying components.

This section will not repeat how these methods work and, instead, it will focus on the results produced by using both approaches (chosen depending on the information of interest): either the estimate of an averaged beat or the reconstruction of the time-course of the cardio-electric events during the whole recording (Comani *et al.* 2004b). To do this, the description of the general characteristics of the systems, along with the recording process, and the resulting multi-channel data will be presented.

4.2.1. MCG systems and signal acquisition

Due to technological development of superconducting quantum interference devices (SQUIDs), MCG systems provide both great sensitivity and multichannel recording. In these systems, reduction of environmental noise in the recorded signals is either obtained by applying a strong physical shielding or by using differential measures. As a result, the FMCG systems allow simultaneous recording of good quality bio-magnetic field variations from several positions over either the chest or the abdomen.

At present, authors in the literature have used systems with different numbers of channels and arrangements:

1. Some authors reported a 31 channel SQUID Biomagnetometer (Phillips Medical Systems) with a total diameter of 145 mm, but without further information about the sensors arrangement (Frank *et al.* 2006; Kahler *et al.* 2002). The system, positioned above the foetal heart (using sonographic localisation), recorded signals over 5 minutes using a sampling rate of 1 kHz and a filtering between 0.3 and 500 Hz. In addition, the maternal ECG was simultaneously recorded. As a result, Frank *et al.* (2006) reported a study where 39 out of 129 recordings (recorded from 1999 to 2003 with gestational ages between 35 and 40 weeks) were analysed, whereas an alternative study by Kahler *et al.* (2002) reported that a total of 163 recordings (between 19 and 42 weeks of gestational age) were used.

2. Lowery *et al.* (2003) have reported the design of a system dedicated to reproductive assessment called SARA (CTF Systems Inc, Port Coquitlam, Canada). This SARA system is specifically dedicated to foetal monitoring during gestation and composed of 151 channels arranged on a curved surface that matches the abdomen shape. In addition, and contrary to other systems, where the mother lies in a supine position; in

the SARA system the mother sits and leans forward against the array surface. Data recording was performed on 39 pregnant women at different gestational ages (from weeks 27 to 39) producing a total of 102 sets. The signals, recorded between 6 and 12 minutes with a sampling rate of 312.5 Hz, were de-noised using information from some sensors and then high-pass filtered with a cut-off frequency of 0.35 Hz (the reasons for using these parameters were not provided by the authors).

3. Other authors have reported multicentre studies using systems with 19, 31, 32, 37, and 67 channels where data was generally sampled at 1 kHz (Stinstra *et al.* 2002; van Leeuwen *et al.* 1999; van Leeuwen *et al.* 2004).

4. Horigome *et al.* (2001) used a nine-channel SQUID system where the sensors were allocated using a square arrangement as detailed by Tsukada *et al.* (1995). The system, positioned above the foetal heart after sonographic localisation, records signals at 1 kHz sampling rate and band-pass filters them from 0.1 and 100 Hz. Data were recorded from a total of 95 foetuses with gestational ages between 20 and 40 weeks, 88 without maternal or foetal complications and the rest with foetal cardiomegalia (an abnormal enlargement of the heart).

5. Comani *et al.* (2004b) have reported a system composed of 77 channels arranged in a honeycomb grid of 230 mm diameter. In this system, 55 magnetometers are used for measuring, whilst the rest are used for residual noise reduction. Besides, as the system can be configured to record a different number of channels (*e.g.* 7, 12, 22 channels), it is possible to change the spatial resolution. Data recording was performed for each volunteer at different gestational ages (from week 22 to delivery) producing a total of 61 sets. The MCG system was positioned after the foetal heart position was established by mode-2D pulsed colour Doppler echocardiogram (used as well to evaluate the foetal heart condition). The signals, recorded during five minutes using a sampling rate of 10 kHz, are filtered from 0.016 to 250 Hz and decimated by a factor of 10 (to reduce the amount of data). In this way, the system generates fifty five signals with a sampling frequency of 1 kHz.

6. Popescu *et al.* (2007, 2008) have reported a system with 83 channels, in a spherical array, that completely covers the maternal abdomen whilst the mother sits on the scanner chair. Data from two foetuses (after positioning the system by using ultrasound information) were acquired in blocks of two minutes at a sampling rate of 1.2 kHz, and a band-pass filter between 0.5 and 300 Hz.

4.2.2. Extraction of foetal signals and further analysis

In general, although the sets of recordings described in the previous section were produced by different protocols, the signal analysis was performed using either template subtraction or ICA. The former was used to process those sets described in points 1, 2, 3, and 4 (Frank *et al.* 2006; Horigome *et al.* 2001; Kahler *et al.* 2002; Lowery *et al.* 2003; Stinstra *et al.* 2002; van Leeuwen 2004; van Leeuwen *et al.* 2009), whereas the latter was used to process those signals described in points 5 and 6 (Comani *et al.* 2004b; Popescu *et al.* 2007; Popescu *et al.* 2008).

a) **Template subtraction** was used to remove the maternal component from the signals by linearly subtracting a template. Such a template was calculated by averaging maternal cycles from (1) each channel in the datasets recorded by Frank *et al.* (2006), Kahler *et al.* (2002), and Horigome *et al.* (2001), (2) probably each channel (although not clearly specified) recorded by Lowery *et al.* (2003), and (3) the channels closer to the maternal heart in the sets recorded by Stintra *et al.* (2002) and van Leeuween *et al.* (1999). Next, the template was used to find the maternal beats in the channels of interest, adjusted, and subtracted to enhance the foetal components. After that, the foetal QRS complexes were detected to:

1. *Calculate the beat-to-beat intervals* in order to (a) automatically identify foetal states (Frank *et al.* 2006), or (b) semi-automatically identify foetal arrhythmias (van Leeuwen *et al.* 1999).

2. *Trigger an averaging process* whose resulting foetal patterns were used to (a) calculate a dipole and search for cardiac hypertrophy (Horigome *et al.* 2001), or (b) verify the existence of P-wave, QRS complex, and T-wave. From these waves, whenever possible, the P-wave, QRS, and T-wave duration as well as PR, PQ, QT, and ST intervals were quantified at different gestational ages (Kahler *et al.* 2002; Lowery *et al.* 2003; Stinstra *et al.* 2002; van Leeuwen 2004).

b) **ICA** was used to decompose the FMCG into its underlying components by considering (a) channels grouped in clusters (according to either the spatial distribution or the intensity of the signals recorded by Comani *et al.* (2004b)), or (b) the whole set obtained by Popescu *et al.* (2007, 2008). In the experiment described by Comani *et al.* (2004b), from each cluster, long, stable (*i.e.* with very low drift from the base-line) and simultaneous segments were chosen, filtered (from 0.4 to 150 Hz), and decimated.

The datasets were processed using different implementations of ICA in order to find independent components that were then used to (a) reconstruct the whole foetal trace (even though a high percentage of those foetal complexes was hidden by the maternal complexes) (Comani *et al.* 2005c; Comani *et al.* 2004a; Comani *et al.* 2004b), detect waveforms,

measure duration and intervals (Comani and Alleva 2007; Comani *et al.* 2005a; Comani *et al.* 2005b; Mantini *et al.* 2005); or (b) reconstruct diaphragmatic activity related to hiccup or sucking (Popescu *et al.* 2007; Popescu *et al.* 2008).

As can be seen, the FMCG analysis has not gone through as many signal processing schemes as the abdominal ECG has gone. This could be because of the higher quality and quantity of the signals that can be obtained during the study. As a result, template subtraction seems to offer a suitable processing method to study features on preselected and averaged data. Conversely, if spatial resolution and time-course analysis are important, then ICA shows good performance. The problem, besides the costs, is that further research needs to be done to properly exploit the power of both, the recording method and ICA. More specific, from the point of view of this review, it is still necessary to establish standard protocols for (1) data recording (*e.g.* number and configuration of sensors), (2) interpretation of extracted sources (*e.g.* foetal, maternal or environmental) (Zarzoso and Nandi 2001), and (3) selection of sources of interest and thus extraction of information to effectively perform foetal surveillance (*e.g.* diaphragmatic activity, temporal and morphological characteristics of the foetal trace like the shape and duration of P-QRS-T waves, beat-to-beat heart rate, and presence of arrhythmias).

4.3. Processing the abdominal phonogram

The abdominal phonogram, recorded by placing an acoustic sensor on the maternal abdomen, carries valuable information about physiological parameters such as FHS, FMs, FBMs, and heart cycle timing (*e.g.* FHR, systolic and diastolic intervals) (Colley *et al.* 1986; Goovaerts *et al.* 1989a; Goovaerts *et al.* 1989b; Holburn and Rowsell 1989; Moghavvemi *et al.* 2003; Zuckerwar *et al.* 1993). Nevertheless, because of the acoustic damping in the maternal tissues, the foetal information in the abdominal phonogram has a low acoustic energy that is easily disturbed by external sources from the environment (*e.g.* speech), biological sources from the mother (*e.g.* placental blood flow, digestive activity, aortic pressure wave, maternal breathing, heart and respiratory sounds), and artifactual sources produced by small movements of the transducer (Holburn and Rowsell 1989; Varady *et al.* 2003; Zuckerwar *et al.* 1993). All these noises may bury the foetal information and therefore make it hard to extract reliable information about foetal activity. The maternal pressure wave (formerly referred to as aortic pressure wave), as mentioned in Chapter 3, is constantly present and may reach an intensity that has been reported to be least 60 dB larger than the intensity of the foetal information (with a broad spectrum centred between 8 and 15 Hz) (Zuckerwar *et al.* 1993).

Traditionally, and contrary to the strategy followed when analysing the abdominal ECG and FMCG, where multiple signals are simultaneously digitised and then processed to

reconstruct foetal traces, the abdominal phonogram is first filtered in the time-continuous domain –to separate either FHS or FBMs– and then digitised (Bassil and Dripps 1989; Goovaerts *et al.* 1989a; Holburn and Rowsell 1989; Talbert *et al.* 1986). This strategy, along with sensors especially designed, aims to separate FHS from FBMs and gives the possibility of independent scaling for each signal, which is important since their amplitudes differ at least by one order of magnitude (*i.e.* FHS typically cause maternal abdominal displacements between 5 and 10 μm, whereas FBMs cause displacements in the order of 100 μm) (Ansourian *et al.* 1993; Holburn and Rowsell 1989). After that, some analyses have been implemented to find general patterns, distinctive features (*e.g.* acoustic signature, frequency spectrum, and amplitude of FHS) (Zuckerwar *et al.* 1993), or to measure heart and breathing rates (Ansourian *et al.* 1993; Bassil and Dripps 1989; Goovaerts *et al.* 1989a; Holburn and Rowsell 1989; Talbert *et al.* 1986; Zuckerwar *et al.* 1993).

a) **Detection of general patterns:** Former analyses used to look for profiles of the major cardiorespiratory and movement patterns over long time periods. To this end, FIR filters with an order of 128 taps and a bandwidth between 0.5 and 2 Hz for breathing patterns (Goovaerts *et al.* 1989a; Goovaerts *et al.* 1989b) or between 50 and 100 Hz (sometimes between 50 and 200 Hz) for FHS (Moghavvemi *et al.* 2003; Talbert *et al.* 1986; Zuckerwar *et al.* 1993) have been used.

b) **Extraction of distinctive features:** It has been focused on the FHS. To do this, a set of good quality heart sounds HS (*i.e.* free of artefacts) was manually chosen and averaged to generate a template whose temporal and frequency features were calculated (Zuckerwar *et al.* 1993).

c) **Rate measurements:** It is performed by measuring distances from (a) consecutive events in the whole recording to produce beat-to-beat measurements from the FHS, or (b) available events in a segment to produce average measurements from the FHS or FBMs. In particular, as they are present during the whole recording, the detection of the events corresponding to FHS have received more attention giving rise to methods based on template matching (Holburn and Rowsell 1989), smoothing in one (Bassil and Dripps 1989) or two frequency bands (Kovacs *et al.* 2000), and cross- or auto- correlation.

It can be seen that there have been efforts to develop methods for foetal well-being based on the detection of FHS or FBMs by filtering the abdominal phonogram. Unfortunately, although the idea may sound easy to implement because the signals cover different frequency bands, it is important to highlight that this deterministic filtering does not necessary remove the noise caused by the environment, the mother or the transducer movement. Thus, the SNR remains very low and, although recent methods have included time-frequency analysis (Jimenez

et al. 2001) and/or adaptive noise cancellation (Varady *et al.* 2003), or highly deterministic criteria (Kovacs *et al.* 2000), it may be still difficult to detect FBMs or FHS and therefore to collect reliable information for surveillance purposes (*e.g.* temporal and morphological characteristics of the foetal breathing movements or the main heart sounds like breathing rate, beat-to-beat heart rate, presence of arrhythmias, and acoustic signatures).

4.4. A novel approach for antenatal surveillance

So far, this chapter has discussed different approaches reported in the literature for extracting foetal information from the abdominal ECG, FMCG, and abdominal phonogram. As noticed, although different methodologies have been explored, the extraction of entire traces –from where temporal and morphological characteristics can be collected to effectively perform foetal surveillance– remains an unsolved problem. In the case of the abdominal ECG, the spectral overlap between maternal and foetal cardiac information –as well as the presence of the vernix caseosa– have made it impossible to recover complete traces of the FECG. As a result, only average values of FHR have been obtained. In the case of the FMCG, although entire traces have been separated by ICA, further research needs to be done to better exploit the advantages of the recording process and ICA. Additionally, and very important in practical terms, is the high cost involved in recording and analysis of FMCG data, which results in prohibitively expensive systems for clinical applications. Finally, the case of the abdominal phonogram, a signal that, although has two essential advantages over the former two (*i.e.* the maternal and foetal cardiac activities do not spectrally overlap as in the former two signals and the recording can be performed using a single-channel configuration), has not been successfully processed to retrieve entire traces of the FHS (*i.e.* the foetal phonocardiogram, FPCG) and/or FBMs.

The research presented in this thesis has paid attention to the problem of extracting information for antenatal surveillance by means of the abdominal phonogram. In this context, this work believes that the methods used so far have been erroneously focused only on the recording/extraction of one source (either FHS or FBMs) and thus generally rely on rigid empirical criteria and/or more than one channel to extract pre-selected information. Hence, once a method has been adjusted according to specific criteria (*i.e.* fixed filters bandwidth), any significant change in the SNR, produced by either the recording conditions or the maternal/foetal behaviour, might not be properly managed by the method. Furthermore, because of the interest in specific foetal information, there might be some extra and valuable foetal/maternal information that is irreversibly discarded such as maternal heart and respiratory rates, for instance.

Some studies have shown some improvement in the SNR of the signals (Goovaerts *et al.* 1989a; Jimenez *et al.* 1999; Kovacs *et al.* 2000; Varady *et al.* 2003), but the extraction of entire traces containing the FBMs or FHS may still be difficult (and therefore the calculation of the beat-to-beat heart rate and the detection of arrhythmias, for instance), and it is clear that the solution requires not only sophisticated signal processing methods, but also a complete different signal processing perspective for the abdominal phonogram. This signal processing perspective, instead of searching for a pre-selected component, should take advantage of the abundance of information in the abdominal phonogram and separate all its components. Thus, by applying a data-dependent analysis, and using only the temporal information present in a single-channel recording, the method should decompose the phonogram into its underlying components. Such a signal processing perspective, referred to and studied as Single Channel Independent Component Analysis (SCICA) by Davies and James (2007), uses higher-order statistics for separation purposes, which makes it more robust than methods based on second-order statistics like PCA or SVD. Hence, SCICA has been successfully applied to biomedical signals such as EEG (James *et al.* 2006; James and Lowe 2000) and MEG (James and Lowe 2001; Woon and Lowe 2004), but never to the abdominal phonogram.

Therefore, in the aim of contributing towards the development of alternatives for antenatal foetal surveillance, the research presented in this thesis studies, for the first time, a methodology based on this single-channel approach for extracting sources contained in noisy abdominal phonograms. Such sources, retrieved as entire traces, should make it possible to collect temporal and morphological characteristics to perform foetal surveillance that, in this work, will be given the beat-to-beat heart rate and the acoustic signature of the FHS (the former, as previously mentioned, drops during the stress of hypoxemia, the latter, as mentioned by Zuckerward *et al.* (1999), reflects the state of the heart valves). To this end, and to make it clear how complex the extraction problem is, a further description of the recording setup and the available dataset will be presented in Chapter 5. After that, Chapter 6 will focus on the fundamentals of SCICA and the decomposition of the abdominal phonogram into its underlying sources.

4.5. Summary

This chapter discussed some approaches reported in the literature to process the abdominal ECG, the FMCG, and the abdominal phonogram in order to extract foetal information. So far, some reconstruction of foetal information has been possible (*i.e.* the average FHR), though there is still some valuable temporal and morphological information that remains inaccessible (*e.g.* beat-to-beat heart rate and typical shapes of the component waves) and whose access would definitely improve the quality of antenatal surveillance.

In general, the abdominal ECG and FMCG techniques are mainly characterised by multi-channel recordings and empirical/rigid processing methods that usually discard valuable information. In addition, they may result expensive due to time-consuming signal processing algorithms, need of trained personal or high-cost consumables. The abdominal phonogram, on the other hand, is easily recorded by using a single-channel configuration and rich in information about foetal activity. Most importantly, the spectral overlapping of foetal and maternal cardiac activities in the abdominal phonogram is not as significant as in the abdominal ECG and FMCG, which is an important advantage. Unfortunately, the resulting signal is usually affected by several interferences and, at present, it is still difficult to extract reliable foetal information by applying signal processing methods usually based on rigid and empirical criteria that discard valuable information.

As an alternative, this work proposes that a different signal processing perspective, which exploits the richness of information in the abdominal phonogram, will provide better results. Thus, by applying a data-dependent analysis perspective given by SCICA, it would be feasible to separate the sources underlying the abdominal phonogram as entire traces from where the beat-to-beat heart rate and the acoustic signature of the FHS will be collected. This SCICA perspective will be discussed in Chapter 6 after a detailed description of the setup and the available dataset is presented in Chapter 5.

5 THE DATASET FOR ANTENATAL SURVEILLANCE

Previous chapters have introduced the problem of obtaining suitable information for antenatal foetal surveillance by non-invasive means. As mentioned, although different signals and processing methods have been explored over the last decades, they have only partially succeeded in doing so and, although an average FHR has been obtained, some temporal and morphological information that could reinforce foetal assessment (*i.e.* beat-to-beat heart rate and shapes of the component waves) remains unreachable. In particular, since it is easily recorded and rich in information about foetal activity, the research presented in this thesis focused on a signal referred to as the abdominal phonogram. However, since the energy of the foetal components in the abdominal phonogram is very low and easily hidden by other sources, their extraction is a challenging task.

This chapter describes the process to record the signals used in this work and, to illustrate how difficult the extraction of foetal information from the abdominal phonograms can be, depicts some examples of the signal to analyse.

5.1. The process for data recording

The dataset for this research was recorded as detailed in the next two sections.

5.1.1. The recording setup

The recording setup, as shown in Figure 5.1, simultaneously recorded five signals corresponding to the abdominal phonogram, the abdominal ECG, the FBM, the FMs, and the maternal breathing (*i.e.* here referred to as the maternal respirogram) respectively (Ortiz-Pedroza 2007). The former, as previously mentioned, is the signal of interest in this research and will be analysed by SCICA in the next chapters. The other signals, as detailed in Chapter 10, will serve as “gold-standard” signals for evaluating the quality of the information extracted

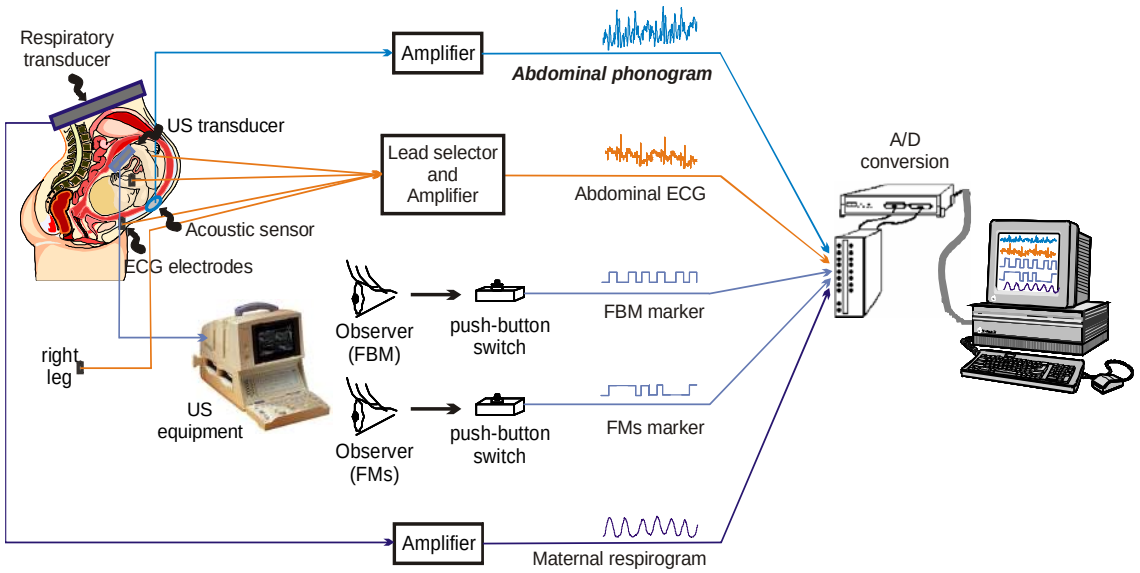

Figure 5.1. Setup used for antenatal recording of the single-channel abdominal phonogram and four gold-standard signals (*i.e.* the abdominal ECG, the FBM marker, the FMs marker, and the maternal respirogram). The transducers for the first four signals were located on the maternal womb and the transducer for the maternal respirogram was located on the maternal chest. The signals were digitised at 500 Hz, displayed on a computer screen, and saved for further processing (Ortiz-Pedroza 2007).

by SCICA from the abdominal phonogram, especially the abdominal ECG, which will provide (1) a temporal reference to identify maternal and cardiac signals in Chapter 9 and (b) a reference beat-to-beat heart rate in Chapter 10. Here, further details on the recording setup are described:

a) **Abdominal phonogram:** This signal was recorded using a single PCG piezoelectric transducer (TK-701T, Nihon Kohden™) connected to a general purpose amplifier (DA100, Biopac Systems™). The transducer was positioned on the maternal abdomen close over the foetal heart, which was located by using ultrasound imaging (SSA-320A, Toshiba™ with a transducer of 3.5 MHz).

b) **Abdominal ECG:** This signal was recorded using four plate electrodes, three plates were placed on the maternal womb to form an equilateral triangle (between 20 and 25 cm side) as in Figure 5.2, whereas the fourth plate (*i.e.* the voltage-reference electrode) was placed on the right leg, close to the ankle. The electrodes were connected to a lead selector-ECG (PB-640G, Nihon Kohden™) to produce a one-lead abdominal ECG that was then provided to an instrumentation amplifier (AB-621G, Nihon Kohden™) for conditioning purposes (*i.e.* amplification and filtering).

The selection of the one-lead abdominal ECG to be recorded was performed by manually switching the lead selector (to combine the signals from the electrodes on the maternal womb each time) and looking at the resulting signal at the output of the amplifier. Thus, the "best" lead was chosen as the signal where the foetal QRS complexes were more evident.

Next, the amplifier gain and cut-off frequencies were carefully adjusted to visually improve the quality of the signal by reducing the effect of low- and high-frequency interferences.

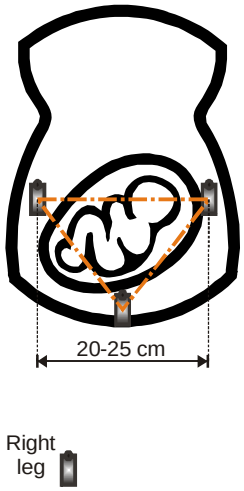

Figure 5.2. Location of the electrodes used to record the abdominal ECG. Three electrodes were positioned on the maternal womb to form an equilateral triangle whilst the voltage-reference electrode was positioned on the right leg.

c) FBM and FMs: The signals corresponding to these movements were produced by two observers watching foetal images, each one controlling a push-button switch that was pressed whenever such movements were spotted in US images. The images, produced by the ultrasound equipment previously mentioned, were simultaneously presented to the observers in M-mode and B-mode to make it possible for one observer focusing on detecting FBM whilst the other observer focused on detecting FMs.

Clearly, the transducer location and orientation were fundamental to produce images from where the foetal movements were detected by the observers (as needed for the work developed by Ortiz-Pedroza (2007)). To this end, the transducer was positioned on the maternal abdomen and oriented to produce a frontal view of the foetus (formally referred to as sagittal view in medical terms) such that (1) the thorax, diaphragm and/or abdomen, and inferior limbs were evident in the B-mode image and (2) any thoracic or abdominal displacement corresponding to the FBM were observed as oscillations in the M-mode image. Figure 5.3 shows the US equipment used in this work and the images obtained by a medical doctor from a foetus at a gestational age of 38 weeks. In (a), the transducer positioned on the maternal abdomen and the electrodes for abdominal ECG, in (b), the images presented to the observers. Notice that, in (b), the B-mode image illustrates the cardiac cavity, the diaphragm, and the inferior limbs, whereas the M-mode image depicts the oscillations produced by the abdominal movements when the FBM appeared.

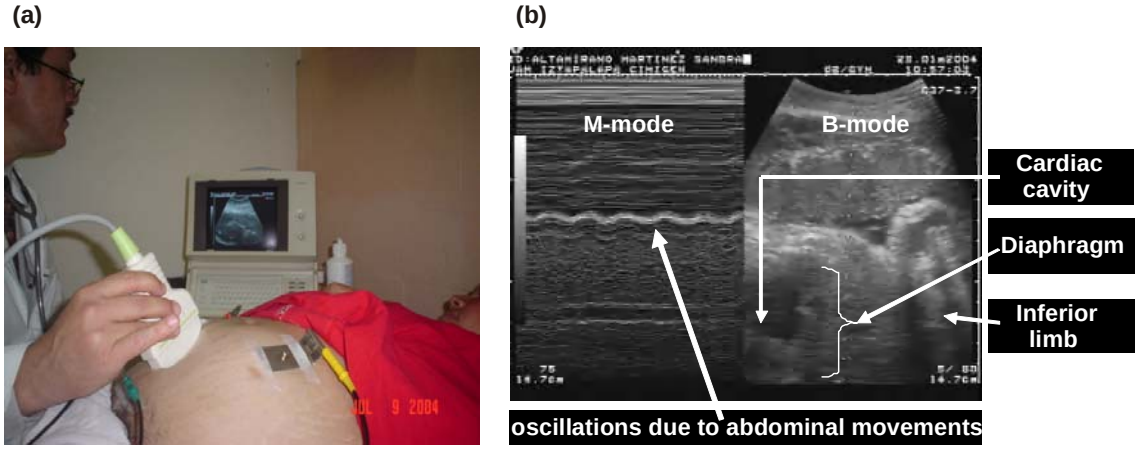

Figure 5.3. US equipment used to detect foetal movements and the abdominal sagittal view of a foetus at a gestational age of 38 weeks. (a) the transducer positioned on the maternal abdomen and the electrodes for abdominal ECG and (b) the images presented to the observers. The B-mode image illustrates the cardiac cavity, the diaphragm, and the inferior limbs whilst the M-mode image depicts the oscillations produced by the abdominal movements when the FBM appeared (Ortiz-Pedroza 2007).

The push-button switches were designed to produce a 5 V signal while pressed and 0 V otherwise. Hence, the FMs observer was instructed to look at the B-mode image, keep the push-button pressed while such movements were present, and release it when they disappeared. The FBM observer, on the other hand, was instructed to look at the M-mode image and to press and release the push-button according to the oscillations in the image.

d) Maternal respirogram: This signal was recorded using a respiratory effort transducer (TSD101B, Biopac Systems™) connected to a respiratory amplifier (RSP100B, Biopac Systems™). The transducer was positioned around the maternal chest.

5.1.2. The facilities and recording staff

The recording setup was installed in a room at the Centro de Investigación Materno Infantil Gen[1] (CIMI-Gen), a clinic that works based on an alternative and low-cost model to improve the quality of the perinatal health services. The room, normally used for ultrasonographic studies, but without any electric or acoustic isolation, was approximately 6 m length and 4 m width. There, once the pregnant woman agreed to participate in the study, the recording procedure was implemented by two medical doctors and an engineer, MD Ramón González-Camarena[2], MD

[1] Created in 1987 by the Asociación Hispano Mexicana I.A.P and located at Av. Tláhuac No. 160, Col. Lomas Estrella, C.P. 09890, Delegación Iztapalapa, México City, México.

[2] Department of Health Sciences, Faculty of Biological Sciences and Health, Universidad Autónoma Metropolitana-Iztapalapa. Av. San Rafael Atlixco No. 186, Col Vicentina, C.P. 09340, Del. Iztapalapa, México City, México.

Alfonso Martínez-Ortiz[3], and Dr. Rocio Ortiz-Pedroza[3].

5.2. The recorded signals

The dataset for this work was obtained from 18 pregnant women (24 ± 3 years old) –with foetal gestational ages ranging between 29 and 40 weeks and low to middle risk factors– who provided their informed consent to participate in the study. The signals, digitised at a sampling frequency of 500 Hz during three or five minutes (MP100 module and Acqknowledge software, Biopac Systems™), were transmitted to a computer and saved for further processing.

Table 5.1 shows the gestational age distribution in the dataset recorded for this work. There, it is important to notice that the number of recordings at weeks 33, 36, 37, and 40 are larger than the number of subjects recorded, which means that some recordings were taken from the same subject. Such extra recordings, according to the recording staff, were obtained whenever a burst of foetal movements appeared at the end of a recording that was free (or almost free) of them. This made it possible be certain that foetal movements were present in some recordings and gave rise to a dataset containing a total of 25 recordings, each one composed of the abdominal phonogram and the gold-standard signals (at least three of them as shown in Table 5.2).

Table 5.1. Distribution of the gestational age in the dataset.

Gestational age	Number of recordings*	Number of subjects recorded
29	1	1
33	2	1
34	2	2
36	10	7
37	2	1
38	4	4
39	1	1
40	3	1
TOTAL	**25**	**18**

* Some recordings were recorded from the same subject in the same session.

[3] Department of Electrical Engineering, Faculty of Basic Science and Engineering, Universidad Autónoma Metropolitana-Iztapalapa. Av. San Rafael Atlixco No. 186, Col Vicentina, C.P. 09340, Del. Iztapalapa, México City, México.

Table 5.2. Set of gold-standard signals simultaneously recorded with the abdominal phonogram.

Recording ID	Gestational age (weeks)	Abdominal ECG	FBM	FMs	Maternal respirogram	Recording length (min)
1	40	√	√	√	√	5
2	36	√	√	√	√	5
3	38	√	√	√	√	3
4	37	--	√	√	↯	5
5	36	√	√	√	√	5
6	36	√	√	√	√	3
7	36	√	√	√	√	3
8	36	--	√	√	↯	5
9	38	--	√	√	↯	3
10	36	√	√	√	√	3
11	38	--	√	√	↯	3
12	34	--	√	√	√	3
13	38	--	√	√	↯	3
14	40	√	√	√	√	5
15	40	√	√	√	√	5
16	36	√	√	√	√	5
17	36	√	√	√	√	5
18	33	√	√	√	√	5
19	36	--	√	√	↯	3
20	36	√	√	√	√	3
21	29	--	√	√	↯	3
22	33	√	√	√	√	5
23	34	√	√	√	√	5
24	37	--	√	√	↯	5
25	39	--	√	√	↯	5

* √ indicates that the signal was properly recorded, ↯ indicates that the signal presents quantisation problems, and -- indicates that the signal was not recorded at all.

Here it is important to highlight that, for unknown reasons, it was impossible to observe the foetal QRS complexes in the abdominal ECG in some subjects. This problem rendered the

abdominal ECG useless as a gold-standard and therefore left the signal out of the recording process. As a result, as shown in Table 5.2, the set of gold-standard signals in some subjects is composed of three instead of four signals.

Figure 5.4 illustrates the time (left-hand side) and frequency (right-hand side) representations of some abdominal phonograms recorded at different gestational ages. The frequency representation, or power spectral density (PSD), was estimated using the Welch's method with a Hanning window of 32 coefficients in length and an overlap of 50% (to produce a smoothed PSD). From top to bottom, signals at (a) 29 weeks, (b) 33 weeks, (c) 34 weeks, (d) 36 weeks, (e) 37 weeks, (f) 38 weeks, (g) 39 weeks, and (h) 40 weeks. In the time domain, three characteristics are visually evident in the signals: (1) they present different levels of noise, although all of them are very noisy, (2) they show a slow component whose large amplitude is more obvious in (c), (e), and (g), and (3) they also show some quasiperiodic peaks (the most evident are indicated by arrows), which are clearer in (b), (d), and (e). In the frequency domain, it can be seen that the power of the signals ranges from 0 to 250 Hz with the main content below 100 Hz (> -50 dB), although (b) and (f) show also some large power after 200 Hz. As can be seen in the signals, the problem is that in most instances the FHS are not immediately evident, at least in these representations.

Alternatively, Figure 5.5 depicts the time-frequency representation of the abdominal phonogram in Figure 5.4 (h). Such a representation, *i.e.* the spectrogram, was calculated using a Short-Time Fourier Transform with a Hanning window, 128 coefficients in length, and an overlap of 120 samples. The red parts show that most of the signal power is below 100 Hz (especially below ~10 Hz), which confirms the observations in the previous paragraph. Additionally, further observation of the section below 100 Hz seems to show three types of signals, one below ~10 Hz and constantly present, one between 10 and 50 Hz (although the boundaries are not very clear sometimes) that appears at about three times per second (as indicated by the downward arrows), and one at about 60 Hz and constantly present as well.

Since the purpose of this section is only to illustrate how the abdominal phonogram in the dataset looks, not further discussion about the origin of information in Figure 5.4 and Figure 5.5 will be presented until further analysis is performed. Such an analysis will be described in the next chapters, where the challenge of separating the components underlying the abdominal phonogram will be tackled by SCICA. Thus, since the recording procedure has been described, and the of noisy abdominal phonogram has been illustrated, the next chapter can focus on the description and implementation of SCICA as an approach to separate the abdominal phonogram into its underlying components, *e.g.* foetal, maternal, and noise.

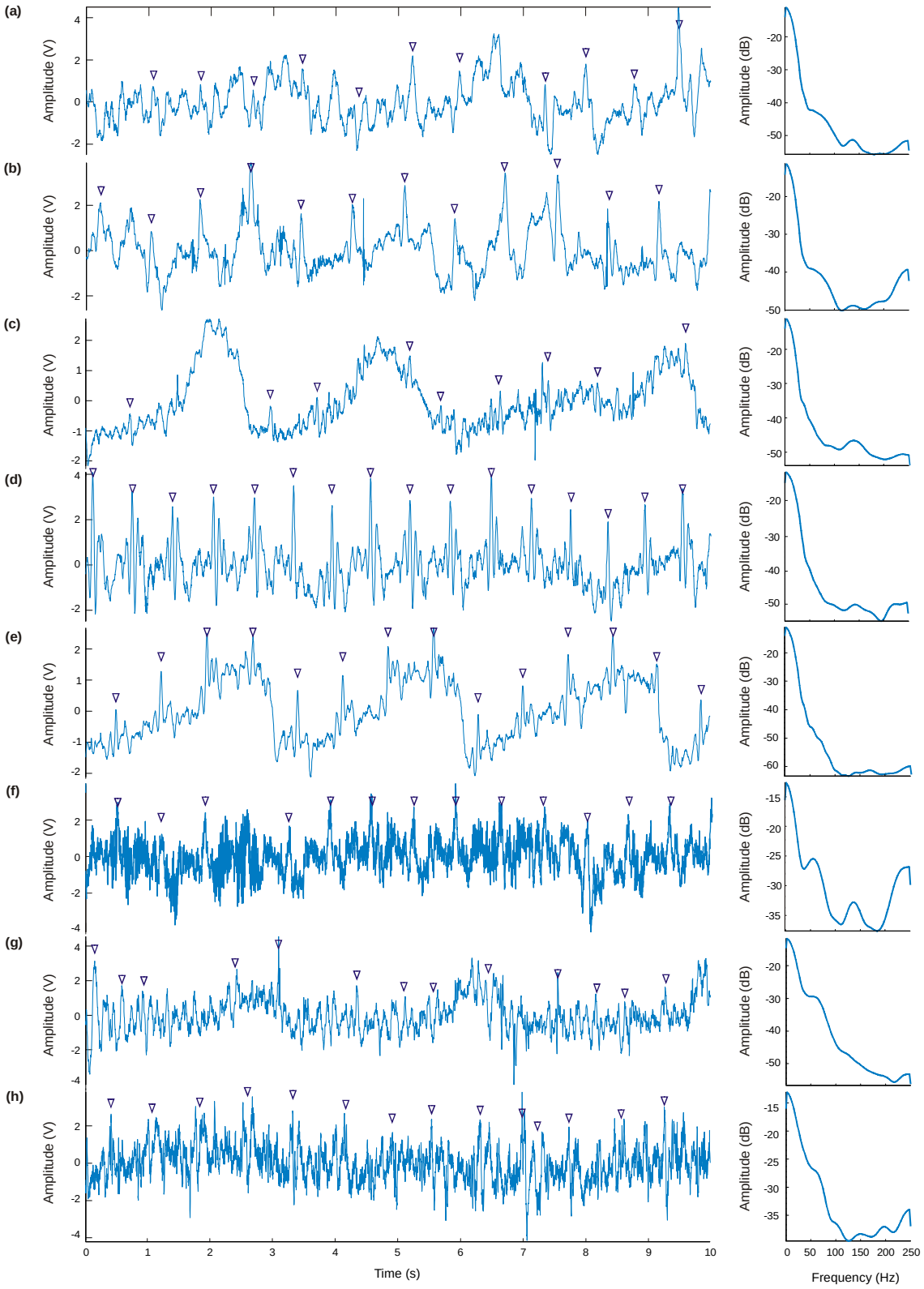

Figure 5.4. Time (left-hand side) and frequency (right-hand side) representations of abdominal phonograms recorded at different gestational ages: (a) 29 weeks, (b) 33 weeks, (c) 34 weeks, (d) 36 weeks, (e) 37 weeks, (f) 38 weeks, (g) 39 weeks, and (h) 40 weeks. As noticed, although the signals may clearly show a slow component along with some quasiperiodic peaks (indicated by downward arrows), there is not a clear evidence of the FHS. The origin of such components will be discussed in the next chapters after further analysis of the signals is performed.

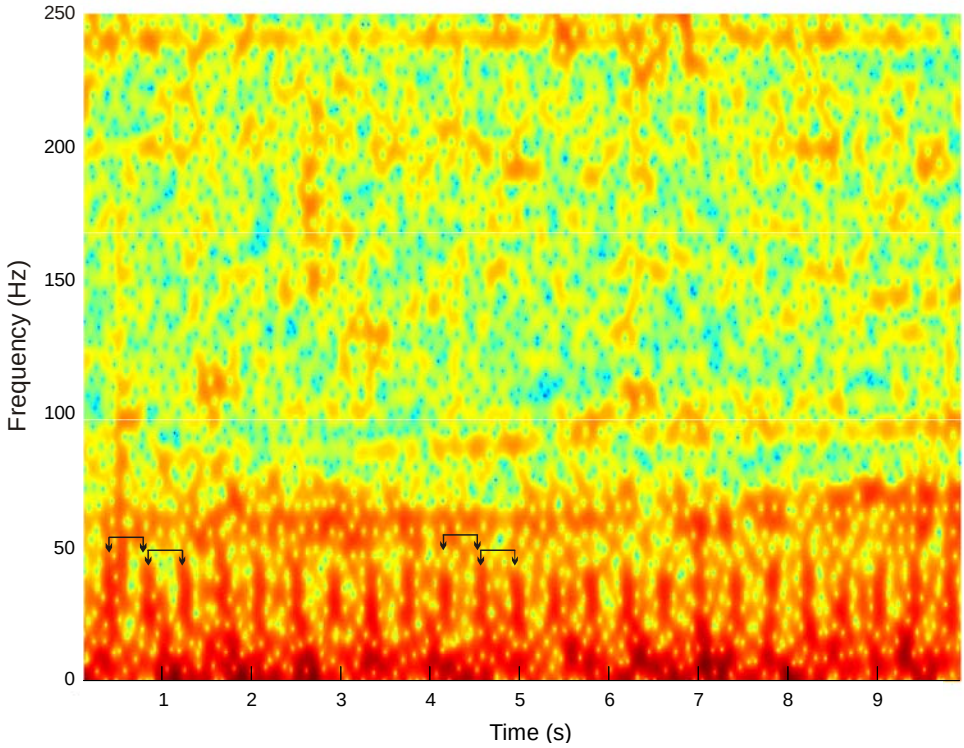

Figure 5.5. Spectrogram of an abdominal phonogram. The red colour indicates the sections were the main power of the signal is present. The downward arrows indicate that there is some information between 10 and 50 Hz (approximately) that appears at about three times per second. Conversely, there is some information below 10 and around 60 Hz that is present almost all the time. The origin of such components will be discussed in the next chapters after further analysis of the signals is performed.

5.3. Summary

This chapter described the procedure used to record the dataset used in this work and illustrated the concept of noisy abdominal phonogram (where the FHS are not immediately evident). The dataset of 25 recordings, each composed of the abdominal phonogram and four gold-standard signals, was recorded at gestational ages ranging between 29 and 40 weeks (between 3 and 5 minutes in length). The next step is to apply a signal processing alternative suitable to recover foetal information from such noisy single-channel signals. This is done in Chapter 6, where SCICA is introduced and used to process the noisy abdominal phonograms used in this work.

6 AN ALTERNATIVE SIGNAL PROCESSING APPROACH FOR ABDOMINAL PHONOGRAM RECORDINGS

Chapter 4 discussed signal processing methods used to extract information for foetal surveillance from the abdominal ECG, the FMCG, and the abdominal phonogram. As mentioned, the abdominal ECG and FMCG (both characterised by multi-channel recordings and temporarily spectral overlapping between foetal and maternal cardiac signals) have been traditionally analysed using signal processing methods that have managed to recover foetal traces from these signals (up to 70% of foetal QRS traces from the abdominal ECG and almost 100% from the FMCG (Kahler *et al.* 2002; Lewis 2003; Pieri *et al.* 2001)). However, these signals are barely considered in routine clinical practice because (a) the SNR in the abdominal ECG is highly dependent on the gestational age (*i.e.* becomes considerably reduced between 24 and 32 weeks of gestation due to the vernix caseosa) and (b) the FMCG is an expensive tool for a clinical environment since it needs trained personal and high-cost facilities/consumables.

The abdominal phonogram, on the other hand, is a signal that conveys abundant information about foetal activity in a single-channel recording. Most importantly, the spectral overlapping of foetal and maternal cardiac activities in the abdominal phonogram is not as significant as in the abdominal ECG and FMCG, which makes it a promising signal for clinical applications (Jimenez-Gonzalez and James 2008a; Jimenez-Gonzalez and James 2008b; Jiménez-González and James 2009). Unfortunately, as discussed in previous chapters, the acoustic energy of the foetal activity in the abdominal phonogram is so low that it becomes easily hidden by environmental, maternal, and artifactual noises (Varady *et al.* 2003), which turns the extraction of foetal information into a challenging task.

To date, with regards to the recovery of foetal information from abdominal recordings, most signal processing methods in the literature have followed the approach of using rigid and empirical criteria to recover pre-selected components (*e.g.* FHS or FBM), but have only partially succeeded to do so and the extraction of entire traces containing FBMs or FHS may

still be difficult. Alternatively, the research presented in this thesis proposes that information of interest can be better recovered by means of a data-dependent signal processing approach that, by exploiting the temporal information in a single-channel recording, freely retrieves the components underlying the abdominal phonogram. Such a signal processing perspective, referred to and studied by Davies and James (2007) as Single-Channel Independent Component Analysis (SCICA), uses higher-order statistics for separation purposes and has been successfully applied to biomedical signals such as EEG (James *et al.* 2006; James and Lowe 2000) and MEG (James and Lowe 2001; Woon and Lowe 2004), but never to the abdominal phonogram.

The research described in this chapter explores, for the first time, a methodology based on this single-channel approach for the extraction of the sources underlying the abdominal phonogram. To this end, this chapter firstly introduces the fundamentals of SCICA, next describes its practical implementation for decomposing the abdominal phonogram and, finally, discusses the development needed for SCICA to truly become a robust signal processing alternative for antenatal surveillance.

6.1. Fundamentals of source separation by SCICA

Since there is only a single-sensor involved, SCICA can be considered as an extreme case of "undetermined" ICA that, according to different works (Cardoso 1998; Casey 2000; Castells *et al.* 2004), can be studied by considering SCICA as a case of multidimensional ICA (MICA), though applied to vectors of delayed samples (Davies and James 2007). This idea is described in more detail next.

This section starts by recalling a popular model of observed data as a random vector, $\mathbf{x} \in \mathbb{R}^m$, which consists of representing $\mathbf{x}$ as a linear superposition of vectors $\mathbf{a}_i$ as

$$\mathbf{x} = \sum_i s_i \mathbf{a}_i = \mathbf{A}\mathbf{s}\,, \tag{6.1}$$

where s_i are the weights or coefficients, $\mathbf{a}_i$ is a vector, $\mathbf{A} = [\mathbf{a}_1, \ldots, \mathbf{a}_m]$ is a square and invertible matrix, and $\mathbf{s}$ is a vector of coefficients s_i. Usually, the vectors $\mathbf{a}_i$ are chosen to form a basis in the signal space such that an inverse equation is uniquely defined as $\mathbf{s} = \mathbf{W}\mathbf{x}$ (where $\mathbf{W} = \mathbf{A}^{-1}$). In this representation, if the coefficients s_i are treated as independent random variables, then the model in Equation 6.1 becomes a generative linear statistical model like the classic model given by ICA (*i.e.* describes how the observed data are generated by a process of mixing components (Hyvarinen *et al.* 2001)) (Davies and James 2007).

Now, to apply this ICA representation to an N_T-valued scalar dataset, $x(n)$, first it is necessary to relax the constraint of ICA separation that requires the presence of at least as many observations as sources (Hyvarinen *et al.* 2001; Hyvarinen and Oja 2000; Stone 2004). This can be achieved by projecting the single-channel mixture onto a higher-dimensional space (Casey 2000; Castells *et al.* 2004; Tufillaro 1998), which is accomplished by breaking $x(n)$ up into a sequence of contiguous blocks of length m and by treating these as a sequence of vector observations, $\mathbf{x}(n)$, given as (Broomhead and King 1986; Sauer *et al.* 1991; Tufillaro 1998)

$$\mathbf{x}(n) = \left[x(nm), ..., x(m(n-1)+1) \right]^T, \tag{6.2}$$

where n in $\mathbf{x}(n)$ works as the block index. After that, a standard ICA implementation applied to $\mathbf{x}$ will learn a basis ($\mathbf{A}$) whose interpretation has been discussed by Davies and James (2007) as follows in the next sections.

6.1.1. SCICA as a filter bank

Understanding the meaning of the basis learnt by ICA requires keeping in mind that $\mathbf{x}$ comes from a scalar time-series (Davies and James 2007). Additionally, it is important to take into account that the components separated by ICA are usually mapped back to the original observation domain, which results in a perfect reconstruction-decomposition as

$$\mathbf{x} = \sum_i \mathbf{x}_s^{(i)}, \tag{6.3}$$

where $\mathbf{x}_s^{(i)}$ is the i^{th} source in the original observation domain.

In standard ICA, it is possible to observe each source in the original domain by applying an unmixing and mixing pair of operations given by

$$\mathbf{x}_s^{(i)} = \mathbf{A}_{(:,i)} \mathbf{W}_{(i,:)} \mathbf{x}. \tag{6.4}$$

Therefore, if Equation 6.4 is applied to the n^{th} block of the scalar time-series as defined in Equation 6.2, then it gives

$$x_s^{(i)}(nm - r + 1) = A_{(r,i)} \sum_{c=1}^{m} W_{(i,c)} x(nm - c + 1), \tag{6.5}$$

where r and c index over m samples.

Equation 6.5 is highly dependent on the block alignment with the data, *i.e.* is shift-variant. This problem is solved by applying cycle-spinning, which is a method originally proposed in wavelet analysis (Coifman and Donoho 1995). Basically, the cycle-spinning works by generating an estimate for each possible block alignment with the data and then, from the m

different estimates, calculates the average to obtain a shift-invariant estimate. Thus, the application of the cycle-spinning method in this case produces

$$x_s^{(i)}(n) = \frac{1}{m}\sum_{r=1}^{m} A_{(r,i)} \sum_{c=1}^{m} W_{(i,c)} x(n-c+r), \tag{6.6}$$

which can be rewritten as (Davies and James 2007)

$$x_s^{(i)}(n) = \frac{1}{m} a_i(-n) * w_i(n) * x(n), \tag{6.7}$$

where each $a_i(n)$ is a finite impulse response (FIR) filter given by the column vector $\mathbf{a}_i$, and each $w_i(n)$ is an FIR filter given by the row vector $\mathbf{w}_i$.

Equation 6.7 can be still simplified by assuming that the signal has been pre-whitened, which implies that the unmixing matrix $\mathbf{W}$ is orthogonal and thus, $a_i(n) = w_i(n)$ (*i.e.* the filter is symmetric around $t = 0$ and has zero-phase). *Therefore, the separation basis learnt by SCICA from pre-whitened data is a bank of zero-phase FIR filters.* Moreover, as the filters commute, a perfect reconstruction-separation in the observation domain is suitable by using only the separation filter, $f_i(n)$, as (Davies and James 2007)

$$f_i(n) = \frac{1}{m} w_i(-n) * w_i(n). \tag{6.8}$$

6.1.2. Notions of independence in SCICA

As mentioned in Section 4.1.4, ICA aims to decompose a set of observations into multiple statistically independent components. Here, it has been seen that, to achieve such a decomposition, ICA learns a set of zero-phase FIR filters (Davies and James 2007). The next step in this chapter is to describe what happens to $x_s^{(i)}(n)$ in Equation 6.7 when such a set of filters $f_i(n)$ is applied to the scalar time-series given by $x(n)$ as

$$x_s^{(i)}(n) = f_i(n) * x(n). \tag{6.9}$$

The answer that immediately arises is that the individual sources would be filtered versions of $x(n)$. However, the question that should be addressed is whether the separate components are truly independent.

In their work, Davies and James (2007) took into account the fact that the basis learnt by ICA generally contains shifted versions of the same filter (Hyvarinen *et al.* 2001), which led them to propose a suitable answer based on the MICA model developed by Cardoso (1998).

In his model, Cardoso (1998) shows that an observed vector $\mathbf{x}$ can be decomposed into a sum of K multidimensional independent vectors, $\mathbf{x}_P$, as

$$\mathbf{x} = \sum_{P=1}^{K} \mathbf{x}_P \,, \tag{6.10}$$

where (a) each $\mathbf{x}_P$ lays in an $N_{\mathcal{E}}$-dimensional subspace, $\mathcal{E}_P$, and (b) the set of subspaces $\mathcal{E}_P = \{\mathcal{E}_1,\ldots,\mathcal{E}_K\}$ are linearly independent. Most importantly, Cardoso (1998) also noted that the multidimensional decomposition in Equation 6.10 can be achieved by standard ICA by first calculating one-dimensional components, and then using dependence to group them in subspaces. As a result, it was possible to reorganise the mixing matrix $\mathbf{A}$ into a set of K submatrices $\mathbf{A}= [\tilde{\mathbf{A}}_1,\ldots,\tilde{\mathbf{A}}_K]$, where the columns of $\tilde{\mathbf{A}}_P$ span the linearly independent subspace $\mathcal{E}_P$.

Applying this reasoning to the time-series, it can be assumed that $x(n)$ can be represented as the sum of mutually independent random processes, $x_P(n)$, as

$$x(n) = \sum_{P} x_P(n) \,, \tag{6.11}$$

where each process $x_P(n)$ is considered as a filtered independent identically distributed random process, $s_P(n)$, given by

$$x_P(n) = h_P(n) * s_P(n) \,, \tag{6.12}$$

where $h_P(n)$ is an N_h-order FIR filter. Notice that, although this model is more restrictive than the model in Equation 6.11, it is similar to Equation 6.9, which is the model considered when ICA is applied to a matrix of delays (*i.e.* SCICA).

Let $\mathbf{x}(n)= [x(n), x(n-1), \ldots, x(n-m+1))]^T$ be the previously mentioned sequence of m-dimensional delay vectors, then Equation 6.11 can be rewritten in matrix form as

$$\mathbf{x}(n) = \sum_{P} \mathbf{H}_P \mathbf{s}_P(n) \,, \tag{6.13}$$

where $\mathbf{H}_P$ is the Toeplitz matrix for the filter $\mathbf{h}_P= [h_P(0),\ldots,h_P(N_h-1)]^T$ and $\mathbf{s}_P(n)= [s_P(n), s_P(n-1),\ldots,s_P(n-m-N_h+2)]^T$ (Davies and James 2007).

In particular, when solving for a single source $s_1(n)$, Equation 6.12 becomes equivalent to the blind deconvolution problem where, according to Davies and James (2007), ICA learns a single separating vector that is equivalent to the Shalvi-Weinstein deconvolution filter. Thus, when used to learn the full unmixing matrix, ICA produces a matrix $\mathbf{W}$ whose rows convey m approximate shifted versions of the deconvolution filter (Hyvarinen *et al.* 2001). Finally, if assuming the presence of multiple components, then each $\mathbf{h}_P$ is non-invertible, the corresponding $\mathbf{H}_P$ is rank deficient and, consequently, the vectors $\mathbf{x}_P(n)= \mathbf{H}_P\, \mathbf{s}_P(n)$ lie in the

subspace $\mathcal{E}_P$. Most importantly, if all the subspaces $\mathcal{E}_P$ are linearly independent, then the model becomes a valid MICA model (Cardoso 1998; Davies and James 2007).

In conclusion, whenever applied to a scalar time-series, ICA manages to decompose any process $\mathbf{s}_P$ into basis vectors $\mathbf{a}_i$ that can be certainly grouped into K subsets λ_P such that $\mathbf{a}_i \subset \mathcal{E}_P$ when $i \in \lambda_P$. Furthermore, since these basis vectors tend to be shifted approximations of the individual filter $\mathbf{h}_P$, all the basis vectors associated with the subset λ_P will have very similar spectral support (Davies and James 2007).

Finally, to estimate the individual independent processes, the contributions of the separate one-dimensional components within each subset must be summed. Recalling from Equation 6.9 that each component contribution can be estimated using the $f_i(n)$ filter, then each $x_P(n)$ can be estimated as

$$x_P(n) = \sum_{i \in \gamma_P} f_i(n) * x(n). \tag{6.14}$$

Thus, the decomposition of a stationary process $x(n)$ by SCICA results in independent stationary random processes $x_P(n)$ that are built from subsets of one-dimensional components with very similar spectral characteristics (Davies and James 2007). *In other words, in SCICA, independence means that the separate sources have disjoint spectral support*.

Notice that in this thesis, since $x(n)$ refers to the single-channel abdominal phonogram, then it is expected that the extracted independent processes (*i.e.* the underlying sources) will be related to foetal, maternal, and environmental activities. The next section details the implementation of SCICA for source separation of the abdominal phonogram.

6.2. Decomposing the abdominal phonogram by SCICA

Following the fundamentals described in Section 6.1, the practical implementation of SCICA follows three steps to decompose a signal into its underlying sources (see Figure 6.1): first, the single-channel signal is mapped into a higher-dimensional space. Next, multiple one-dimensional independent components (ICs) are calculated using a standard implementation of ICA (FastICA or TDSEP in this work). Finally, after projecting the ICs back to the measurement space, the resulting signals are clustered (based on their spectral similarity) to recover the multidimensional independent sources underlying the abdominal phonogram. The next sections will expand on each step.

6.2.1. Transforming a single-channel signal into a multidimensional dataset

This step can be thought of as a preprocessing stage, which is necessary to fulfil one of the two primary conditions to apply ICA (Hyvarinen *et al.* 2001; Hyvarinen and Oja 2000; Stone 2004), *i.e.* the number of observations available is at least as large as the number of sources to be extracted (Woon and Lowe 2004). Therefore, since the abdominal phonogram is a single scalar time-series, and ICA is applied to a "multi-channel" representation of data, the abdominal phonogram recording must be mapped into a higher-dimensional representation (Cardoso 1998; Casey 2000; Castells *et al.* 2004; Golyandina *et al.* 2001; Salgado and Alonso 2006; Teixeira *et al.* 2006; Woon and Lowe 2004). In this work, to exploit the characteristic temporal structure (*i.e.* presence of rhythmic patterns or oscillations) of the physiological sources underlying the abdominal phonogram (Castells *et al.* 2004), the mapping is done by using the method of delays (MD), also otherwise known as dynamical embedding (Sauer *et al.* 1991).

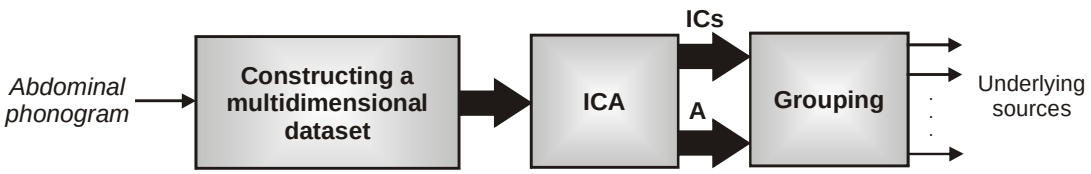

Figure 6.1. SCICA, an alternative methodology for decomposing the single-channel abdominal phonogram into its underlying sources.

The premise in dynamical embedding is that there is a system underlying the recorded time-series (*i.e.* a phonogram generator) that can be modelled as a nonlinear system whose dynamics reside on some unobservable system manifold embedded in the phase space. Furthermore, it is assumed that a relatively small number of underlying nonlinear source generators contribute to this unobservable manifold. Thus, it is possible to think of the abdominal phonogram as the result of nonlinear interactions of just a few degrees of freedom (*D*) with additive noise. Takens' theorem[1] (Takens 1981) allows for the reconstruction of such a *D*-dimensional dynamical system that generated the measured time-series, this by constructing an empirical state phase based on successive observations of the time-series (this is the method of delays) (Broomhead and King 1986).

[1] In his work, by considering M as a compact manifold of dimension *D* and $x \in M$, Takens theorem states that "For pairs (φ, y), $\varphi: M \rightarrow M$ as smooth diffeomorphism and $y: M \rightarrow \mathbb{R}$ a smooth function, it is a generic property that the map $\Phi_{(\varphi, y)}$ $M \rightarrow \mathbb{R}^{2m+1}$, defined by $\Phi_{(\varphi, y)} = (y(x), y(\varphi(x)), \ldots, y(\varphi^{2m}(x)))$ is an embedding." Note that the symbols and characters have been used as in the original paper.

The basic idea of the MD is to construct an *m*-dimensional matrix of delay vectors from $x(n)$ by simply extracting consecutive overlapped segments of length *m* from the time-series as

$$\mathbf{v}_m(k) = \left[x(k), x(k+\tau), \ldots, x(k+(m-1)\tau)\right]^T, \tag{6.15}$$

and using them (for successive values of *k*) as vectors to form the matrix of delays, **v**, as (Broomhead and King 1986; Woon and Lowe 2004)

$$\mathbf{v} = \begin{bmatrix} x(k) & x(k+\tau) & \cdots & x(k+N\tau) \\ x(k+\tau) & x(k+2\tau) & \cdots & x(k+(N+1)\tau) \\ \vdots & \vdots & \ddots & \vdots \\ x(k+(m-1)\tau) & x(k+m\tau) & \cdots & x(k+(m+N-1)\tau) \end{bmatrix},$$

where τ is the time-lag, *m* is the embedding dimension, and *N* is the number of consecutive delay vectors (Broomhead and King 1986). Each vector represents a point on the system manifold and together all the columns trace a trajectory on this manifold generated by the Euclidean embedding. In Takens (1981), it was shown that the Euclidean embedding dimension, $\hat{e}$, must be at least as large as *D*, but in practice it must be at least

$$\hat{e} > 2D + 1. \tag{6.16}$$

In particular, when applied to real world data, because of dependencies in the time-series and inherent noise in the system, *m* needs to be significantly larger than $\hat{e}$. In fact, *m* needs to be "big enough" to capture the information content necessary, especially when the time-series data is heavily correlated (James and Lowe 2001). Thus, provided the data were sampled using a reasonable rate (according to the Nyquist criterion), and by setting τ to one, it is possible to choose the practical minimum size for *m* only by considering the lowest frequency of the periodic components of interest as (Golyandina *et al.* 2001; James and Lowe 2001; Teixeira *et al.* 2006)

$$m \geq f_s / f_l, \tag{6.17}$$

where f_s denotes an appropriate sampling frequency and f_l is the lowest frequency of interest in the measured signal. For instance, considering a phonogram that was sampled at 500 Hz, and knowing that the lowest frequency of the FHS is 20 Hz (Holburn and Rowsell 1989), then a value of f_l = 10 Hz seems appropriate and, consequently, *m* = 50.

Once the value for *m* is found, **v** is constructed using *N* consecutive delay vectors. This value is determined by the length of the signal to be analysed (*i.e.* N_A) as

$$N = N_A - (m-1). \tag{6.18}$$

To select N, a matrix of delays that covered a quasi-stationary signal of length N_A, rather than a non-stationary entire signal of length N_T, is considered (James and Lowe 2003). Here, after testing different segments of size N_A (*i.e.* 250, 500, 1000, 2500, 5000, and 10000 samples), it was found that N_A = 5000 samples (*i.e.* 10 s) made it suitable to build up a matrix of delays that was successfully processed by the FastICA algorithm (*i.e.* the algorithm converged to a solution (Hyvarinen and Oja 1997)) as described in the next section. Conversely, for lower and larger values of N_A, where the amount of data was not enough for the statistical analysis required by SCICA or where the segment became so large that is was not a quasi-stationary segment anymore, FastICA had difficulties to converge.

Finally, once the choice of τ, m, and N is made, $\mathbf{v}$ conveys information about the states of the underlying system that generated the time-series (Broomhead and King 1986; Sauer *et al.* 1991), and its data is now ready to be represented by a convenient spanning basis such as ICA (Davies and James 2007; Sauer *et al.* 1991).

6.2.2. Transforming a multidimensional dataset into multiple independent components

This step solves the BSS problem in Equation 4.1 by applying ICA. To do this, the input data – the matrix of delays, $\mathbf{v}$– is transformed so that the statistical dependences between the output components $\hat{\mathbf{s}}$ are minimised as (Hyvarinen *et al.* 2001; Hyvarinen and Oja 2000; James and Hesse 2005)

$$\hat{\mathbf{s}} = \mathbf{W}\mathbf{v} \,. \tag{6.19}$$

a) Extracting statistically independent components: Currently, depending on the method used to seek/define statistical independence (*i.e.* higher-order statistics or time-structure based methods), different ICA algorithms have been developed (Hyvarinen *et al.* 2001; Hyvarinen and Oja 2000; James and Hesse 2005; Stone 2004). Here, two of them have been considered, FastICA and Temporal Decorrelation source SEParation (TDSEP):

1. *FastICA:* Proposed by Hyvarinen *et al.* (1997), it is an ICA algorithm that has become very popular due to its speed and stability of convergence.

   FastICA belongs to the higher-order statistics based methods (HOS), which means that the output components are found by maximising their non-Gaussianity. Therefore, since a Gaussian distributed signal possesses zero kurtosis (*i.e.* the fourth-order cumulant of the signal is zero), the aim of FastICA is maximising the magnitude of the kurtosis to make $\hat{\mathbf{s}}$ as non-Gaussian as possible (*i.e.* statistically independent). To do this, FastICA treats the problem in Equation 6.19 as an optimisation problem with $\hat{\mathbf{s}}$

(better known as the ICs) as its solution (Hyvarinen and Oja 1997; James and Hesse 2005), where **W** is estimated by searching for directions of maximum kurtosis as

$$kurt\left(\mathbf{W}\ \mathbf{z}\right) = E\left\{\left(\mathbf{W}\ \mathbf{z}\right)^4\right\} - 3\left(E\left\{\left(\mathbf{W}\ \mathbf{z}\right)^2\right\}\right)^2, \tag{6.20}$$

for a zero-mean random variable **z** (*i.e.* the whitened version of **v**).

2. *TDSEP:* Proposed by Ziehe *et al.* (1998), it is a computationally simple and efficient ICA algorithm that is suitable for data with a significant temporal structure, *e.g.* speech or biomedical signals.

   TDSEP belongs to the methods that, instead of considering higher-order statistics, consider the time-structure of the sources. In these implementations, independence is defined as the absence of cross-correlations amongst the sources (Ziehe and Muller 1998). In addition, TDSEP assumes that the sources have temporal structure and, consequently, that all time-delayed correlation matrices, $R^{\mathbf{s}}_{k_\mathbf{s}}$, should be diagonal (Wubbeler *et al.* 2000). Hence, TDSEP captures the dependence structure of the observed signals, **v** in this work, by creating a set of square matrices, and then finds the joint diagonaliser of that set, which turns out to be the mixing matrix (**A**) (James and Hesse 2005; Wubbeler *et al.* 2000; Ziehe and Muller 1998). To this end, TDSEP calculates a set of time-lagged correlation matrices of **v** as

$$R^{\mathbf{v}}_{k_\mathbf{v}} = \sum_{k_\mathbf{v}=0} \mathbf{v}\left(n\right)\mathbf{v}\left(n+k_\mathbf{v}\right), \tag{6.21}$$

   where $k_\mathbf{v}$ (= 0, 1, 2, …, $k_{\mathbf{v}max}$) represents the time-lag. Then, as for independent components these matrices have to be diagonal, TDSEP performs a joint diagonalisation of $R^{\mathbf{v}}_{k_\mathbf{v}}$ to estimate **A** along with the ICs. Finally, after calculating **W** (which is the inverse of **A**), it is possible to substitute it in Equation 6.19 to estimate the sources, better known as the ICs.

   For this implementation to work, it is important to highlight that the value of $k_{\mathbf{v}max}$ becomes essential as it defines the number of time-lags and the quality of the separation. Here, in absence of a theoretical choice of $k_{\mathbf{v}max}$, results from several tests have shown that $k_{\mathbf{v}max}$= 1 is suitable to extract ICs with a well defined single-peak spectrum (Jimenez-Gonzalez and James 2008b).

b) Assumptions for recovering independent components: Before applying ICA, some assumptions about the composition of the data are necessary: (i) the sources are statistically independent (*i.e.* they have non-Gaussian distributions, for the FastICA algorithm, and they have non-delta autocorrelations and non-cross correlations, for the TDSEP algorithm)

(Hyvarinen *et al.* 2001; Hyvarinen and Oja 2000; Stone 2004; Ziehe and Muller 1998), (ii) the abdominal phonogram is a linear summation of signals produced by the foetal heart and different maternal/external sources, (iii) the sources underlying the abdominal phonogram have disjoint spectral support (Davies and James 2007), and (iv) the matrix of delays, **v**, successfully conveys a quasi-stationary signal (James and Hesse 2005).

As a BSS method, the first assumption is fundamental for FastICA and TDSEP to work whilst the second simplifies the solution to the BSS problem by considering linear mixtures of ICs (Hyvarinen *et al.* 2001; Hyvarinen and Oja 2000; Stone 2004; Ziehe and Muller 1998). The third assumption is fundamental to the successful application of SCICA since it defines how well the method is going to separate sources through the zero-phase FIR filter bank learnt by ICA when **v** is processed (Davies and James 2007). The final assumption is important to provide FastICA and TDSEP with a stable segment to work with and enough data to perform the higher-order statistical analysis required by FastICA to converge (Hyvarinen and Oja 1997).

6.2.3. Transforming multiple independent components into underlying sources

Once **v** has been constructed and transformed by a standard ICA algorithm, multiple one-dimensional ICs are recovered (some of them associated to the same source or process) (Cardoso 1998; Davies and James 2007). This implies that some post-processing is necessary to group the relevant ICs together, although identifying ICs of interest is not a trivial task.

a) Restoring components in the measurement space: The step described in Section 6.2.2 produces at most 50 one-dimensional ICs (due to m= 50) that are projected back to the measurement space using

$$\mathbf{Y}^i = \mathbf{a}_i \ \mathbf{s}_i^T , \tag{6.22}$$

where $\mathbf{s}_i$ is the i^{th} IC (i= 1,…,50), $\mathbf{a}_i$ is the corresponding column of the mixing matrix **A** (which is the inverse of **W**), and $\mathbf{Y}^i$ is a matrix of delays for that component (James and Lowe 2001). Next, this elementary matrix is transformed into the i^{th} projected IC (IC_p^i) by applying a linear transformation known as diagonal averaging or Hankelization (Golyandina *et al.* 2001; Salgado and Alonso 2006) as

$$\text{IC}_p^i = \frac{1}{m}\sum_{z=1}^{m} \mathbf{Y}_{z,(n+z-1)}^i \ . \tag{6.23}$$

Once the whole set of IC_ps have been calculated, and because some of them correspond to the same process (*i.e.* FHS, maternal or line-noise), they must be grouped to construct the related independent sources. More specifically, as ICA "learns" a zero phase filter bank

(expressed in each column of **A**), every IC_p corresponds to a filtered sequence of signals that can be grouped by taking into account their spectral similarities (Davies and James 2007; James and Lowe 2001).

b) Grouping similar components: The Power Spectral Density (PSD) seems to be a suitable attribute for the *K*-means algorithm to identify and cluster components corresponding to the same process or activity. Here, this PSD information has been estimated using the Welch's method with a Hanning window of 32 coefficients in length and an overlap of 50%. The resulting *m* PSDs, composed of N_{FFT} points each, are then provided to the *K*-means algorithm (Nabney 2004) to be iteratively clustered into *K* disjoint and therefore independent groups ($\mathbf{IG}_P$, P= 1,…,K), where each $\mathbf{IG}_P$ is represented by its mean vector and each PSD^i (i= 1,…,50) is assigned to the $\mathbf{IG}_P$ with the closest vector.

In more detail (Teknomo 2006), once the PSDs are provided to *K*-means, the algorithm treats each PSD as a vector ($\mathbf{psd}^i \in \mathbb{R}^{N_{FFT}}$) whose coordinates are given by the values in its frequency bins (f_b)[2], *i.e.* $PSD^i_{f_b}$. Next, to define whether two vectors $\mathbf{psd}^i$ and $\mathbf{psd}^P$ ($\mathbf{psd}^P \in \mathbb{R}^{N_{FFT}}$) belong to the same group in this work, the algorithm calculates the cosine angular separation, θ^i_P, between them as

$$\theta^i_P = \frac{\sum_{f_b=1}^{N_{FFT}} \left(\mathrm{PSD}^i_{f_b} - \mu_{\mathrm{PSD}^i}\right)\left(\mathrm{PSD}^P_{f_b} - \mu_{\mathrm{PSD}^P}\right)}{\sqrt{\sum_{f_b=1}^{N_{FFT}} \left(\mathrm{PSD}^i_{f_b} - \mu_{\mathrm{PSD}^i}\right)^2 \sum_{f_b=1}^{N_{FFT}} \left(\mathrm{PSD}^P_{f_b} - \mu_{\mathrm{PSD}^P}\right)^2}}, \tag{6.24}$$

were

$$\mu_{\mathrm{PSD}^i} = \frac{1}{N_{FFT}} \sum_{f_b=1}^{N_{FFT}} \mathrm{PSD}^i_{f_b}, \tag{6.25}$$

and

$$\mu_{\mathrm{PSD}^P} = \frac{1}{N_{FFT}} \sum_{f_b=1}^{N_{FFT}} \mathrm{PSD}^P_{f_b}. \tag{6.26}$$

[2] In a simple example, if N_{FFT} were equal to four, and the PSD values of the first IC_p at each bin were PSD^1_1= 0.1, PSD^1_2= 0.5, PSD^1_3= 0.2, and PSD^1_4= 0 respectively, then the coordinates of $\mathbf{psd}^1$ would be (0.1, 0.5, 0.2, 0.0).

Then, since for closer vectors the cosine angular separation moves towards one, *K*-means uses θ_P^i as the criterion to define whether the vector psdi belongs to the group represented by the vector $\mathbf{psd}^P$ as its centre, *i.e.* $\mathbf{IG}_P$.

In this way, *K*-means becomes a nice first clustering trial method because it converges quickly as it minimizes the *error* function described by

$$error = \sum_{P=1}^{K} \sum_{\text{PSDs} \in \mathbf{IG}_P} \theta_P^i \,, \tag{6.27}$$

However, although *K*-means is easy to implement, it requires the user to predefine the *K* number of **IG** or clusters to be formed. In this work, after performing some experimental work and empirical observations on the classification outcome for values of *K* between three and fifteen, it can be said that:

1. A value of *K larger than 10* is more likely to make *K*-means create more than one group for the foetal group, sometimes including only one IC_p.
2. A value of *K smaller than 4* is more likely to make *K*-means break down and misclassify either foetal components in the maternal group, or noise components in the foetal/maternal groups.
3. A value of *K between 4 and 10 (inclusive)* is more likely to make *K*-means group foetal and maternal components in different subspaces with less misclassified cases.

Being cautious, and because the work presented in this chapter is exploring the SCICA methodology, *K*= 10 proves to be a good value so that *K*-means groups the 50 one-dimensional IC_ps into 10 independent-multicomponent groups called $\mathbf{IG}_P$ (*P*= 1,…,10).

c) Recovering independent sources: After clustering similar components, the time-series of the independent sources (is_P) are recovered by summing the IC_ps grouped in each $\mathbf{IG}_P$ as (Golyandina *et al.* 2001; Salgado and Alonso 2006)

$$is_P = \sum_{\text{IC}_p\text{s} \in \mathbf{IG}_P} \text{IC}_p\text{s} \tag{6.28}$$

Finally, time and frequency information must be considered to manually identify sources as foetal, maternal or line-noise.

6.3. SCICA for well-being surveillance: practical issues

So far, this chapter has gone from the presentation of the fundamentals of SCICA to its practical implementation for decomposing the abdominal phonogram (see Figure 6.2). To this end, as

already noted, parameters like the embedding dimension (m), the length of the segment to be decomposed (N_A), and the number of sources to be separated (K), have been adjusted to decompose the abdominal phonogram. As a result, in a preliminary test, the current proposal has managed to decompose the single-channel abdominal phonogram into ten independent sources (Jiménez-González and James 2009). This is an essential achievement in this study since it demonstrates the feasibility of SCICA to separate the sources underlying the abdominal phonogram. However, before claiming that the problem has been solved, it is imperative to consider the current SCICA implementation in the interest of this research, which is the extraction of entire traces from where information for surveillance purposes can be collected (*i.e.* monitoring foetal well-being). This will be discussed in the next sections.

6.3.1. Working with segmented data

When creating the matrix of delays, **v**, the abdominal phonogram of length N_T is chopped up into segments of length N_A, which provides the ICA algorithms with a suitable quasi-stationary set of observations to work with. This means that, to decompose the entire abdominal phonogram, a number of N_A-segments have to be processed and, most importantly, that the recovered sources will be also N_A in length (*i.e.* SCICA is producing ten *segmented* independent sources). For that reason, once the sources have been separated from all the segments, they must be concatenated to assemble entire independent sources from where suitable information about well-being can be obtained.

The task may sound easy to implement since each segment produces ten independent sources and thus it should be simple to *attach the equivalent sources* between adjacent segments. Unfortunately, there are two important ambiguities in ICA (and consequently in SCICA) that make the task hard to achieve and require to be dealt with first:

a) Uncertainty in the order of components/sources (*i.e.* permutation ambiguity): Recalling the BSS problem expressed in Equation 4.1, where both **s** and **A** are unknown, it can be seen how easy it is for the ICA algorithm to freely change the position of the columns in **A** and randomly name any of the ICs as IC^1 (and thus any of the IC_ps as $IC^1{}_p$). As a result, every time the ICA algorithm runs, even on the same abdominal phonogram segment, the order of the components at the output will be different (*i.e.* the components are randomly sorted) (Hyvarinen and Oja 2000). Besides, to complicate matters –because K-means randomly initialises its centres μ_i as well–, such an arrangement uncertainty also appears in the separate is_P.

In practical terms, this permutation ambiguity means that the components/sources separated from the segment s_β will probably be sorted in a different way than the equivalent sources

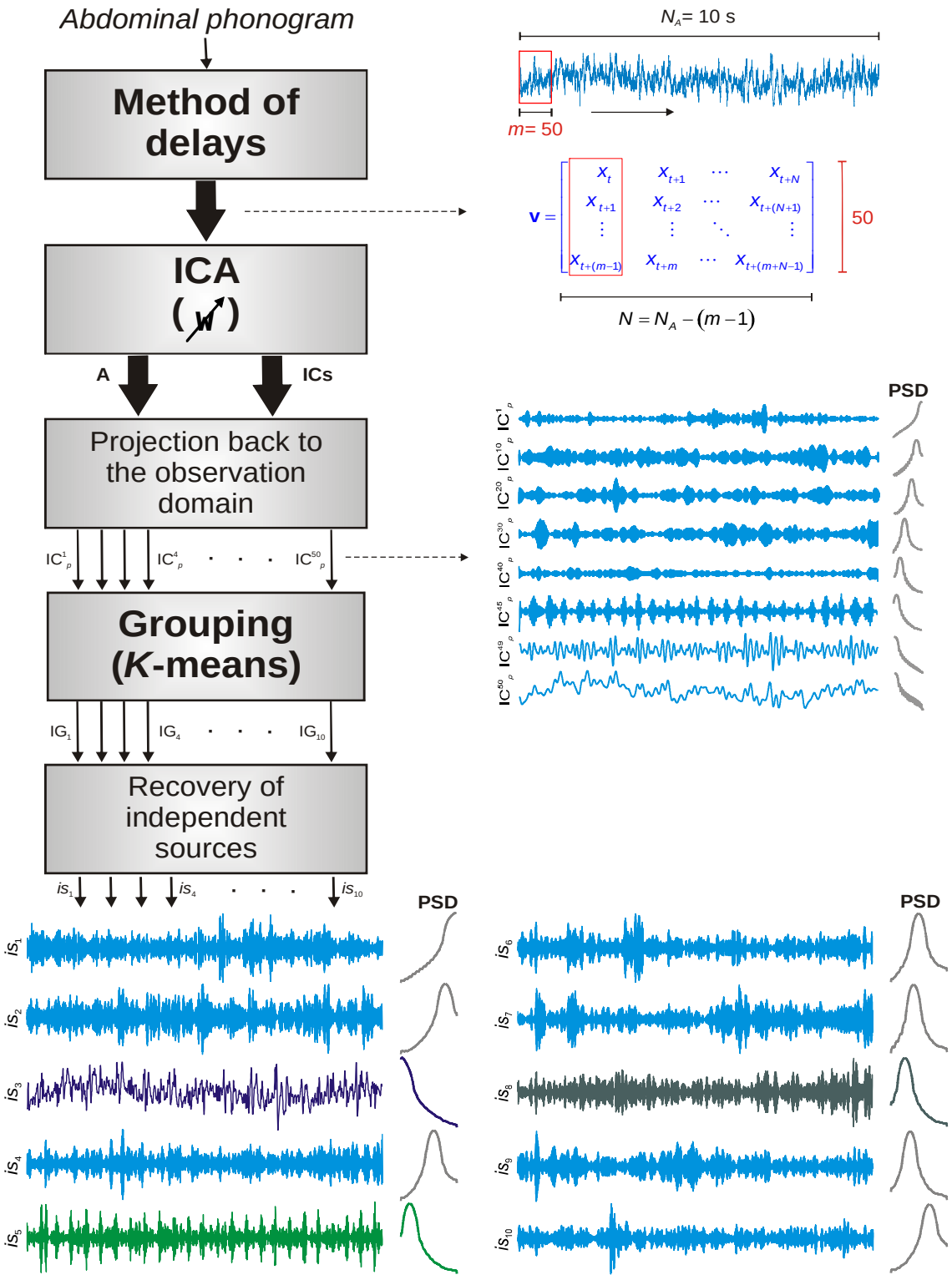

Figure 6.2. Implementation of SCICA for decomposing the *abdominal phonogram* into ten independent sources (is_P). The left-hand side shows the steps followed to process the single-channel signal, whereas the right-hand side illustrates the corresponding outputs. From top to bottom, the projection of the signal into a higher dimensional space (by the method of delays) along with the matrix of delays (**v**), the extraction/projection of independent components (by TDSEP) along with eight of fifty one-dimensional components (in the observation domain, IC^i_p) and, finally, the grouping (by *K*-means) and recovery of ten spectrally disjoint sources (*i.e.* independent sources). Notice that the PSDs show single and well-defined peaks and that is_3 is still a mixture of a slow component and some peaks.

in the adjacent segments (*i.e.* $s_{\beta-1}$ and $s_{\beta+1}$). Thus, even though adjacent segments are being processed, it is impossible to predict which components belong to each source or the arrangement of the sources finally separated by SCICA.

b) Uncertainty in the energy of components/sources (*i.e.* scaling ambiguity): As some information may not be present in some segments, and the current proposal requires from SCICA to recover (i) 50 ICs and then (ii) 10 sources, it is possible that, from each segment (i) ICA extracts shifted versions of the same filter (Davies and James 2007; Hyvarinen *et al.* 2001) and (ii) *K*-means recovers more than one source for the same process (*e.g.* two sources corresponding to the FHS). As a result, adjacent segments s_β and $s_{\beta'}$ may show a different number of components/sources for the same process. Consequently, when those components are summed as in Equation 6.28 to recover the is_P in each segment, the resulting energy will be different (depending on the number of components used). Thus, the amplitude of equivalent sources between adjacent segments may be different by a scaling factor that, unfortunately, cannot be predicted.

In conclusion, further processing is still required for this proposal to reconstruct an entire source across multiple recording windows. A possible solution will not be discussed here and, for the moment, this chapter will leave open the question of *how to take the segmented sources produced by SCICA and reconstruct entire time-series that are suitable for surveillance?* (This will be further discussed in Chapter 10, where a solution will be presented).

6.3.2. Working with overcomplete data representations

So far, the blindness of ICA has been a convenient attribute for this work. In fact, such blindness makes it possible to decompose a set of observations (knowing almost nothing about the sources and the mixing matrix) only by assuming that the underlying sources are statistically independent (*i.e.* spectrally disjoint). Thus, as illustrated in Figure 6.2, it is possible to recover *m*-components/*K*-sources underlying the abdominal phonogram (Jiménez-González and James 2009). However, the implementation of the algorithm requires the assumption of values for *m* and *K* that, due to the lack of *a priori* information about the real number of underlying components/sources, is not easy to define. To avoid this problem, higher values are commonly used to produce an *overcomplete representation* from where the *components/sources of interest* are manually selected. Unfortunately, finding components of interest is not an easy task. Here, to emphasize how difficult it is to deal with an overcomplete representation, the 50 one-dimensional IC_ps produced in Section 6.2.2 will be analysed in terms of their relevance, redundancy, and interpretation.

a) Relevance: As mentioned in Section 6.2.2, Equation 6.17 provides a criterion to separate periodic components as far as f_l Hz, which is an objective and consistent way to do so. In

particular, as the current SCICA implementation aims to extract the FHS, this equation indicates that 50 one-dimensional components must be extracted by ICA. Unfortunately, amongst these 50 components, only some are related to physiological processes, whilst the rest are related to environmental processes. This means that, in an overcomplete representation, there is an unknown number of components that are relevant for surveillance so that only these components should be considered in the postprocessing step.

The main advantage of working with relevant components would be to certainly focus on physiological data and reduce postprocessing time. This would be especially useful since the current SCICA implementation is applied not to one, but to a number of segments. Unfortunately, finding relevant components (*i.e.* dimension reduction) can become a subjective and demanding task that, at least for the components underlying the abdominal phonogram (where no previous studies exist about their features), requires experience and time to properly recognise them.

b) Redundancy: As mentioned in Section 6.2.3, another characteristic of the components (either relevant or irrelevant) is that some of them correspond to the same process, either maternal, foetal or noise and, because of that, they have to be grouped to recover the sources. However, grouping components is not as easy to do as it might sound, especially in the aim of surveillance, where the is_P must be correctly extracted to be meaningful (*i.e.* without contamination produced by misclassified or noisy components).

The current implementation of SCICA uses a solution that, although manages to quickly group components, may fail at correctly classifying, which results in either redundant sources or misclassified components. The redundancy problem in the sources, which is a consequence of using an algorithm that *a priori* requires the number of groups to form, could be acceptable for a first implementation of SCICA. The components misclassification, on the contrary, is totally unacceptable since it may contaminate the source and render it useless for surveillance purposes. Therefore, since the classification given by *K*-means has presented problems in distinguishing components belonging to different processes, it should not be used for surveillance purposes. This will be further discussed in Chapter 8, where a formal evaluation of *K*-means will be presented as part of the solution of the redundancy problem (Jiménez-González and James 2010).

c) Interpretation: This is one of the most important and perhaps difficult tasks of analysing biomedical signals by using BSS methods, establishing the relationship between a recovered trace and a physiological process. Clearly, the task is far from the objective of any decomposition method, but for practical purposes –as the one presented in this thesis–, extracting the traces is meaningless *per se* unless they can be associated with specific

processes, physiological or otherwise. Then, by assuming that the traces of the sources were correctly extracted and associated with a physiological process of interest, it would be possible to start the reconstruction of the entire time-series, which is necessary for surveillance.

The task would be easier if there were precise information about the processes underlying the abdominal phonogram –not only their number, but also their characteristics or properties–. However, since such information is unavailable, visual examination of the sources becomes the default way to identify them, which makes the analysis slow and highly subjective.

In conclusion, although an overcomplete representation makes SCICA feasible to extract components underlying the abdominal phonogram, further research needs to be done on how to find/group relevant components so that the separate is_P become suitable for surveillance purposes. The solution is not described in this chapter, mainly because there is not any previous research (*i.e.* knowledge) about the components underlying the abdominal phonogram. Alternatively, since the separation by TDSEP has nicely separated the components underlying the abdominal phonogram to produce spectrally disjoint IC_ps as in Figure 6.2 (Jimenez-Gonzalez and James 2008b), the next natural step is to study, for the first time, the IC_ps characteristics in the aim of establishing an appropriate strategy to postprocess them. Hence, due to the significance of both (i) the study of the separate components and (ii) the adjustment of the postprocessing step, an entire chapter will be dedicated to each one. Consequently, Chapter 7 will focus on the study of the components underlying the abdominal phonogram, whereas Chapter 8 will focus on the method proposed to postprocess them.

6.4. Summary

This chapter introduced SCICA as an alternative signal processing approach for decomposing the single-channel abdominal phonogram (a signal rich in temporal information about foetal activity, but buried in unpredictable maternal and environmental noises). Contrary to traditional signal processing schemes, where empirical filters are used to extract single pre-selected information, SCICA performs a data-dependent analysis that separates out not one, but all the sources underlying the abdominal phonogram (foetal, maternal, and noise).

Successfully applied to other biomedical signals such as the EEG and the EMG, SCICA works in three steps: (1) the single-channel signal is projected into a multidimensional dataset, (2) the dataset is transformed to extract statistically independent components by using a standard algorithm of ICA (FastICA or TDSEP) and, (3) components corresponding to the same

process/activity are grouped by *K*-means and used to recover the independent sources underlying the abdominal phonogram.

As currently implemented, SCICA based on TDSEP is feasible to separate the components related to different activities underlying the abdominal phonogram. This is an important first achievement for this thesis, although still in need of further research in the context of well-being surveillance, which is more rigorous about the length and quality of the separate sources. Fortunately, although such requirements are not fulfilled by the current implementation, it is evident which step of SCICA requires further development, which is the grouping step. Indeed, preliminary results have made it possible to observe that *K*-means is unreliable to group components and therefore inadequate for surveillance purposes (Jiménez-González and James 2009). However, in a more critical analysis, at this stage it is impossible for this chapter to certainly specify where the classification problem comes from: the classifier, the attribute used (*i.e.* the PSD) or both of them. Hence, rather than testing more classifiers using the same attribute (or other attributes using the same classifier), this research considered that a more natural approach would be (1) to study the separate components (*i.e.* gain knowledge about their characteristics) and then, (2) to propose an appropriate strategy for postprocessing them (*i.e.* grouping). Thus, Chapter 7 will focus on the study of the components underlying the abdominal phonogram and the chapters after that will present the solutions proposed to make SCICA suitable for well-being surveillance.

7 ON THE EXAMINATION OF THE INDEPENDENT COMPONENTS SEPARATED FROM THE ABDOMINAL PHONOGRAM

Chapter 6 introduced SCICA as an alternative signal processing methodology to extract the components underlying the single-channel abdominal phonogram (Jiménez-González and James 2009). Preliminary results showed that SCICA based on TDSEP manages to separate components whose PSDs are characterised by a well-defined single-peak (*i.e.* band-limited) (Jimenez-Gonzalez and James 2008), which are promising results from a decomposition perspective. However, from a physiological perspective, which aims not only to separate, but also to comprehend/infer the meaning of the components, these results need further analysis. Hence, as the current problem is not related to the separation by SCICA but rather to the interpretation of its outputs, a logical solution points towards the study of these components.

The work presented in this chapter aims to gain knowledge, from a physiological perspective, about the components underlying the abdominal phonogram. To this end, methods usually applied to the analysis of other physiological signals have been selected. Such methods, proved to provide different perspectives about a time-series (*i.e.* descriptive, spectral, complexity, and time-structure), seem promising for a study of the components underlying the abdominal phonogram. This chapter starts with a description of such methods, next proceeds towards their application to a dataset of ICs and, finally, discusses the physiological relevance of the components separated from the abdominal phonogram.

7.1. Measures for physiological signal analysis

Physiological signals are traditionally described in terms of features such as amplitude and frequency (*e.g.* the ECG ranges between 10 μV and 5 mV in amplitude and between 0.04 and 100 Hz in frequency, whereas the EMG ranges between 20 μV and 5 mV in amplitude and between 5 and 2000 Hz in frequency, to mention a couple of signals (VuBovy 1978)). Such parameters, although provide a general idea of the signal characteristics, do not really give any

insight about the regulatory processes underlying the signal dynamics (*e.g.* the heart rate in the ECG case), which requires the extraction of appropriate features. Unfortunately, finding *representative features* usually becomes a difficult task. Certainly, the description of the abdominal phonogram components is an excellent example of such a difficulty, especially because of (1) the lack of prior knowledge about how a component should look (*e.g.* any pattern), either foetal or maternal, and (2) the lack of *a priori* information about which physiological process produced the components (*e.g.* foetal or maternal). Consequently, a description of the components underlying the abdominal phonogram requires one to find representative features that are not only sensitive (to distinguish components related to different processes), but also specific (to identify whether a physiological process is either foetal or maternal). This section describes four methods that might accomplish such sensitivity/specificity requirements and thus become useful for the examination of the components separated from the abdominal phonogram.

7.1.1. Traditional analysis: measures in the time and frequency domains

In a very preliminary analysis, physiological signals are traditionally characterised using features related to the time and frequency domains. In general, a descriptive analysis in the time domain looks for the mean (μ), standard deviation (σ), and skewness (γ) of an N_T-valued scalar time-series, $x(n)$, as

$$\mu = \frac{1}{N_T}\sum_{n=1}^{N_T} x(n), \tag{7.1}$$

$$\sigma = \sqrt{\frac{1}{N_T - 1}\sum_{n=1}^{N_T}\left(x(n)-\mu\right)^2}\,, \tag{7.2}$$

and

$$\gamma = \frac{\frac{1}{N_T}\sum_{n=1}^{N_T}\left(x(n)-\mu\right)^3}{\sigma^3}. \tag{7.3}$$

On the other hand, frequency information is usually obtained by the Fourier Transform, which makes it possible to estimate the PSD of a signal, $\hat{S}_x(f)$. The PSD reveals the distribution of power in the signal as a function of frequency and, when properly used, may become an essential guide to further analysis like short-term correlations, for instance (Eke *et al.* 2000). The PSD can be estimated by the periodogram, which is calculated as

$$\hat{S}_x(f) = \frac{1}{f_s N_T}\left|\sum_{n=1}^{N_T} x(n)\, e^{-j(2\pi f/f_s)n}\right|^2, \tag{7.4}$$

where f_s is the sampling frequency and N_T is the number of samples in the time-series.

If $x(n)$ is weighted by a window $w(n) = \left[w(1), \ldots, w(N_T) \right]$, then a modified periodogram is produced as

$$\hat{S}_x(f) = \frac{1}{f_s} \frac{\left| \sum_{n=1}^{N_T} x(n) w(n) e^{-j(2\pi f / f_s)n} \right|^2}{\sum_{n=1}^{N_T} |w(n)|^2}, \tag{7.5}$$

whose characteristic high variance can be reduced by using Welch's method as in the following steps:

1. The time-series is divided into l overlapping segments of size *window*.
2. The modified periodogram of each segment is calculated.
3. The set of modified periodograms is averaged to produce $\hat{S}_x(f)$.

Figure 7.1 illustrates the power spectral density $\hat{S}_x(f)$ of a signal composed of a 200 Hz sinusoid and additive random noise (normally distributed with an amplitude equal to 10% the amplitude of the sinusoid): (a) depicts the estimation of $\hat{S}_x(f)$ by the modified periodogram and (b) depicts the estimation of $\hat{S}_x(f)$ by Welch's method (using a Hamming window of 128 samples in length and an overlap of 120 samples).

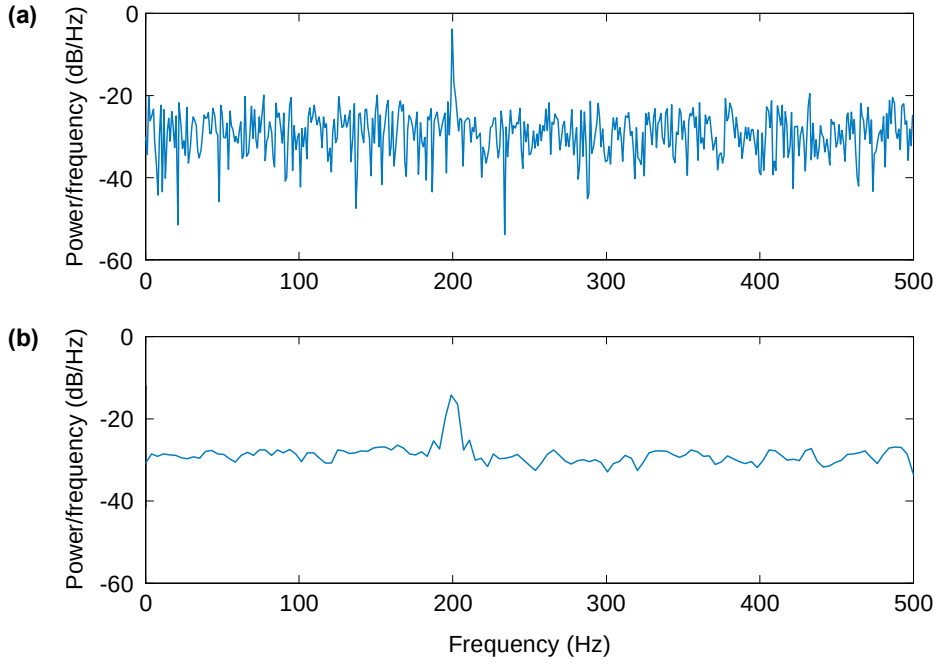

Figure 7.1. Power spectral density $\hat{S}_x(f)$ of a signal composed of a sinusoid and random noise: (a) estimation by using the modified periodogram and (b) estimation by using Welch's method.

The PSD analysis is widely used since it is easy to implement on a computer. Besides, when properly applied, it gives a good overview about the frequency content of a signal.

7.1.2. Entropy analysis: a measure of irregularity/complexity

Visual examination of signals' behaviour some times gives the observer an intuitive idea of their complexity. For instance, some signals show an extremely random behaviour (higher complexity) whilst other signals show regular patterns at different intervals (lower complexity) (Rezek and Roberts 1998). Frequently found in biological signals, such a complex behaviour has been widely studied from the perspective of dynamical systems and chaos theory, which has proven to be a powerful approach for studying biological systems (Eke *et al.* 2000; Pincus and Goldberger 1994; Richman and Moorman 2000). In the field of cardiovascular research, for instance, the degree of complexity/irregularity of a signal has been correlated with physiological conditions, which shows potential for this work (Dawes *et al.* 1992; Ferrario *et al.* 2006; Lipsitz *et al.* 1997; Nelson *et al.* 1998). Consequently, to consider this idea of complexity in a biological signal, the research in this chapter also explores a method referred to as sample entropy (SampEn), which uses the rate of generation of new information as an estimate of irregularity (Pincus and Goldberger 1994; Richman and Moorman 2000).

As part of the methods for entropy analysis, SampEn has the advantage of enhancing relevant features of a signal even though the amount of data is small (Ferrario *et al.* 2006; Pincus and Goldberger 1994; Richman and Moorman 2000). In addition, SampEn overcomes the characteristic shortcomings of its biased predecessor, approximate entropy (ApEn), which is highly dependent on the signal length as well as highly inconsistent across datasets (Pincus and Goldberger 1994; Richman and Moorman 2000). Thus, designed as an unbiased method by discarding all self-matches, SampEn can be consistently applied to short and noisy time-series like the ones used in this work (Comani *et al.* 2007; Richman and Moorman 2000).

SampEn quantifies the rate of generation of new information (*i.e.* irregularity) by looking for similar patterns in a time-series, $x(n)$. Thus, in a regular signal, which generates new information at lower rates than an irregular signal does, the presence of more frequent and similar patterns produces lower values of SampEn (Richman and Moorman 2000). In a formal description, SampEn uses the conditional probability that two sequences in the time-series, which are similar for m_s samples, remain similar for $m_s + 1$ samples (within a tolerance α) (Richman and Moorman 2000). This is further described in the next paragraphs.

SampEn requires two parameters to work: m_s, which specifies the pattern length and α, which defines the criterion of similarity between patterns. This information is used to build a subvector containing m_s consecutive values of $x(n)$. Such a vector, referred to as the pattern

$p_{m_s}(u)$, begins at the u^{th} position of $x(n)$ ($1 \le u \le N_T - m_s$). Next, similar patterns are searched by sliding $p_{m_s}(u)$ through the signal, where two patterns $p_{m_s}(u)$ and $p_{m_s}(v)$ will be considered similar whenever the difference between any pair of corresponding measurements is less than or equal to α as

$$\left| y(u+k) - y(v+k) \right| \le \alpha, \quad \text{for } 1 \le k \le m_s \quad \text{and} \quad u \ne v. \tag{7.6}$$

Now, by considering $P_{m_s} = \left\{ p_{m_s}(1), p_{m_s}(2), \ldots, p_{m_s}(N_T - m_s) \right\}$ as the set containing all the patterns of length m_s in $x(n)$, it is possible to define the quantity $C_u^{m_s}(\alpha)$ as

$$C_u^{m_s}(\alpha) = \frac{n_u^{m_s}(\alpha)}{N_T - m_s}, \tag{7.7}$$

where $n_u^{m_s}(\alpha)$ is the number of patterns in P_{m_s} that are similar to $p_{m_s}(u)$, and $C_u^{m_s}(\alpha)$ is the probability that two sequences will match for m_s samples in the set P_{m_s} (Comani *et al.* 2007; Richman and Moorman 2000).

Using Equation 7.7 it is suitable to define the probability, $C^{m_s}(\alpha)$, that any pattern $p_{m_s}(u)$ is within α of P_{m_s}

$$C^{m_s}(\alpha) = \frac{1}{N_T - m_s} \sum_{u=1}^{N_T - m_s} C_u^{m_s}(\alpha), \tag{7.8}$$

and finally calculate SampEn as (Comani *et al.* 2007)

$$\text{SampEn}(m_s, \alpha, N_T) = \ln\left(\frac{C^{m_s}}{C^{m_s+1}} \right), \tag{7.9}$$

where C^{m_s} / C^{m_s+1} represents the conditional probability that the patterns $p_{m_s}(u)$ and $p_{m_s}(v)$, which are similar for m_s points, remain similar within a tolerance α for m_s +1 points.

In this way, by discarding all self-matches, SampEn performs a more accurate (*i.e.* unbiased) and faster evaluation of the irregularity of short time-series than ApEp does (Richman and Moorman 2000). As a result, SampEn produces a single index that, being independent of the amplitude and frequency of the signal, is suitable for comparison of datasets (Rezek and Roberts 1998). Unfortunately, although SampEn gives a picture of the general behaviour of the time-series, it does not identify the dynamics of the underlying "signal generator" (Ferrario *et al.* 2006). In other words, the SampEn values of two signals will only reveal which signal is more regular, but they will not say anything about the signal "generators". Furthermore,

regarding Equation 7.9, it is important to highlight that, since SampEn does not consider self-matches, the occurrence of either ln(0) or ln(∞) is unavoidable and must be carefully interpreted. The former happens whenever no regularity is detected (*i.e.* $C^{m_s}(\alpha) = 0$) so that the conditional probability is zero. The latter happens when $C^{m_s+1}(\alpha) = 0$ and thus the conditional probability is infinite. In those cases SampEn will be undefined and, most importantly, meaningless. These possibilities must be taken into account when analysing time-series and interpreting their SampEn values.

7.1.3. Rhythmicity analysis: a measure of time-structure

Today, it is well known that biological phenomena like heart beat, breathing, locomotion, states of consciousness, bacterial protein synthesis, and photosynthesis (to mention a few) are regulated by rhythmic dynamical processes (Barman and Kenney 2007; Giebultowicz 2001; McAuley *et al.* 1997; Mor and Lev-Tov 2007; Vandenhouten *et al.* 2000). Clearly, this is fundamental for living systems since it makes it possible for them to adapt to changes of internal and external conditions, either by initiating/stopping or by accelerating/decelerating individual processes or subsystems (Barman and Kenney 2007; Vandenhouten *et al.* 2000).

As a consequence of such a rhythmic regulation, signals recorded from biological phenomena have time-structure (*i.e.* present rhythmic patterns or oscillations) that, depending on the underlying process, range from fractions of a second to days or even years (Barman and Kenney 2007; Huang *et al.* 2000; McAuley *et al.* 1997; Mor and Lev-Tov 2007; Vandenhouten *et al.* 2000). Therefore, since the time-structure of a signal is caused by underlying process(es), the analysis of its time-structure should provide information about such processes. To this end, and because the time-structure is observed through rhythmic patterns or oscillations, a measure of those oscillations disclose the processes underlying the signal (Barman and Kenney 2007; Giebultowicz 2001; McAuley *et al.* 1997; Mor and Lev-Tov 2007; Vandenhouten *et al.* 2000).

Time-series oscillations can be measured either in the time or frequency domains, the former by autocorrelation analysis and the latter by power spectral analysis (*i.e.* autospectrum) (Barman and Kenney 2007). Autocorrelation analysis quantifies the correlation between the same time-series at times n and $n + k_x$ for $k_x = 1,\ldots, N_T$. Thus, it provides a measure of how well a signal matches a time-shifted version of itself as a function of the time-lag k_x as

$$R^x_{k_x=1,\ldots,N_T} = \sum_{k_x=1}^{N_T} x(n)\,x(n+k_x), \tag{7.10}$$

where $R^x_{k_x}$ is referred to as the autocorrelogram of $x(n)$. In this way, even though the signal is contaminated by noise, the autocorrelogram conveys a good representation of the dependence structure of the time-series (*i.e.* its oscillations or rhythmic patterns) (Barman and Kenney 2007;

D'Urso and Maharaj 2009). Next, in a further processing step, the autocorrelogram can be transformed into the frequency domain so that the estimation of the oscillation(s) rate becomes easier from the resulting $\hat{S}_x(f)$ (also referred to as autospectrum) (Barman and Kenney 2007). Figure 7.2 depicts an example of a signal composed of three sinusoids oscillating at different amplitude and frequency, and the subsequent rhythmic patterns (*i.e.* oscillations) obtained in both (a) time and (b) frequency domains (Barman and Kenney 2007).

As can be seen in Figure 7.2, the rhythmic pattern in the form of $\hat{S}_x(f)$ makes it a lot easier to identify the oscillations present in the mixed signal. Indeed, in a more detailed observation of (b), is it suitable to establish not only the number of processes underlying the signal, but also their characteristics, which becomes promising for this work. Thus, the time-structure analysis clearly discloses the presence of three rhythmic processes, each one oscillating at different frequency and intensity (assuming one process per sinusoid).

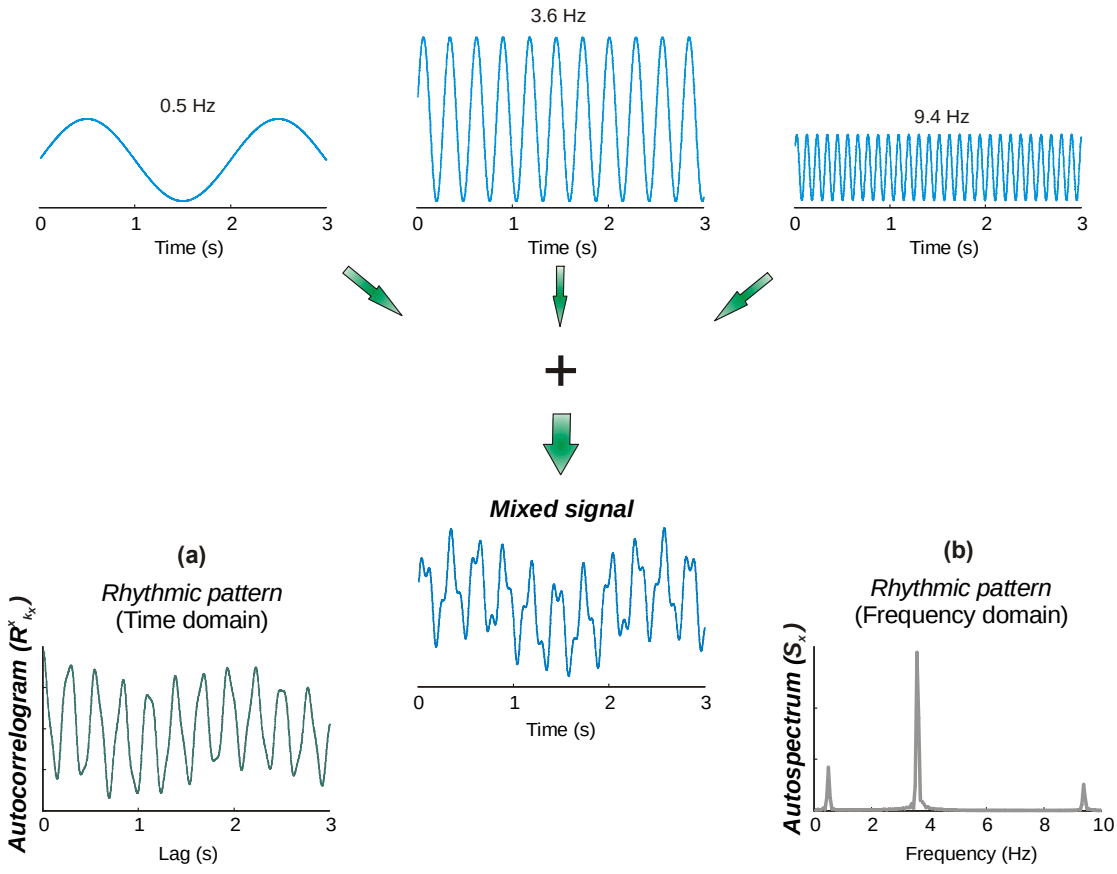

Figure 7.2. Rhythmic patterns (oscillations) obtained for a signal composed of three sinusoids oscillating at different amplitude and frequency (Barman and Kenney 2007). (a) Estimation in the time domain by the autocorrelogram ($R^x_{k_x}$) and (b) estimation in the frequency domain by the PSD ($\hat{S}_x$).

At this stage, this chapter has described four methods normally used to analyse physiological time-series. Amongst the many methods available for such an analysis, these four

were selected mainly because they study the signals from different points of view, which provide a wider perspective for studying the behaviour of the time-series. These methods, previously used to analyse some cardiovascular signals, have been applied to the study of the components underlying the abdominal phonogram for the first time in this work.

7.2. Measuring the components underlying the abdominal phonogram

This section details the practical application of the traditional, entropy, and rhythmicity analyses on the components separated from the abdominal phonogram by SCICA. First, some details about the construction of the dataset of separate components are presented, and then the preprocessing stage and the dataset analysis are described.

7.2.1. Constructing the components dataset

The twenty five signals in the dataset of abdominal phonograms have been processed by using a slight modification of the methodology described in Chapter 6. In this modification, the abdominal phonogram is fragmented into overlapped segments rather than in non-overlapped segments. Such an overlapping, which consists of 50% of the segment, does not have any effect on the stage for separating components, and will be useful for reconstructing the entire time-series later on, in Chapter 10.

To recall the procedure followed by SCICA, Figure 7.3 illustrates the methodology for extracting the one-dimensional components underlying the abdominal phonogram (IC^i_p).

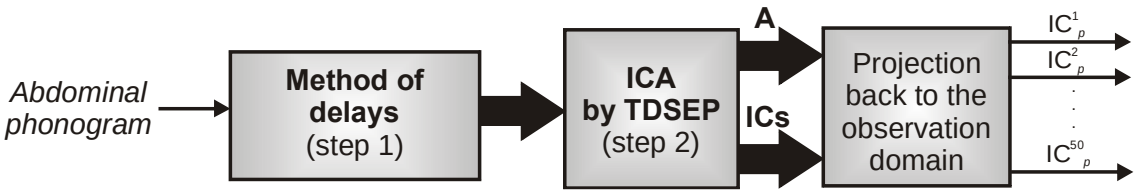

Figure 7.3. Methodology for extracting one-dimensional components (IC^i_p) underlying the abdominal phonogram by using SCICA (steps 1 and 2). The second step is implemented by TDSEP because it produces components whose spectra present a single and well-defined peak (Jimenez-Gonzalez and James 2008).

This methodology has been applied to the dataset of abdominal phonograms described in Chapter 5. As a result, a number of one-dimensional components (10 s in length) is available for the analysis described in this chapter, which would be too much data to be presented in this thesis. Alternatively, to ease the analysis, only three segments per phonogram are used: one at the beginning, one in the middle, and one at the end of each recording. In this way, the dataset

of separate components to be analysed in this chapter was constructed by using 75 segments of abdominal phonograms that, producing 50 components per segment (as shown in Figure 7.3), ended up with a total of 3,750 one-dimensional components.

7.2.2. Preprocessing components

This stage is required only for the analysis of rhythmicity, and its purpose is enhancing the time-structure of the IC_ps, which is achieved as follows:

a) Envelope generation: This is performed by using the Hilbert Transform ($H[\cdot]$), a method that has been successfully applied to narrowband signals where the envelope, $e(n)$, is slow compared to the temporal variations of the signal (*e.g.* the heart sounds) (Choi and Jiang 2008; Godinez *et al.* 2003; Xu *et al.* 2000). Thus, $e(n)$ is calculated from the analytical form, $x_a(n)$, of the signal under analysis $x(n)$ as

$$x_a(n) = x(n) + jH\left[x(n)\right] = e(n)\exp\left(j\varphi(n)\right), \tag{7.11}$$

where $H[\cdot]$ represents the Hilbert Transform given by

$$H\left[x(n)\right] = x(n) * \frac{1}{\pi n}, \tag{7.12}$$

and,

$$e(n) = \sqrt{x(n)^2 + H\left[x(n)\right]^2}, \tag{7.13}$$

$$\varphi(n) = \tan^{-1}\left(\frac{H\left[x(n)\right]}{x(n)}\right). \tag{7.14}$$

b) Detrend: This removes the linear trend in $e(n)$ to reduce its influence on further calculations.

7.2.3. Processing components

The components extracted from each segment of abdominal phonogram are processed by the methods earlier described according to the specific parameters indicated herein. The result, as illustrated in Figure 7.4, is a set of features corresponding to:

a) Descriptive analysis: To calculate the mean (μ), standard deviation (σ), and skewness (γ) of the IC_p.

b) Spectral analysis (S_I): Implemented by the Welch's method, it makes use of a Hanning window of 32 coefficients of length and an overlap of 50% (Jimenez-Gonzalez and James 2008; Jiménez-González and James 2009). Next, from the characteristic single-peak in $\hat{S}_x$

(Jimenez-Gonzalez and James 2008), its central frequency (S_I) is used as the index to represent the frequency content of the IC_p as

$$S_I = \arg_f \max \hat{S}_x(f). \tag{7.15}$$

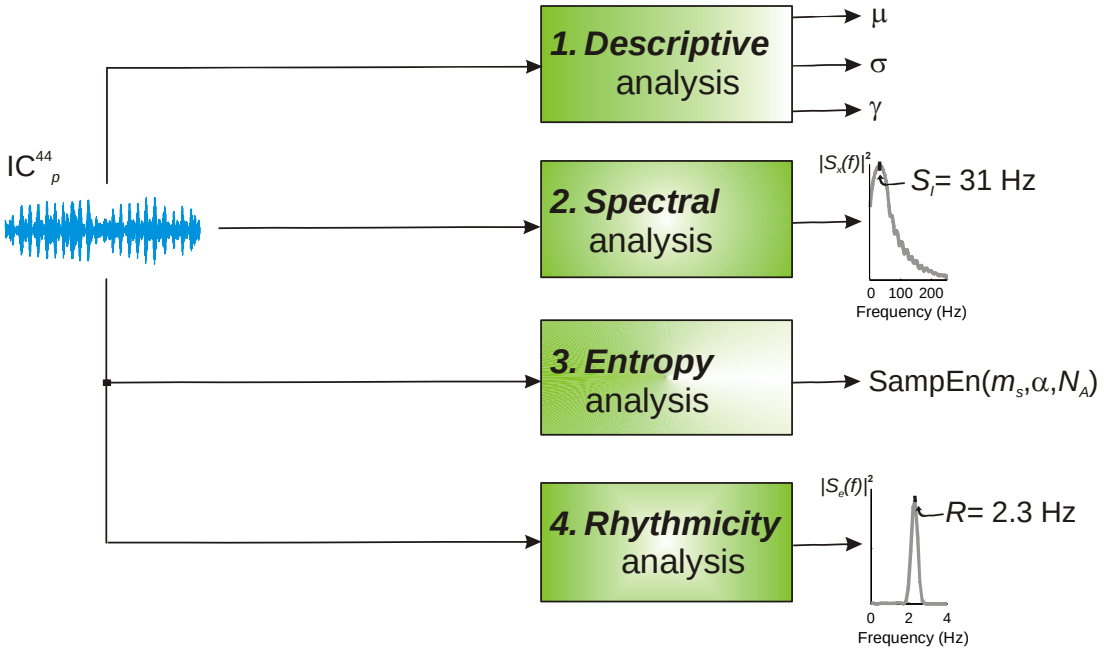

Figure 7.4. Methods used to analyse components separated from the abdominal phonogram. Each method analyses the time-series from a different point of view and provides information about: time statistics (mean μ, standard deviation σ, and skewness γ), frequency content (S_I), complexity (SampEn), and time-structure (R).

c) Entropy analysis (SampEn): Implemented by Sample Entropy (Richman and Moorman 2000), it uses a pattern length of one sample (m_s= 1), a criterion of similarity equal to 0.2 times the standard deviation of the IC_p, *i.e.* α= 0.2·std(IC_p), and a time-series length given by the length of the IC_p, which is therefore defined by N_A, *i.e.* 5000 samples. The former two parameters were already used by Comani *et al.* (2007) to perform a sample-by-sample analysis of independent components extracted from the FMCG.

d) Rhythmicity analysis (R): After preprocessing the IC_ps to generate a detrended $e(n)$, the autocorrelogram of such an envelope is calculated as

$$R^e_{k_e=1,\ldots,N_A} = \sum_{k_e=1}^{N_A} e(n)\,e(n-k_e) \tag{7.16}$$

and transformed to the frequency domain using the Welch's periodogram to produce $\hat{S}_e(f)$. In particular, due to the interest in the cardiac activity (which generates the HS), the length of the window is chosen to enclose a suitable amount of information from the two possible

processes, maternal and/or foetal. Thus, a *window* size of 2048 samples (~ 4 s since the signals were sampled at 500 Hz) is used to include an average of four maternal and/or eight foetal heart beats. Finally, from the resulting $\hat{S}_e$, the frequency of the largest peak is taken as the measure of rhythmicity[1], *i.e.* R.

Figure 7.5 and Figure 7.6 depict a set of 50 IC_ps extracted by SCICA from one segment of abdominal phonogram (25 components per figure) and the measures obtained when analysed by using the methods described in this chapter. In Figure 7.5, from top to bottom, a segment of abdominal phonogram and its first 25 one-dimensional components separated by SCICA (*i.e.* from IC^1_p to IC^{25}_p). In Figure 7.6, from top to bottom, the same segment of abdominal phonogram and its last 25 one-dimensional components separated by SCICA (*i.e.* from IC^{26}_p to IC^{50}_p). In both figures, on the right-hand side of each IC_p, the information provided by the four methods of analysis considered in this chapter: descriptive, spectral, entropy, and rhythmicity.

Visual examination of Figure 7.5 and Figure 7.6 reveals some aspects about the time-series and their measured features: firstly, that in the abdominal phonogram it is possible to distinguish a slow component and some peaks (indicated by red upwards arrows), but not the FHS. Secondly, that the first 40 IC_ps show some spontaneous but unrecognisable activities, whereas the last 10 IC_ps show some periodic information that alternates (1) at more than two times per second (*e.g.* IC^{44}_p), (2) at more than one time per second (*e.g.* IC^{49}_p), (3) or much less than that (IC^{50}_p). Thirdly, that the amplitude of the last IC_ps is larger than the amplitude of the first IC_ps.

Regarding the features, it can be seen that, whilst the entropy directly produces a single value, the other methods generate a waveform (*i.e.* a pattern) from where specific measurements are taken in this work. Additionally, in a more detailed examination of such patterns, it can be seen that the histogram usually presents a unimodal distribution, although there is a possibility that it shows a bimodal distribution as in IC^{50}_p. The $\hat{S}_x$ patterns, on the other hand, consistently produce a single and well defined peak (from where S_I is easily taken), whereas the $\hat{S}_e$ patterns may produce many peaks of which only the largest one is chosen to quantify R. Furthermore, a closer observation of those measurements shows that those corresponding to S_I, SampEn, and R change from IC_p-to-IC_p, whereas σ and γ seem to remain similar[2] (except for IC^{50}_p, whose γ is higher than the skewness of the other components by one order of magnitude).

[1] Note that in this work the term "rhythmicity" is being used as a measure of the frequency of the rhythm in a signal. I should not be understood as a measure of how rhythmic the signal is.

[2] The value of μ has been excluded because it is zero by construction in ICA (Hyvarinen *et al*. 2001).

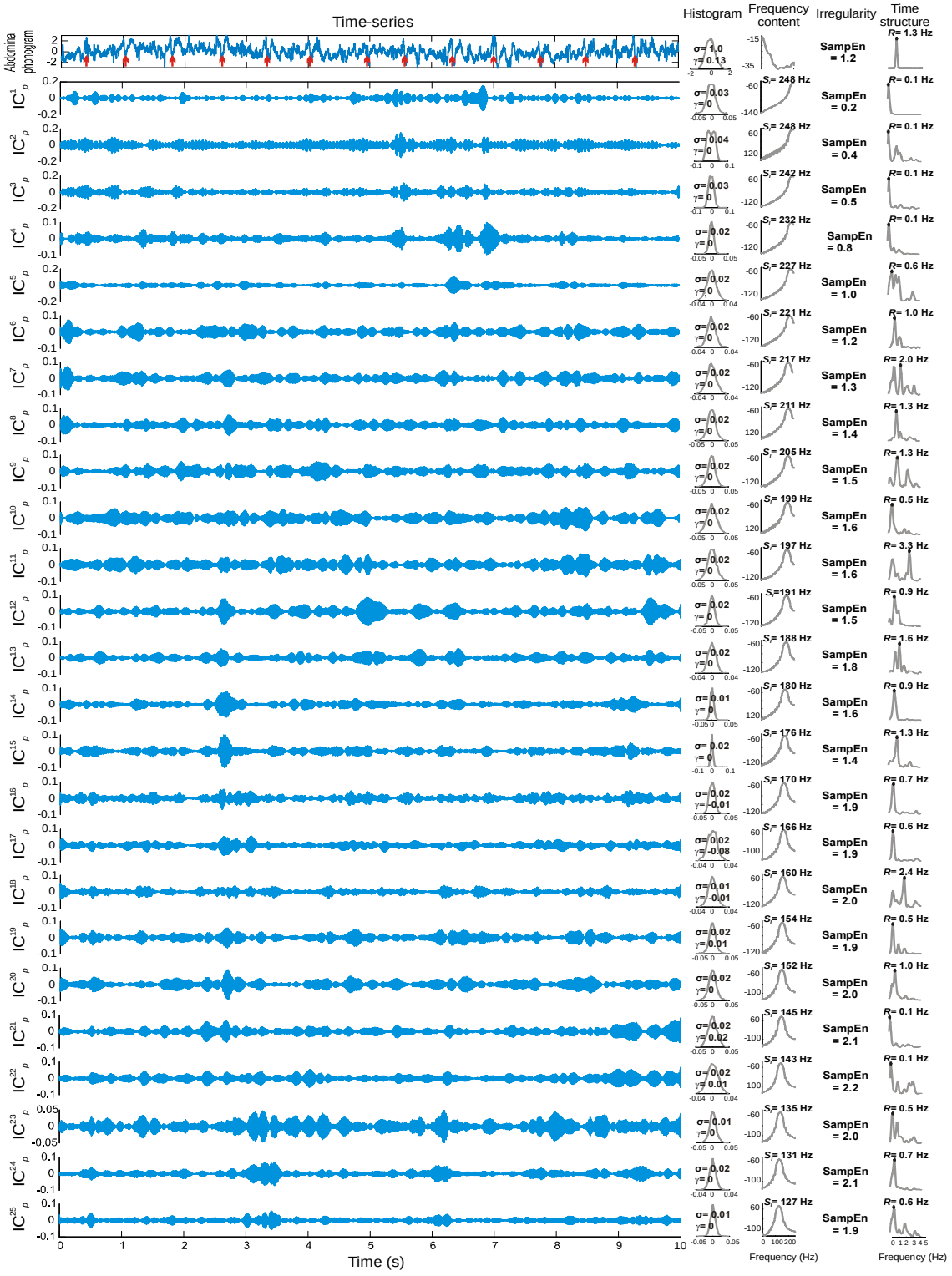

Figure 7.5. Example of the first 25 one-dimensional components underlying an abdominal phonogram segment along with the features measured by using descriptive, spectral, entropy, and rhythmicity analyses. From left to right: the time-series, the histogram with its statistics (standard deviation σ, and skewness γ), $\hat{S}_x$ with the frequency of its characteristic single-peak (S_I), the irregularity value (SampEn), and $\hat{S}_e$ with its rhythmicity value (R) –which is taken from the largest peak–. From top to bottom: a segment of abdominal phonogram (10 s in length) and 25 of its 50 one-dimensional components (*i.e.* from $IC^1{}_p$ to $IC^{25}{}_p$). The mean value, μ, has been deleted from the histograms because it is zero by construction in ICA (Hyvarinen and Oja 2000).

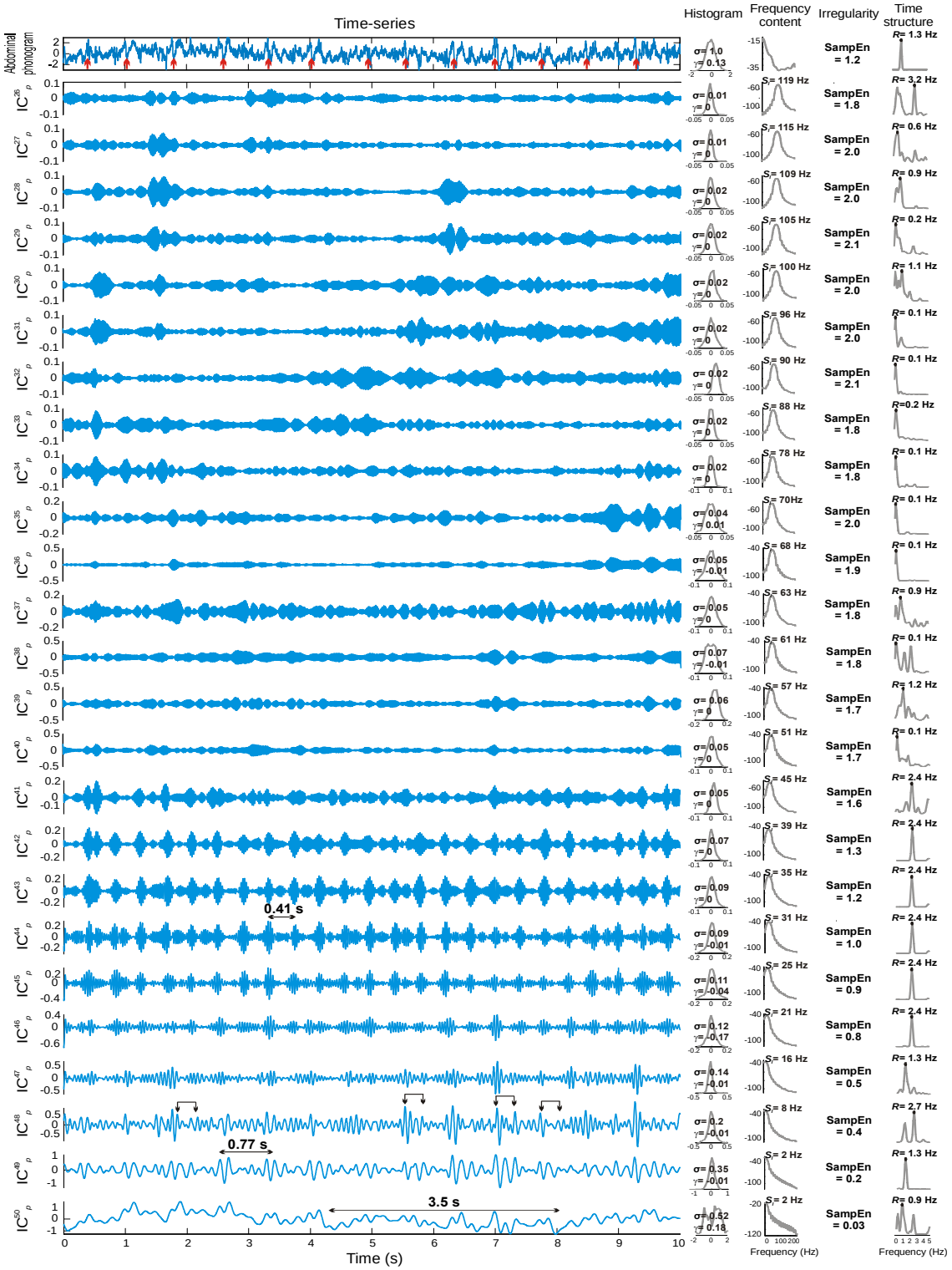

Figure 7.6. Example of the last 25 one-dimensional components underlying an abdominal phonogram segment along with the features measured by using descriptive, spectral, entropy, and rhythmicity analyses. From left to right: the time-series, the histogram with its statistics (standard deviation σ, and skewness γ), $\hat{S}_x$ with the frequency of its characteristic single-peak (S_I), the irregularity value (SampEn), and $\hat{S}_e$ with its rhythmicity value (R) –which is taken from the largest peak–. From top to bottom: a segment of abdominal phonogram (10 s in length) and 25 of its 50 one-dimensional components (*i.e.* from $IC^{26}{}_p$ to $IC^{50}{}_p$). The mean value, μ, has been deleted from the histograms because it is zero by construction in ICA (Hyvarinen and Oja 2000).

This behaviour is more evident in Figure 7.7, where the features obtained from each IC_p are depicted (except for the descriptive measurements, which were discarded for the reason previously expressed).

As can be seen in Figure 7.7, S_I and SampEn clearly show a particular tendency. In (a), it is manifest that the S_I of each component (except for the first and last couples) consistently decreases as long as i increases (i= 1,…,50). In (b), the SampEn reveals different levels of irregularity in the IC_ps and, most interesting, some similarities in the degree of regularity between the first and last IC_ps (*i.e.* a symmetric behaviour). Hence, according to SampEn, the most regular components are located both, at the beginning and at the end of the sequence of IC_ps, whereas the less regular –or more complex components– are located in the middle. In (c), where the rhythmicity is shown, finding a trend is a bit difficult at first sight, especially after the evident tendencies shown in (a) and (b). In despite of this, focusing on the last ten IC_ps, it is possible to see that (1) from IC^{41}_p to IC^{46}_p, the rhythmicity value is 2.4 Hz and (2) for IC^{47}_p and IC^{49}_p, the rhythmicity value is 1.3 Hz. Regarding the other components, their rhythmicity is between 0.1 and 0.2 Hz.

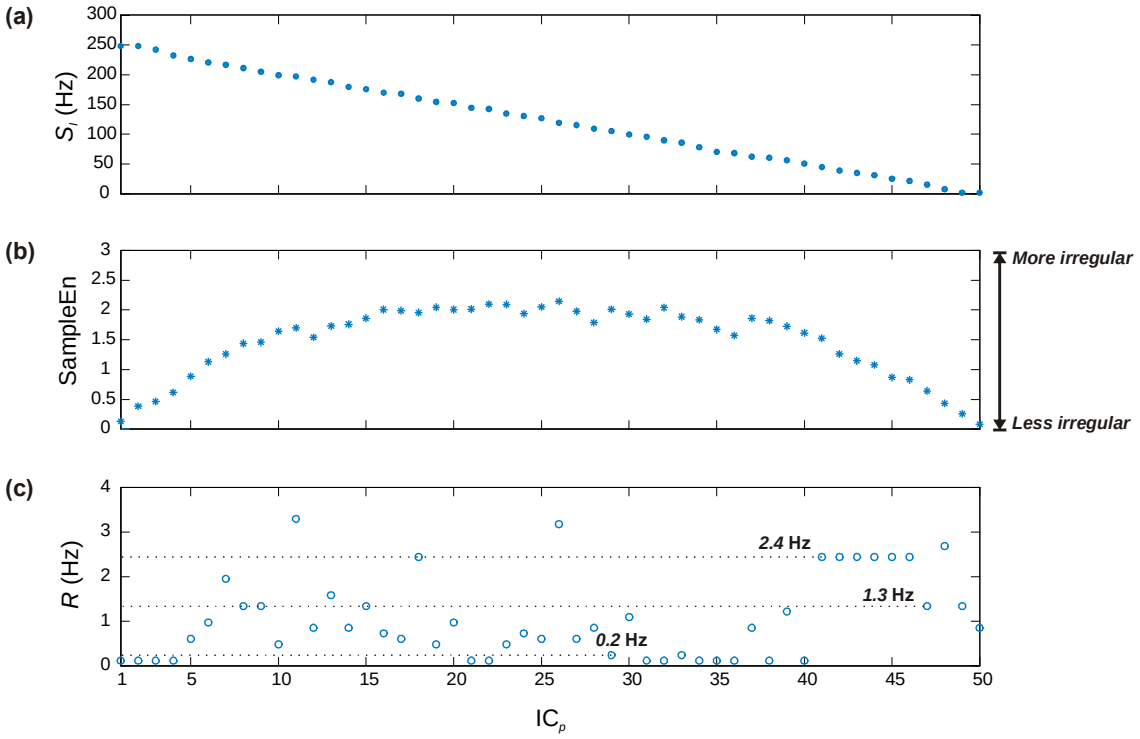

Figure 7.7. Behaviour of the features measured from the set of IC_ps underlying an abdominal phonogram segment: (a) the frequency content by S_I, (b) the irregularity by SampEn, and (c) the time-structure by R.

Figure 7.8 depicts the features as a function of S_I. In (a), the amplitude of the power spectrum at S_I (*i.e.* the amplitude of the peak in the $\hat{S}_x$ pattern, aS_I) versus S_I is shown, in (b),

SampEn versus S_I is depicted, and finally, (c), illustrates the rhythmicity versus S_I. As shown by the grey areas, some regions in (a) and (b) present interesting behaviours as a function of S_I. In (a), two groups of IC_ps have larger power, those with the lowest and those with the highest frequencies, which are also the last and first components in the sequence of IC_ps respectively. In (b), the same two groups are clearly more regular than the other components. Conversely, in (c), such two groups are not evident, although the rhythms at 1.3 and 2.4 Hz mentioned in Figure 7.7 (c) are clearly located in the region where the slowest components are found, which means that they correspond to the last IC_ps in the sequence. Regarding the rhythm at 0.2 Hz, it appears in both the medium high and high frequency ranges (*i.e.* in the medium fast and the fastest components).

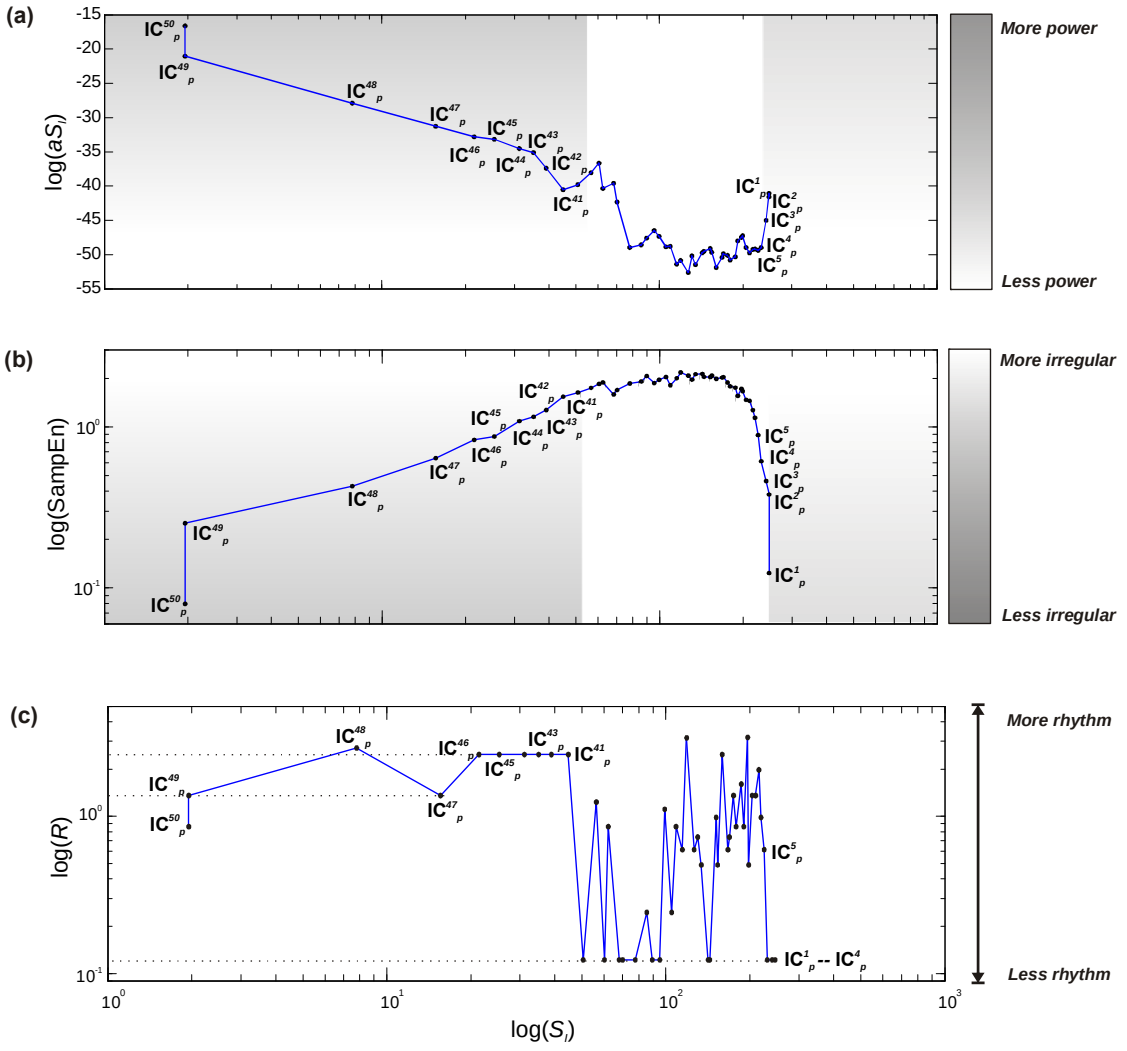

Figure 7.8. Dependence of features on S_I (*in log-log coordinates*) measured from the set of IC_ps underlying an abdominal phonogram segment: (a) the amplitude of the peak in the $\hat{S}_x$ pattern versus S_I, (b) the SampEn versus S_I, and (c) the rhythmicity versus S_I. The grey areas mark the regions where the features show some correlation with S_I.

So far, only the features obtained from the set of IC_ps of *a single* abdominal phonogram segment have been presented. This has made it easier to observe their behaviour along components and detect some trends or particular characteristics, although the reader could be already wondering whether such a behaviour remains throughout the whole dataset. This is answered in Figure 7.9, which illustrates the typical tendencies and dependences of S_I and SampEn all through the dataset used in this chapter (R is not included since currently it is difficult to see any trend due to multiple variations in its value). As can be seen, both S_I and SampEn keep their tendencies throughout the dataset.

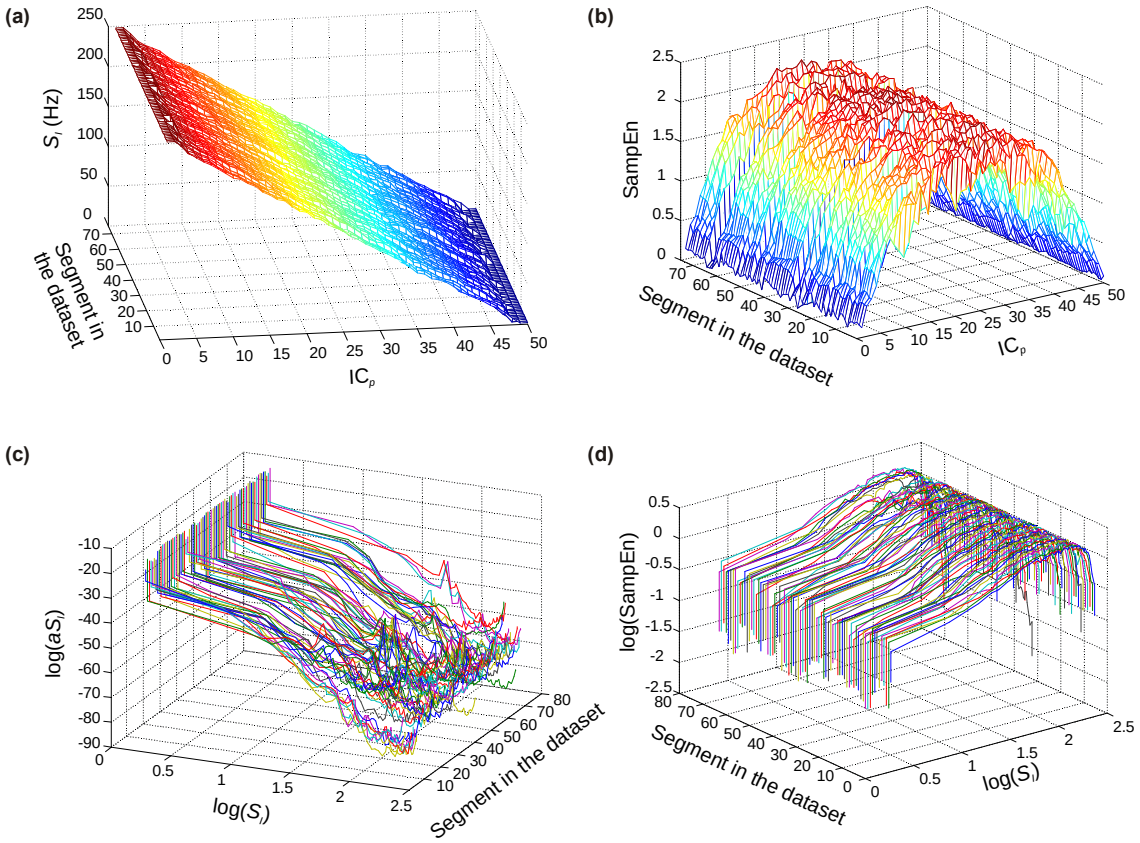

Figure 7.9. Typical tendencies and dependencies of S_I and SampEn throughout the whole dataset of components: (a) frequency content by S_I, (b) irregularity by SampEn, (c) aS_I versus S_I, and (d) SampEn versus S_I.

7.3. Analysis of physiological relevance

In the previous section, IC_ps features were obtained using methods that analyse time-series from different points of view such as statistical, spectral, complexity, and time-structure. By themselves, the features obtained by the latter three methods show not only consistent, but also interesting behaviours along the IC_ps dataset. This is an important step towards the comprehension of the IC_ps since it provides quantitative information about different aspects of the time-series (*i.e.* the frequency content, irregularity, and rhythmicity). For the next step, this

section analyses such information (both individually and as a whole) in order to establish their physiological relevance and then, the potential meaning of the IC_ps that underlie the abdominal phonogram.

7.3.1. The waveforms or patterns

As seen in Figure 7.5 and Figure 7.6, only the waveforms of the last ten IC_ps consistently show periodic information. Indeed, according to the intervals measured in such time-series, this information oscillates at: (1) ~2.5 Hz from $IC^{41}{}_p$ to $IC^{46}{}_p$, which is in the interval reported for the foetal heart rate (Guijarro-Berdinas *et al.* 2002), (2) ~1.3 Hz from $IC^{47}{}_p$ to $IC^{49}{}_p$, which is in the interval reported for the maternal heart rate (Ogueh *et al.* 2009), and (3) ~0.28 Hz in $IC^{50}{}_p$, which is in the interval reported for the maternal breathing (van Leeuwen *et al.* 2009). Therefore, based on this visual examination of the *evident periodic information* in the time-series, it is possible to say that, at least, there are three physiological rhythms in the "last" IC_ps separated from the abdominal phonogram that are more likely to correspond to: the maternal breathing rate (R_{MB}), the maternal heart rate (R_{MH}), and the foetal heart rate (R_{FH}). From now on, this *a priori* knowledge will be used to give the calculated features a physiological interpretation and thus, to study the IC_ps.

Further considering Figure 7.5 and Figure 7.6, and focusing on the waveforms or patterns from where the features are measured, a profound difference between the waveforms produced by $\hat{S}_x(f)$ and $\hat{S}_e(f)$ is noticed, which is the number of peaks. In $\hat{S}_x(f)$, due to the band-limited filters learnt by ICA (Jimenez-Gonzalez and James 2008), there is always a single-peak that makes it easier to measure S_I. In $\hat{S}_e(f)$, multiple peaks might be present and make it necessary to choose the largest peak to measure R, which might not be the best strategy. Indeed, a closer inspection of $IC^{50}{}_p$, $IC^{48}{}_p$, and $IC^{38}{}_p$, for instance, makes it possible to see that their $\hat{S}_e$ patterns also have peaks centred at 0.24 and 2.6 Hz in $IC^{50}{}_p$, at 1.3 Hz in $IC^{48}{}_p$, and at 1.4 and 2.4 Hz in $IC^{38}{}_p$, which are values more consistent with the rhythms measured from the last ten IC_ps (*i.e.* R_{MB}, R_{MH}, and R_{FH}). Furthermore, $IC^{48}{}_p$ shows an interesting pattern where the rhythm of the largest peak (2.7 Hz) is twice the rhythm of the smaller peak (1.3 Hz). Another interesting pattern appears in those components where the largest peak is centred at a very low rate (0.1-0.2 Hz) and whose amplitude is so large that makes the contribution of other rhythms look insignificant (*e.g.* first IC_ps and those from $IC^{31}{}_p$ to $IC^{36}{}_p$).

From these observations, it is clear that the multi-peak pattern in $\hat{S}_e$ currently affects the measuring of R and distorts the time-structure results, which would not be an issue if such a pattern were an isolated case. Unfortunately, as shown in Figure 7.5 and Figure 7.6, this pattern appears so frequently that the measured R presents behaviours that are difficult to interpret, like the one in Figure 7.7 (c). This means that, before having a final, and perhaps wrong, opinion

about the time-structure analysis, this multi-peak pattern must be carefully analysed so that the circumstances that give rise to an incorrect measurement of R are understood and then, a more reliable way to measure R in $\hat{S}_e$ can be proposed.

First of all, a multi-peak pattern in $\hat{S}_e$ means that more than one rhythm is present in the IC_p, *i.e.* that a complete separation was not reached by SCICA. As a first impression, this result might seem to conflict the former affirmation in Chapter 6 that SCICA learns a set of band-limited filters, which would be a wrong interpretation. In fact, from these results it is possible to better understand what SCICA does when processes the abdominal phonogram. Hence, after carefully considering these results, it is possible to infer that, although SCICA successfully learns a set of filters to separate a signal into disjoint spectral components (Davies and James 2007), it may fail to separate the physiological rhythms underlying the abdominal phonogram (which happens whenever the signals regulated by such rhythms do not have disjoint spectral support).

In other words, *independent components by SCICA do not always mean independent physiological components in the abdominal phonogram*. This is an interesting finding regarding SCICA performance that must be taken into account from now on when referring to the "independent components" separated by this signal processing approach.

Now it is time to have a detailed look at the multi-peak patterns, not in terms of the separation quality (*i.e.* the method), but in terms of the physiological evidence provided by them (*i.e.* the underlying generator). To this end, this discussion will be based again on Figure 7.5 and Figure 7.6 results, where three physiological rhythms have been clearly identified: a slower rhythm at 0.2 Hz given by R_{MB}, a middle rhythm at 1.3 Hz given by R_{MH}, and a faster rhythm at 2.4 Hz given by R_{FH}. Ideally, as these rhythms contribute to the IC_p with different rate and power, they should not have any effect on each other. Hence, there should be reliable to identify the dominant rhythm (previously referred as R) only by looking for the one whose power overrules the power of other rhythms. However, in real world signals, where harmonic frequencies exist, such a dominant rhythm might be the result of either (a) an actual physiological rhythm or (b) another rhythm (whose larger power was coincidentally produced by the contribution of some harmonic information). Here, such harmonic information comes from the physiological rhythms given by R_{MB}, R_{MH}, and R_{FH}, whose harmonics do not affect each other all the time. However, as it is still possible to have a pseudo-dominant rhythm, it is necessary to know the cases that produce it and, whenever possible, prevent its occurrence (as described in the next chapter).

a) Harmonics from R_{MB}: Possessing the slowest rhythm, this is the one whose harmonics cover the broadest range. As a result, the breathing harmonics may add power to a cardiac

rhythm (either maternal or foetal), fake its contribution to the IC_p, and thus wrongly point at it as R (a potential situation when the power of R_{MH} and R_{FH} is similar).

b) Harmonics from R_{MH}: This rhythm may add its harmonic power to R_{FH} making it incorrectly look as R (a situation only possible whenever the maternal heart rate is half the foetal rate which, although rarely, may happen).

c) Harmonics by S1-S2: This is a very exceptional case that, as far as this study goes, only happens in those IC_ps that perfectly enclose the pair of heart sounds S1 and S2. Indeed, as observed during this study, the occurrence of these two events at every heart beat produces a double-rhythm (*i.e.* composed of two rates) rather than a single-rhythm, one centred at the heart rate (R_{HR}, either maternal or foetal) and another at twice this value ($2R_{HR}$). This behaviour, although physiologically interesting, affects the measurement of R since the harmonic power of R_{HR} certainly increases the power at $2R_{HR}$. As a result, the rhythm at $2R_{HR}$ becomes a pseudo R and, consequently, a maternal IC_p containing S1-S2 would erroneously "produce" a foetal rhythm, whereas a foetal IC_p containing S1-S2 (*i.e.* the main FHS) would "produce" a rhythm out of the normal physiological range. This may explain what happened in IC^{48}_p, where the rate calculated directly from the time-series (~1.3 Hz) differs with the rhythm measured by R in $\hat{S}_e$ (2.7 Hz). After knowing this result, and by carefully observing the time-series in IC^{48}_p, some double-oscillations can be noticed (as indicated by downwards arrows in Figure 7.6).

In summary, it can be said that, as soon as the harmonic effect is reduced[3] to properly measure and interpret R, *the time-structure analysis* provides a valuable feature that, as expected, conclusively *reveals the physiological process(es)* that generated the IC_p (*e.g.* maternal breathing activity, maternal cardiac activity or foetal cardiac activity). Also important, and unanticipated, (1) in those IC_ps generated by a cardiac process, *R may also reveal the presence of the pair S1-S2* and (2) it has made it possible to interpret the degree of independence amongst the components in *a physiological sense.*

7.3.2. The measured features

Once the physiological origin of some components has been established by both visual and time-structure analyses, it is suitable to say that, in the sets of IC_ps depicted in Figure 7.5 and Figure 7.6, those components from IC^{41}_p to IC^{46}_p are generated by the foetal cardiac activity, those from IC^{47}_p to IC^{49}_p are generated by the maternal cardiac activity, and that IC^{50}_p contains a

[3] For practical purposes, this discussion assumes that the harmonic effect has been somehow reduced so that R is reliably measured. The solution to this problem requires some extra pre-processing that will be presented in the next chapter.

mixture of breathing and cardiac activities. The other IC_ps, however, cannot be definitely interpreted without first considering the tendencies of the features given by the frequency content and irregularity.

a) Regularity: As seen in Figure 7.7 (b), SampEn shows a trend where the less regular components are clearly positioned in the middle of the sequence of IC_ps, whereas the most regular are at the beginning and ending of it. This means that the IC_ps in the middle of the sequence are more complex time-series and therefore closer to noise (or perhaps only noisier) than the other IC_ps. To see whether such IC_ps are noise, or only contaminated by noise, the time-structure becomes a helpful feature that, as shown in Figure 7.5 and Figure 7.6, detects one or more rhythms in the components (although some of them are currently unidentified). According to this, those IC_ps are not pure noise, but rhythmic components contaminated by such an amount of noise that they become less regular than, for instance, the last IC_ps. This can be confirmed by looking at the time-series in Figure 7.5 and Figure 7.6 where, whilst it is virtually impossible to visually identify physiological information in the component with the largest SampEn value ($IC^{24}{}_p$), it is easier to do so in the component with the smallest value ($IC^{50}{}_p$). Such an interesting behaviour is seen in Figure 7.8 (b) where, in addition, the correlation between the SampEn and S_I shows that the more regular IC_ps are also those components with the lowest and highest frequency contents.

Thus, as confirmed by Figure 7.9 (cases (b) and (d)), the *entropy analysis* consistently shows that (independently on the segment/subject in the dataset), amongst the 50 IC_ps extracted by SCICA from one segment, the information of those components in the middle of the sequence is mostly noise, whereas the information in the first and last IC_ps is less noisy. Furthermore, by taking into account the former observations it can be said that, amongst such highly regular components, the last IC_ps are the components whose information is more likely to be physiological and, most importantly, strongly related to maternal and foetal processes of interest (whereas the first IC_ps might be related to some unidentified regular processes). In other words, according to the entropy analysis, *only a few regular* IC_ps *in the sequence are more likely to be useful to reconstruct the physiological independent sources underlying the abdominal phonogram*.

b) Frequency content: As can be seen in Figure 7.7 (a), every IC_p (except the first and last two) has a different S_I value, which has been previously explained as the consequence of the band-limited set of filters learnt by SCICA. More interesting, and completely unexpected, is to see that the IC_ps extracted by SCICA are consistently sorted from the highest to the lowest frequency, as confirmed by Figure 7.9 (a). Moreover, as shown in Figure 7.8 (a) and confirmed by Figure 7.9 (c), such highest and lowest frequencies belong

to the first and last components in the sequence respectively. Hence, *the spectral analysis* shows that SCICA *sorts the separate components by frequency content*, where IC^{1}_{p} and IC^{50}_{p} have the highest and lowest frequencies respectively.

According to these results, and recalling that the most regular-physiological components of interest are at the end of the sequence of IC_ps, then the physiological IC_ps are also the components with the lowest central frequency S_I. Regarding the first IC_ps, also regular as indicated by SampEn, but with an origin currently unknown, they have been temporary discarded until further research reveals whether they belong to a physiological process useful for foetal surveillance purposes or otherwise.

Thus, according to the spectral analysis, *only the slowest IC_ps in the sequence are more likely to be usable to reconstruct the physiological independent sources*.

7.3.3. The performance of SCICA

After focusing attention on understanding the information in the IC_ps, now it is time to go through the results about how SCICA is working when decomposing the abdominal phonogram dataset. As mentioned in Section 6.3.1, one of the most important ambiguities of ICA is the uncertainty about how it will arrange the components at the output (Hyvarinen *et al.* 2001; Hyvarinen and Oja 2000; Stone 2004). Here, contrary to expectation, SCICA consistently sorts the IC_ps by frequency content from the highest to the lowest frequencies, where the slowest IC_ps tend to be the physiological components of interest. Also, in such an interesting trend it has also been seen that the first and last couples of IC_ps (outer frequencies) have the same S_I value. Here both situations will be analysed:

a) Ranking by frequency: To understand this behaviour, it is necessary to recall a couple of details about the methodology used to extract the components underlying the abdominal phonogram. First of all, as shown in Figure 7.3, TDSEP is the ICA implementation used to separate the IC_ps since it produces components with disjoint spectral support (Jimenez-Gonzalez and James 2008). Second, as highlighted in Section 6.2.2, the implementation of TDSEP used in this research works on a stack of only two time-lagged correlation matrices (*i.e.* $R^{\mathbf{v}}_{k_{\mathbf{v}}=0}$ and $R^{\mathbf{v}}_{k_{\mathbf{v}}=1}$), which is a very special case of TDSEP (Ziehe *et al.* 2000).

In general, as proposed by Ziehe and Muller (1998) and Ziehe *et al.* (2000), TDSEP estimates the mixing matrix **A** by jointly diagonalising the time-lagged correlation matrices in two combined steps as

$$\mathbf{A} = \mathcal{W}^{-1}\mathbf{Q}, \tag{7.17}$$

where $\mathcal{W}$ is a whitening transformation of **v**. This step produces a transformed dataset, **z**= $\mathcal{W}$ **v**, from where $R^{\mathbf{z}}_{k_z=1}$ can be exactly diagonalised by a unique orthogonal transformation **Q** (*i.e.* the temporal correlation is minimised by a rotation matrix such that $\mathbf{QQ}^T = \mathbf{I}$) (Ziehe *et al.* 2000).

In particular, for the case considered in this research, where *only two matrices are diagonalised*, **Q** is obtained by the eigenvalue decomposition of $R^{\mathbf{z}}_{k_z=1}$, which turns out to be a *spectral decomposition* given by

$$R^{\mathbf{z}}_{k_z=1} = \mathbf{Q}^T R^{\mathbf{z}}_{k_z=1} \mathbf{Q} = \mathbf{Q}^T \Lambda_{k_z=1} \mathbf{Q} \,. \tag{7.18}$$

where (1) the eigenvalues ($\Lambda_{k_z=1}$) equal the largest possible variances of the projections of **z** on the eigenvectors of $R^{\mathbf{z}}_{k_z=1}$ (**Q**), (2) the direction of the largest variance of a projection of **z** is defined by the eigenvector associated to the largest eigenvalue of $R^{\mathbf{z}}_{k_z=1}$, and (3) the projections of **z** onto the eigenvectors are uncorrelated.

In practical terms, a detailed study of the code created in MATLAB by Ziehe *et al.* (1998) showed that the eigenvalue decomposition in Equation 7.18 is implemented using a built-in function (EIG.m). Furthermore, EIG utilises the DSYEV Fortran sub-routine that –found in LAPACK (Linear Algebra PACKage) (LAPACK 2006)–, is an algorithm that always returns the eigenvalues in ascending order. Thus, since the eigenvectors in **Q** follow the order given by the eigenvalues in $\Lambda_{k_z=1}$, the column vectors in the mixing matrix **A** at Equation 7.17 follow the same order (*i.e.* the first column is associated to the smallest eigenvalue whilst the last column is associated to the largest eigenvalue). Moreover, since an eigenvalue reflects the largest possible variance of a projection, the columns in **A** are sorted according to such projections, therefore ranked from the projection with the smallest variance to the projection with the largest variance.

Thus, as depicted in Figure 7.10, the fastest components, whose information contributes the less to the variance, are more likely to be noisy IC_ps. Conversely, the slowest components, whose information contributes the most to the variance, are more likely to be physiological IC_ps and, most importantly, correspond to the processes of interest in this research. In other words, when applied to the abdominal phonogram, the spectral decomposition given by SCICA returns a set of spectrally disjoint components that are sorted depending on the energy of the underlying process that produced them. As a result, from the first to the last, the IC_ps are arranged as (1) noisy activity (that could be regular information buried in

noise), (2) foetal cardiac activity, (3) maternal cardiac activity, and (4) maternal breathing activity.

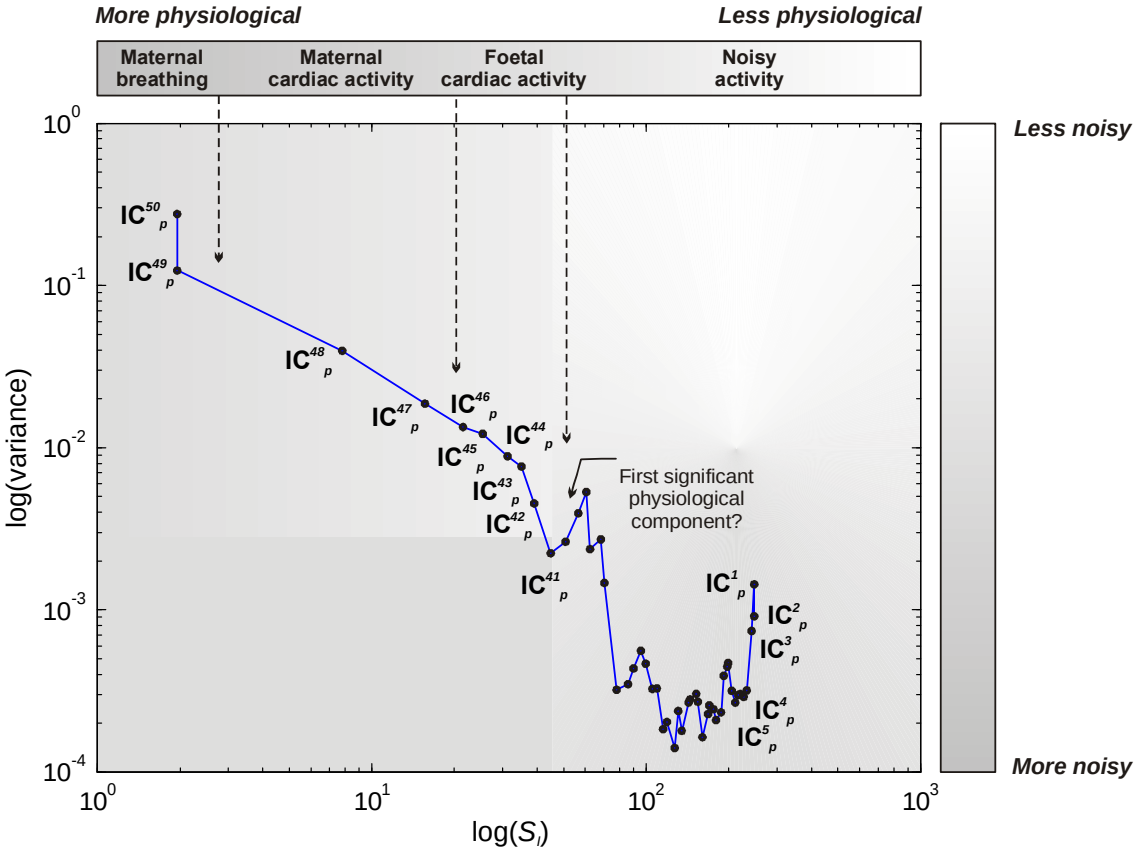

Figure 7.10. Summary of the spectral decomposition performed by SCICA (based on TDSEP) on the abdominal phonogram. The IC_ps are sorted by frequency due to the characteristics of the processes underlying the abdominal phonogram. The strongest physiological components, which respectively correspond to the maternal breathing, maternal cardiac activity, and foetal cardiac activity, are the last IC_ps in the sequence. The other components could contain physiological information, but buried in noise.

b) Resolution at outer frequencies: The other unexpected result shows that the first and last pairs of IC_ps have the same S_I. This is a curious result since consistently happens only to the two slowest and the two fastest IC_ps and therefore could be produced because SCICA may not properly resolve between such outer frequencies. In the former case, a suitable explanation comes by recalling the criterion used to define the embedding dimension (m) during the construction of the matrix of delays (**v**). As explained in Section 6.2.1, Equation 6.17 provides an objective criterion to calculate m by considering the lowest frequency of the periodic *components of interest*, which was 10 Hz for extracting the FHS. Thus, since SCICA is being constrained to resolve frequencies as far as 10 Hz, and some underlying physiological processes are slower than such a value, the filters learnt for them will probably have the same S_I, which has not been an issue so far. In fact, as only the breathing process seems to be slower than 10 Hz, the 50 IC_ps successfully manage to recover not only

the FHS, but also the maternal activity in the form of cardiac, and breathing activity[4] (this latter always in IC^{50}_{p}).

Regarding the two fastest components, a frequency constraint seems to be the reason for such behaviour as well, although in this case it has been assumed that such a constraint is given by the frequency used to record the data (*i.e.* 500 Hz). Further research will have to explore whether changes in m and f_s truly affect the resolution at outer frequencies as mentioned in this chapter.

In conclusion, when applied to a biomedical signal like the abdominal phonogram, where the energy of the underlying physiological processes is likely to be different, and where the slowest processes are likely to have the highest power (*e.g.* the breathing signal), the spectral decomposition implemented by SCICA is likely to return a set of spectrally disjoint components sorted from high to low frequency[5]. Thus, only the *last components in the sequence of* IC_ps *seem suitable to reconstruct the physiological information underlying the abdominal phonogram*. Furthermore, considering the rhythms found in such IC_ps, combined with the trends/correlations of the features along the whole dataset (as shown in Figure 7.8 and Figure 7.9), it can be said that, amongst such last IC_ps, three physiological rhythms are evident: (1) the last and slowest IC_p (*i.e.* IC^{50}_{p}) conveys the slowest physiological rhythm (given by the maternal breathing, R_{MB}), (2) the next group conveys a faster physiological rhythm (given by the maternal heart, R_{MH}), and finally, (3) the fastest IC_ps convey the fastest physiological rhythm (given by the foetal heart, R_{FH}). The problem now, as indicated by the downwards arrows in Figure 7.10, is to objectively define (1) how many IC_ps are significant to represent the physiological information (*i.e.* dimension reduction) and amongst them, as shown in Figure 7.8 (c), (2) which IC_ps belong to each physiological process or subspace (*i.e.* maternal breathing, MB, maternal cardiac, MC, or foetal cardiac, FC). These questions will be addressed in the next chapters.

7.4. Summary

This chapter presented a comprehensive study that aimed to gain knowledge, from a physiological perspective, of the components underlying the abdominal phonogram (separated by SCICA). For this purpose, looking for a complete perspective to interpret the meaning of the

[4] Further research must be performed to verify the origin of such breathing information, either exclusively maternal (as assumed in this work) or maternal and foetal (whenever the FBMs are present).

[5] Further research on simulated data (with different energy and frequency content), could reveal whether the energy and frequency content of the underlying components truly defines how the components are sorted by TDSEP.

IC_ps, different methods for time-series analyses were considered. Such methods, based on descriptive, spectral, entropy, and rhythmicity analyses, revealed essential characteristics of the ICs and TDSEP that provided the bases needed for improving the performance of SCICA.

In particular, the frequency content and time-structure information were useful to establish a couple of interesting results of SCICA when processing the abdominal phonogram: (1) although SCICA succeeds to spectrally separate components, it may fail to separate independent physiological components, and (2) SCICA based on TDSEP consistently sorts the IC_ps by frequency content. Regarding the IC_ps, it was established that, amongst the 50 components separated by SCICA (as described in Chapter 6), only some of them are suitable to reconstruct the physiological sources underlying the abdominal phonogram. Indeed, according to the measured features, such IC_ps are not only very regular, but also the slowest time-series in the set of IC_ps, consequently, they always appear at the end of the sequence of IC_ps. Also, and promising for this research, the rhythmicity analysis disclosed the physiological process(es) driving the IC_ps, which were clearly identified as maternal breathing activity, maternal cardiac activity, and foetal cardiac activity.

Now the question to address is how to use this promising outcome to define the number of IC_ps in the significant physiological group and, amongst them, automatically identify which IC_ps belong to each physiological activity. These will be addressed in the next chapter, where a novel idea for grouping IC_ps will be presented.

8 TIME-STRUCTURE BASED CLASSIFICATION OF PHYSIOLOGICAL COMPONENTS UNDERLYING THE ABDOMINAL PHONOGRAM

The previous chapter detailed a study of the components underlying the abdominal phonogram that revealed valuable information about SCICA (based on TDSEP) and the IC_ps. According to the study, when applied to the abdominal phonogram, TDSEP performs a spectral decomposition that, in addition, sorts the components according to their frequency content. Furthermore, amongst the m IC_ps separated by TDSEP, only the last components in the sequence are relevant for reconstructing the physiological sources underlying the abdominal phonogram. Also, and essential for this research, the rhythmic patterns in such physiological IC_ps identifies three physiological processes driving the components: R_{FH}, R_{MH}, and R_{MB}.

Certainly, this study provides knowledge about the IC_ps properties, but also with a proper idea of the performance of SCICA based on TDSEP. Indeed, since TDSEP was sorting the components according to their frequency content, it could be seen that: (1) the permutation ambiguity had been tackled by TDSEP (at least for the case considered in this work), (2) only the slowest components were significant to retrieve the physiological sources of interest and, most importantly, (3) such meaningful IC_ps were generated by physiological processes that could actually be identified as foetal cardiac, maternal cardiac or maternal breathing activities. These were valuable outcomes for this research, but still represented a partial solution of the bigger problem of *recovering* reliable estimates of the *physiological sources underlying the abdominal phonogram*.

As mentioned in Chapter 6, recovery of reliable sources means that, once a good-quality separation has been achieved, the estimates of the underlying sources can be carefully reconstructed by excluding non-physiological or noisy IC_ps. Therefore, *similar IC_ps* must be somehow identified and correctly *grouped* prior to retrieving estimates of the physiological sources corresponding to foetal and maternal activities.

At present, some studies in the literature have visually defined similarity and manually grouped physiological components (Comani *et al.* 2004a; Comani *et al.* 2004b; Jimenez-Gonzalez and James 2008a; Zarzoso and Nandi 2001), which is not only subjective, but also a demanding and time-consuming task due to the number of components to be classified, which is usually large. Alternatively, some studies have proposed automatic methods to group similar ICs based on time and/or frequency content (Castells *et al.* 2004; Jimenez-Gonzalez and James 2008b; Jiménez-González and James 2009; Mantini *et al.* 2005; van Leeuwen *et al.* 2004), entropy (Comani *et al.* 2007), or mutual information (Kraskov *et al.* 2005). The methods based on time-frequency content are easy to implement and fast to execute, but perform poorly (Jiménez-González and James 2009; Mantini *et al.* 2005). On the other hand, the methods based on entropy and mutual information perform better, but are slower to execute due to much larger computational loads (Comani *et al.* 2007; Kraskov *et al.* 2005).

Here, it is proposed that grouping can be reliable and yet still efficiently executed, and this is done by exploiting the time-structure of the physiological components underlying the phonogram as the measure of similarity. So, based on the results in Chapter 7, this chapter presents a *rhythmicity-based analysis* scheme that aims to automatically group the physiological IC_ps underlying the abdominal phonogram. To this end, this chapter first describes an upgraded version of the method used in Chapter 7 to measure time-structure. Then, once an enhanced measurement of the rhythmicity has been achieved, the IC_ps with similar rhythms can be automatically classified into physiological groups. Finally, a quantitative evaluation of the performance of such a time-structure based classifier is presented.

8.1. Measuring time-structure: revisited

As mentioned in Chapter 7, biological processes commonly involve a rhythmic regulatory process. As a result, signals recorded from those systems posses time-structure, *i.e.* present rhythmic patterns. Such a time-structure is an evident feature of the physiological sources underlying the abdominal phonogram (both cardiac and breathing) that, in addition, and essential for this research, shows different periodicities (see Figure 8.1). In normal conditions, it has been reported that the maternal heart rate ranges from 1.2 to 1.4 Hz (Ogueh *et al.* 2009) whilst the foetal heart rate ranges from 2.0 to 2.7 Hz (Guijarro-Berdinas *et al.* 2002). The maternal breathing rate, on the other hand, is considerably lower and ranges from 0.16 to 0.33 Hz (van Leeuwen *et al.* 2009). Therefore, by analysing the IC_ps rhythms it is possible to find similar components and cluster them into: maternal breathing (MB), maternal cardiovascular (MC), foetal cardiac (FC), and even noise (N) groups. To this end, it is essential to have a reliable measurement of rhythmicity (R), which was partly achieved in Chapter 7, mainly because of the harmonic effects. Therefore, this section revisits the method proposed to measure

rhythmicity and, by considering the observations in Chapter 7, discusses an upgrade that aims, not only to reduce the harmonic effects, but also to validate the measurement or *R*.

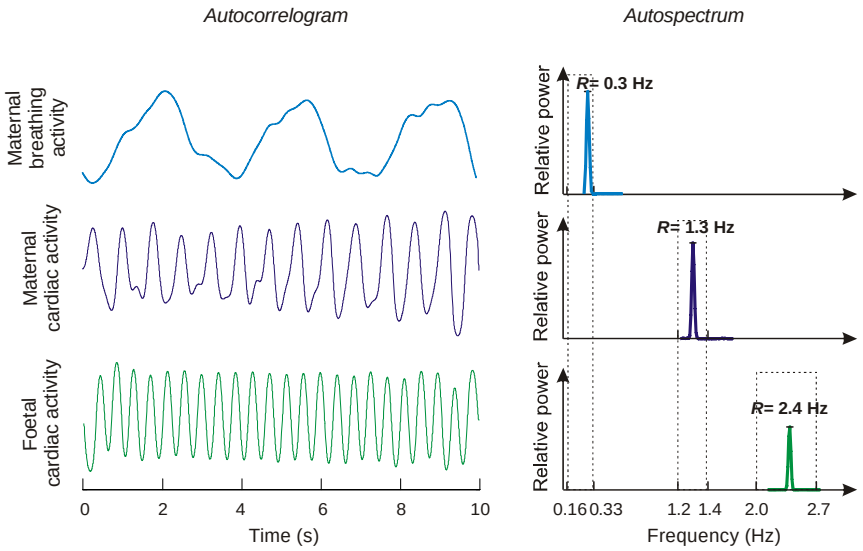

Figure 8.1. Rhythmic patterns of the physiological sources underlying the abdominal phonogram in time (left) and frequency (right) domains. From top to bottom: maternal breathing, maternal cardiac, and foetal cardiac activities. The dotted box in the frequency domain shows the normal intervals reported by Guijarro-Berdinas *et al.* (2002), Ogueh *et al.* (2009), and van Leeuwen *et al.* (2009), whereas the peak within corresponds to a typical rate or rhythmic value (*R*). © 2010 IEEE. Reprinted, with permission, from IEEE Transactions on Biomedical Engineering, Time-structure based reconstruction of physiological independent sources extracted from noisy abdominal phonograms, Jiménez-González A and James CJ.

8.1.1. An improved measurement of rhythmicity

As mentioned in Chapter 7, time-series rhythmicity can be measured either in the time or frequency domains, the former by autocorrelation analysis and the latter by power spectral analysis (Barman and Kenney 2007). Here, the benefits of working in both domains are exploited by enhancing the time-structure in the former and by measuring *R* in the latter by means of a modified version of the procedure described in Section 7.2.3 (d). Thus, the procedure is as follows:

a) **Generation of a detrended envelope,** $e(n)$, as described in Section 7.2.2.

b) **Autocorrelogram generation:** This is the step that discovers the dependence structure in $e(n)$ (even though it may be masked by background noise) (Barman and Kenney 2007; D'Urso and Maharaj 2009). It uses autocorrelation analysis to compare the signal with a replica of itself that is gradually shifted in time as

$$R^{e}_{k_e=1,\ldots,N_A} = \sum_{k_e=1}^{N_A} e(n)\,e(n-k_e), \tag{8.1}$$

where $R^{e}_{k_e}$, referred to as the autocorrelogram of $e(n)$, conveys a good representation of the dynamics in the IC_p, *i.e.* its rhythmic pattern.

Ideally, the dependence structure in $R^{e}_{k_e}$ should produce a single rhythmic pattern, either from FC (R_{FH}), MC (R_{MH}) or MB (R_{MB}) activities. However, since a physiological separation by SCICA is not always possible (*i.e.* the IC_p does not always contain clean components from one underlying source), $R^{e}_{k_e}$ may convey more than one pattern, although oscillating at different frequencies and intensities. In this case, the obvious solution would be to choose R as the rhythm of the most significant pattern (*i.e.* the pattern with the largest energy). However, as the rhythmic patterns also bring harmonic frequencies, there is a chance of harmonics-rhythms overlapping that, as a result, would add "harmonic" energy to any pattern, diminish its actual contribution, and more importantly, wrongly point to it as the most significant pattern. Thus, unless the harmonic effects are reduced, the classifier would have to deal with unreliable information about R and probably misclassify some IC_ps, which might considerable contaminate the group and the reconstructed source. To prevent this problem, and based on the observations in Chapter 7 about the harmonic effects, this section adds a simple step given by

c) Filtering: This reduces the harmonic effects due to R_{MB} and R_{FH}, which is possible because of their different rates (as shown in Figure 8.1). To this end, $R^{e}_{k_e}$ is decimated[1] by a factor of 20 and the resulting signal is filtered, first by a low-pass filter (using a 10th-order FIR filter with cut-off frequency of 3.1 Hz), and then by a high-pass filter (using a 10th-order FIR filter with cut-on frequency of 0.7 Hz). Finally, the filtered signal is restored to the original sampling frequency and detrended to produce R^{e}_{f}.

The cut-off frequency of 3.1 Hz was chosen to remove the R_{FH} harmonic and to leave intact the information at lower frequencies. The cut-on frequency of 0.7 Hz, on the other hand, removes the effects of the maternal breathing by directly removing R_{MB} from the IC_p. This idea was implemented to easily deal with the wider frequency range influenced by R_{MB} and, as a result, reduced the problem into the reliable measurement of cardiac rhythms, either foetal or maternal. Here it is important to mention that this idea took into account the *a priori* knowledge that the breathing information is consistently concentrated in the last component of the IC_ps sequence (IC^{50}_{p}). Thus, although the breathing rhythm is not present

[1] The decimation process first filters the input data with a low-pass filter, to avoid antialiasing problems, and then resamples the resulting signal at a lower rate.

at the stage of measuring R, the IC_p that mainly conveys such information remains intact to represent the breathing group, *i.e.* MB.

d) Autospectrum: This step makes it easier to calculate R by transforming R_f^e into a frequency domain representation, $\hat{S}_f(f)$, using the Welch's method as described in Section 7.2.3 (d), *i.e.* with a Hanning window of 2048 samples in length and an overlap of 50%. Finally, from the autospectrum $\hat{S}_f$, as illustrated in Figure 8.1, the frequency of the largest peak is taken as the measurement of rhythmicity (R).

8.1.2. A procedure to validate rhythmicity in noise

Once the harmonic effects due to R_{MB} and R_{FH} have been reduced, R should be easily categorised as maternal or foetal. However, as some IC_ps may still contain some degree of mixture (Davies and James 2007), the classification is not a straightforward step, especially because a "noisy" IC_p can contaminate the physiological group and, as a result, render the reconstructed source useless for further analysis. For this reason, some extra and *a priori* information (learnt in Chapter 7) is necessary to assess how prevailing R is over the noise and thus, the pertinence of the IC_p to a group. Thus, three types of noisy IC_ps (*i.e.* mixtures, M) may appear when SCICA decomposes the abdominal phonogram: (1) the $M_{MB\text{-}MC}$ type, which presents the maternal breathing and the maternal heart rhythms, (2) the $M_{MC/FC\text{-}N}$ type, which presents a heart rhythm (either maternal or foetal) and background noise, and (3) the $M_{FC\text{-}MC}$ type, which presents foetal and maternal heart rhythms.

In particular, and important to be highlighted, the $M_{MB\text{-}MC}$ type is a unique IC_p that always seems to be dominated by the maternal breathing as its main source. Therefore, as discussed in Chapter 7, whenever $M_{MB\text{-}MC}$ happens, it consistently appears at the very end of the sequence of IC_ps (*i.e.* $IC^{50}{}_p$). Regarding the cardiac mixtures, either $M_{MC/FC\text{-}N}$ or $M_{FC\text{-}MC}$, which may easily degrade the FC group (by introducing either maternal cardiac information or background noise), also have characteristics that, although empirical, become helpful for validating R. Hence, as discussed in Chapter 7, a well separated IC_p (both spectrally and physiologically independent) is characterised not only by a single R (as in Figure 8.1), but also by a spectrum whose single-peak (S_I) appears in typical ranges depending on the IC_p type (as exemplified in Figure 8.2). On the other hand, the noisy version of such an IC_p would show the same R in presence of either (a) background noise and a different S_I or (b) another cardiac source and a secondary rhythm (R'). Therefore, this chapter uses S_I as one mechanism to validate R. Besides, to find out whether the IC_p is noisy due to R', it uses a steadiness index (S_t). In this way it is suitable to find not only a noisy R, but also the best group for it: N, MC or FC. The steps used to calculate S_I and S_t are as follows:

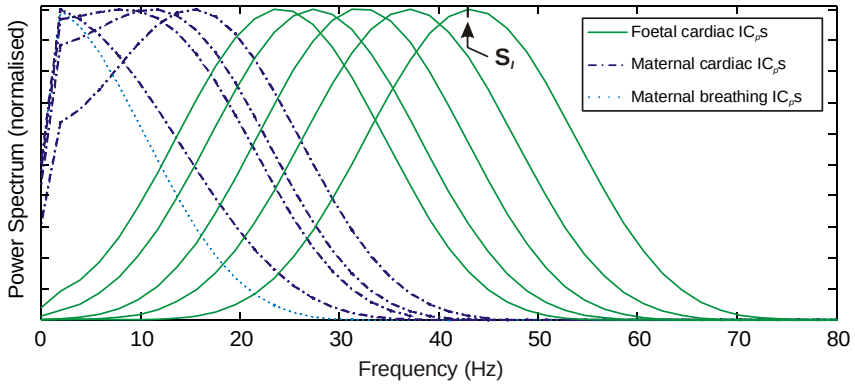

Figure 8.2. An example of the spectra observed in the physiological IC$_p$s separated from the abdominal phonogram by SCICA (based on TDSEP). Each curve depicts the spectral content of a component in the sequence of IC$_p$s, whereas S_I corresponds to the frequency of its single-peak. From lower to higher frequencies: a maternal breathing IC$_p$, four maternal cardiac IC$_p$s, and five foetal IC$_p$s. © 2010 IEEE. Reprinted, with permission, from IEEE Transactions on Biomedical Engineering, Time-structure based reconstruction of physiological independent sources extracted from noisy abdominal phonograms, Jiménez-González A and James CJ.

a) Spectral content index (S_I): This was found as described in Section 7.2.3 (b) and illustrated in Figure 8.2.

b) Steadiness index (S_t)**:** This index is focused on those IC$_p$s that, composed of two high-energy cardiac periodicities (*R* and *R'*), need further analysis as to which group they better belong to. Such IC$_p$s are found by taking into account that an ideal well-separated IC$_p$ contains only one rhythmic pattern along the whole segment. Consequently, the autospectrum of either the whole segment or large parts of it should produce the same rate (*i.e.* a steady pattern). On the other hand, in those IC$_p$s where two cardiac rhythms were present, some parts would produce partial autospectra different to the whole autospectrum (*i.e.* an unsteady pattern). Here, to evaluate such steadiness, a second rhythmic (*R'*) is calculated from R_f^e, though this time using a variation of the Welch's periodogram. Such a variation removes the step were the windowed FFTs are averaged so that it better detects the frequencies in all the segments. After that, by comparing *R* and *R'*, the IC$_p$ is labelled as steady (*i.e.* free of *R'*) and ready to be classified, or unsteady (*i.e.* contaminated by an *R'*) and in need of further analysis.

Next, for the unsteady IC$_p$s, the idea is to identify the most persistent process and then, the best cardiac group. This is done by comparing R_f^e against two ideal autocorrelograms, one foetal and one maternal. These autocorrelograms are produced by using sinusoid signals of amplitude one and frequencies given by the maternal and foetal *R*s obtained from the stable

IC_ps. Then, Pearson's coefficients between R_f^e and each sinusoid (P_f, P_m) are calculated to see how much of an ideal maternal and an ideal foetal cardiac component is present in the IC_p.

Figure 8.3 sketches the rhythmicity-based analysis proposed to extract reliable information about the time-structure in an IC_p. In addition, to keep in mind the parameters provided to the classifier, R, S_I, P_f, and P_m are also indicated.

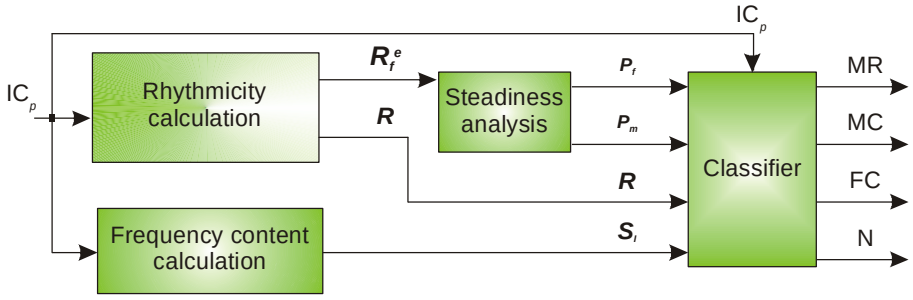

Figure 8.3. Rhythmicity-based analysis proposed to find similar IC_ps and cluster them into physiological groups. R represents the rhythmicity, whereas S_I, P_f, and P_m assess its dominance over noise (*i.e.* R reliability). The information is provided to the classifier in order to build groups corresponding to maternal breathing (MB), maternal cardiac (MC), foetal cardiac (FC), and noise (N) activities.

8.2. A time-structure based classifier

Once some features about the time-structure of the IC_p have been obtained, the next part of this methodology requires defining the set of rules that, by considering such information, cluster similar IC_ps into their proper group: MB, MC, FC or N (as illustrated in Figure 8.3). Here, such a set of rules has been designed based on knowledge obtained during the study described in Chapter 7. Hence, this section starts by briefly pointing to the empirical information considered to design the classifier. Next, Table 8.1 presents the time-structure based algorithm proposed to automatically group the physiological components underlying the abdominal phonogram.

a) Empirical criteria:

(1) MB is significantly represented by $IC^{50}{}_p$.

(2) Whenever a disagreement between features appears, the information given by S_I always overrules the information given by R (Jiménez-González and James 2010a) and $P_{(f, m)}$.

(3) The ranges observed for R in the abdominal phonogram dataset are slightly wider than those reported in other works (Guijarro-Berdinas *et al.* 2002; Ogueh *et al.* 2009; van Leeuwen *et al.* 2009). Therefore, in this proposal, the ranges used by the algorithm are different to the values previously reported as follows

b) Empirical ranges per physiological group:

* *For frequency content* (*SI*):

1. S_I_MC= (0.5 – *thrS*] Hz, which represents the frequency content assumed for a maternal cardiac IC_p.
2. S_I_FC= (*thrS* – 44.5] Hz, which represents the frequency content assumed for a foetal cardiac IC_p.
3. S_I_N > 44.5 Hz, which represents the frequency content assumed for either a noisy or noise IC_p.

* *For rhythmicity* (*R*):

1. *R*_MC= [0.83 – *thrR*] Hz (*i.e.* between 49.8 and *thrR* beats/min), which is the range assumed for the maternal cardiac rate.
2. *R*_FC= (*thrR* – 3.0] Hz (*i.e.* between *thrR* and 180 beats/min), which is the range assumed for the foetal cardiac rate.

Table 8.1. A time-structure based algorithm for automatic classification of the IC_ps separated from the abdominal phonogram.

```
FOR i FROM 1 TO m DO
    IF i = = 50 THEN                    % the component is more likely to represent the breathing
        Put IC_p^i in the MB group
    ELSE                                % the component is either cardiac or noise
        IF R and S_I disagree about the group THEN     % verify background noise
            Put IC_p^i in the group indicated by S_I (either MC, FC or N)
        ELSE                            % R and S_I agree
            IF IC_p^i is a steady component THEN     % looking for another cardiac R
                Put IC_p^i in the group indicated by R (either MC or FC)
            ELSE
                IF P_(m, f) and S_I disagree about the group THEN
                    Put IC_p^i in the group indicated by S_I (MC, FC, N)
                ELSE    % P_(m, f) and S_I agree
                    Put IC_p^i in the group indicated by P_(m, f) (either MC or FC)
                END
            END
        END
    END
END
```

8.3. Classifier evaluation

A typical problem when recovery estimates of underlying sources is the natural absence of a gold standard, which makes it difficult to quantify the quality of the decomposition and thus, the quality of the retrieved sources. In an attempt to deal with this uncertainty, some studies have used synthetic data to test the separation results by measuring the error between the "original" sources and the sources estimated by their methods (Klemm *et al.* 2009; Mantini *et al.* 2006; Wallstrom *et al.* 2004). This approach, although "evaluates" the decomposition performance, has not been used in this research because it is frequently criticised due to the lack of knowledge about (1) the true sources underlying the observations and (2) the mixing process. Consequently, even though synthetic data attempt to emulate real sources and mixtures, since the simulations strongly rely on assumptions not only about the number of underlying processes, but also about their interactions, it is still impossible to know how representative of the actual sources they are (Klemm *et al.* 2009). Hence, unless the real sources and mixing processes are known (which is especially complicated for non-invasive recordings like the abdominal phonogram), the simulated data will never actually represent the phenomena under study (Klemm *et al.* 2009). Alternatively, although this work is not yet estimating sources, it is necessary to find a way to quantify its performance so far, at least in terms of the grouping because, if wrongly done, it would give rise to sources that are useless for further analysis. The next section presents the methodology followed to perform such an evaluation on the time-structure based classifier proposed in this research.

8.3.1. A manually pre-classified dataset

The classifier was tested on a pre-classified dataset built from the dataset described in Chapter 7. Indeed, the difference between these two datasets is only the number of IC_ps per sequence contained in each one. The original dataset[2] contains the whole sequences of 50 IC_ps extracted per segment of abdominal phonograms (*i.e.* from IC^1_p to IC^{50}_p), whereas the pre-classified dataset contains subsequences composed of the last 10 IC_ps of each sequence (*i.e.* from IC^{41}_p to IC^{50}_p). Consequently, as shown in Figure 8.4, this new dataset is composed of 75 subsequences whose IC_ps were manually categorised as MB, MC, FC, or N (*i.e.* a total of 750 IC_ps).

The reason behind using only the last 10 IC_ps was that they consistently show physiological information over the background noise, which made it possible to manually classify them in order to create the *reference* needed to quantify the classifier performance.

[2] Recall that there are 25 abdominal phonograms and, from each phonogram, three segments of 10 s length were selected. Next, each segment was decomposed to extract sequences of 50 IC_ps (from IC^1_p to IC^{50}_p). Therefore, the original dataset contains 75 sequences of 50 IC_ps each.

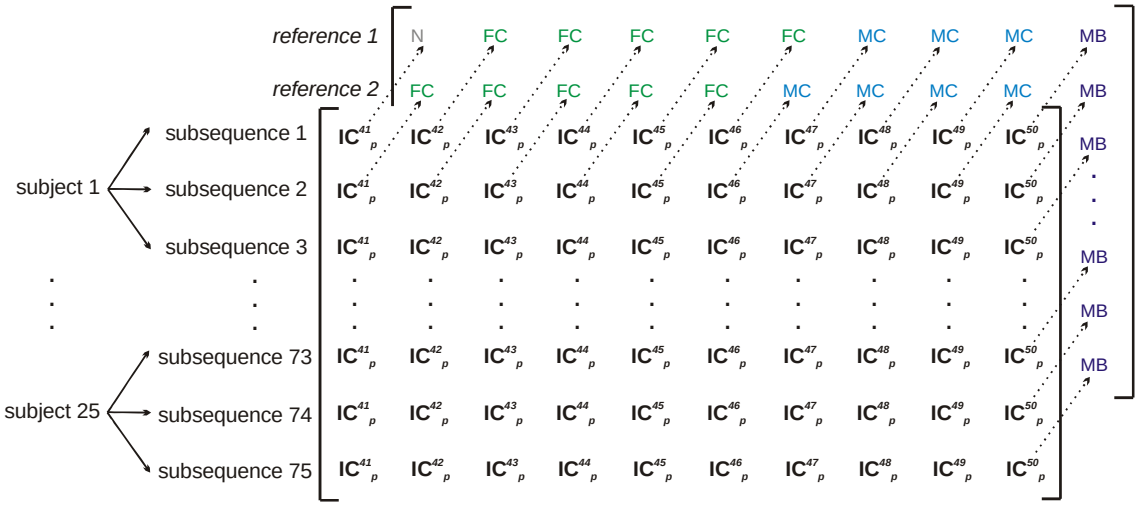

Figure 8.4. Dataset used to test the performance of the time-structure based classifier. This dataset contains subsequences of 10 IC_ps because of their strong physiological content, which made it easier to manually categorise them as FC, MC, MB or N and thus, to construct the *reference* to evaluate the classifier.

8.3.2. Testing the classifier

Each subsequence of 10 IC_ps in the dataset was analysed and automatically grouped as described in the previous section, although now the index i of the algorithm in Table 8.1 is taken from $m - 9$ to m. After that, the automatic classification results were compared with the reference by calculating the Sensitivity (Se) and Specificity (Sp) as in Equation 8.2 and Equation 8.3 respectively

$$Se = \frac{TP}{TP + FN}, \tag{8.2}$$

where TP is the number of true positives, FN is the number of false negatives, and

$$Sp = \frac{TN}{TN + FP}, \tag{8.3}$$

where TN is the number of true negatives and FP is the number of false positives.

Here it is important to mention that, as MB has been consistently composed only of IC_p^{50} and, as seen in Table 8.1, R is not used to create this group, MB is not included in this evaluation. In other words, Se and Sp measure the reliability of the classifier to distinguish between foetal and maternal cardiac IC_ps, which are the components whose misclassification causes a larger contamination. In addition, as this rhythmicity-based analysis scheme is composed of two parts (measurement and validation of R), the classifier was tested in order to see the impact of the validation stage as follows:

a) Test 1 (classification *without* validation of *R*): This tested the sensitivity and specificity of *R* as the criterion for grouping. To this end, *Se* and *Sp* were measured not as a single value, but as a function of *thrR*, which defines the limit between maternal and foetal rhythms. Thus, by taking into account the rhythmicity range in Section 8.2 (b), *thrR* changed from 0.83 to 3.0 Hz in steps of 0.2 Hz and, in each case, the corresponding *Se* and *Sp* values were calculated.

b) Test 2 (classification *with* validation of *R*): This tested the sensitivity and specificity of the whole grouping algorithm, *i.e. R* and its validation. To this end, *Se* and *Sp* were measured as a function of *thrS*, which defines the limit between maternal and foetal frequency contents. Thus, after fixing *thrR* at 1.6 Hz (as discussed in the next section), and by taking into account the frequency content range in Section 8.2 (b), *thrS* changed from 0.5 to 44.5 Hz in steps of 2 Hz and, in each case, the corresponding *Se* and *Sp* were calculated. In addition, to see how active the validation is during the classification process, the average numbers of times that S_I and $P_{(f, m)}$ disagreed with *R* (and so overruled it) were also calculated.

8.4. Performance of the time-structure based proposal

Figure 8.5 summarises the time-structure based methodology proposed for grouping the physiological components underlying the abdominal phonogram. Based on rhythmicity analysis, the first six blocks aim to obtain significant features (*R*, P_f, and P_m) so that, in combination with S_I, the method automatically clusters similar components into groups corresponding to maternal breathing activity in MB, maternal cardiac activity in MC, foetal cardiac activity in FC, and, in this example, noise (or noisy activity) in N. Notice that, amongst the 10 IC_ps considered in this example, the classifier is grouping one component in MB (IC^{50}_p), four components in MC (from IC^{46}_p to IC^{49}_p), four components in FC (from IC^{42}_p to IC^{45}_p), and one component in N (IC^{41}_p). In particular, regarding the steps followed to achieve such a grouping results, the observation of the signals in Figure 8.5 reveals interesting information about:

a) The rhythmicity measurement stage: The outputs of the first five blocks illustrate the signals obtained during the procedure used to enhance/measure the time-structure in two IC_ps of the subsequence (IC^{42}_p on the left-hand side and IC^{48}_p on the right-hand side). In each case, from top to bottom, the figure depicts the time and frequency representations of the normalised envelope, the autocorrelogram, and the filtered and normalised autocorrelogram. As can be seen in both cases, even though $e(n)$ is a noisy signal, *every subsequent step better defines the time-structure* in the IC_p, which is clear in both domains.

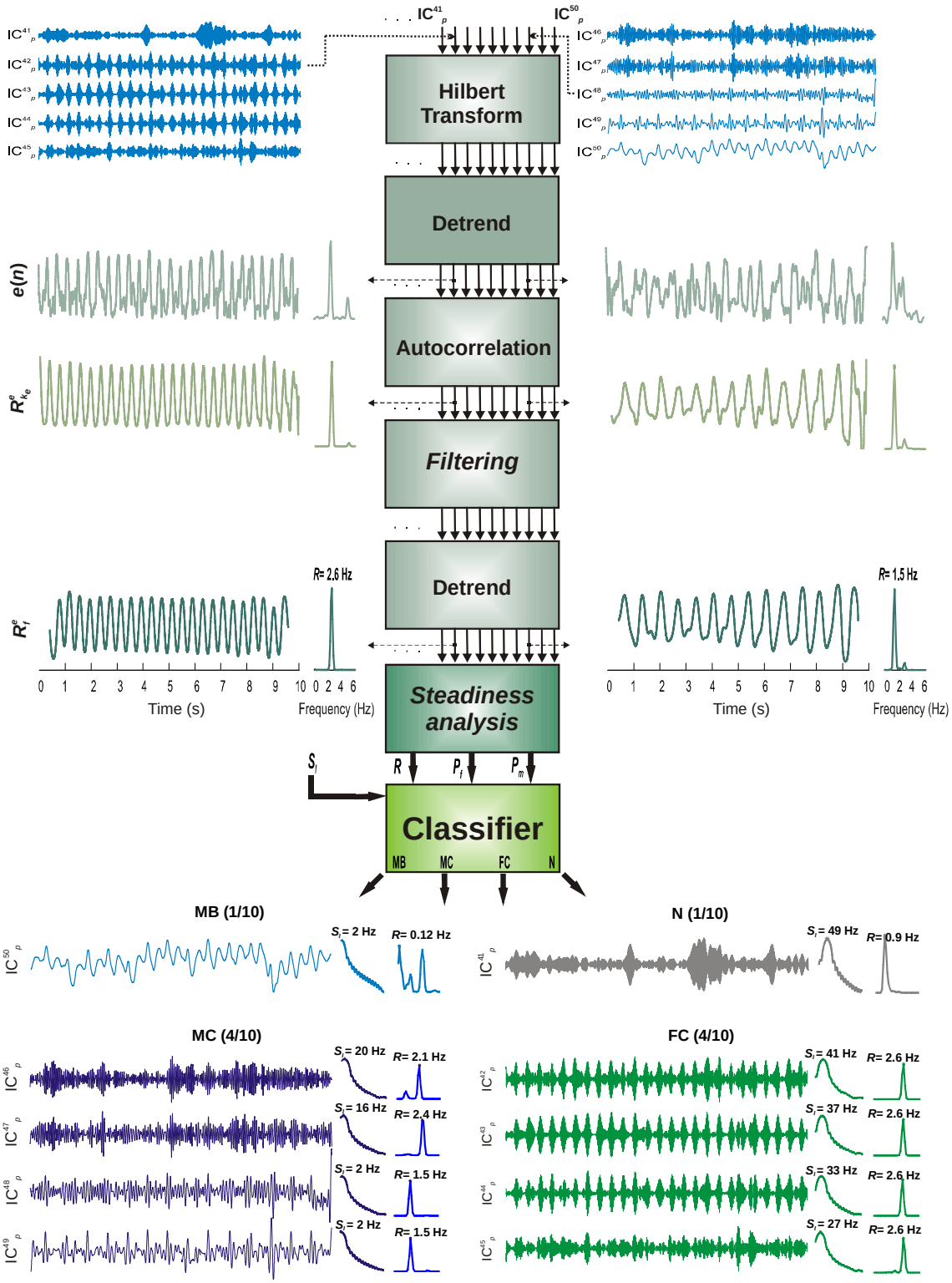

Figure 8.5. An upgraded time-structure based methodology for grouping the physiological components underlying the abdominal phonogram. Based on rhythmicity analysis, the method obtains significant features (R, P_f, P_m, S_I) that are used to automatically classify similar components in groups corresponding to foetal cardiac activity (FC, oscillating at 2.6 Hz), maternal cardiac activity (MC, oscillating at 1.5, 2.1 and 2.4 Hz), maternal breathing activity (MB, oscillating at 0.9 Hz) and, in this example, noise (N). The example illustrates a subsequence of 10 IC_ps that were grouped as: $IC^{50}{}_p$ in MB, from $IC^{46}{}_p$ to $IC^{49}{}_p$ in MC, from $IC^{42}{}_p$ to $IC^{45}{}_p$ in FC, and $IC^{41}{}_p$ in N. The signals amplitude has been modified for visual purposes.

Thus, R_f^e becomes more like a sinusoid wave, whereas $\hat{S}_f$ tends more to a well defined single-peak spectrum. Most importantly, the time-structure revealed in these IC_ps *oscillates at different frequencies*: 2.6 Hz for the $IC^{42}{}_p$ (which is in the foetal cardiac range) and 1.5 Hz for the $IC^{48}{}_p$ (which is in the maternal cardiac range).

b) The rhythmicity grouping stage: As predefined in the algorithm, $IC^{50}{}_p$ is used to construct MB and, as seen in the corresponding $\hat{S}_f$, this component does posses the slowest rhythm, which is 0.12 Hz. Furthermore, both the time-series and $\hat{S}_f$ show additional rhythms that, according to $\hat{S}_f$, oscillate at 1.5 and 3.0 Hz, where the latter is almost as large in amplitude as R_{MB}. Regarding the MC group, the $\hat{S}_f$ of each component shows single-peak patterns, although centred at different frequencies such as 2.1, 2.4 and 1.5 Hz. Furthermore, the time-series corresponding to $IC^{46}{}_p$ and $IC^{47}{}_p$ seem to be noisier than $IC^{48}{}_p$ and $IC^{49}{}_p$ although, with some effort, it is possible to see some patterns aligned with $IC^{46}{}_p$ and $IC^{47}{}_p$. In the FC group, the single-peak patterns of all its constituent IC_ps are centred at 2.6 Hz, although $IC^{45}{}_p$ seems to be noisier than the other components in the group (and still showing activity aligned with the other IC_ps). Finally, in the N group, although there is no visual evidence of periodic patterns in the time-series, $\hat{S}_f$ reveals one rhythm at 0.9 Hz.

Figure 8.6 shows the distribution of the R values measured by using (a) the methodology described in Chapter 7 and (b) the methodology described in this chapter that reduces some harmonic effects. As can be seen, both cases clearly have a three-modal distribution centred at physiological rhythms (R_{MB}, R_{MH}, and R_{FH}) and covering ranges wider than those reported by other authors (Guijarro-Berdinas *et al.* 2002; Ogueh *et al.* 2009; van Leeuwen *et al.* 2009). More detailed, in (a), the R values range from 0.1 to 5.0 Hz and the number of IC_ps oscillating at R_{MB} is larger than the number of components oscillating at R_{MH} and R_{FH}. In (b), the R values are scattered from 0.1 to 3.0 Hz and redistributed so that the number of IC_ps oscillating at R_{MB} is smaller than the number of components oscillating at R_{MH} and R_{FH}, which is more consistent with the observations in Chapter 7 (*i.e.* there is a single component in each sequence of IC_ps consistently associated to the maternal breathing, which is the slowest physiological rate).

Figure 8.7 shows the performance of the classifier at categorising cardiac IC_ps as maternal or foetal (a) *without* and (b) *with* validation of R. In addition, (c) shows the average number of times (per subsequence) that S_I and $P_{(f,\,m)}$ found R unreliable and overruled it. As expected, *Se* and *Sp* change depending on the thresholds (*thrR*, *thrS*) used to decide between maternal and foetal groups. *Se* increases whereas *Sp* decreases as the threshold increases, which makes it possible to see the trade-off between them and look for the optimal threshold (*i.e.* their intersection point). Thus, as shown by the dash-dotted vertical line, the optimal threshold appears in (a) when *thrR*= 1.6 Hz, and in (b) when *thrS*= 18.8 Hz, which respectively produces

values for *Se* and *Sp* of 0.77 and 0.96. In (c), the activity of S_I is always more frequent than the activity of $P_{(f,\,m)}$. Furthermore, at the optimal *thrS*, where the validated method reaches the best performance for *Se* and *Sp*, the average number of corrections performed by S_I is 2.25 whilst by $P_{(f,\,m)}$ is 1.3.

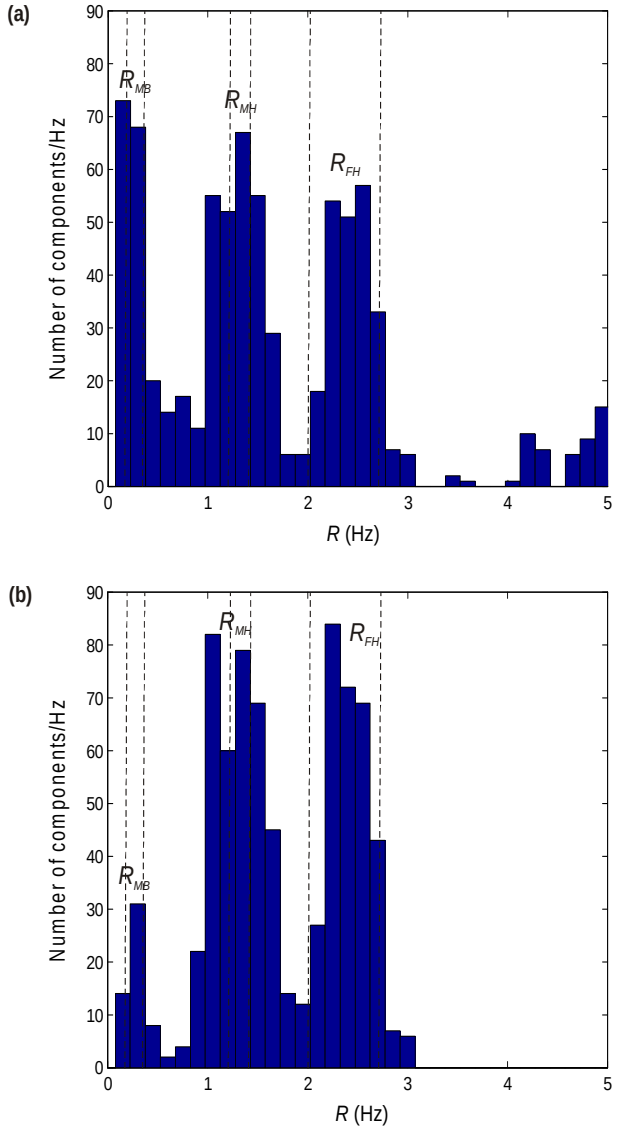

Figure 8.6. Distribution of the *R* values measured by using (a) the methodology described in Chapter 7 and (b) a new methodology that reduces the harmonic effects. Both cases show three-modal distributions; although in (a) the values are spread from 0.1 to 5 Hz and the number of components at R_{MB} is larger than the number of components at R_{MH} and R_{FH}. In (b), the values range from 0.1 to 3 Hz and the number of components at R_{MB} is considerable smaller than the number of components at R_{MH} and R_{FH}. The dotted lines show the normal intervals reported in other works (Guijarro-Berdinas *et al.* 2002; Ogueh *et al.* 2009; van Leeuwen *et al.* 2009).

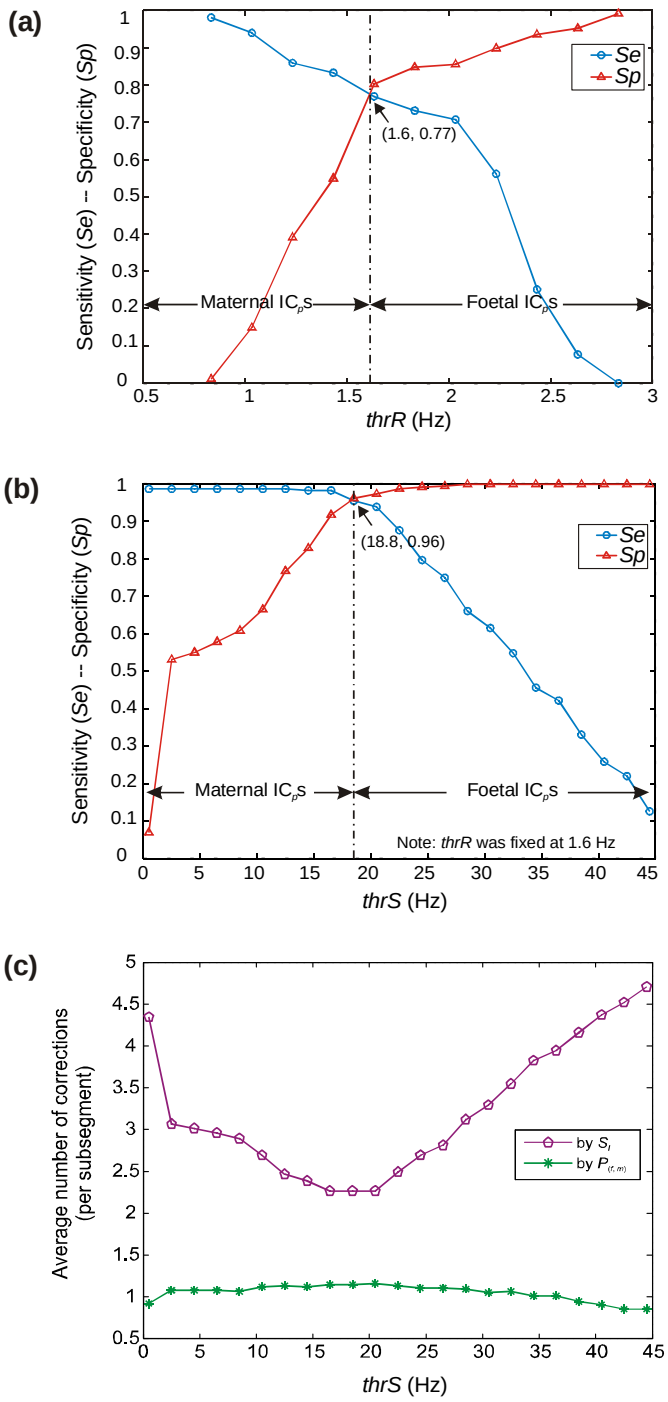

Figure 8.7. Performance of the time-structure based classifier on categorising cardiac IC$_p$s as foetal or maternal (a) *without* and (b) *with* the validation of R by S_I and $P_{(f, m)}$. In (c), the average number of times (per subsequence) that S_I and $P_{(f, m)}$ found R unreliable and overruled it. The dash dot vertical line shows the optimal threshold to distinguish IC$_p$s in each case. The optimal classifier performance increases from (a) 0.77 to (b) 0.96 in as soon as the validation of R is included and, at that point, the average numbers of corrections by S_I and $P_{(f, m)}$ are 2.5 and 1.3 respectively.

8.5. How far from well-being surveillance?

This chapter described a time-structure based method that aimed to automatically classify physiological, and therefore relevant, IC_ps underlying the abdominal phonogram extracted by TDSEP (Jiménez-González and James 2010b). The scheme, applied to a total of 750 IC_ps extracted from segments of 25 single-channel phonograms (and organised by subsequences of 10 IC_ps), uses rhythmicity-analysis to progressively reveal and validate the time-structure in each IC_p. Then, by using such rhythmicity, it has been possible not only to *group similar IC_ps, but also to associate the resulting groups to physiological phenomena*, which is a further achievement for this methodology. Thus, the method manages to successfully classify components into groups corresponding to *maternal breathing activity*, *maternal cardiac activity*, *foetal cardiac activity*, and *noise*.

Regarding the rhythmicity patterns found in the groups (see Figure 8.5), they present interesting characteristics that deserve to be analysed in more detail. In MB, for instance, a detailed observation of the multi-peak pattern not only shows that IC^{50}_p was partly separated by SCICA (as evident in the time-series), but also that the extra component, whose apparent main rhythm oscillates at 3 Hz, could be wrongly interpreted as FC rather than as MC. Indeed, $\hat{S}_f$ shows a third and small peak centred at 1.5 Hz, which means that the second largest peak in the pattern is oscillating at twice this rhythm. In other words, the peaks in $\hat{S}_f$ represent two rhythmicities, one single-rhythm at 0.12 Hz that belongs to R_{MB}, and one double-rhythm centred at f_0 = 1.5 Hz and $2f_0$ = 3.0 Hz that, consequently, belongs to R_{MC} and its harmonic $2R_{MC}$. This double-rhythm, as mentioned in Chapter 7, reveals not only the presence of cardiac information in IC^{50}_p, but also the origin of such information, which is the maternal heart sounds pair (S1-S2). Here, although in this particular case the multi-peaks $\hat{S}_f$ is harmless for classification purposes (as IC^{50}_p is classified regardless R), it was considered as important to be highlighted because the *rhythmicity-based analysis not only reveals improperly separated* IC_ps (in a physiological sense), but also the *origin of the extra physiological information*. Such information, when properly interpreted and validated, may even reveal the presence of the HS pair.

For the MC group, where a few $\hat{S}_f$ would wrongly have made the classifier put IC^{46}_p and IC^{47}_p into FC, the validation given by S_I correctly identified them as belonging to MC and thus, avoided the introduction of wrong and contaminating information into FC. Such components, as previously mentioned, can be visually related to the maternal cardiac activity, but the rhythms at 2.1 and 2.4 Hz (which are different to the rhythms for the clearest maternal and foetal components), remain as yet unidentified. For the FC group, although in this example the whole IC_ps showed the same rhythm, the validation was still important to determine the best group for IC^{45}_p, either FC or N. Finally, for the N group, although there is a rhythm in its single

component (whose origin is currently unknown), it is so immersed in noise that it cannot be visually recognised and so safely[3] belongs to N.

So far, these results show the impact of the rhythmicity-analysis proposal that, by combining an enhanced measurement of R (as shown in Figure 8.6) with the validation of it, manages to properly group, not only well separated, but also noisy IC_ps. In addition, as this rhythmicity-analysis is implemented by using autocorrelation and PSD methods, the scheme manages a classification which is not only automatic, but also faster than those methods based on entropy or mutual information (Comani *et al.* 2007; Kraskov *et al.* 2005). On a PC with a Core2 Duo processor at 2.40 GHz, the whole rhythmicity-based analysis scheme takes no longer than 5 s to process a subsequence of ten IC_ps, whereas the implementation by Comani *et al.* (2007) takes almost 800 s only to calculate the Sample Entropy of the same subsequence. However, although these results are promising, since the classifier deals with imperfectly separated IC_ps (contaminated by other rhythms or background noise), it is important to be conscious that groups completely free from contamination cannot be retrieved without losing some physiological information. Therefore, this chapter considered a trade-off between the quality of the grouping and the risk of contamination so that only the best quality (*i.e.* validated) IC_ps are used to form the physiological groups. Consequently, some physiological but noisy information may be assigned to N and therefore missed at the time of reconstructing the physiological sources. The unique exception is MB that, even though may contain a highly contaminated IC^{50}_p (as discussed), is never discarded because it consistently contains the maternal breathing.

For the classifier performance, Figure 8.7 shows the specificity and sensitivity values enhanced from 0.77 to 0.96 after including the validation by S_I and $P_{(f,\ m)}$. These values, compared with the Se= 0.68 and Sp= 0.99 values produced by testing K-means once on the same dataset, show that, whilst K-means may be better at identifying maternal cardiac components, it poorly performs at identifying foetal cardiac components. On the other hand, the scheme described in this chapter performs well at distinguishing between both components. Additionally, this evaluation has also made it possible to corroborate/find the optimal thresholds for both *thrR* and *thrS* so that the physiological intervals for foetal and maternal IC_ps, required by the algorithm in Table 8.1, have been established according to Figure 8.7 (*i.e.* *thrR*= 1.6 Hz and *thrS*= 18.8 Hz). The former had already been proposed by considering other works (Guijarro-Berdinas *et al.* 2002; Ogueh *et al.* 2009; van Leeuwen *et al.* 2009). The latter, however, had not been previously proposed and therefore becomes an empirical value that

[3] Note that there are other noisy components that were disregarded in the IC_ps between IC^1_p and IC^{40}_p.

certainly requires further analysis, especially because of its level of activity in the validation stage, which averages 2 corrected IC_ps per subsequence. This number of average corrections may indicate that the IC_ps are noisy due to background noise rather than due to cardiac mixtures.

At this stage results show that the classification problem has been successfully dealt with, although it is still desirable to reduce the dependence on empirical values to make the method more robust (*e.g.* better to deal with harmonic effects and independent from preset values like *thrS* and the number of components to be classified). Therefore, it is considered that further and more specific analysis of the features obtained in Chapter 7 should make it possible to find more robust criteria to (a) measure[4] *R*, (b) calculate *thrS*, and (c) reduce the dimension of the components to classify (*e.g.* 10 or 15 rather than 50 IC_ps). By now, it is clear that the redundancy issue of SCICA has been dealt with and therefore, the next step is the reconstruction of the estimates of the segmented physiological sources underlying the 25 abdominal phonograms in the dataset. This will be performed in Chapter 9 where, to emphasize the evolution of this SCICA methodology, sources retrieved by the implementations discussed in this thesis will be presented.

8.6. Summary

This chapter presented a method that exploits the time-structure of the physiological components underlying the abdominal phonogram to automatically classify them into groups corresponding to maternal breathing activity (MB), maternal cardiac activity (MC), foetal cardiac activity (FC), and noise (N). To this end, a rhythmicity-based analysis scheme was proposed and tested on a dataset composed of 750 ICs extracted by SCICA from segments of 25 single-channel phonograms (recorded at foetal gestation ages between 29 and 40 weeks). Based on autocorrelation and PSD analysis, this scheme not only managed to quickly and automatically group similar IC_ps, but also correlated the groups with specific physiological phenomena (either maternal or foetal), which is an additional achievement.

Further research should be conducted to explore alternatives to make the method more robust and less dependent of empirical criteria. Now, and because this reliable grouping has already solved the redundancy issue of SCICA described in Chapter 6, the next chapter will retrieve the traces of the segmented physiological sources underlying the 25 abdominal

[4] Further research will have to explore whether the filtering and steadiness analysis steps are the best options to deal with the harmonic effects when measuring rhythmicity.

phonograms in the dataset. In a later chapter, the solution to recover entire time-series suitable for well-being surveillance will be presented.

9 RETRIEVING THE PHYSIOLOGICAL SOURCES UNDERLYING THE ABDOMINAL PHONOGRAM

Previous chapters in this thesis have discussed different aspects associated with antenatal well-being surveillance. First, antenatal foetal surveillance was introduced as a key part of maternal and foetal care. Next, different methods (both standard and alternative) used for monitoring foetal condition were analysed. After that, to exploit the advantages of the abdominal phonogram over the abdominal ECG and the FMG (*i.e.* single-channel recordings where the maternal and foetal cardiac activities do not spectrally overlap as significantly as in the latter two signals), SCICA was presented as an alternative approach for recovering significant physiological information from the single-channel abdominal phonogram (see Figure 9.1). The method, developed through three implementations, has shown promising results (Jimenez-Gonzalez and James 2008a; Jimenez-Gonzalez and James 2008b; Jiménez-González and James 2009; Jiménez-González and James 2010).

In a *first implementation* of SCICA (based on FastICA (Hyvarinen and Oja 1997) and *K*-means), the phonogram was separated into components corresponding to FHS, maternal breathing, maternal cardiovascular activity, and line-noise (Jiménez-González and James 2009). Thus, the outcome of this implementation showed, for the first time, the suitability of SCICA for decomposing the abdominal phonogram and, most importantly, for recovering foetal information (*i.e.* FHS). However, in that implementation the components were still contaminated by some noise, a problem solved later on by Jimenez-Gonzalez and James (2008b) by using TDSEP (Ziehe and Muller 1998), which is an ICA algorithm that utilises time-structure to define independence rather than higher-order statistics.

As a result of the *second implementation* of SCICA (based on TDSEP and *K*-means), the components separated by TDSEP always had spectra with a single and well-defined peak, whereas those separated by FastICA usually had spectra with more than one peak (attributed to contamination from other sources due to residual mixing after ICA) (Jimenez-Gonzalez and James 2008b). This outcome was promising since it showed that SCICA improved its

performance at separating foetal, maternal, and noise components. However, the enhanced separation reached by this second implementation was still far from solving the problem of recovering reliable estimates of the physiological sources underlying the abdominal phonogram, which required a better-quality grouping step.

As an alternative solution, after further studying the components features, their rich time-structure was exploited at the grouping stage, which led to a *third implementation* of SCICA (based on TDSEP and rhythmicity-based analysis) that successfully groups spectrally independent components into physiological groups (Jiménez-González and James 2010). Such groups, related to foetal cardiac (FC), maternal cardiac (MC), maternal breathing (MB), and noise (N) activities, are ready to be used for retrieving the estimates of the physiological sources underlying the abdominal phonogram. This will be performed in this chapter where, to show the evolution of the SCICA proposal in this research, both IC_ps and sources produced by the three implementations of SCICA will be presented.

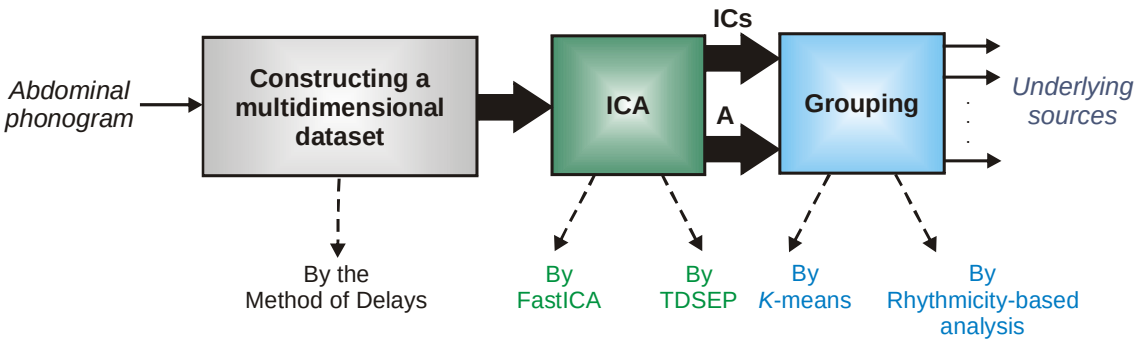

Figure 9.1. SCICA, an alternative methodology for decomposing the single-channel abdominal phonogram into its underlying sources. In this research two ICA algorithms (FastICA and TDSEP) and two methods for grouping (*K*-means and rhythmicity-based analysis) have been explored.

9.1. Aiming to decompose the abdominal phonogram: the first implementation of SCICA

This section shows results achieved by the *first implementation* of SCICA that, as detailed in Chapter 6, extracted *m* one-dimensional components by using FastICA and then formed 10 independent groups (composed of spectrally similar components) using *K*-means.

9.1.1. The IC_ps extracted by FastICA and grouped by *K*-means

Figure 9.2 depicts one segment of a noisy abdominal phonogram and sixteen of a total of fifty IC_ps separated by FastICA and grouped by *K*-means. From the abdominal phonogram, in the time domain, it is only possible to distinguish a slower component (with large amplitude

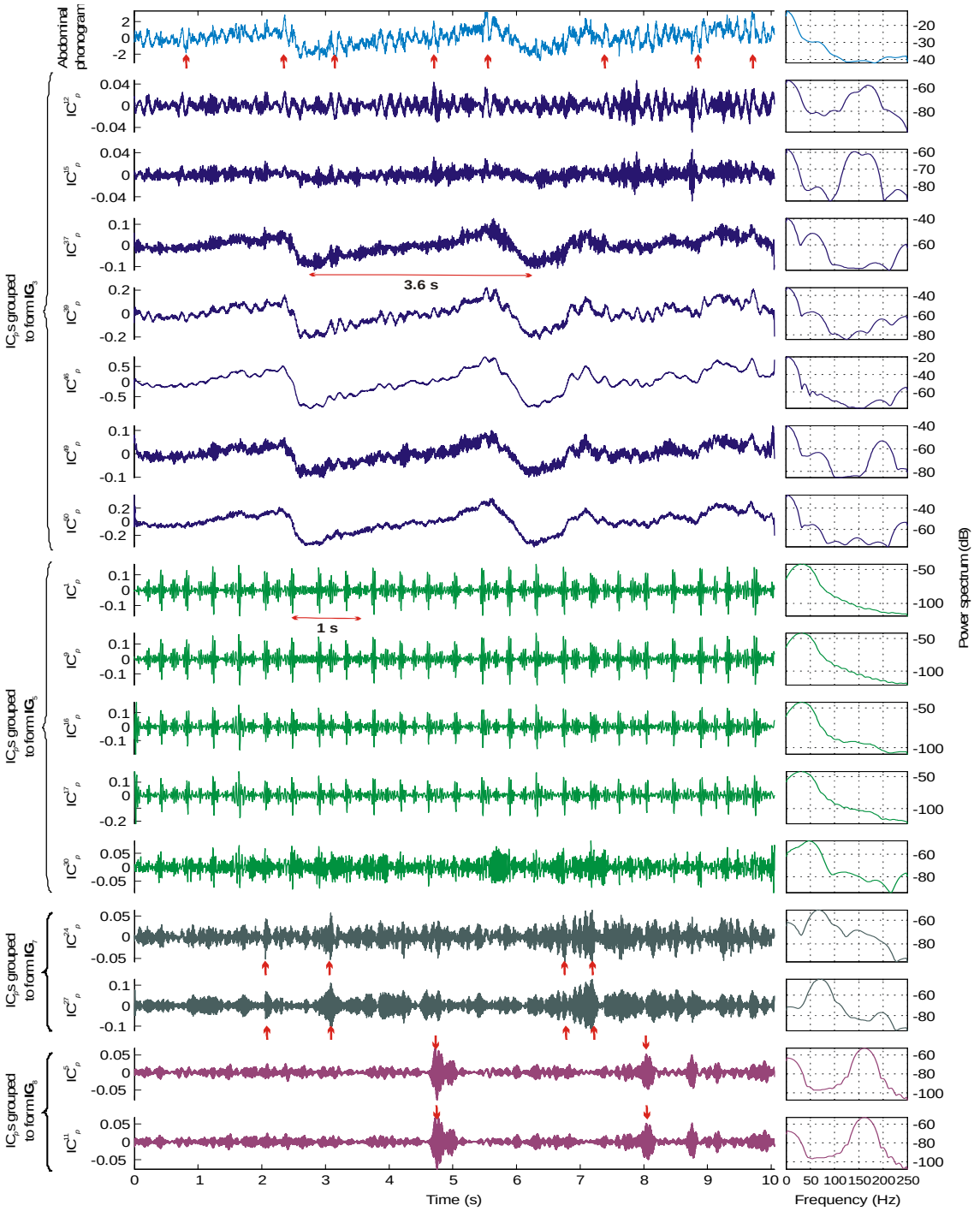

Figure 9.2. Four independent groups formed by *K*-means after clustering one-dimensional IC$_p$s separated by FastICA from a segment of noisy abdominal phonogram. From top to bottom: the recorded abdominal phonogram (normalised), **IG**$_3$: IC$_p$s with activity mainly below 25 Hz, **IG**$_5$: IC$_p$s with activity between 10 and 60 Hz and a peak close to 30 Hz, **IG**$_7$: IC$_p$s with activity between 50 and 100 Hz and a peak close to 60 Hz, and **IG**$_8$: IC$_p$s with activity between 140 and 190 Hz and a peak at 160 Hz. The corresponding power spectrum of the abdominal phonogram and its underlying IC$_p$s is shown on the right-hand side. The arrows in the abdominal phonogram point at some evident peaks in the signal, whereas the arrows in **IG**$_7$ and **IG**$_8$ point at some spontaneous activity apparently aligned with the activity in **IG**$_5$. © 2009 Springer Science+Business Media. Reprinted, with kind permission from Medical & Biological Engineering & Computing, Extracting sources from noisy abdominal phonograms: a single-channel blind source separation method, 2009, 47(6): 655-664, A. Jiménez-González and C. J. James, Fig. 1.

between ± 2 volts) and some peaks (the most evident indicated by arrows). However, there is not any clear evidence of FHS. In the frequency domain, it can be seen that the power of the signal ranges from 0 to 250 Hz with most power below 75 Hz (> -30 dB).

Regarding the sixteen IC_ps, grouped by *K*-means (based on their spectral similarity) to form the independent groups $\mathbf{IG}_3$, $\mathbf{IG}_5$, $\mathbf{IG}_7$, and $\mathbf{IG}_8$, it can be seen that: (i) $\mathbf{IG}_3$ is composed of seven low frequency IC_ps whose power is mainly distributed below 25 Hz. The first two, recovered as IC^{12}_p and IC^{15}_p, show the peaks previously referred to along with a signal between 150 and 160 Hz. The next five, IC^{37}_p, IC^{39}_p, IC^{46}_p, IC^{49}_p, and IC^{50}_p, show the slower component along with other signals in IC^{37}_p (60 Hz) and IC^{49}_p (200 Hz). In addition, it is also possible to distinguish periodic activity in the slower component almost every 3.6 s. (ii) $\mathbf{IG}_5$ is composed of five low frequency IC_ps between 10 and 50 Hz with a well defined peak centred close to 30 Hz. The first four, recovered as IC^1_p, IC^9_p, IC^{16}_p, and IC^{17}_p, clearly show periodic information that alternates at more than two times per second. The last component, IC^{30}_p, shows this periodic information as well, although contaminated by a signal that shifted the spectral peak from 30 to 50 Hz. (iii) $\mathbf{IG}_7$ is composed of two low frequency IC_ps whose power is mainly limited to between 50 and 100 Hz (> -80 dB) with a well defined peak centred at 60 Hz. These IC_ps, recovered as IC^{24}_p and IC^{27}_p, show some spontaneous activity, and some of it seems temporally aligned with the IC_ps in $\mathbf{IG}_5$ (the most obvious ones indicated by arrows). Finally, (iv) $\mathbf{IG}_8$ is composed of two high frequency IC_ps whose power ranges mainly from 140 to 190 Hz (> -80 dB) with a well defined peak at 160 Hz. As in $\mathbf{IG}_7$, these IC_ps, separated as IC^5_p and IC^{11}_p, also show some activity aligned with $\mathbf{IG}_5$ (a couple of arrows point to the most evident), although this time contaminated by some low frequency information below 25 Hz.

9.1.2. The sources estimated by SCICA based on FastICA and *K*-means

Figure 9.3 illustrates the estimates of the ten independent sources (is_P) retrieved by the first implementation of SCICA from the noisy abdominal phonogram depicted in Figure 9.2. From top to bottom, the abdominal phonogram, the separate is_P (P= 1,…,10) and, additionally, as a visual reference to identify the cardiac sources (*i.e.* foetal and maternal) in the set of is_P, the abdominal ECG is shown.

The sources, constructed by adding the IC_ps in the groups formed by *K*-means, can be described as follows: (i) is_1 clearly involves the peaks referred to at the beginning of the previous section (the most obvious of which are indicated by arrows) and, as shown in the figure, the main power (> -40 dB) of this source is below 50 Hz. Also, every time these peaks appear in is_1, they show some delay in relation to the maternal QRS complex (indicated by a dotted vertical line in a couple of complexes), which means that they are likely to represent

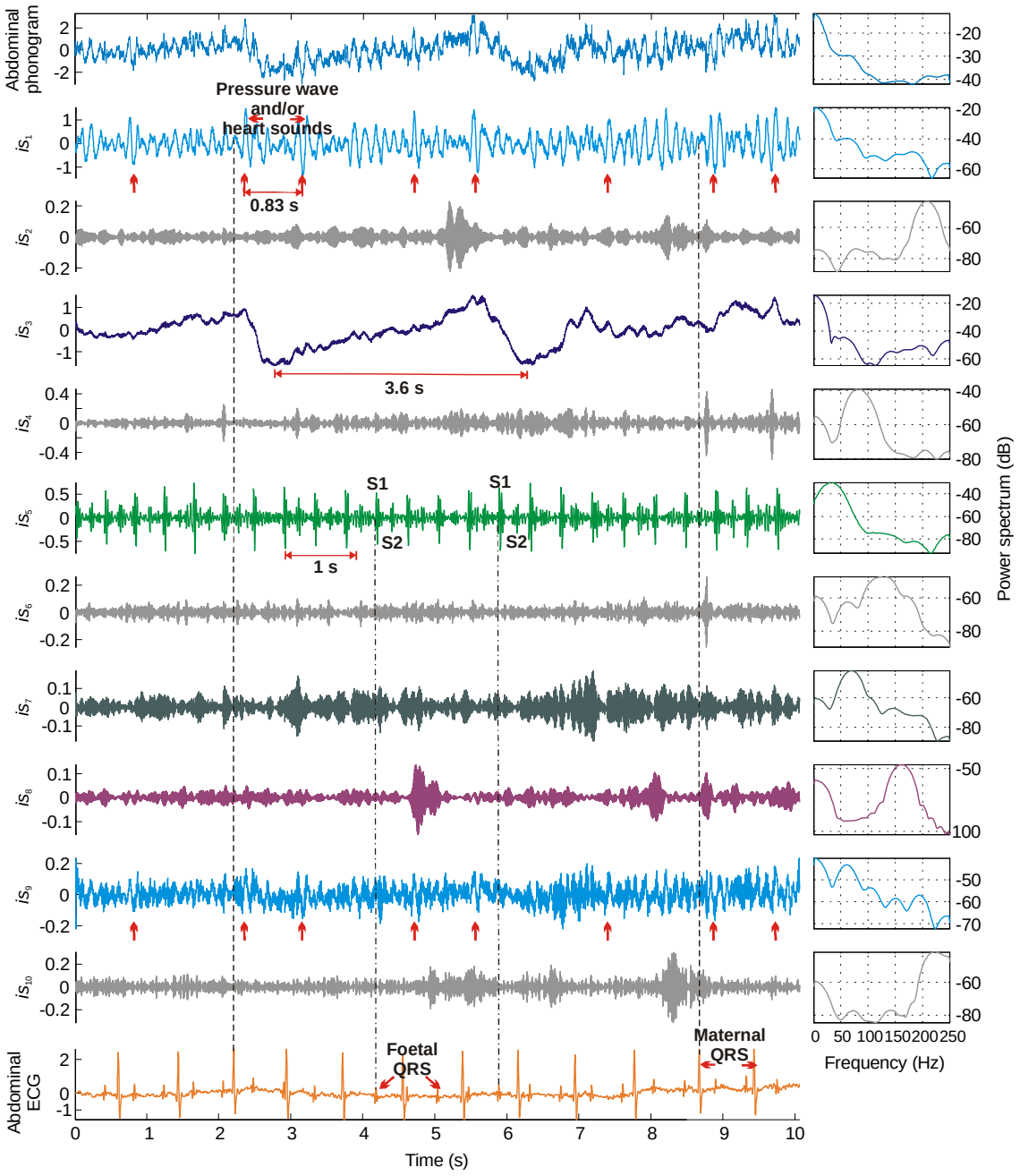

Figure 9.3. Ten independent sources (is_P) retrieved from a segment of noisy abdominal phonogram by the first implementation of SCICA (based on FastICA and *K*-means). From top to bottom: the recorded abdominal phonogram (normalised), its sources (maternal cardiovascular information in is_1, an unidentified source with activity at 207 Hz in is_2, a slow motion artifactual source associated with the maternal breathing in is_3, an unidentified source with activity at 82 Hz in is_4, the FHS (S1 and S2) in is_5, an unidentified source at 130 Hz in is_6, a 68 Hz source in is_7 (line-noise), an unidentified source with activity at 160 Hz in is_8, maternal cardiovascular information plus noise source in is_9, and an unidentified high frequency source in is_{10}), and the abdominal ECG (only as a visual reference to identify the foetal and maternal cardiac sources). The corresponding power spectrum of the abdominal phonogram and the sources is shown on the right-hand side. The arrows in is_1 and is_9 point at some peaks that are also present in the abdominal phonogram. © 2009 Springer Science+Business Media. Reprinted, with kind permission from Medical & Biological Engineering & Computing, Extracting sources from noisy abdominal phonograms: a single-channel blind source separation method, 2009, 47(6): 655-664, A. Jiménez-González and C. J. James, Fig. 2.

some *maternal cardiovascular activity* (*e.g.* the maternal pressure wave and/or the maternal heart sounds). (ii) is_2 represents a high frequency source whose power is mainly contained between 175 and 245 Hz (> -80 dB) with a well defined peak centred at 207 Hz. In this signal it is possible to see some spontaneous and high frequency activity from time to time. (iii) is_3, constructed from the $\mathbf{IG}_3$ described previously, shows a lower frequency source below 25 Hz with periodic activity almost every 3.6 s that could be related to the *maternal breathing*. (iv) is_4 shows a low frequency source whose power is mainly limited between 50 and 125 Hz (> -60 dB) with a well defined peak centred at 82 Hz. As in is_2, some spontaneous activity is present, although with shorter duration. (v) is_5, constructed from the $\mathbf{IG}_5$ described earlier, shows a low frequency source with a well defined peak centred close to 30 Hz. As mentioned previously, there is periodic activity in this signal, and from the figure it is clear that such activity is fully aligned with the foetal QRS complex (indicated by a dashed-dotted vertical line in a couple of peaks), which means that this source almost certainly corresponds to the *FHS*. Moreover, this FHS source clearly shows the two main heart sounds, S1 and S2, the former with the highest amplitude and always present, and the latter with lower amplitude and hard to detect in some heart cycles. (vi) is_6 shows a medium frequency source whose power is mainly restricted between 80 and 180 Hz with a peak at 130 Hz. (vii) is_7, constructed from the $\mathbf{IG}_7$ described previously, shows a low frequency source with a well defined peak centred close to 60 Hz. In this signal the presence of sporadic activity is particularly evident in the entire segment, and because of its frequency and time morphology, it could be mainly associated to *line-noise*. (viii) is_8, constructed from the $\mathbf{IG}_8$ described earlier, shows a high frequency source with a well defined peak centred at 160 Hz and additional information at frequencies below 25 Hz. As in is_2 and is_4, some sporadic activity appears from time to time. (ix) is_9, shows a source mainly composed of two frequencies, one lower than 25 Hz and another with a peak centred at 60 Hz. By comparing this source with is_1 and is_7, it can be said that there is a composition between the *maternal pressure-wave/heart-sounds* (the peaks mentioned in is_1 are indicated by arrows) and the *line-noise*. Finally, (x) is_{10} shows a higher frequency source whose power is mainly above 200 Hz. This signal also depicts some sporadic activity over the whole segment as well, although with different amplitude and duration.

Figure 9.4 depicts the *FHS sources* retrieved from two different segments of the noisy abdominal phonograms recorded on three subjects. Before going into more detail, it is important to notice that, for subject 1, one segment has been omitted. This “missing” segment corresponds to the one presented in figures and paragraphs above, therefore, it was considered unnecessary to repeat the segment and its analysis. As shown in the three subjects, in the time domain, even though it is virtually impossible to distinguish the FHS in the abdominal phonograms, the

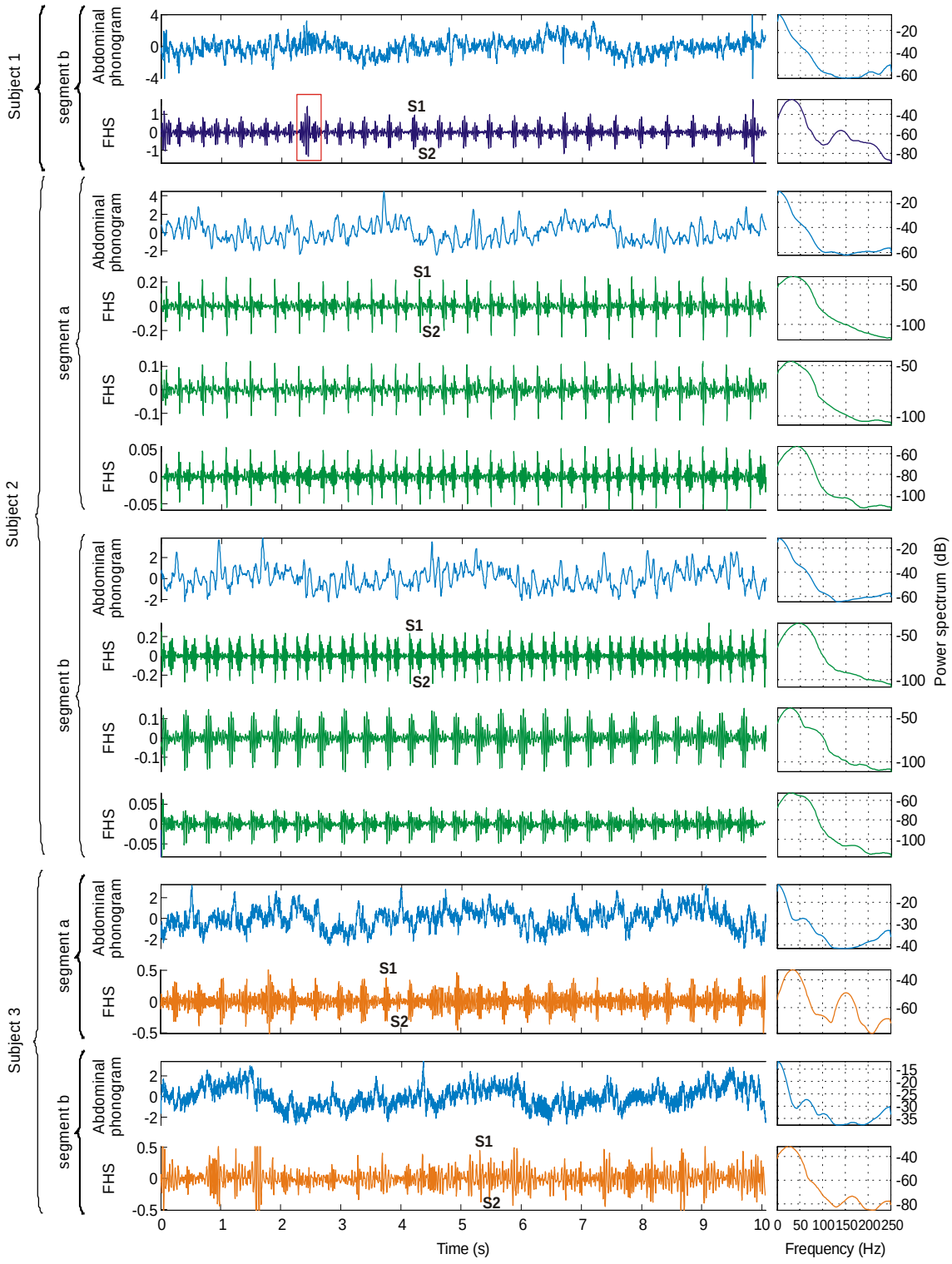

Figure 9.4. FHS sources recovered from two different segments of the abdominal phonograms recorded on three subjects. From top to bottom: Subject 1, segment b (one source); subject 2, segment a (three sources), segment b (three sources); subject 3, segment a (one source), segment b (one source). The corresponding power spectrum of the abdominal phonogram and its FHS sources is shown on the right-hand side.

method successfully extracted the corresponding sources, although with different number of sources and amplitude. In the frequency domain, all the FHS sources show components from 10 to 60 Hz with a well defined peak between 30 and 50 Hz. More specifically, from subject 1-segment *b*, the extraction looks quite good, it is not only possible to see one FHS source but also to clearly distinguish the main two sounds, S1 and S2. In addition, there is a heart cycle at 2.3 s where S2 is immersed in a transient source. For subject 2, even though the method extracted three FHS sources from each segment, the extraction looks quite good in both segments. In segment *a*, the three sources clearly show both S1 and S2 and slight differences in the frequency components of each source. In segment *b*, both the first and third FHS sources show S1 and S2, although they are better defined in the former. On the other hand, the second FHS source only shows clearly S1 and less so S2. Again, as in segment *a*, there are slight differences in the frequency components of each source. For subject 3, one noisy FHS source was extracted, so only S1 can be seen in each cardiac cycle and S2 from time to time. In the frequency domain, two well defined peaks close to 30 Hz and 150 Hz are present.

Figure 9.5 exemplifies the *maternal sources* recovered from those abdominal phonograms discussed in the previous paragraph. These sources, previously described as a slower component (with large amplitude) and some peaks (one of them indicated by an arrow), can be distinguished in these abdominal phonograms, but mixed with other sources. Again, as in the FHS case, only one segment for subject 1 is presented.

As illustrated in Figure 9.5, the maternal sources extracted by the method are different from segment to segment in both number and amplitude, and they can still be related to the maternal breathing activity and the maternal cardiovascular activity (for each source there is an arrow pointing to a well defined peak only as a visual aid). For subject 1-segment *b*, for example, only one maternal source, composed of both the respirogram (*i.e.* the breathing signal) and the cardiovascular signals, was extracted. For subject 2, a different number of sources was extracted from segments *a* and *b*. In segment *a*, three maternal sources appeared, the first one composed of the breathing and pressure wave signals. The other two sources, which are free of such a breathing component, contain either some pressure wave peaks (whose frequency is slightly higher than that of the peaks presented in the first source) or the maternal heart sounds. From these results it looks like the method did not completely separate the maternal information into *breathing* and *cardiovascular sources*, but the maternal cardiovascular sources in a low and high frequency parts (perhaps the *pressure wave* and *heart sounds*). In segment *b*, only one maternal source was extracted, which is composed of both the respirogram and cardiovascular signals. In subject 3-segment *a*, two maternal sources were extracted, one composed of the

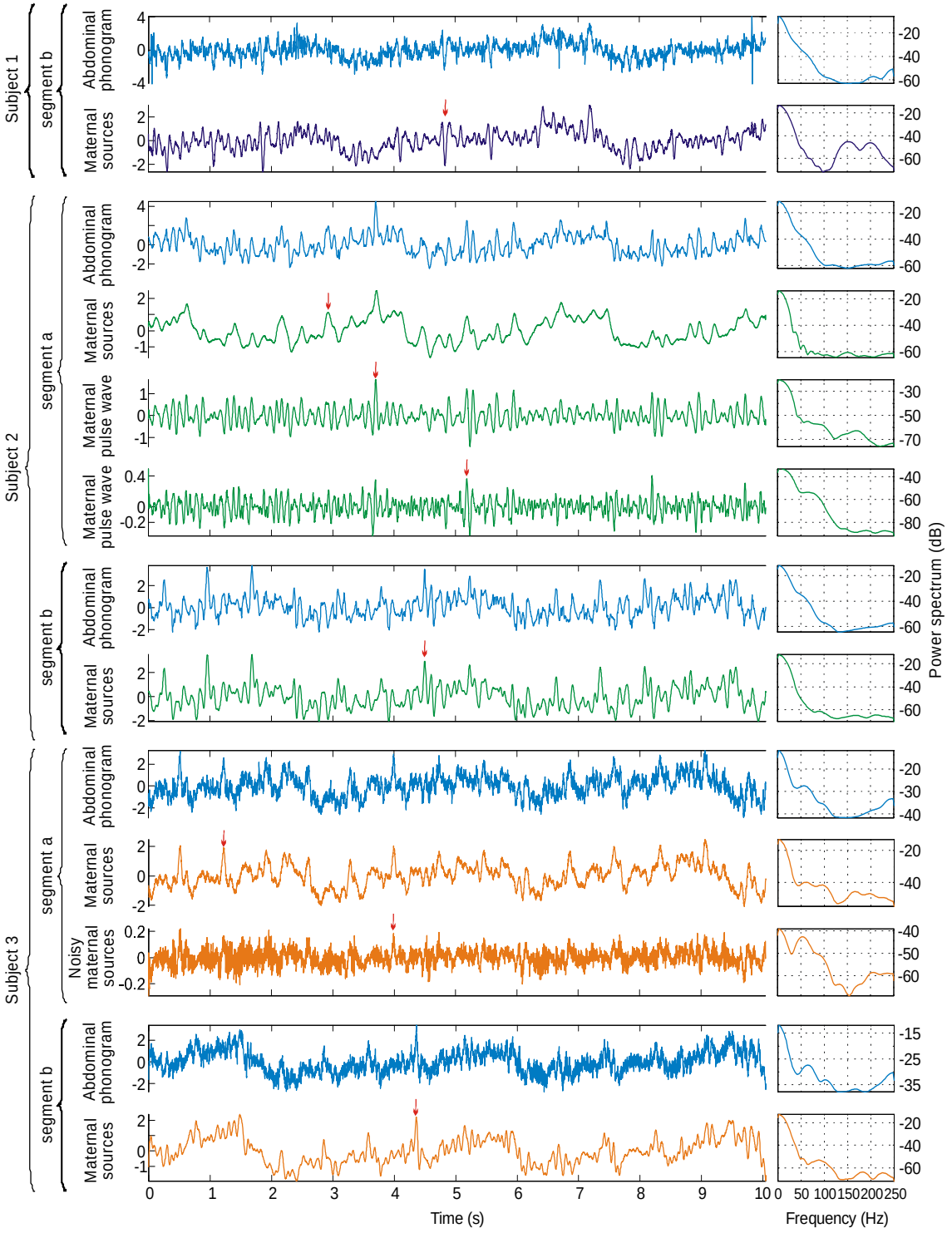

Figure 9.5. Maternal sources recovered from two different segments of the abdominal phonograms recorded on three subjects. From top to bottom: Subject 1, segment b (one source); subject 2, segment a (three sources), segment b (one source); subject 3, segment a (two sources), segment b (one source). The corresponding power spectrum of the abdominal phonogram and its maternal sources is shown on the right-hand side. The peaks pointed at by an arrow represent the peaks that might be associated to the maternal cardiovascular activity, either the pressure wave or the heart sounds.

respirogram and cardiovascular signals, and another composed of the cardiovascular signal along with a 60 Hz source. In segment *b* only one maternal source was extracted, which is composed of both the breathing and cardiovascular signals.

Figure 9.6 depicts the performance on the extraction of FHS by a "*general filter*" versus the SCICA-FastICA implementation. In this way it has been compared, in a visual manner, the quality of the FHS extracted by two zero-phase filter banks. The former, whose coefficients were generated once and remained invariable all over the signal; and the latter, whose coefficients were learnt (in each column of **A** that corresponds to the FHS groups (Davies and James 2007)) and changed from segment to segment according to the characteristics of the abdominal phonogram. Hence, to calculate the coefficients for the general filter, the coefficients learnt by FastICA for the FHS from five different segments were considered (segment 2, segment 8, segment 14, segment 20 and segment 26), and their median value was used to calculate the invariable coefficients. After that, the filter was applied to the abdominal phonogram of subject 1 on two of those segments used to generate the filter (segments 8 and 26), and on two new segments (segments 23 and 29). As can be seen, the general filter successfully extracted FHS in all segments as well, although it also included a slow component that has been previously associated to the maternal breathing. This slow component is also noticed in the power spectrum, where the general filter shows a wider response from 0 to 40 Hz in comparison to the one by SCICA-FastICA, which not only shows a band limited spectrum from 10 to 60 Hz but also a well defined peak centred close to 30 Hz.

9.1.3. Relevance of SCICA based on FastICA and *K*-means

As previously mentioned, this first implementation of SCICA produced promising results and raised the possibility of consistently retrieving foetal information from the abdominal phonogram (*i.e.* from different segments and different subjects). In addition, this implementation performed better than a "general" filter (whose coefficients remained the same over the time). Hence, the filters learnt by FastICA (Davies and James 2007) seem to be more selective, and this is because they are both band-limited and adaptive to the changes of the physiological signals from segment to segment, and subject to subject. At first sight, it appears that, even though the coefficients of an ordinary filter designed to extract the FHS (or any other source) may be known, the varying characteristics of the physiological sources are more likely to be better extracted by applying an adaptive data-driven method like the one studied in this research. However, since the filtering outcome in Figure 9.6 illustrates that the general filter is not removing as much of the lower frequencies as SCICA is removing, some of the filters used to construct such a general filter were not truly for FHS, but for maternal

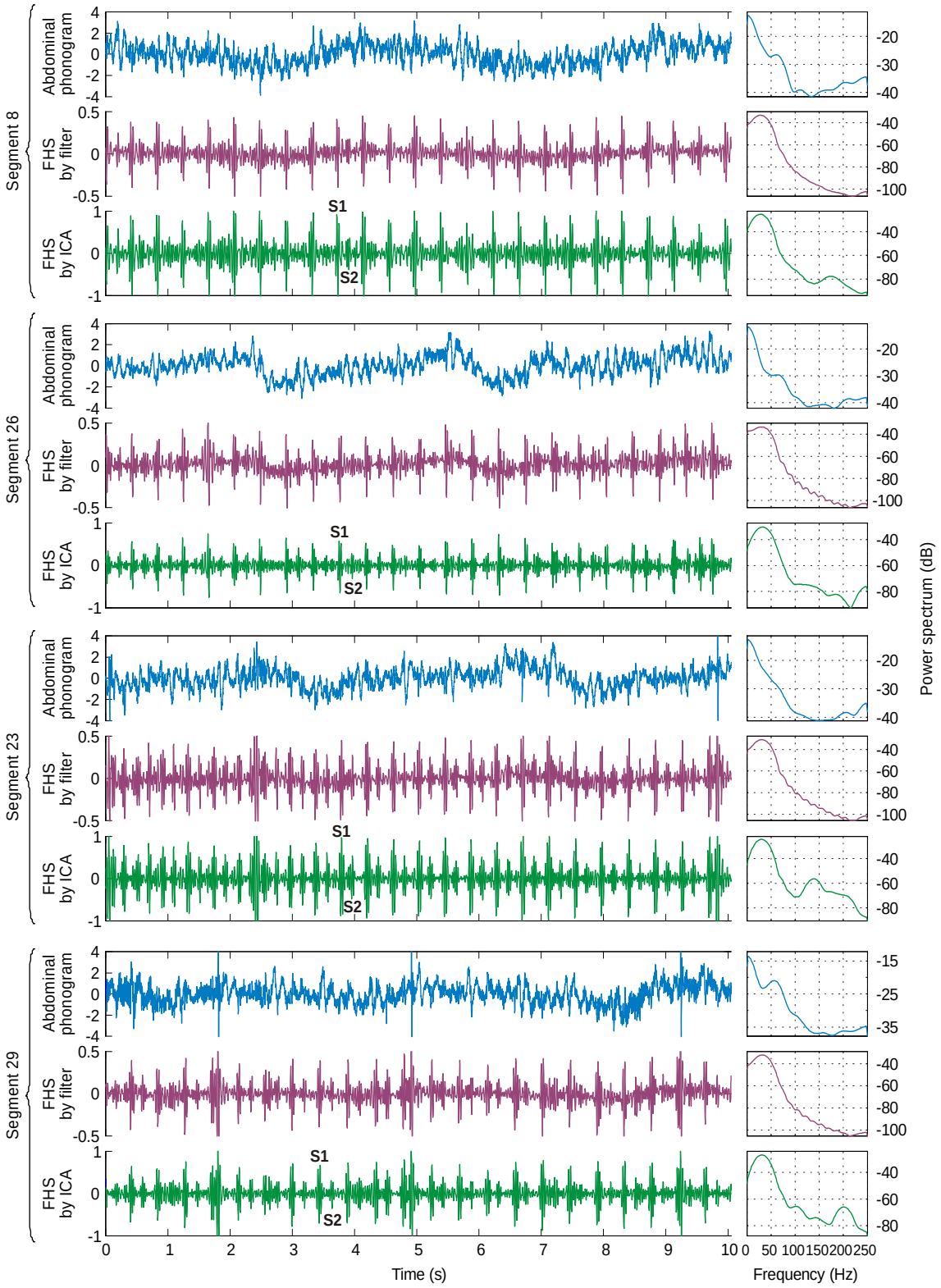

Figure 9.6. FHS extracted from different segments (same subject) by using a general filter and the proposed method. From top to bottom: Abdominal phonogram, FHS extracted by the general filter and FHS extracted by the proposed method in segments 8, 26, 23 and 29. The corresponding power spectrum of the abdominal phonogram and the FHS sources extracted is showed on the right-hand side.

components, which means that *K*-means probably misclassified some maternal components as foetal. Thus, to properly verify whether this SCICA approach overrules a general filter (or vice versa), further research will have to quantitatively characterise the performance of both filtering options, *i.e.* the data-driven filtering and the "general" filtering, especially on a larger dataset (this will conducted in Chapter 10).

The value of the embedding dimension (*m*) must be carefully chosen as it affects the quality of the separation of the underlying components. In fact, the appropriate selection of *m* depends on the problem in hand and on preliminary information extracted from the time series (Golyandina *et al.* 2001). For this work, due to the presence of periodic components such as FHS, Equation 6.17 provided a clear criterion indicating a value for *m* (Golyandina *et al.* 2001). In addition, although *m* is fundamental, the length of the segment N_A is also important for this single-channel approach, not only to construct the matrix of delays but also to provide enough data for FastICA to converge (Hyvarinen and Oja 1997; Hyvarinen and Oja 2000). On the face of it, it might appear that using a large N_A would be better for FastICA to converge more easily, but it is also necessary to consider that the stationarity of the signal is also fundamental for FastICA to work. So, N_A must be selected by considering a trade-off between the amount of data and its stationarity, otherwise FastICA may not converge. In this work, a value of that N_A = 5000 points (for a sampling frequency of 500 Hz) has been used to produce a matrix of delays that provides enough data for FastICA to converge and, as has been seen, the results obtained from three subjects are promising and show that the method extracts sources that can be related to different activities such as *foetal*, *maternal*, *line-noise*, and some "*unidentified*" *activities*.

Regarding the foetal activity, which is virtually impossible to distinguish from the original phonograms, it was effectively extracted in the form of FHS sources. These FHS sources, extracted in different number and amplitude, show the presence of the two main heart sounds, S1 and S2, the former with the largest amplitude. In addition, all the FHS sources showed a band limited behaviour from 10 to 60 Hz and a well-defined peak between 30 and 50 Hz. Regarding the maternal activity, composed of the respirogram and/or some cardiovascular sources (present from time to time with an unpredictable contribution to the phonogram and covering the bandwidth below 25 Hz), the method extracted most of it in all segments and subjects. This extraction was not necessarily as separate sources such as breathing and pressure-wave/heart-sounds (sometimes the signals were mixed with noise as well), but usually separate from the FHS. Considering these foetal and maternal activities in more detail, it is essential to point out the high performance of the method to extract these as separate sources. Thus, this separation is especially significant because the maternal cardiovascular information may overlap the FHS in the same way that the maternal QRS overlaps the foetal QRS in the abdominal ECG, and the most outstanding feature is that it was achieved by using a *single-channel method*. In

addition, because of the classifier used to group IC_ps, the method converges fast to produce 10 independent sources. As a first implementation, considering a fixed value of 10 groups is quite acceptable, since it is better having more than one group for one source (without misclassification) than having IC_ps misclassified into the wrong groups.

In summary, this *first implementation* of SCICA demonstrated the possibility of retrieving physiological information underlying the abdominal phonogram (*e.g.* FHS). However, the main problem was that some components still presented some degree of mixing that made them noisier and misclassified by *K*-means (a problem especially important when foetal or maternal cardiac components were placed into the wrong group).

9.2. Aiming to enhance the separation stage: the second implementation of SCICA

This section presents results achieved by the *second implementation* of SCICA that, as detailed in Chapter 6, extracted *m* one-dimensional ICs by using TDSEP and then formed 10 independent groups (composed of spectrally similar components) by using *K*-means.

9.2.1. The IC_ps extracted by TDSEP and grouped by *K*-means

Following the structure of the previous section, Figure 9.7 depicts the same segment of a noisy abdominal phonogram along with sixteen of a total of fifty IC_ps separated this time by TDSEP and grouped by *K*-means. From the abdominal phonogram, as described in Figure 9.2, it is only possible to distinguish a slower component and some peaks (the most evident indicated by arrows), but there is not any clear evidence of FHS. The power of the signal ranges from 0 to 250 Hz with its main part below 75 Hz (> -30 dB).

Regarding the IC_ps, grouped into clusters by *K*-means (based on their spectral similarity) to form independent groups like in $\mathbf{IG}_3$, $\mathbf{IG}_6$, $\mathbf{IG}_7$, and $\mathbf{IG}_8$, it can be seen that, as shown by their power spectra, the signals are more band-limited so that all of them present a single and well-defined peak. In a more detailed observation of the groups, it can be seen that: (i) $\mathbf{IG}_3$ is this time composed of six low frequency IC_ps whose power is mainly distributed below 50 Hz. The first three components, separated as IC^{45}_p, IC^{46}_p, and IC^{47}_p, show periodic activity at more than two times per second. The next two, separated as IC^{48}_p and IC^{49}_p, show the peaks previously referred to in the abdominal phonogram and, as shown by the arrows, periodically appear as a rate slightly larger than one per second. The last component, IC^{50}_p, resembles the slower component previously mentioned in the abdominal phonogram, which periodically appears almost every 3.6 s. (ii) $\mathbf{IG}_7$ is composed of four low frequency IC_ps between 10 and 75 Hz with

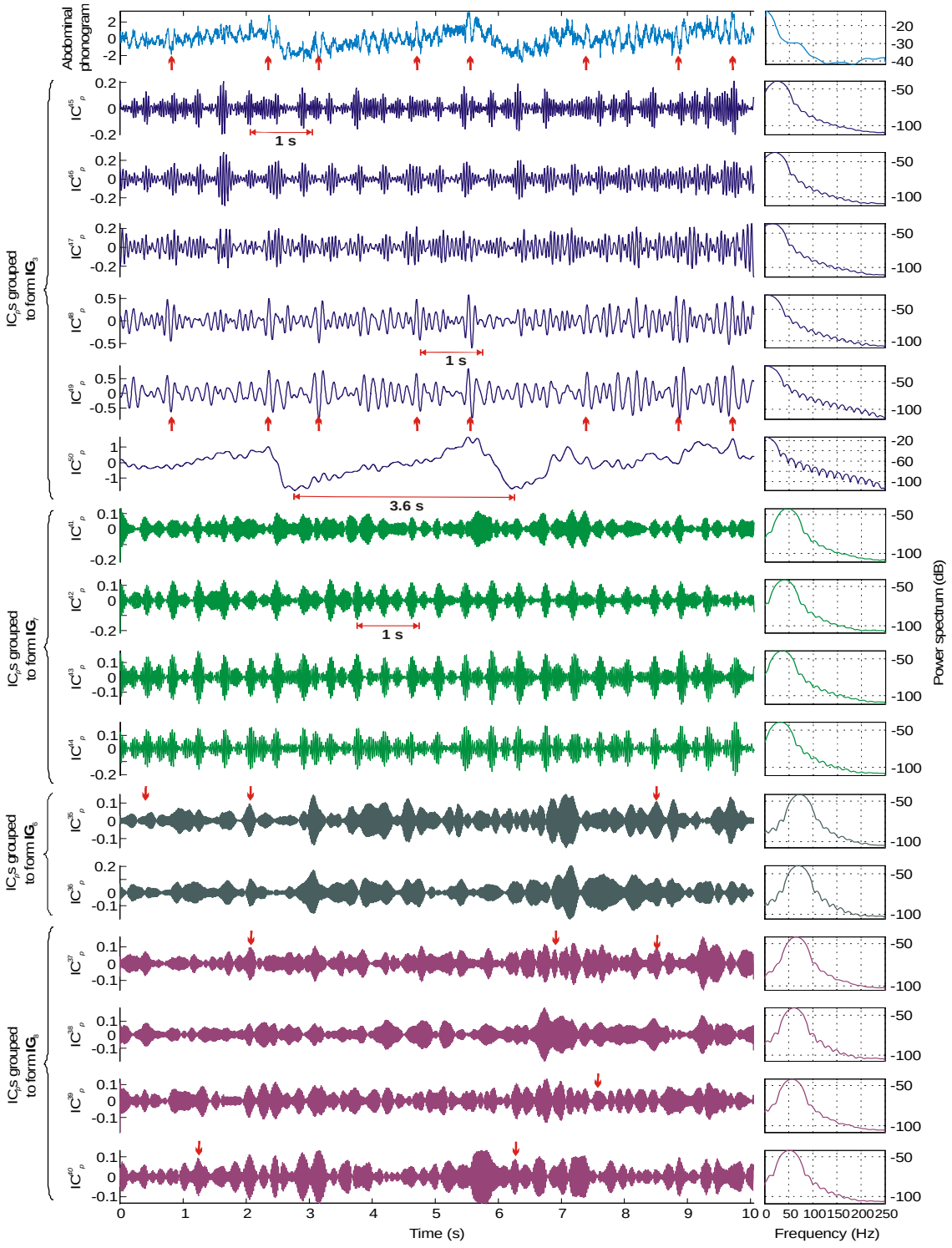

Figure 9.7. Four independent groups formed by *K*-means after clustering one-dimensional IC$_p$s extracted by TDSEP from a segment of noisy abdominal phonogram. From top to bottom: the recorded abdominal phonogram (normalised), **IG**$_3$: IC$_p$s with activity mainly below 50 Hz, **IG**$_7$: IC$_p$s with activity between 10 and 75 Hz and a single-peak close to 40 Hz, **IG**$_6$: IC$_p$s with activity between 50 and 100 Hz and a single-peak close to 70 Hz, and **IG**$_8$: IC$_p$s with activity between 25 and 75 Hz and a single-peak close to 60 Hz. The corresponding power spectrum of the abdominal phonogram and its underlying IC$_p$s is shown on the right-hand side. The arrows in the abdominal phonogram point at some evident peaks in the signal (also present in $IC^{48}{}_p$ and $IC^{49}{}_p$), whereas the arrows in **IG**$_6$ and **IG**$_8$ point at some spontaneous activity apparently aligned with the activity in **IG**$_7$.

a well defined peak centred close to 40 Hz. Such components, extracted as IC^{41}_p, IC^{42}_p, IC^{43}_p, and IC^{44}_p, also show periodic information that alternates at more than two times per second. (iii) $\mathbf{IG}_6$ is composed of two low frequency IC_ps whose power is mainly limited to between 50 and 100 Hz (> -80 dB) with a well defined peak close to 70 Hz. These IC_ps, extracted as IC^{35}_p, and IC^{36}_p, show some spontaneous activity, and some of it seems temporally aligned with the IC_ps in $\mathbf{IG}_7$ (the most obvious ones indicated by arrows). Finally, (iv) $\mathbf{IG}_8$ is composed of four IC_ps whose power ranges from 25 to 75 Hz with a well defined peak close to 60 Hz. As in $\mathbf{IG}_6$, these IC_ps, extracted as IC^{37}_p, IC^{38}_p, IC^{39}_p, and IC^{40}_p, show some activity aligned with $\mathbf{IG}_7$ (the arrows point to the most evident).

9.2.2. The sources estimated by SCICA based on TDSEP and *K*-means

Figure 9.8 shows the estimates of the ten is_P retrieved by the second implementation of SCICA from the noisy abdominal phonogram depicted in Figure 9.7. In addition, at the bottom, as a visual reference to distinguish between foetal and maternal cardiac sources, the abdominal ECG is shown.

The sources, constructed using the IC_ps in the groups formed by *K*-means, can be described as follows: (i) is_1 shows a medium frequency source whose power is mainly restricted between 80 and 150 Hz with a single-peak at 115 Hz. (ii) is_2 shows a medium frequency source whose power is mainly limited between 75 and 125 Hz (> -60 dB) with a well defined peak centred at 100 Hz. As can be seen, some spontaneous activity is present in is_1 and is_2. (iii) is_3, constructed from the $\mathbf{IG}_3$ described previously, shows a mixture whose frequency content is mainly below 50 Hz. There, the signal looks like a low-pass filtered version of the abdominal phonogram and it is possible to distinguish both, the slow periodic activity almost every 3.6 s (that could be related to the *maternal breathing*) and the peaks referred to at the beginning of the previous section (the most obvious indicated by arrows). Also, every time these peaks appear in is_3, they show some delay in relation to the maternal QRS complex (indicated by a dotted vertical line in a couple of peaks), which means that they are representing some *maternal cardiovascular activity* (*e.g.* the *maternal pressure wave* and/or the *maternal heart sounds*). (iv) is_4 shows a higher frequency source whose power is mainly above 200 Hz. This signal also depicts some sporadic activity over the whole segment, although of different amplitude and duration. (v) is_5 shows a high frequency source with a single-peak centred at 170 Hz. As in is_1, is_2, and is_4, some sporadic activity is present. (vi) is_6, constructed from the $\mathbf{IG}_6$ described earlier, shows a low frequency source with a single-peak centred at 70 Hz. (vii) is_7, constructed from the $\mathbf{IG}_7$ described earlier, shows a low frequency source with a single-peak centred close to 40 Hz. As mentioned previously, there is periodic activity in this signal, and from the figure it is clear that

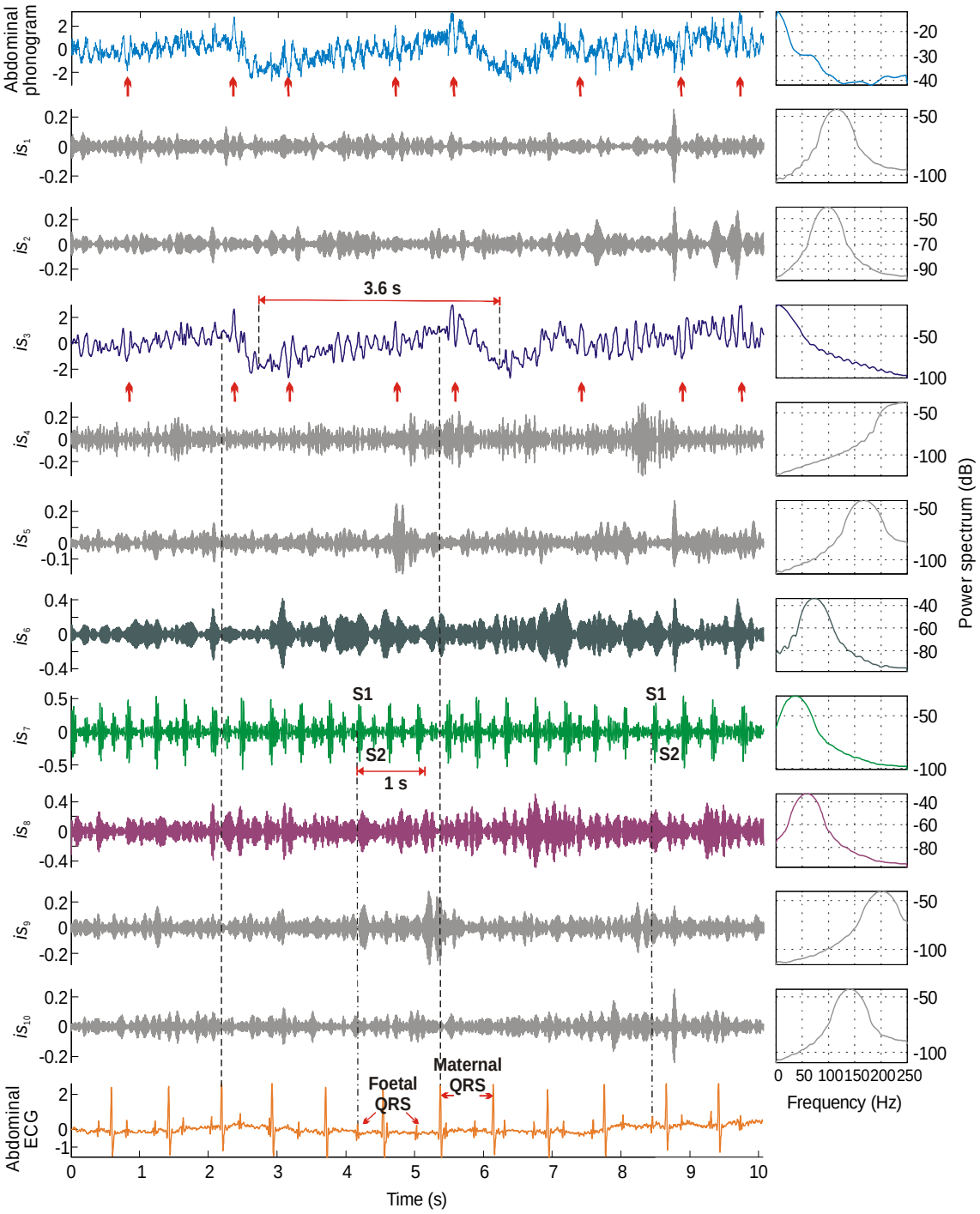

Figure 9.8. Ten independent sources (is_P) retrieved from a segment of noisy abdominal phonogram by the second implementation of SCICA (based on TDSEP and *K*-means). From top to bottom: the recorded abdominal phonogram (normalised), its sources (two unidentified sources with activities at 115 Hz in is_1 and 100 Hz in is_2, a mixture of maternal breathing and cardiovascular activities in is_3, three unidentified sources with activities at 200 Hz in is_4, 170 Hz in is_5, and 70 Hz in is_6, the FHS (S1 and S2) in is_7, the line-noise at 60 Hz in is_8, and two unidentified sources at 200 Hz in is_9, and 140 Hz in is_{10}), and the abdominal ECG (used only as a visual reference to identify the foetal and maternal cardiac sources). The corresponding power spectrum of the abdominal phonogram and the sources is shown on the right-hand side. The arrows in the abdominal phonogram point at some evident peaks in the signal that are also present in is_3.

such activity is fully aligned with the foetal QRS complex (indicated by a dashed-dotted vertical line in a couple of peaks), which suggests that this source corresponds to the *FHS*. Moreover, this FHS source clearly shows the two main heart sounds, S1 and S2, the former with the highest amplitude and always present, and the latter with lower amplitude and hard to detect in some of the heart cycles. (viii) is_8, constructed from the $\mathbf{IG}_8$ described earlier, shows a low source with a single-peak centred at 60 Hz. In this signal the presence of sporadic activity is evident in the entire segment, and because of its frequency and time morphology, it could be mainly associated to *line-noise*. (ix) is_9 shows a high frequency source whose power is mainly contained between 175 and 245 Hz (> -80 dB) with a peak centred at 200 Hz. In this signal it is possible to see some spontaneous and high frequency activity from time to time. Finally, (x) is_{10} shows a medium frequency source whose power is mainly restricted between 125 and 175 Hz with a peak at 140 Hz. This signal also depicts some sporadic activity over the whole segment as well, although of different amplitude and duration.

Figure 9.9 depicts a 10 s segment of noisy abdominal phonogram (subject 1- segment *b* described in Figure 9.4) and three of ten *is* (a, b, and c) retrieved by using the SCICA-FastICA and SCICA-TDSEP implementations (Jimenez-Gonzalez and James 2008b). The sources have been visually identified as: (a) FHS (S1-S2), (b) maternal activity (cardiovascular information superimposed on a slow-breathing component), and (c) line-noise. At the bottom, and only as a visual time reference, the abdominal ECG is shown. In addition, on the right-hand side of the phonogram and its sources, the corresponding PSDs are shown.

In the time domain, for the physiological sources in (a) and (b), it is difficult to visually distinguish differences between sources extracted by SCICA-FastICA and SCICA-TDSEP implementations, except that the amplitude in the FHS by TDSEP is a bit larger than the amplitude in the FHS by FastICA. In (c), it is clear that the line-noise amplitude by TDSEP is larger than that by FastICA. In the frequency domain, there is a clear difference between sources extracted by both methods in terms of the number of peaks in the PSD. For the signals extracted by TDSEP, the PSDs always show a single and well-defined peak, whereas for FastICA the PSDs usually show more than one peak. Similar results are present in different segments and subjects, *i.e.* both implementations extract these sources, and the amplitude of the sources retrieved by SCICA-TDSEP is larger than the amplitude of the sources retrieved by SCICA-FastICA. In addition, the PSDs are more band-limited in the SCICA-TDSEP implementation than in the SCICA-FastICA implementation.

9.2.3. Relevance of SCICA based on TDSEP and *K*-means

In general, as shown in the previous section, the second implementation of SCICA also manages to retrieve estimates of the sources underlying the abdominal phonogram, both

physiological and environmental and, again, foetal and maternal cardiac activities are extracted separately from each other. In particular, by comparing the features of the sources extracted by both implementations, it is clear that considering the temporal structure of the signal (by using TDSEP) produces a better-quality band-limited separation. As a result, SCICA-TDSEP retrieves sources whose PSDs have a single and well-defined peak and, consequently, that are less dependent on each other than those extracted by SCICA-FastICA.

In summary, considering the time-structure in this *second implementation* helped ICA find a more selective filter bank. However, in terms of the grouping stage, as seen in $\mathbf{IG}_3$ (Figure 9.7), *K*-means failed to differentiate amongst components corresponding to FHS, maternal cardiovascular, and maternal breathing activities, which compromised the enhanced separation achieved by TDSEP.

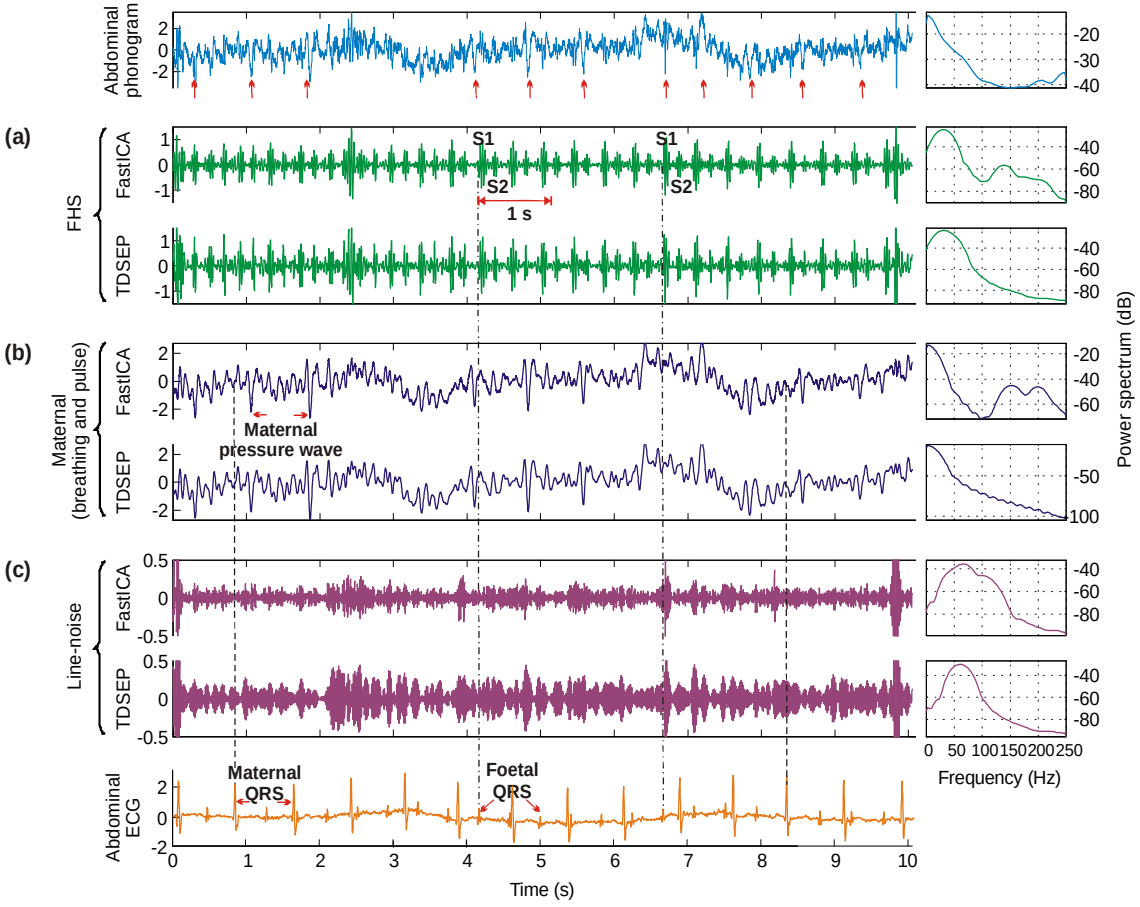

Figure 9.9. A segment of noisy abdominal phonogram and three independent sources retrieved by using the first (SCICA-FastICA) and second (SCICA-TDSEP) implementations of SCICA. From top to bottom: the recorded abdominal phonogram (normalised), its sources ((a) FHS, (b) maternal activity, and (c) line-noise), and the abdominal ECG (used as a visual reference to distinguish between maternal and cardiac sources). The corresponding power spectrum of the abdominal phonogram and its independent sources is shown on the right-hand side. The arrows in the abdominal phonogram point at some evident peaks in the signal.

9.3. Enhancing the grouping stage: the third implementation of SCICA

This section shows results achieved by the *third implementation* of SCICA, which extracted *m* one-dimensional ICs by using TDSEP and then formed physiological groups (composed of components with similar rhythm) only using rhythmicity-based analysis.

9.3.1. The IC_ps extracted by TDSEP and grouped by rhythmicity-based analysis

Figure 9.10 depicts the results of analysing a segment of a noisy abdominal phonogram and sixteen of a total of fifty IC_ps separated by TDSEP and grouped this time by using rhythmicity-based analysis. The abdominal phonogram, as described in Figure 9.2, presents little evidence of FHS, whereas its power spectrum is mainly below 75 Hz (> -30 dB). Additionally, as can be seen on the right hand-side, its strongest rhythm appears at 0.24 Hz.

Regarding the IC_ps, grouped into clusters by rhythmicity-based analysis to form four independent groups physiologically identified as $\mathbf{IG}_{FC}$, $\mathbf{IG}_{MC}$, $\mathbf{IG}_{MB}$, and $\mathbf{IG}_{N}$, it can be seen that: as shown by the power spectra, the signals are band-limited so that present a single and well-defined peak. More specifically, a detailed observation of the groups shows that: (i) $\mathbf{IG}_{FC}$ is composed of five slow IC_ps whose power is mainly distributed below 45 Hz and, most importantly, whose rhythm is centred at 2.3 Hz. Such components, extracted as IC^{42}_p, IC^{43}_p, IC^{44}_p, IC^{45}_p, and IC^{46}_p, show periodic activity almost every 0.42 s and are very clean (except for some small disturbances indicated by the downwards arrows). (ii) $\mathbf{IG}_{MC}$ is composed of three slower IC_ps whose power is mainly below 20 Hz, and whose rhythms are centred at 2.3 and 1.2 Hz. The last two components, extracted as IC^{48}_p and IC^{49}_p, present the peaks previously referred to in the abdominal phonogram and show periodic activity almost every 0.83 s. The first component, extracted as IC^{47}_p, shows some of such peaks (indicated by the upwards arrows) along with some of the information in $\mathbf{IG}_{FC}$ (indicated by the downwards arrows). (iii) $\mathbf{IG}_{MB}$ is composed of a single IC_p whose power is below 20 Hz and whose rhythm is centred at 0.24 Hz. This IC_p, extracted as IC^{50}_p, corresponds to the slowest component referred to in the abdominal phonogram and, as seen, periodically appears almost every 3.6 s. Finally, (iv) $\mathbf{IG}_{N}$ is composed of seven IC_ps whose power is larger than 45 Hz and whose rhythms range between 0.7 and 3.1 Hz. These IC_ps, extracted as IC^{35}_p, IC^{36}_p, IC^{37}_p, IC^{38}_p, IC^{39}_p, IC^{40}_p, and IC^{41}_p show spontaneous activity, some aligned with $\mathbf{IG}_{MC}$ and some with $\mathbf{IG}_{FC}$ (the downwards arrows illustrate the most evident).

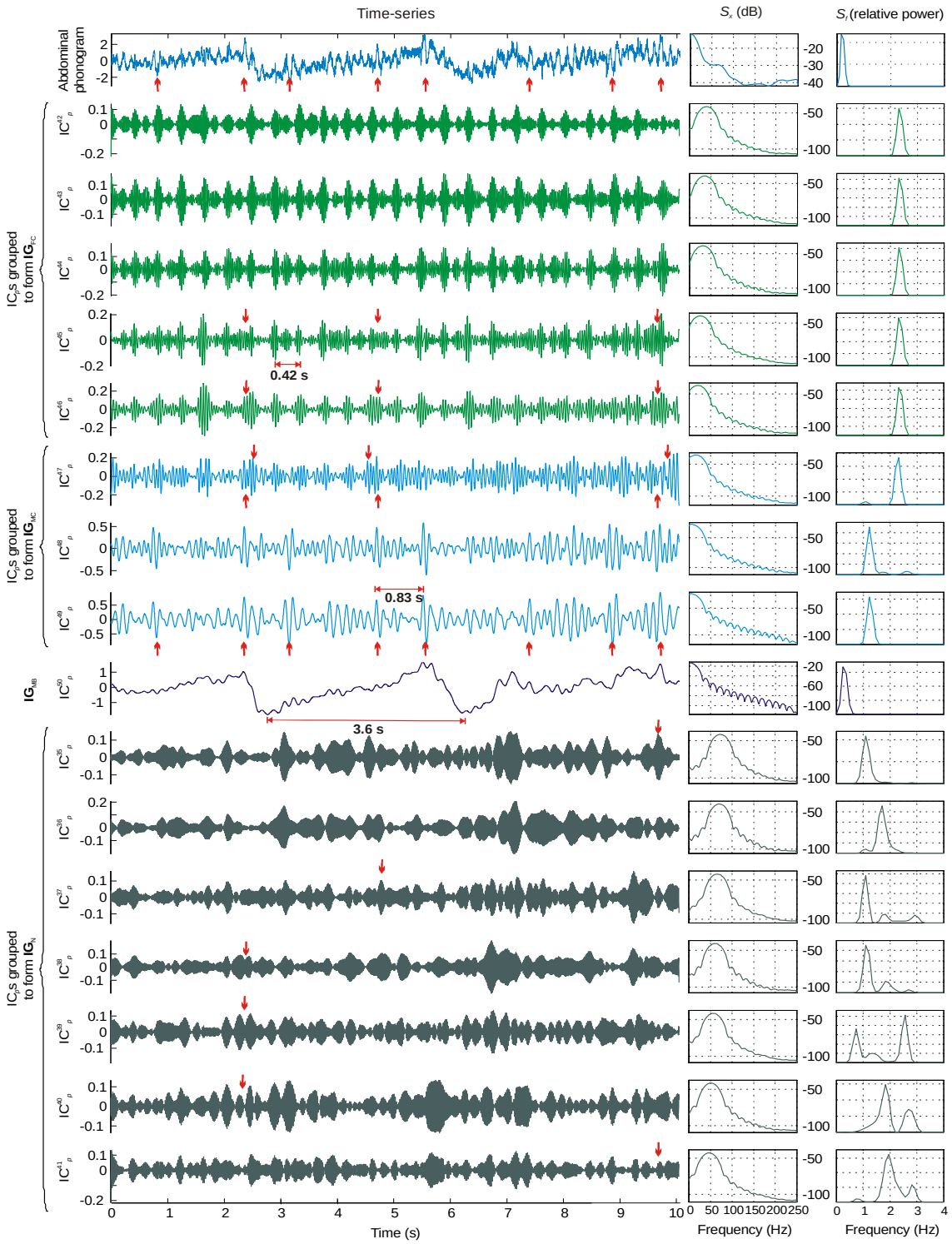

Figure 9.10. The physiological groups formed by rhythmicity-based analysis after clustering one-dimensional IC_ps (extracted from a segment of noisy abdominal phonogram by TDSEP). From top to bottom: the recorded abdominal phonogram (normalised), $\mathbf{IG}_{FC}$: IC_ps containing foetal cardiac activity at 2.3 Hz, $\mathbf{IG}_{MC}$: IC_ps containing maternal cardiovascular activity at 1.2 Hz, $\mathbf{IG}_{MB}$: a single IC_p containing maternal breathing activity at 0.24 Hz, and $\mathbf{IG}_N$: noise or noisy IC_ps. The corresponding power spectrum ($\hat{S}_x$) and rhythm ($\hat{S}_f$) of the abdominal phonogram and its underlying IC_ps are shown on the right-hand side. The upwards arrows in the abdominal phonogram point at some evident peaks in the signal (also present in $IC^{48}{}_p$ and $IC^{49}{}_p$), whereas the downwards arrows in $\mathbf{IG}_N$ point at some spontaneous activity apparently aligned with the activity in $\mathbf{IG}_{FC}$.

9.3.2. The sources estimated by SCICA based on TDSEP and rhythmicity-based analysis

Figure 9.11 depicts a segment of noisy abdominal phonogram and the estimates of the physiological sources (*is*) retrieved from a set of IC_ps classified by the rhythmicity-based analysis proposed in this research. From top to bottom, the time and frequency representations of: the abdominal phonogram, three physiological traces, the noise trace, and the abdominal ECG (used here to confirm the identity of the cardiac sources retrieved by this SCICA implementation rather than to identify them, as in the previous sections) are shown. The frequency representation, on the right hand side, shows two curves, the inner is the frequency content (from where S_I is calculated) and the outer is the autospectrum (which gives R).

The sources, constructed using the IC_ps in the groups formed by rhythmicity-based analysis, can be described as follows: (i) is_{FC}, constructed using the five IC_ps in $\mathbf{IG}_{FC}$, shows a low frequency source whose power spectrum is centred at 30 Hz and whose double-pattern rhythm is centred at 2.3 and 4.6 Hz. As previously mentioned, the time-series shows periodic activity every 0.42 s that is clearly aligned with the foetal QRS complex (indicated by a dotted vertical line), which means that this foetal cardiac trace corresponds to the *foetal PCG* (where the heart sounds can be seen*)*. Thus, the time-series clearly shows the two main heart sounds, S1 and S2, the former with the highest amplitude and always present, and the latter with lower amplitude and hard to detect in some heart cycles. (ii) is_{MC}, constructed using the three IC_ps in $\mathbf{IG}_{MC}$, shows a lower frequency source whose power spectrum is centred at 2 Hz and whose single-pattern rhythm is centred at 1.2 Hz. As seen in the time-series, this trace clearly presents the peaks referred to when the abdominal phonogram was described (the most obvious indicated by arrows) and show periodic activity almost every 0.83 s. Furthermore, every time these peaks appear in is_{MC}, they show some delay in relation to the maternal QRS complex (indicated by a dotted vertical line), which means that they are likely to be related to some *maternal cardiovascular activity* (*e.g.* the *maternal pressure wave* and/or the *maternal PCG*). (iii) is_{MB}, constructed using the single IC_p in $\mathbf{IG}_{MB}$, shows another slower source whose power spectrum is centred at 2 Hz and whose rhythm is centred at 0.24 Hz (calculated by using the FFT to make it easier to see the lowest frequencies). As can be seen, the time-series presents a slow periodic activity almost every 3.6 s, which could be related to the *maternal breathing*. (iv) is_N, constructed using the seven IC_ps in $\mathbf{IG}_N$, shows a low frequency source whose power spectrum is centred at 63 Hz, and whose multi-pattern rhythm shows frequencies at 0.12, 1.1, 2.2, 2.5, and 5.2 Hz. As can be seen in the time-series, the presence of sporadic activity is evident in the entire segment, and because of its frequency and time morphology, it could be mainly associated to *line-noise*.

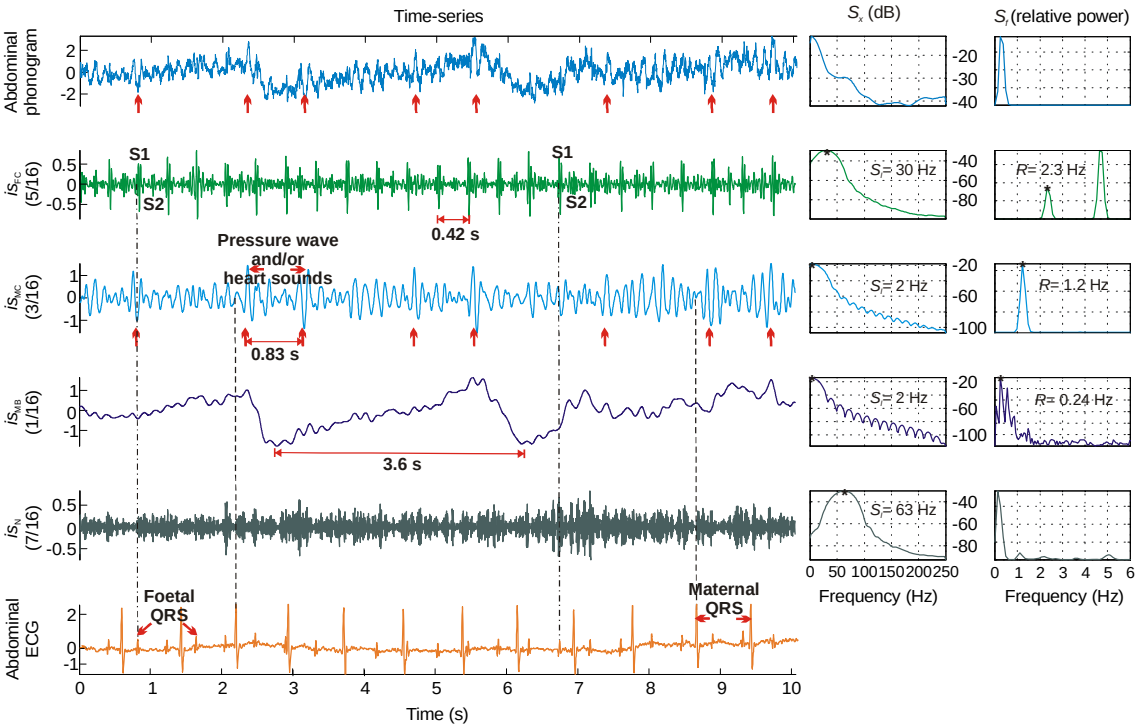

Figure 9.11. Physiological sources (*is*) retrieved from a segment of noisy abdominal phonogram by the third implementation of SCICA (based on TDSEP and rhythmicity-based analysis). From top to bottom: the recorded abdominal phonogram (normalised), its sources (foetal PCG in is_{FC}, pressure wave and/or PCG in is_{MC}, maternal respirogram in is_{MB}, and line-noise in is_{N}), and the abdominal ECG (used to confirm the identity of the cardiac sources retrieved by this SCICA implementation and to identify S1-S2 and the maternal pressure-wave/heart-sounds). The corresponding power spectrum ($\hat{S}_x$) and rhythm ($\hat{S}_f$) of the abdominal phonogram and its sources are shown on the right-hand side. The arrows in the abdominal phonogram point at some evident peaks in the signal that are also present in is_{MC}.

9.3.3. Relevance of SCICA based on TDSEP and rhythmicity-analysis

As described in the previous sections, the third implementation of SCICA has made it possible not only to better group similar IC$_p$s, but also to associate the groups directly to physiological phenomena (*i.e.* FC, MC, and MB), which is an extra achievement of this implementation. Thus, the method manages to successfully group similar IC$_p$s and, from them, to retrieve estimates corresponding to *foetal cardiac activity* (*i.e.* the FHS), *maternal cardiovascular activity* (composed of the heart sounds and/or the pressure wave), *maternal breathing*, and *noise*. Certainly, as mentioned in Chapter 7, because the method sometimes deals with imperfectly separated IC$_p$s, it is important to be conscious that a perfect trace will not always be retrieved. Here, a trade-off between the quality of the signal and the risk of contamination was considered so that only the best quality IC$_p$s (*i.e.* less contaminated by noise) were used to retrieve the estimates of the sources underlying the abdominal phonogram. Future work will focus on the reconstruction of entire time-series suitable for well-being surveillance.

In summary, considering the time-structure of the signal in this *third implementation* helps SCICA find not only a more selective filter bank, but also a more robust way to classify the separate components. As a result, it is possible to say that the performance of SCICA has been enhanced so that it better retrieves the physiological sources underlying the segmented abdominal phonogram than the previous implementations. The next chapter will be focused on recovering entire time-series suitable for well-being surveillance as here only short segments were considered.

9.4. Summary

This chapter presented the sources retrieved from the noisy abdominal phonogram by the implementations of SCICA discussed in this thesis (*i.e.* SCICA based on FastICA and *K*-means, SCICA based on TDSEP and *K*-means, and finally, SCICA based on TDSEP and rhythmicity-based analysis). Results showed the evolution of the SCICA methodology and how its performance is enhanced by using TDSEP –for separating ICs–, and rhythmicity-based analysis –for grouping ICs–. As a result, the current implementation of SCICA not only retrieves the sources underlying the abdominal phonogram, but also identifies the physiological processes that originate them (foetal and maternal). Next, this work will focus on the last requirement for SCICA, which is the reconstruction of entire time-series for well-being surveillance. This will be presented in the next chapter as part of the procedure needed to extract information for antenatal foetal surveillance in the form of beat-to-beat FHR and average morphology of the FHS.

10 WELL-BEING SURVEILLANCE THROUGH THE SOURCES ESTIMATED BY SCICA: A FEASIBILITY STUDY

This research has studied SCICA as an alternative signal processing approach to estimate the sources underlying the abdominal phonogram. Such a study, conducted through the development of three SCICA implementations, has given risen to a methodology that not only performs a spectral decomposition of the abdominal phonogram, but also identifies the origin of its physiological components, which are essential contributions of this work (Jimenez-Gonzalez and James 2008a; Jimenez-Gonzalez and James 2008b; Jiménez-González and James 2009a; Jiménez-González and James 2010a; Jiménez-González and James 2010b). Thus, as discussed in Chapter 9, the current implementation of SCICA automatically retrieves estimates of the sources corresponding to foetal cardiac activity (FC), maternal cardiovascular activity (MC), maternal breathing activity (MB), and noise or noisy activity (N) (Jiménez-González and James 2010b).

In particular, these separation results are especially significant since cardiac information from maternal and foetal sources is being retrieved in separate traces even though the former may temporarily overlap the latter (just like the maternal QRS overlaps the foetal QRS in the abdominal ECG). Furthermore, since MC and FC are clearly aligned with maternal and foetal QRS complexes respectively (as illustrated in Figure 9.11), it can be said that (a) MC is more likely to represent the maternal phonocardiogram (PCG) and/or the pressure wave, whereas (b) FC is more likely to represent the foetal PCG, a signal where the main foetal heart sounds (S1 and S2), can be seen. Hence, when applied to the abdominal phonogram, the foetal information retrieved by SCICA corresponds to the FHS which, as discussed in Chapter 3 and Chapter 4, are useful for monitoring well-being.

Now, since such foetal information is actually available, the work presented in this thesis can proceed towards its last stage, which is the collection of parameters for antenatal well-being surveillance. This task requires one to work on entire time-series rather than on the segmented

traces currently retrieved by SCICA. Therefore, the segmented traces must be first concatenated to assemble entire time-series from which well-being information can be collected. These were performed as described in this chapter to produce the final results of this research, which will be given by (a) the reconstruction of entire time-series of the sources underlying the abdominal phonogram and (b) the recovery of preliminary information for performing foetal well-being surveillance. The next sections detail the procedures proposed to do this, firstly by solving the energy uncertainty between adjacent segments (s_β and $s_{\beta'}$) described in Section 6.3.1, and then by detecting the temporal positions of S1 and/or S2 so that the beat-to-beat foetal heart rate (FHR) and the heart sounds' morphology can be estimated.

10.1. Transforming segmented traces into entire time-series

In order to concatenate segmented traces to form entire time-series, the two ambiguities of ICA have to be overcome (*i.e.* permutation and scaling). The permutation ambiguity, as discussed in Chapter 9, has been resolved due to the spectral decomposition performed by TDSEP and the grouping given by the rhythmicity-based analysis, which make it possible to arrange the retrieved traces as FC, MC, MB, and N. The scaling ambiguity, on the other hand, is tackled in this section by finding an appropriate scaling factor between adjacent segments.

First of all, before going into the description of how such a scaling factor can be calculated, it is important to be aware of the characteristics of an entire time-series reconstructed without correcting the scaling ambiguity. Hence, Figure 10.1 illustrates an example of the abdominal phonogram, five PCG segments retrieved by SCICA and, at the bottom, the entire time-series reconstructed by directly concatenating them. As can be seen, even though the PCG traces are extracted from overlapped segments (sharing 50% of their samples), their energies are different[1]. Consequently, when these traces are directly used to reconstruct the entire time-series, these differences in energy turn into sudden variations in the signal amplitude. Most importantly, since such amplitude variations are unpredictable because of the scaling ambiguity, they might be wrongly associated to changes in the foetal position and lead to erroneous interpretations about foetal activity, *e.g.* presence of foetal movements.

Now that the consequences of directly reconstructing entire time-series have been illustrated, it is time to describe the procedure followed to scale and concatenate segmented

[1] As mentioned in Section 6.3.1, empirical observations in this work indicate that such differences in energy are likely to depend on the number of IC_ps used to retrieve the sources rather than on the energy of the IC_ps.

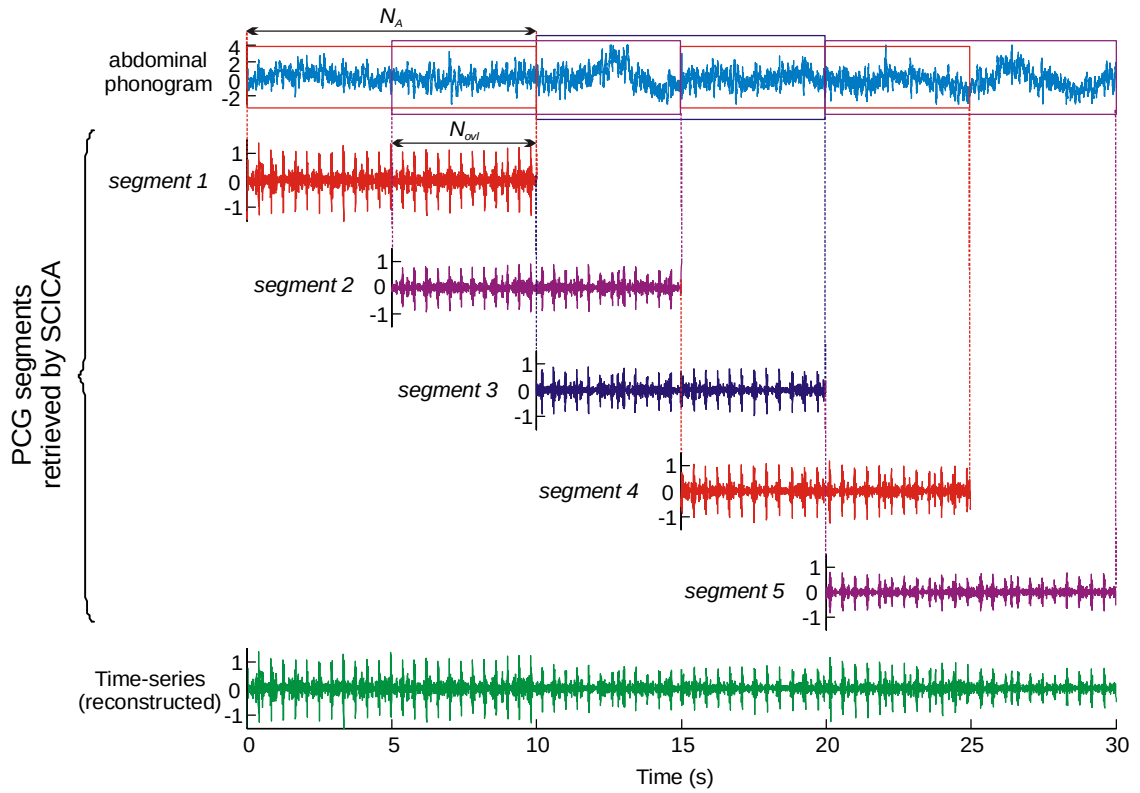

Figure 10.1. The scaling ambiguity between adjacent segments and its effect on the reconstructed time-series. From top to bottom: the abdominal phonogram divided into five overlapped segments, the PCG retrieved by SCICA from each segment, and the entire time-series directly reconstructed by concatenating such PCGs. The segments have a length of N_A samples and overlap each other by N_{ovl} samples.

traces for reconstructing entire time-series. For this purpose, and by following the idea by Corsini *et al.* (2006), this work uses the information in the overlapped sections to estimate a scaling factor that, by adaptively reducing the energy differences from segment to segment, aims to smooth sudden variations in the amplitude of the entire time-series.

In their work, focused on electroencephalographic signals (EEG) for seizure prediction, Corsini *et al.* (2006) estimated the scaling factor by comparing the variances within the overlapped sections between segments s_β and $s_{\beta'}$. The idea, although managed to recover entire time-series, failed to maintain continuity in cases where the EEG segments were corrupted (Corsini *et al.* 2006). Therefore, for longer recordings, where the number of corrupted segments usually increases, the authors argue that such a scaling methodology becomes an unreliable option. Here, to test such a scaling methodology on the segmented traces retrieved by SCICA, three entire time-series of foetal PCGs (composed of 59, 59, and 35 overlapped segments respectively) were reconstructed as proposed by Corsini *et al.* (2006). The results, given by empirical observations of the continuity produced on the reconstructed time-series, showed that the scaling factor did not manage to reduce the energy differences from segment-to-segment, but to increase them. Moreover, it was observed that such a scaling factor kept significantly

changing from segment-to-segment[2] to become either larger (in the former signal) or smaller (in the two latter signals). Consequently, after scaling and concatenating a few segments, the energy differences became so large that it was impossible to see the reconstructed signal using a single amplitude scale, which indicated that the estimation of the scaling factor by means of the variance was not a suitable option for the foetal PCG.

As an alternative, this work explored the calculation of the scaling factor by comparing the area under the curves (a_β and $a_{\beta'}$) within the overlapped sections of s_β and $s_{\beta'}$ as

$$a_\beta = \sum_{k=\frac{1}{2}N_A}^{N_A} \left| s_\beta(k) \right|, \tag{10.1}$$

and

$$a_{\beta'} = \sum_{k=1}^{\frac{1}{2}N_A} \left| s_{\beta'}(k) \right|, \tag{10.2}$$

where the resulting scaling factor, given by $a_\beta/a_{\beta'}$, was steadier than the one proposed by Corsini *et al.* Consequently, when applied to $s_{\beta'}$, this alternative scaling factor produced a scaled segment , $\hat{s}_{\beta'}$, suitable to be concatenated to s_β as (Corsini *et al.* 2006)

$$s_\beta(n + N_A) = \frac{a_\beta}{a_{\beta'}} s_{\beta'}(n + N_A - N_{ovl}), \qquad \text{for } n = 1, \ldots, N_{ovl}, \tag{10.3}$$

or alternatively

$$s_\beta(n + N_{ovl}) = \frac{a_\beta}{a_{\beta'}} s_{\beta'}(n), \qquad \text{for } n = 1, \ldots, N_A, \tag{10.4}$$

where N_A and N_{ovl} are the length of the segments and the overlapped sections respectively, and the concatenation uses either Equation 10.3 or Equation 10.4 to retain the segment with the largest energy.

The whole scaling-concatenating procedure, as detailed in Table 10.1, is repeated until all the segmented traces retrieved from an abdominal phonogram have been adaptively scaled and concatenated into an entire time-series. The resulting time-series, free of sudden amplitude

[2] Further research needs to be done to understand why the scaling factor is presenting such behaviour on the foetal PCGs that, according to the results on the tests conducted in this research, seems to be likely to exponentially change its value from segment-to-segment.

variations due to ICA, and corresponding to an underlying physiological activity, should be now ready for further analysis and recovery of information for well-being surveillance.

Table 10.1. Algorithm to reconstruct entire time-series by scaling-concatenating segmented traces retrieved by SCICA from the abdominal phonogram.

BEGIN

$\beta \leftarrow 1$

$scaled\_signal \leftarrow s_\beta$

FOR β' FROM 2 TO $number\_of\_segments$ DO

$N_S \leftarrow$LENGTH($scaled\_signal$)

$a_\beta \leftarrow \sum_{k=\frac{1}{2}N_A}^{N_A} \left| s_\beta(k) \right|$ % calculating the area under the second half of the curve

$a_{\beta'} \leftarrow \sum_{k=1}^{\frac{1}{2}N_A} \left| s_{\beta'}(k) \right|$ % calculating the area under the first half of the curve

$\hat{s}_{\beta'} \leftarrow \frac{a_\beta}{a_{\beta'}} s_{\beta'}$ % scaling the segment that will be attached

IF VARIANCE(s_β) > = VARIANCE($\hat{s}_{\beta'}$) THEN

$scaled\_signal(k + N_S) \leftarrow \hat{s}_{\beta'}(k + N_A - N_{ovl}),$ for $k = 1, \ldots, N_{ovl}$

ELSE

$scaled\_signal(k + N_S - N_{ovl}) \leftarrow \hat{s}_{\beta'}(k),$ for $k = 1, \ldots, N_A$

END

$s_\beta \leftarrow \hat{s}_{\beta'}$

END

END

10.2. On the collection of information for foetal surveillance

Once the energy uncertainty has been sorted out and entire time-series are available, it is time to focus on the analysis of such signals and collection of information for foetal surveillance purposes. Here, in a preliminary study, the entire foetal PCG is analysed to estimate (a) the beat-to-beat FHR and (b) the average morphology of the main FHS (S1, S2). To this end, as detailed next, the temporal positions of S1 and/or S2 are first detected in the PCG. Then, by using those positions, it is possible to (a) measure the distance between consecutive pairs and (b) align sounds to produce an average morphology.

10.2.1. Detecting the main heart sounds in the foetal PCG

Defining a temporal position for a heart sound is not a straightforward procedure, especially because there is not a consistent and well-known peak like the QRS in the ECG. Thus, as described in the next paragraphs, the task first requires preprocessing the PCG to produce

single-peaks (related to the FHS) that can be detected by setting a threshold. Next, whenever necessary, manual corrections can be performed to improve the detection. The procedure, implemented in four stages and applied to windows containing 5000 samples[3] (10 s in length), is as follows:

a) Peaks generation: This stage enhances the FHS to ease their visual identification in the window under analysis. It works in three steps

1. *Normalisation:* The PCG in each window is normalised as

$$\mathrm{PCG}' = \frac{\mathrm{PCG} - mean(\mathrm{PCG})}{std(\mathrm{PCG})} \tag{10.5}$$

to produce a signal with variance one (PCG'). Next, since large differences between low and high intensity sounds might complicate to notice low-intensity FHS, PCG' is normalised by a sigmoid function given by

$$\mathrm{PCG}_{norm}(n) = \frac{\exp(\vartheta) - 1}{\exp(\vartheta) + 1}, \tag{10.6}$$

where

$$\vartheta(n) = \frac{\mathrm{PCG}' - mean(\mathrm{PCG}')}{std(\mathrm{PCG}')}. \tag{10.7}$$

In this way, Equation 10.6 produces a signal where the differences between amplitudes of high and low intensity sounds are shortened so that it is easier to visualise most of the FHS in the window.

2. *Envelope calculation:* An envelope of PCG_{norm} is produced by means of the Hilbert Transform as detailed in Section 7.2.2.

3. *Smoothing:* This step is implemented by an FIR band-pass filter with cut-off frequencies of 4 and 11 Hz. The filter, adjusted to produce a single-peak envelope per heart sound, makes it easier to seek a single point related to each heart sound, which in this work is given by the maximum of the filtered envelope, $e_f(n)$.

[3] Note that this value of 5000 samples per window has nothing to do with the value of N_A in the decomposition by SCICA. The value of 5000 samples in this chapter has been chosen for each window to contain about 25 heart beats, which makes it easier to conduct manual corrections on the detected peaks whenever necessary. On the other hand, the value of N_A was chosen in Chapter 6 to provide ICA with a "quasi-stationary" segment for the algorithm to converge, and thus, to extract the independent components underlying the abdominal phonogram.

b) Peak detection: In this stage, the peaks of interest are found by manually establishing a threshold (*thr*) for $e_f(n)$. As a result, all the peaks whose amplitude is larger than *thr* are detected.

c) Peak correction: Due to the importance of an appropriate detection of the FHS positions in this study, and knowing that the thresholding produces false positives (FP) and/or false negatives (FN), it is necessary be certain that the peaks detected in this stage truly correspond to peaks of interest. To this end, some manual correction is performed, either to remove high-intensity peaks (due to artefacts) or to insert detections for low-intensity peaks (due to FHS). In those cases where the abdominal ECG is available, the positions of the foetal QRS are used as a visual aid.

The procedure, illustrated in Figure 10.2 for the detection of S1, is repeated segment to segment until the entire foetal PCG has been processed so that the beat-to-beat temporal positions of the *visually enhanced* FHS are known[4]. As noticed, the visual aid given by the foetal QRS positions (shown by the downwards triangles) makes it easier to identify the peaks corresponding to S1.

d) Final detection: This stage is implemented to remove the influence of the enhancing procedure on the "original" positions in the PCG, if any (produced by the second normalisation). Thus, the positions estimated on the enhanced FHS become the reference to automatically find the peaks on the smoothed envelope of the original PCG (*i.e.* without enhancing), which are the positions used in the methods described in the next sections.

10.2.2. Calculating foetal heart rate and heart sounds morphology

Once the HS positions are known, it is time to obtain information for foetal surveillance. In this work, as a preliminary study, the FHS positions are used to estimate (a) the instantaneous FHR and (b) the average morphology of the FHS. The former, as described in Chapter 2, makes it possible to promptly spot variations in the sympatho/vagal balance due to foetal oxygenation changes. The latter, as described in Chapter 4, gives information about the status of the foetal heart valves during the heart cycle.

a) Instantaneous foetal heart rate (FHR): This is calculated by measuring the beat-to-beat distance between heart sounds (*i.e.* S1-S1 or S2-S2), which makes it suitable to monitor the

[4] S1 and S2 are detected only in those cases where their intensity is large enough to distinguish them from background noise. In this study, only S1 is large enough to be easily detected by using a simple methodology like the one described herein.

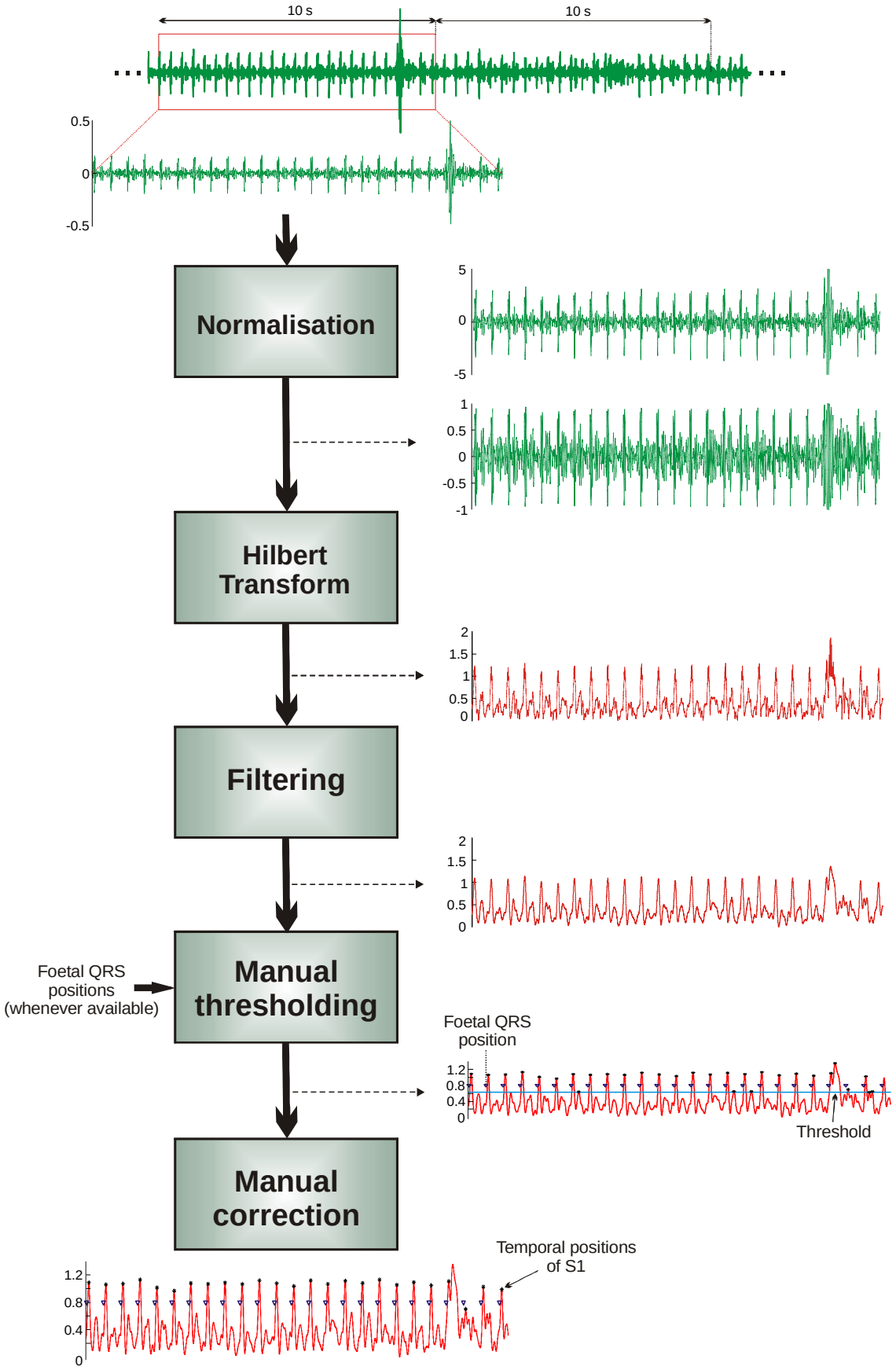

Figure 10.2. Analysis of the foetal PCG to ease the detection of beat-to-beat temporal positions of the FHS. In this example, the detection of the first heart sound (S1) is illustrated.

FHR by means of the FHS. The procedure, either implemented by using S1 or S2[5], is as follows:

1. *Cardiotachogram generation (CTG)*, which is performed by measuring beat-to-beat intervals given by the FHS.

2. *CTG examination and correction*: This is developed in two steps, inspection and manual correction. The former, visually performed, carefully examines abnormal intervals in the CTG (*i.e.* sudden variations towards either lower or higher heart rates) to establish whether they are caused by peaks wrongly detected, or by real variations in the cardiac intervals. In those cases where peaks are incorrectly detected, the CTG is manually corrected by removing wrong peaks and by inserting right peaks.

   Here it is important to mention that this step is often necessary in those subjects where the QRS positions are unavailable. In those cases, the presence of artefacts around the FHS and the lack of a reference signal complicate the selection of the right peak, whose wrong selection becomes evident until the CTG is generated.

3. *CTG trend estimation*, which is performed by smoothing the CTG to produce the FHR trend over time. For this purpose, the CTG is interpolated at 4 Hz by using a spline function. Next, the interpolated CTG is low-pass filtered by using an FIR filter with cut-off frequency of 0.3 Hz and 20 coefficients, parameters that preserve the CTG trend.

b) Average heart sounds morphology (avgS): This is implemented by processing the foetal PCG as follows:

1. *Extraction of FHS:* By considering results in previous work (Jiménez-González and James 2009b), the FHS are extracted from the foetal PCG by using a window. The window, of length 0.3 s for S1 and 0.2 for S2, is centred at the positions detected in Section 10.2.1.

2. *Selection of similar FHS:* Useful FHS are chosen based on their similarity, which in this work is measured by looking at the correlation between adjacent heart sounds. Firstly, the extracted FHS are normalised so that their maximum amplitude is one. Secondly, adjacent FHS are compared and only those showing correlations larger than

[5] When using S2 it should be taken into account that the resulting FHR is likely to include not only the beat-to-beat variations, but also systolic variations (*i.e.* changes in the intervals between S1 and S2 due to chronotropic changes in the heart function).

80% are chosen. Finally, the selected heart sounds are aligned by using their maximum cross-correlation.

3. *Averaging FHS:* The mean value of the aligned FHS is calculated to produce an estimate of the average morphology of S1 (avgS1) or S2 (avgS2) in intervals of 60 s. Such a morphology, as stated by Zuckerwar *et al.* (1993), provide information about the status of the heart valves.

10.3. Complementing foetal observations

Before going into the final analysis of the foetal parameters already obtained, it is essential to be aware that there is still some additional information that can be collected and, most importantly, that such information can be used to complement the foetal CTG and help perform surveillance. This information, present in the other physiological signals recovered by SCICA as well as in the "gold standard" signals recorded simultaneously with the abdominal phonogram (as detailed in Chapter 5), is here collected in the form of complementary parameters that will be finally used in the analysis and discussion of the feasibility of SCICA for antenatal surveillance. Hence, this section gives an overview of the set of signals currently available and describes the procedures followed to collect additional parameters of interest.

10.3.1. Set of available signals

The available signals are classified depending on the method used to obtain them. Hence, FC, MC, MB, and N, which result from the decomposition of the abdominal phonogram, will be from now on referred to as *the estimated signals*. On the other hand, the additional variables, which were recorded simultaneously with the abdominal phonogram, will be referred to as *the reference signals*.

a) The estimated signals: As may be recalled, four physiological sources are retrieved by SCICA here, the foetal PCG, the maternal PCG and/or pressure wave, the maternal respirogram, and noise. Such signals have been consistently retrieved by applying SCICA to a total of 25 single-channel abdominal phonograms.

b) The reference signals: To recall Chapter 5, at the time the abdominal phonogram was recorded, whenever possible, the abdominal ECG was recorded. Also, the FBM, the FMs, and the maternal respirogram were recorded. The FBM and FMs signals were produced as event markers by two observers that pressed a push-button switch whenever such movements were spotted in US images. The maternal respirogram, on the other hand, was recorded by using a piezoelectric sensor positioned around the maternal chest. Thus, in those cases where the abdominal ECG was available, a total of five variables were

measured per recording session: the abdominal phonogram, the abdominal ECG, the FBM, the FMs, and the maternal respirogram (see Table 5.2 for more details).

10.3.2. Additional parameters of interest

Given this important set of signals is available it is essential to be cautious and avoid ambitious and complex analysis of them (*i.e.* attempt to collect as many parameters as possible by means of different signal processing approaches). Thus, by keeping in mind that the objective of the work presented in this chapter is exploring the feasibility of SCICA for antenatal surveillance, the quest has been focused on the recovery of simple but significant parameters reflecting the vital signs such as FHR, maternal heart rate (MHR), and maternal breathing rate (MBR). Additionally, the average morphology of the main heart sounds and the SNR of the PCG have been considered as information of interest. The next paragraphs describe the methods used to collect additional parameters from the estimated and the reference signals.

a) Beat-to-beat signal to noise ratio (SNR(n)): Whilst the observation of FHR and FHS average morphology provide information for well-being surveillance, this research considers that observing the SNR in the foetal PCG will determine how reliable such information is. Hence, as a rough beat-to-beat estimation, the SNR is calculated by using the FHS positions and the smoothed envelope e_f(n). To this end, as shown in Figure 10.3, since the FHS are represented by peaks in the envelope, the amplitude of each peak is taken as the instantaneous signal value (hs_{val}), whereas the minimum point between adjacent peaks is taken as noise. Next, to define an instantaneous noise value ($noise_{val}$) per peak, its adjacent noise values (*i.e.* the one on the left-hand side, $noise_L$, and the one on the right-hand side, $noise_R$) are averaged. Finally, the SNR(n) is calculated as

$$\mathrm{SNR}(n) = 20 \cdot \log_{10} \frac{hs_{val}(n)}{noise_{val}(n)}. \tag{10.8}$$

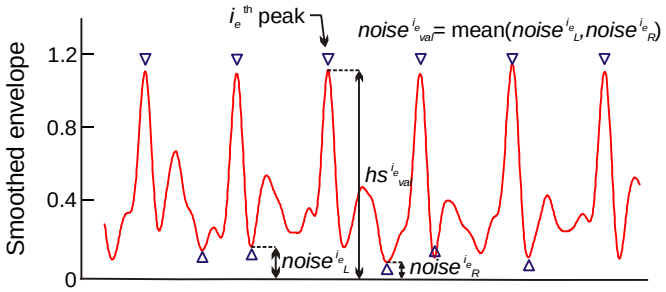

Figure 10.3. Parameters used to estimate the instantaneous SNR in the foetal PCG according to S1. The downwards triangles point at the peaks considered as signal ($hs^{i_e}_{val}$), whereas the upwards triangles point at the valleys considered as background noise ($noise^{i_e}_{L}$, $noise^{i_e}_{R}$).

In this way, by using either S1 or S2, variations in the SNR of the foetal PCG have been collected.

b) Instantaneous maternal heart rate (MHR): This is calculated to sketch the maternal status at the time of recording and observe whether it has some influence on the foetal CTG. To obtain it, the estimated maternal PCGs were processed as in Section 10.2.1 to detect peaks associated to the maternal heart beat and then to generate a CTG that could be finally examined and corrected as formerly described.

c) Reference maternal heart rate: Calculation of this parameter is useful to judge the quality of the CTG generated by means of the maternal PCG, at least in those cases where the abdominal ECG is actually available. To do so, since the SNR of the maternal QRS complexes is typically higher, the maternal QRS complexes in the abdominal ECG are detected and then the R-R intervals are measured as follows:

1. *Band-pass filtering:* Implemented by an FIR filter with cut-off frequencies at 10 and 40 Hz, it removes breathing and high frequency noise from the abdominal ECG so that the maternal QRS is easily detected. Next, the filtered signal is processed in windows containing 5000 samples (10 s in length) as next described
2. *Maternal QRS detection:* This step detects QRS complexes that are larger than a threshold manually established according to the window under analysis.
3. *Manual correction:* In cases where QRS complexes are wrongly detected, they are manually corrected by removing artefacts and by inserting missing complexes.

Steps 2 and 3 are repeated window by window until the entire filtered ECG has been processed and the positions of the maternal QRS complexes are known.

4. *CTG generation:* This is performed by measuring R-R distances.
5. *CTG examination and correction:* As described in Section 10.2.2, this step carefully reviews the CTG and corrects any abnormal intervals produced by QRS complexes wrongly detected.

d) Reference foetal heart rate: As in the previous case, calculation of this parameter is useful to judge the quality of the CTG generated, this time by means of the foetal PCG. To this end, the filtered ECG is processed window by window again, although this time to detect the foetal QRS complexes as

1. *QRS detection:* This step is performed by setting a manual threshold to detect foetal QRS complexes. This means that, in those signals where foetal and maternal complexes have the same sign, not only foetal but also maternal complexes are detected.

2. *Removing maternal QRS complexes:* Whenever foetal and maternal complexes are detected, the already known maternal positions (used to calculate MHR) are subtracted from the overall QRS vector so that the remaining peaks are mostly foetal complexes.

3. *Manual correction:* In cases where QRS complexes are wrongly detected, they are manually corrected by either removing artefacts or inserting missing complexes.

Steps 1, 2, and 3 are repeated window by window until the entire filtered ECG has been processed and the positions of the maternal QRS complexes are known.

4. *CTG generation:* This is performed by measuring R-R distances, this time from the foetal complexes.

5. *CTG examination:* Again, this step carefully reviews the CTG and corrects any abnormal intervals produced by QRS complexes wrongly detected. Here it is essential to mention that these abnormal intervals are usually due to a maternal complex overlapping a foetal QRS, which makes it impossible to truly establish the position of the foetal complex. As an alternative, the position of such a missing foetal complex is estimated as in the middle of its foetal neighbours.

e) Maternal breathing rate (MBR): This vital sign is calculated to observe the maternal status and determine whether it has some influence on the foetal CTG. To do so, the entire estimated respirogram is processed using the FFT.

f) Reference maternal breathing rate: This is calculated by using the FFT as well, although this time on the reference respirogram recorded by the piezoresistive sensor.

10.4. Foetal surveillance: the collected parameters

10.4.1. The estimates of the physiological time-series

Figure 10.4, Figure 10.5, and Figure 10.6 plot the entire time-series reconstructed by concatenating the segmented traces retrieved by SCICA from subjects 1, 2, and 3 respectively. From top to bottom, the time and frequency representations of (a) the foetal PCG, (b) the maternal PCG and/or pressure wave, (c) the maternal breathing, and (d) noise. In the time domain, the unscaled and scaled versions of each time-series are depicted along with a magnified section of the scaled signal. In the frequency domain, the spectrum and autospectrum of each time-series are illustrated, the unscaled case by a continuous black line and the scaled case by a dashed-dotted red line. Additionally, the values of the frequency content (S_I) and rhythmicity (R) indexes are presented.

In general, by observing the time-series in these figures, it can be seen that the scaled signals are more continuous than the unscaled ones (*i.e.* present less sudden variations in amplitude), which is especially clear in the foetal PCG. Furthermore, as shown in Figure 10.4 (a), Figure 10.5 (a), and Figure 10.6 (a), the two main FHS (*i.e.* S1 and S2) can be observed in the foetal PCG, although with different intensity. In the frequency domain, the spectra and autospectra shapes do not show important differences between the unscaled and scaled signals, except for the noise autospectrum, which in the scaled cases presents an additional and prominent peak within the interval corresponding to the maternal heart rate. Also, and important to be noticed, is that every autospectrum shows a very slow rhythm within the maternal breathing interval (van Leeuwen *et al.* 2009).

In particular, by looking at the magnified section in Figure 10.4 (a), it can be seen that the intensity of S1 is considerably larger than the intensity of S2, which makes the former more obvious along the signal. Considering the scaled time-series, it can be observed that their amplitude is not only more continuous, but also larger than in the unscaled signals. In addition, as noticed in the interval between 160 and 220 s, some large-intensity peaks (*i.e.* spikes) are more obvious in the scaled signal than in the unscaled one, which is a phenomenon observed in (b), (c), and (d) as well. In the frequency domain, the overall frequency content and rhythmicity indexes are centred at S_I = 29.3 Hz and R= 2.3 Hz for the foetal PCG, at S_I = 2.0 Hz and R= 1.3 Hz for the maternal PCG, at S_I = 2.0 Hz and R= 0.24 Hz for the maternal breathing, and at S_I = 56.7 Hz for the noise. In (b), besides the slowest rhythm, the autospectrum shows another rhythm centred at 2.6 Hz.

In Figure 10.5, the magnified section in (a) shows that both S1 and S2 are evident, being the former the sound with the largest intensity along the signal. This pattern can be also observed in the magnified section in (d), where the noise time-series seems to present information related to cardiac activities. With regards to the time-series, it can be seen that the overall amplitude of the scaled signals is this time smaller than in the unscaled versions. In the frequency domain, the frequency content and rhythmicity indexes are centred at S_I = 27.3 Hz and R= 2.6 Hz for the foetal PCG, at S_I = 2.0 Hz and R= 1.3 Hz for the maternal PCG, at S_I = 2.0 Hz and R= 0.24 Hz for the maternal breathing, and at S_I = 52.7 Hz for the noise. In (b), besides the slowest rhythm, the autospectrum shows a secondary rhythm centred at 2.6 Hz. In (c), the autospectrum shows two secondary rhythms centred at 1.3 and 2.6 Hz respectively.

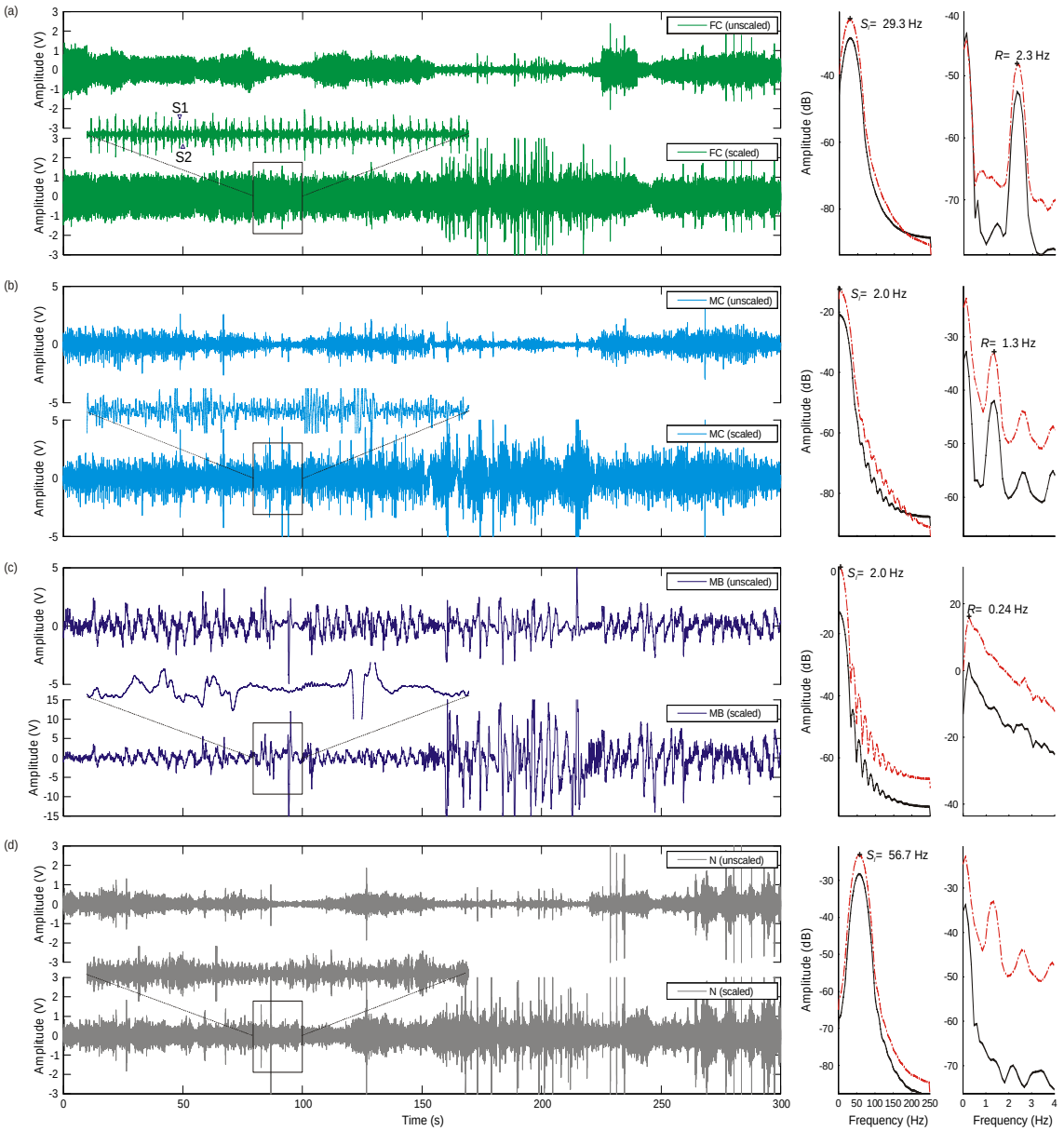

Figure 10.4. Physiological time-series reconstructed by concatenating segmented traces retrieved by SCICA from the abdominal phonogram of subject 1 (40 weeks of gestational age). (a) Foetal PCG, (b) maternal PCG and/or pressure wave, (c) maternal breathing, and (d) noise. The plots on the right-hand side represent the frequency content and rhythmicity of the unscaled (continuous black line) and scaled (dashed-dotted red line) signals. The zoomed section shows a 20 s portion of the scaled time-series.

In Figure 10.6, the magnified section in (a) shows that the intensities of S1 and S2 change beat-to-beat, being still S1 the sound with the largest intensity and thus easier to visualise than S2. In the frequency domain, the indexes are centred at S_I = 33.2 Hz and R= 2.6 Hz for the foetal PCG, at S_I = 2.0 Hz and R= 1.3 Hz for the maternal PCG, at S_I = 2.0 Hz and R= 0.24 Hz for the maternal breathing, and at S_I = 60.6 Hz for the noise. As in previous cases, the autospectra show extra rhythms centred in (b) at 2.6 Hz and in (c) at 1.3 and 2.6 Hz.

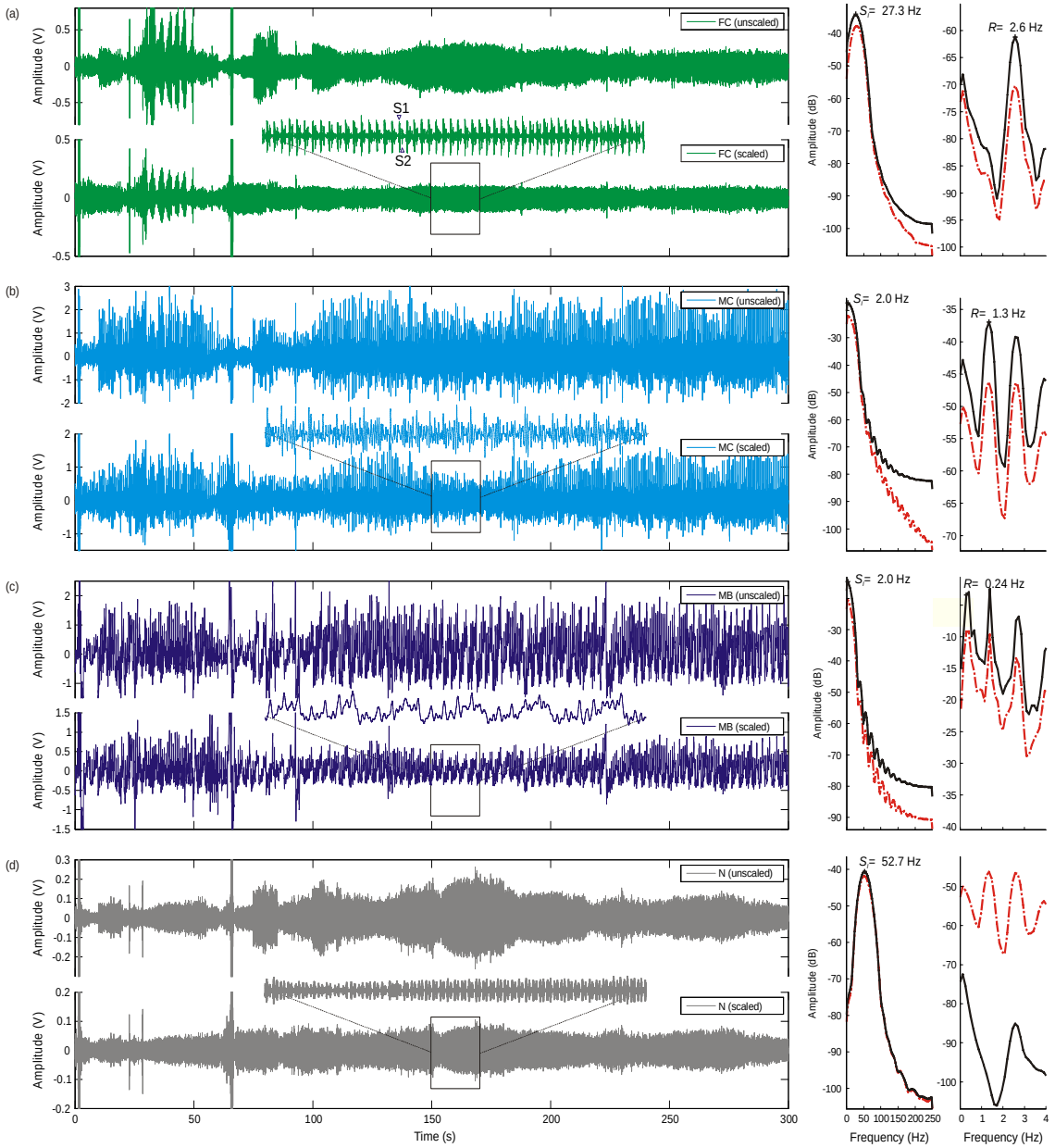

Figure 10.5. Physiological time-series reconstructed by concatenating segmented traces retrieved by SCICA from the abdominal phonogram of subject 2 (36 weeks of gestational age). (a) Foetal PCG, (b) maternal PCG and/or pressure wave, (c) maternal breathing, and (d) noise. The plots on the right-hand side represent the frequency content and rhythmicity of the unscaled (continuous black line) and scaled (dashed-dotted red line) signals. The zoomed section shows a 20 s portion of the scaled time-series.

Similar results have been observed on the time-series reconstructed from the other single-channel abdominal phonograms processed in this work. They can be summarised as follows:

1. From every abdominal phonogram, four scaled time-series are reconstructed, the foetal PCG, the maternal PCG/pressure-wave, the maternal breathing, and the noise.

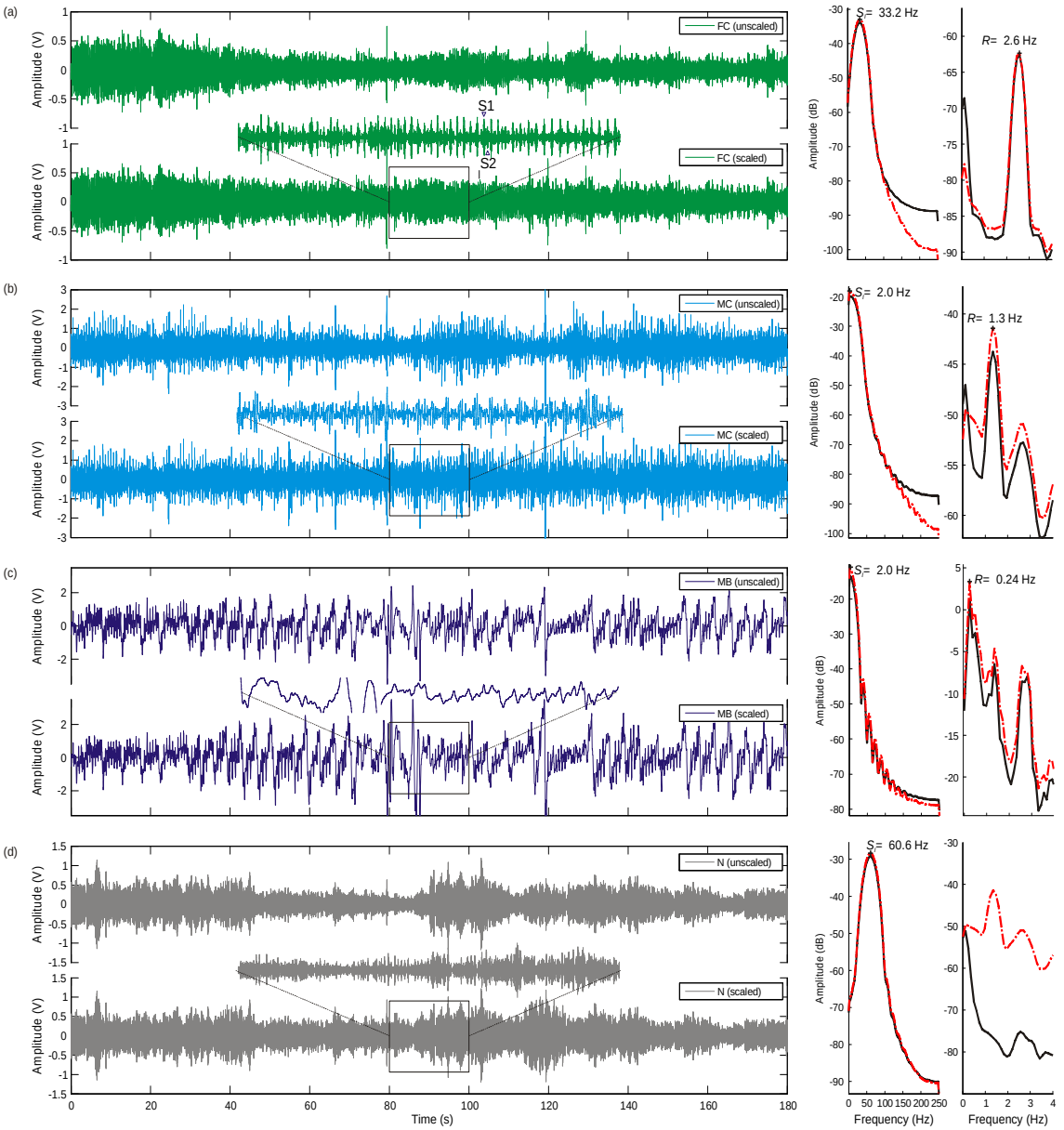

Figure 10.6. Physiological time-series reconstructed by concatenating segmented traces retrieved by SCICA from the abdominal phonogram of subject 3 (38 weeks of gestational age). (a) Foetal PCG, (b) maternal PCG and/or pressure wave, (c) maternal breathing, and (d) noise. The plots on the right-hand side represent the frequency content and rhythmicity of the unscaled (continuous black line) and scaled (dashed-dotted red line) signals. The zoomed section shows a 20 s portion of the scaled time-series.

2. The reconstructed foetal PCG shows the main FHS, S1 and S2, being S1 the sound with the largest intensity and thus easier to visualise in the signals processed in this research.

3. Some portions of the reconstructed noise may still contain physiological information of cardiac origin.

4. The time-series spectrum is characterised by a single and well-defined peak that is centred at different frequencies depending on the physiological activity underlying the time-series.

5. Independently of the time-series, the autospectrum always presents a very slow rhythm centred in the maternal breathing interval. Consequently, the time-series autospectrum is composed of more than one rhythm (either MBR and FHR or MBR and MHR). In some cases, as discussed in Chapter 7, there might be an additional evident rhythm centred at either 2·MHR or 2·FHR.

Table 10.2 presents the overall frequency content and rhythmicity indexes of the time-series reconstructed from 25 single-channel abdominal phonograms processed in this research. As can be seen, the physiological time-series in this work present the next features:

a) Foetal PCG: Its frequency content is centred at [30.5 ± 2.1] Hz and, according to the autospectrum, the FHR is centred at [2.4 ± 0.2] Hz (*i.e.* [144 ± 12] Beats/min).

b) Maternal PCG and/or pressure wave: Its frequency content is centred at [2.0 ± 0.0] Hz and, according to the autospectrum, the MHR is centred at [1.3 ± 0.2] Hz (*i.e.* [78 ± 12] Beats/min).

c) Maternal breathing: Its frequency content is centred at [2.0 ± 0.0] Hz and, according to the autospectrum, the MBR is centred at [0.30 ± 0.08] Hz (*i.e.* [18 ± 4.8] Breaths/min).

d) Noise: Its frequency content is centred at [56.0 ± 1.9] Hz, which is close to the line-noise frequency.

Now that the overall frequency content and rhythm of the reconstructed time-series have been presented, it can be seen that some global information about foetal and maternal status can be actually inferred from *R*. However, the information obtained in this way represents only an overview about the foetal and maternal condition and thus misses valuable details about temporal variations due to temporal changes in the general status, which reduces the possibility to promptly detect problems in foetal oxygenation. Alternatively, as discussed in Chapter 3 and Chapter 4, some specific information can be obtained through the analysis of the foetal PCG, which makes it suitable to collect parameters for foetal surveillance (*i.e.* the beat-to-beat FHR and FHS morphology). Also, as mentioned in Section 10.3, complementary parameters can be collected to verify foetal observations by means of a reference FHR, MHR, and MBR. The next two sections show the specific information collected from the signals used in this work.

Table 10.2. Overall frequency content (S_I) and rhythmicity (R) values of the sources retrieved from the abdominal phonogram.

Recording ID	Gestational age (weeks)	Foetal PCG		Maternal PCG and/or pressure wave		Maternal respirogram		Noise
		S_I (Hz)	R (Hz)	S_I (Hz)	R (Hz)	S_I (Hz)	R (Hz)	S_I (Hz)
1	40	29.3	2.3	2.0	1.3	2.0	0.24	56.7
2	36	29.3	2.6	2.0	1.3	2.0	0.24	52.7
3	38	33.2	2.6	2.0	1.3	2.0	0.24	60.6
4	37	31.3	2.6	2.0	1.3	2.0	0.37	54.7
5	36	29.3	2.2	2.0	1.1	2.0	0.24	54.7
6	36	27.3	2.6	2.0	1.3	2.0	0.24	54.7
7	36	27.3	2.3	2.0	1.7	2.0	0.24	54.7
8	36	29.3	2.6	2.0	1.5	2.0	0.37	56.6
9	38	29.3	2.3	2.0	1.1	2.0	0.37	54.7
10	36	29.3	2.4	2.0	1.5	2.0	0.24	54.7
11	38	31.3	2.1	2.0	1.1	2.0	0.37	54.7
12	34	29.3	2.0	2.0	1.2	2.0	0.37	56.6
13	38	27.3	2.7	2.0	1.5	2.0	0.37	54.7
14	40	31.3	2.4	2.0	1.2	2.0	0.24	58.6
15	40	33.2	2.4	2.0	1.7	2.0	0.24	56.6
16	36	27.3	2.2	2.0	1.1	2.0	0.24	56.6
17	36	29.3	2.3	2.0	1.2	2.0	0.24	60.5
18	33	35.2	2.6	2.0	1.2	2.0	0.49	54.7
19	36	31.3	2.1	2.0	1.5	2.0	0.37	54.7
20	36	31.3	2.3	2.0	1.3	2.0	0.24	56.6
21	29	31.3	2.3	2.0	1.5	2.0	0.24	56.6
22	33	33.2	2.6	2.0	1.2	2.0	0.37	56.6
23	34	31.3	2.7	2.0	1.3	2.0	0.24	54.7
24	37	33.2	2.6	2.0	1.3	2.0	0.37	54.7
25	39	31.3	2.6	2.0	1.5	2.0	0.37	58.6
Mean	36.3	30.5	2.4	2.0	1.3	2.0	0.30	56.0
Std	2.5	2.1	0.2	0.0	0.2	0.0	0.08	1.9

10.4.2. The estimated foetal PCG

Figure 10.7, Figure 10.8, and Figure 10.9 depict the instantaneous FHR and some complementary parameters collected from subjects 1, 2, and 3 respectively. In (a), the reference CTG obtained by using the foetal QRS positions, in (b), the estimated CTG by using the positions of S1, in (c), the estimated CTG by using the positions of S2, in (d), from top to bottom, the signal to noise ratio of S1 and S2, and in (e), from top to bottom, the manual markers that indicate presence of foetal breathing movements or foetal movements. In (b), the red regions indicate segments where the CTG presents lower (on the left-hand side) and higher (on the right-hand side) variance values. In addition, the PCG portions and thus the FHS that gave rise to such variances are shown.

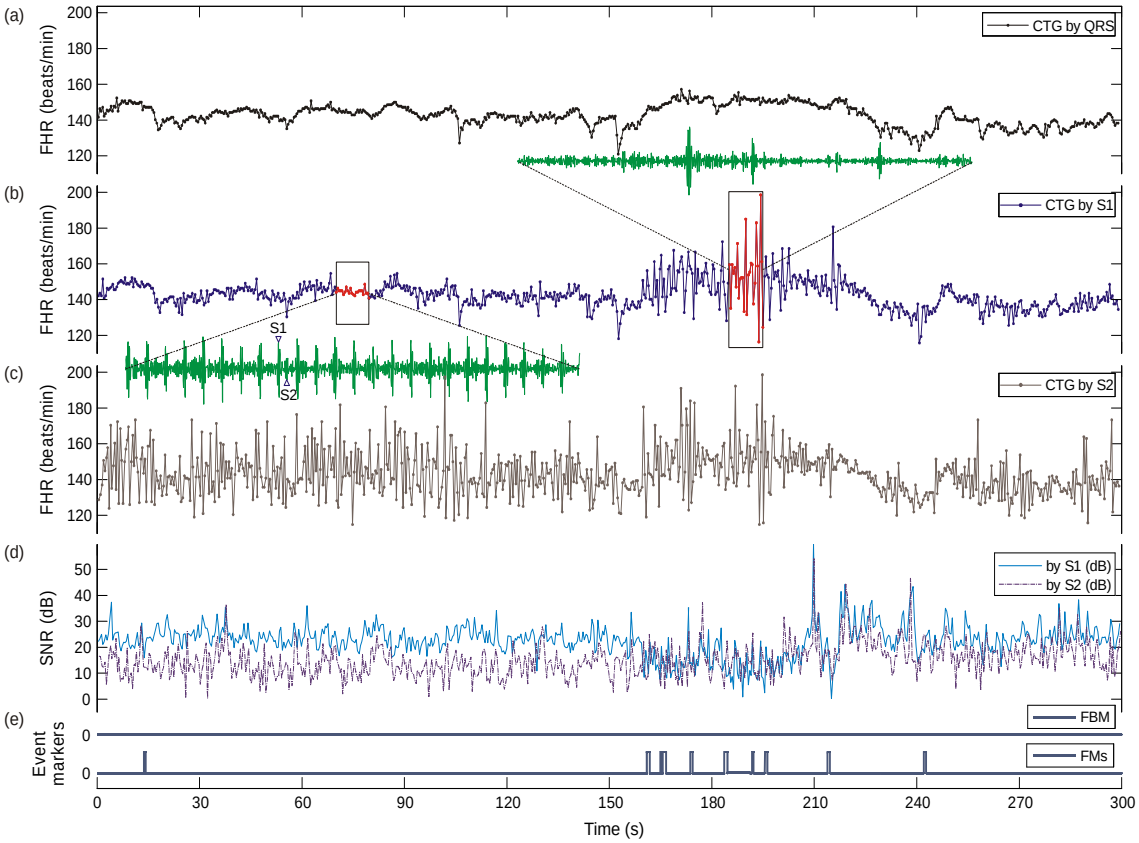

Figure 10.7. Instantaneous foetal heart rate and some complementary parameters collected from subject 1. (a) CTG by the foetal QRS, (b) CTG by S1, (c) CTG by S2, (d) SNR (of S1 and S2), and (e) manual markers to indicate presence of FBM or FMs. In (b), the red region on the left-hand side indicates a small-variance CTG section that comes from a PCG portion with evident S1s, whereas the red region on the right-hand side highlights a large-variance section that comes from a PCG portion with unclear S1s.

By having a look at the plots in these figures, four observations can be made:

a) **CTG quality:** Depending on the temporal position used to generate them (*i.e.* the QRS, S1 or S2), the noise level (*i.e.* beat-to-beat variations) in the CTGs changes, being the CTG by

QRS the least noisy and the CTG by S2 the noisiest. Also, as shown by the red regions in Figure 10.7 (b), Figure 10.8 (b), and Figure 10.9 (b), the level of noise in the CTG changes over time, some times to improve and others to deteriorate the quality of the signals. The same situation can be seen in Figure 10.7 (c), Figure 10.8 (c), and Figure 10.9 (c), where the beat-to-beat variations in some portions of the CTG by S2 are larger than the variations in other portions of the same signal.

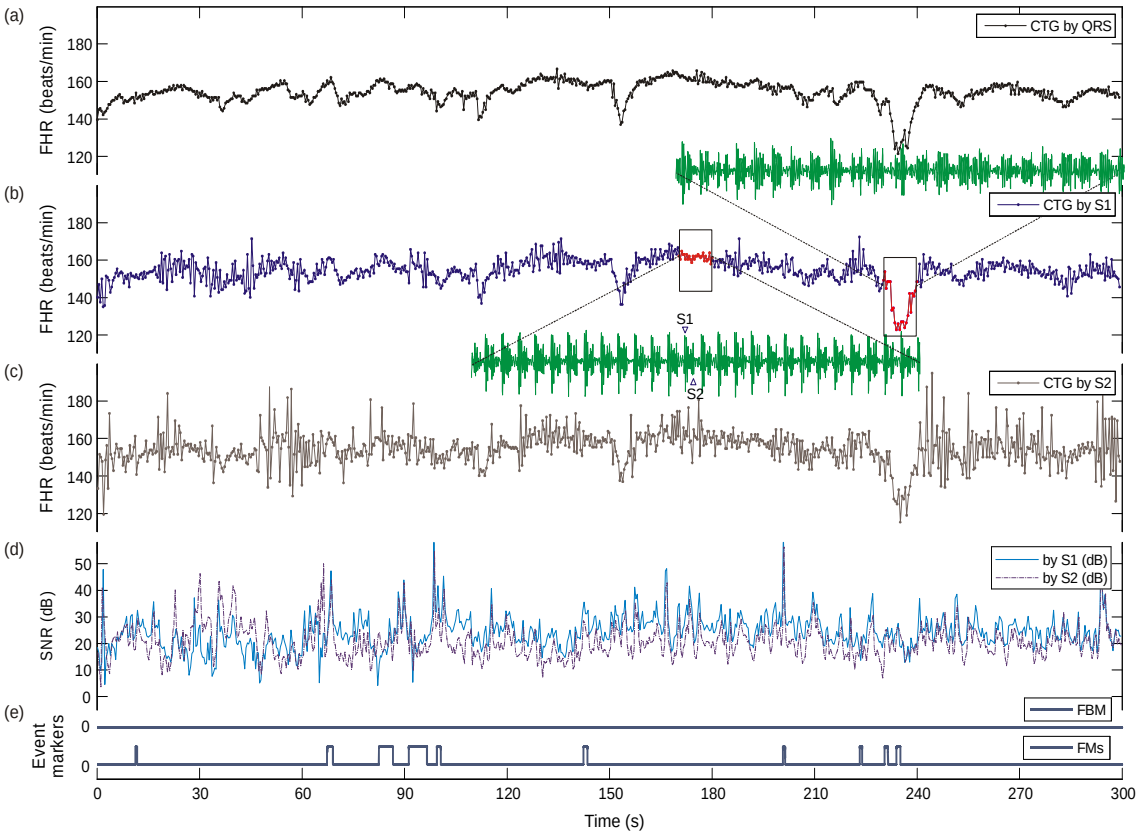

Figure 10.8. Instantaneous foetal heart rate and some complementary parameters collected from subject 2. (a) CTG by the foetal QRS, (b) CTG by S1, (c) CTG by S2, (d) SNR (of S1 and S2), and (e) manual markers to indicate presence of FBM or FMs. In (b), the red region on the left-hand side indicates a small-variance CTG section that comes from a PCG portion with evident S1s, whereas the red region on the right-hand side highlights a large-variance section that comes from a PCG portion with unclear S1s.

b) FHS intensity: According to the PCG portions that produced the red regions in the CTGs in Figure 10.7 (b), Figure 10.8 (b), and Figure 10.9 (b), the FHS intensity seems to be directly related to the CTG quality. It can be noted that in the PCGs from where the CTG small-variance regions were obtained, where S1 is evident. On the other hand, as shown by the PCGs from where the CTG large-variance regions were obtained, S1 is not as obvious as before. These observations are confirmed by the SNR of S1 plotted in Figure 10.7 (d), Figure 10.8 (d), and Figure 10.9 (d), whose intervals with values below < 20 dB match the

intervals with larger variance in the CTGs. The same case applies to S2 which, having less intensity than S1 in this work, presents lower SNR values and therefore gives rise to noisier CTGs.

c) Foetal movements: Presence of FMs sometimes affects the SNR of the FHS, which is especially evident in Figure 10.7. In the interval between 150 and 240 s there were some FMs, the SNR of both S1 and S2 seems to have a slight reduction below 20 dB, which affects the CTGs in (b) and (c) by producing larger variations that are more obvious in (b). In this particular case it is important to highlight that, although the presence of FMs made the CTGs noisier, once they stopped the CTG by S1 returned to its previous variations, whereas the CTG by S2 became less noisy than before.

d) CTG trend: This observation is especially important for the aim of this research and is related not to the noisiness of the CTG by FHS, but to its trend. Such a trend, independently on the point used to produce the CTG (either S1 or S2), seems to have a behaviour that is similar to the trend given by the reference CTG.

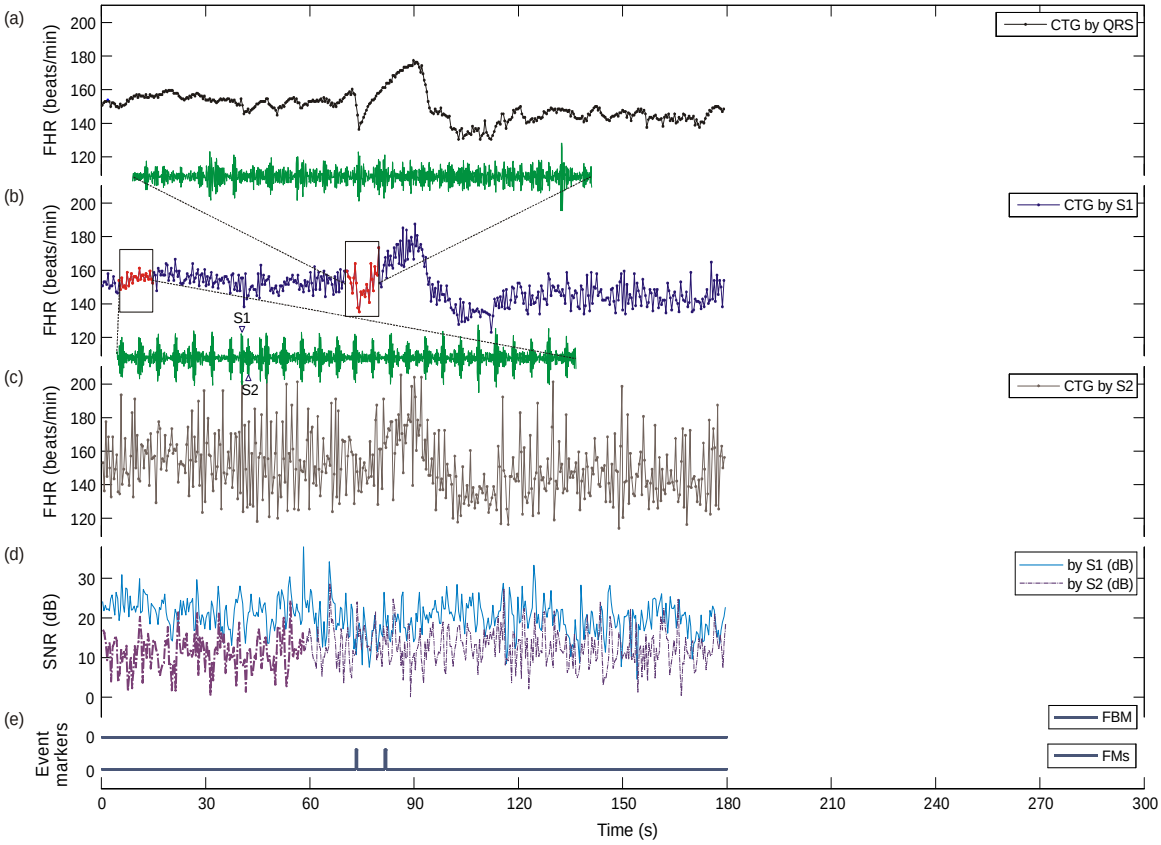

Figure 10.9. Instantaneous foetal heart rate and some complementary parameters collected from subject 3. (a) CTG by the foetal QRS, (b) CTG by S1, (c) CTG by S2, (d) SNR (of S1 and S2), and (e) manual markers to indicate presence of FBM or FMs. In (b), the red region on the left-hand side indicates a small-variance CTG section that comes from a PCG portion with evident S1s, whereas the red region on the right-hand side highlights a large-variance section that comes from a PCG portion with unclear S1s.

Figure 10.10 shows the CTGs collected from subjects 1, 2, and 3 as well as their estimated trends. In (a), the CTGs of subject 1, in (b), the CTGs of subject2, and in (c), the CTGs of subject 3. In each subject, from top to bottom, the reference CTG, the CTG by S1 with its baseline (red line), and the CTG by S2 with its baseline (red line) are plotted. As can be seen from the trends, even though the original CTGs are noisier, the low-pass filtering described in Section 10.2.2 effectively smoothes them. As a result, an estimate of the FHR (here referred to as the trend), whose beat-to-beat variations better resemble the variations in the reference CTG, is obtained. The arrows in each case indicate whenever the reference trace (*i.e.* CTG by QRS) goes either downwards or upwards, the trends follow the same direction.

Figure 10.11, Figure 10.12, and Figure 10.13 plot the information finally collected from the foetal PCG of subjects 1, 2, and 3 respectively. Such information, given by the beat-to-beat FHR baseline and the average morphology of the FHS minute-to-minute is presented as: (a) the trend of the CTG by S1, (b) the average morphology of S1 every minute, (c) the baseline of the CTG by S2, and (d), the average morphology of S2 every minute. In addition, for visual confirmation in (a) and (c), the reference CTG is shown in black colour.

As can be seen in the (a) and (c) plots on each subject, the beat-to-beat FHR obtained in this work (*i.e.* by means of the estimated foetal PCG) resembles the trend given by the reference CTG. Furthermore, and important to highlight, the CTG estimated by S1 seems to match the reference CTG better than the CTG estimated by S2 does, which has been consistently observed in the dataset processed in this research. Hence, when visually comparing the CTGs by S1 and by S2 against the CTG by QRS, it is more likely to find larger and more frequent variations in the CTG by S2 than in the CTG by S1.

On the subject of the average morphology of the FHS, the plots in (b) and (d) in Figure 10.11, Figure 10.12, and Figure 10.13 show the average patterns calculated every minute. In each subject, by visually comparing the duration of S1 versus the duration of S2, it seems that S1 lasts longer than S2. Now, about the average morphology over time, in subject 1, the plots in Figure 10.11 (b) show a repetitive S1 waveform that is composed of three obvious peaks. In subject 2, only three of five plots in Figure 10.12 (b) –corresponding to the second, third, and fourth minutes– depict an avgS1 waveform that is also composed of three evident peaks, but different to the avgS1 in subject 1. Finally, in subject 3, although the three plots in Figure 10.13 (b) show a repetitive avgS1 waveform, it is composed not of three, but of five peaks, which is completely different to the avgS1 in the other subjects.

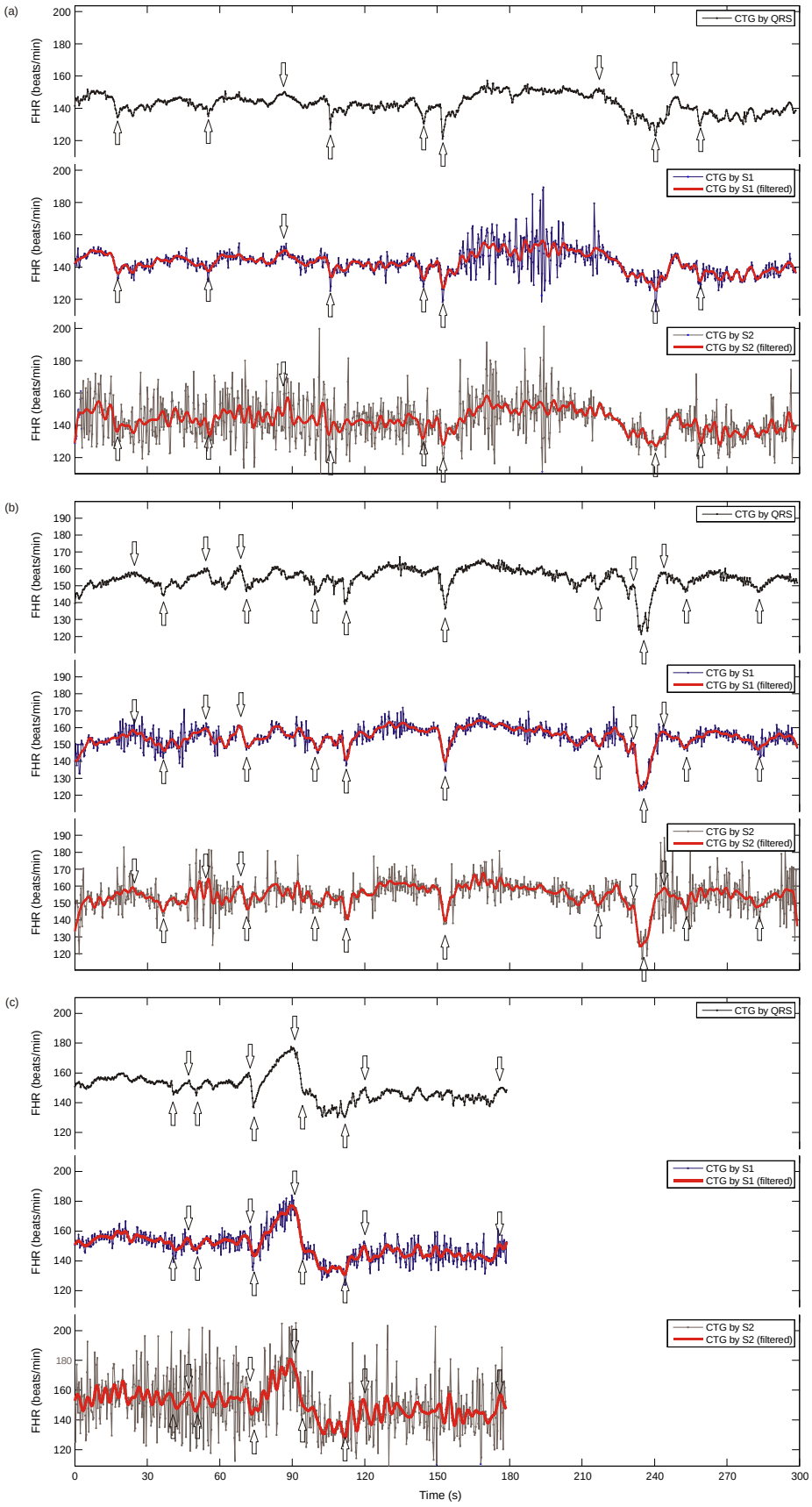

Figure 10.10. Trends of the CTGs collected by means of the FHS from three subjects. (a) CTGs of subject 1, (b) CTGs of subject 2, and (c) CTGs of subject 3. From top to bottom in each case: the reference CTG, the CTG by S1 with its baseline (red line), and the CTG by S2 with its baseline (red line).

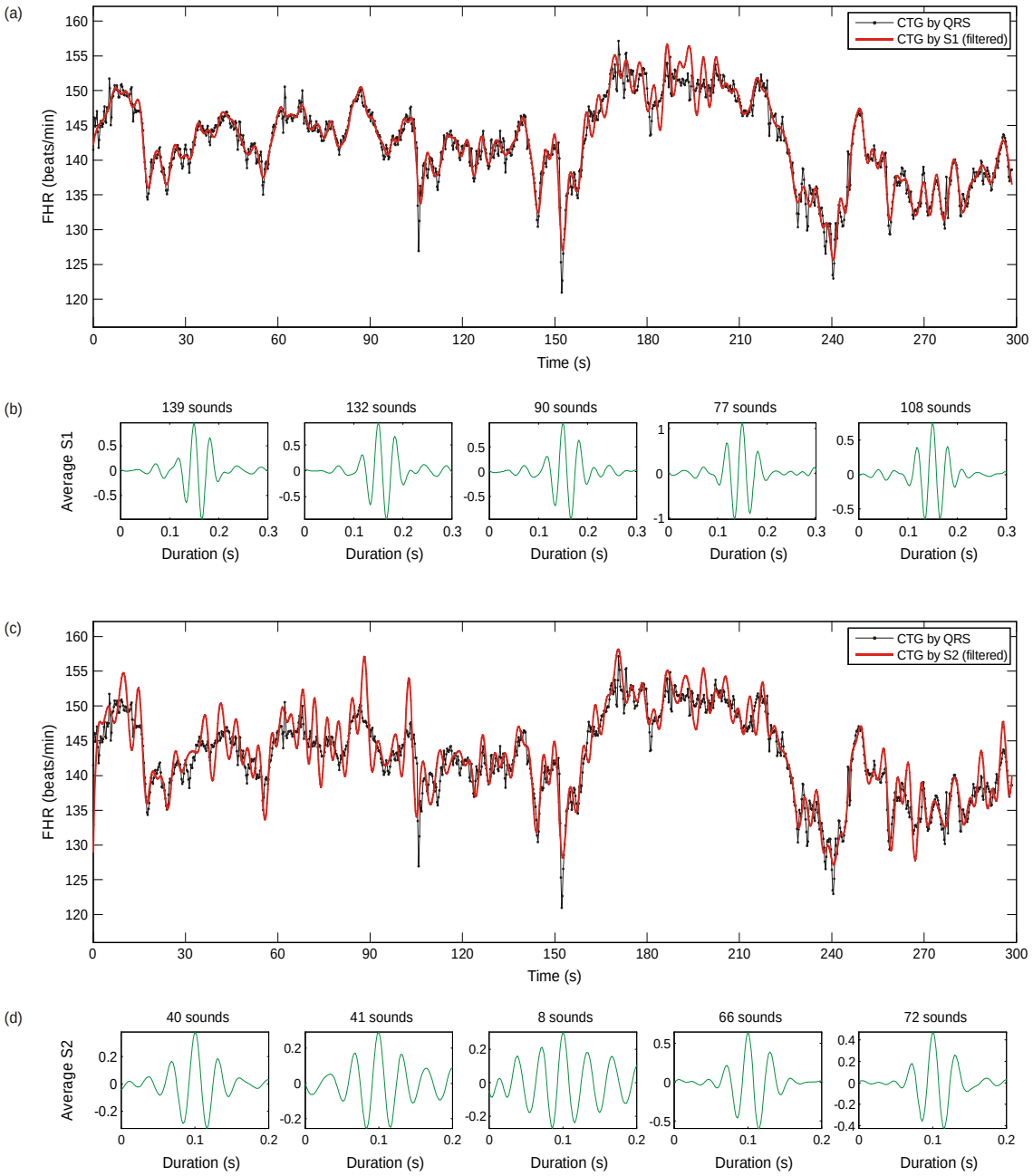

Figure 10.11. Beat-to-beat foetal heart rate and average morphology of the FHS collected from subject 1. (a) Trend of the CTG by S1 (red trace), (b) average morphology of S1 minute-to-minute, (c) trend of the CTG by S2 (red trace), and (d) average morphology of S2 minute-to-minute. The black trace in (a) and (c) corresponds to the reference CTG given by the foetal QRS. The number on top of each morphology represents the number of similar sounds used in its calculation.

Regarding the average morphology of S2, in subject 1, Figure 10.11 (d) shows an avgS2 that changes from a three peaks waveform (in the first minute) to a five peaks waveform (in the next two minutes) and then back to a three peaks pattern in the last two minutes. Also, as shown on the top of each pattern, the number of similar sounds used to calculate every avgS2 is considerable lower than the number of sounds used to calculate every avgS1. In subject 2, the

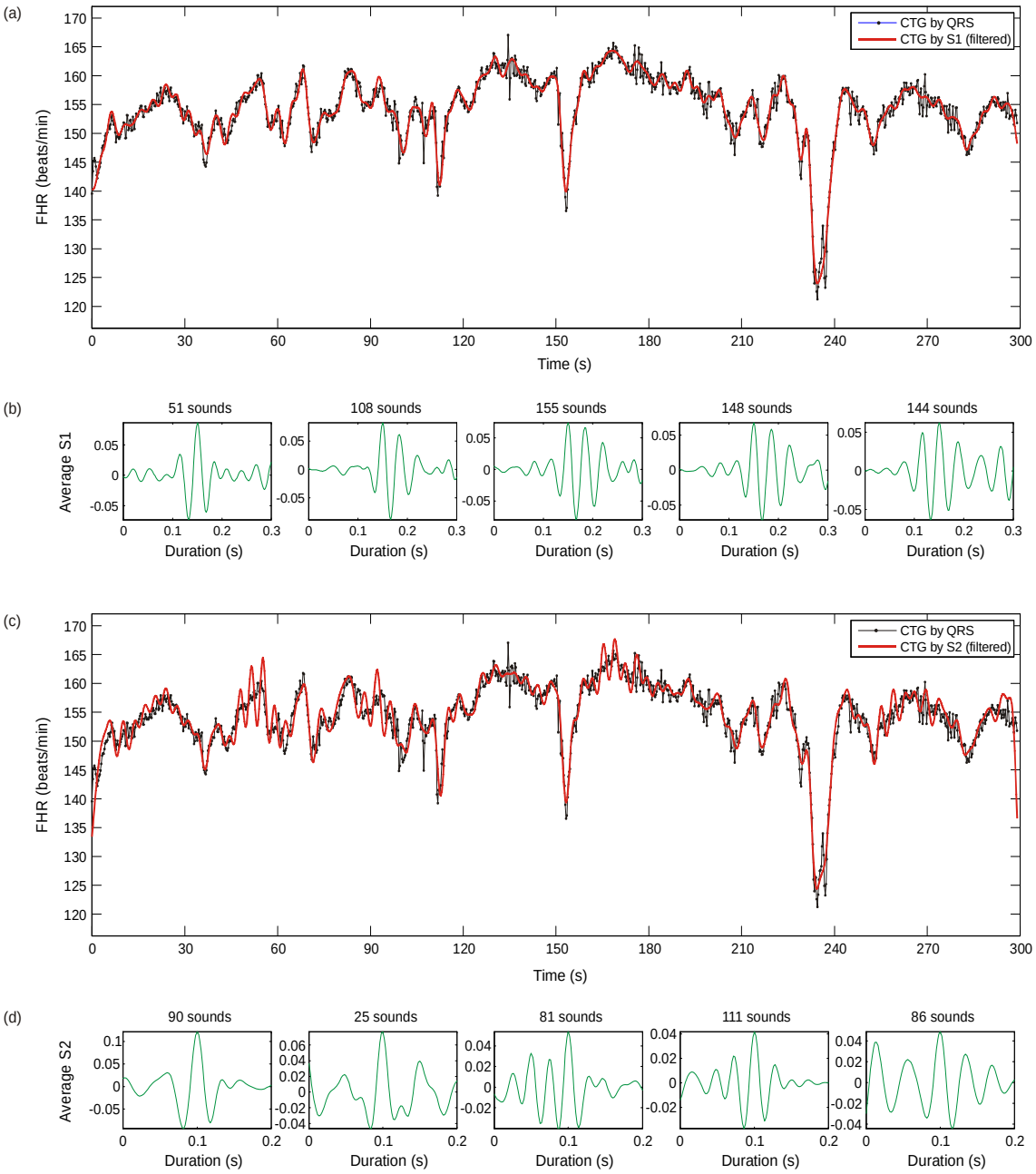

Figure 10.12. Beat-to-beat foetal heart rate and average morphology of the FHS collected from subject 2. (a) Trend of the CTG by S1 (red trace), (b) average morphology of S1 minute-to-minute, (c) trend of the CTG by S2 (red trace), and (d) average morphology of S2 minute-to-minute. The black trace in (a) and (c) corresponds to the reference CTG given by the foetal QRS. The number on top of each morphology represents the number of similar sounds used in its calculation.

plots in Figure 10.12 (d) show dissimilar patterns from where it is difficult to find a typical morphology. In this case, what seems to consistently appear minute-to-minute is a large peak centred at 100 ms. In subject 3, Figure 10.13 (d) shows an average morphology that presents five peaks in the first minute, three peaks in the second minute, and five peaks again in the last minute of recording can be seen. Additionally, like in subject 2, the number of similar sounds used to calculate avgS2 is lower than the number of sounds considered to calculate avgS1.

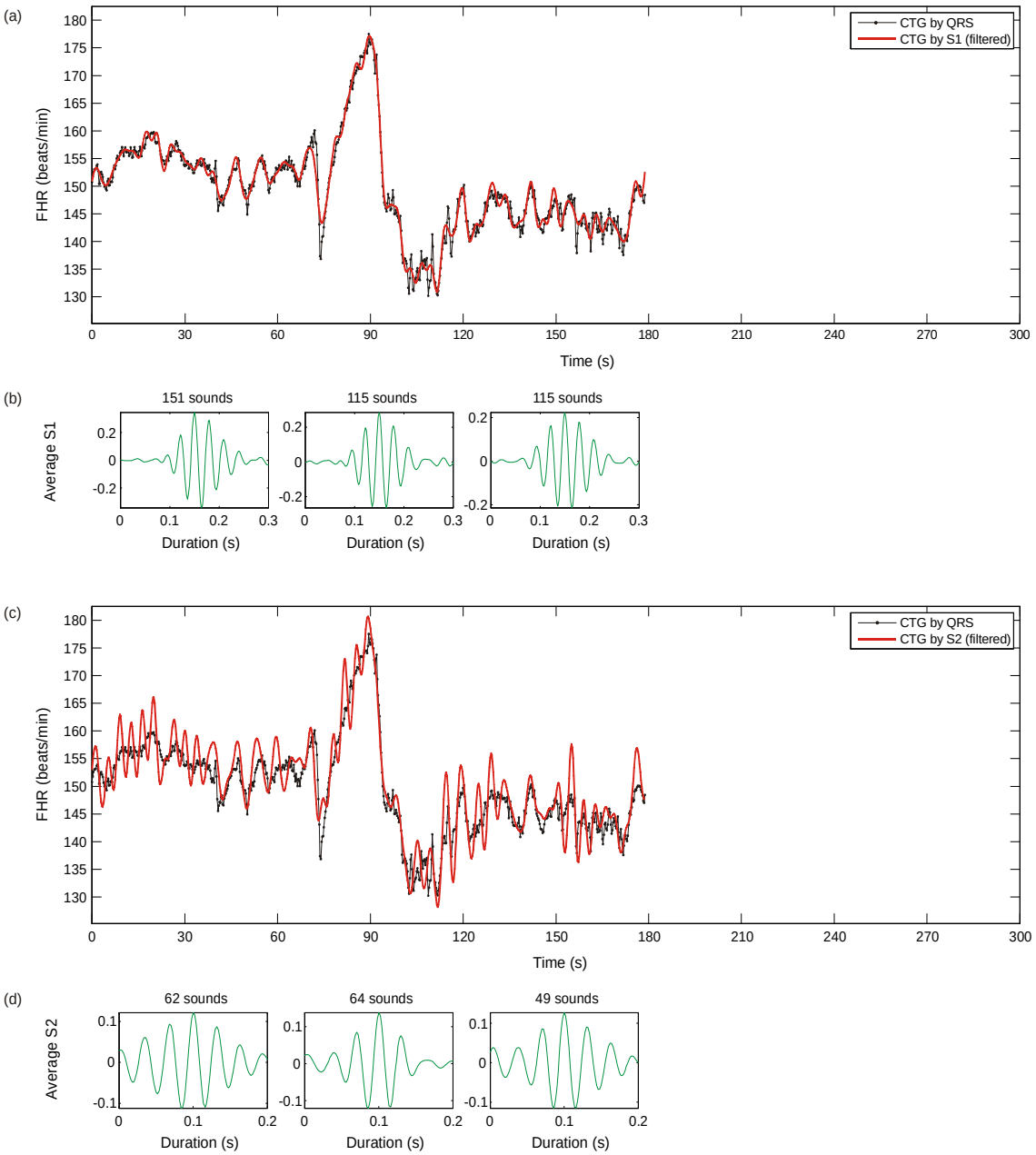

Figure 10.13. Beat-to-beat foetal heart rate and average morphology of the FHS collected from subject 3. (a) Trend of the CTG by S1 (red trace), (b) average morphology of S1 minute-to-minute, (c) trend of the CTG by S2 (red trace), and (d) average morphology of S2 minute-to-minute. The black trace in (a) and (c) corresponds to the reference CTG given by the foetal QRS. The number on top of each morphology represents the number of similar sounds used in its calculation.

Similar results have been observed in the morphologies estimated from the other signals in the dataset, *i.e.* different morphologies, not only amongst cases, but also over time in the same signal have been found.

10.4.3. Complementary information

As mentioned in Section 10.3, since different signals are available in this work, it is suitable to achieve a wider perspective of the antenatal status (at least at the time of recording) by complementing the information collected from the foetal PCG with maternal vital signs such as the heart and breathing rates. Thus, as part of this study, Figure 10.14 depicts the beat-to-beat HR collected from the foetus and the mother in the cases corresponding to (a) subject 1, (b) subject 2, and (c) subject 3. These traces, collected by means of the abdominal ECG (due to the availability of the signal in these subjects), show the foetal CTG in black colour and the maternal CTG in blue colour.

By looking at these traces, it can be seen that the maternal heart rate remained within a physiologically reasonable range (Ogueh *et al.* 2009) during the recording sessions. In addition, the periodic information clearly identifiable along the whole trace in (a), mostly evident during the first and third minutes in (c), and apparently missing in (b), oscillates at about 0.24 Hz in these three cases. For the other signals, whenever the MHR was collected (either from the abdominal ECG or from the estimated maternal PCG), such oscillations have been found to range between 0.24 and 0.49 Hz.

Figure 10.15 illustrates segments of the maternal respirogram of (a) subject 1, (b) subject 2, and (c) subject 3. In each case, the trace on the top represents the reference signal (*i.e.* recorded by a piezoelectric sensor and multiplied by minus one for visual comparison), whereas the two traces on the bottom represent, in blue colour, the signals estimated in this work (*i.e.* from the abdominal phonogram) and, in red colour, a low-pass filtered version that is free of heart rate information (*i.e.* filtered at 0.5 Hz).

As can be seen in the estimated respirograms, they contain information from maternal cardiovascular origin. This is especially clear in (b) and (c) and means that some further processing is necessary on the estimated respirogram to remove undesirable information and ease the visual comparison against the reference signal. After low-pass filtering the signal at 0.5 Hz to produce the red trace, it can be noticed that the filtered signal better resembles the slow oscillations given by the reference respirogram, which has been consistently observed along the whole dataset.

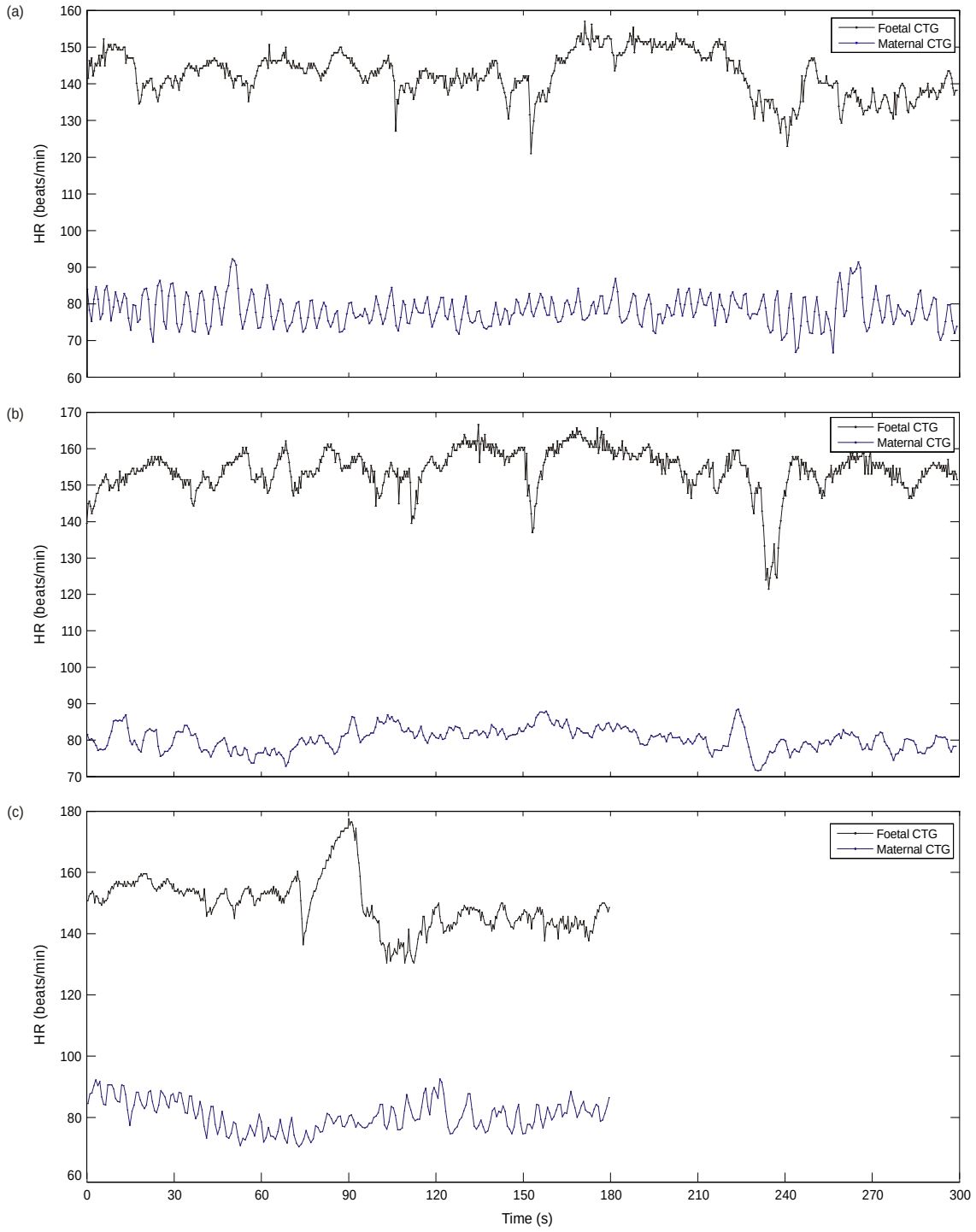

Figure 10.14. Cardiac information collected by means of the abdominal ECGs recorded from (a) subject 1, (b) subject 2, and (c) subject 3. In each case, two beat-to-beat heart rate traces are presented: the foetal CTG (in black colour) and the maternal CTG (in blue colour).

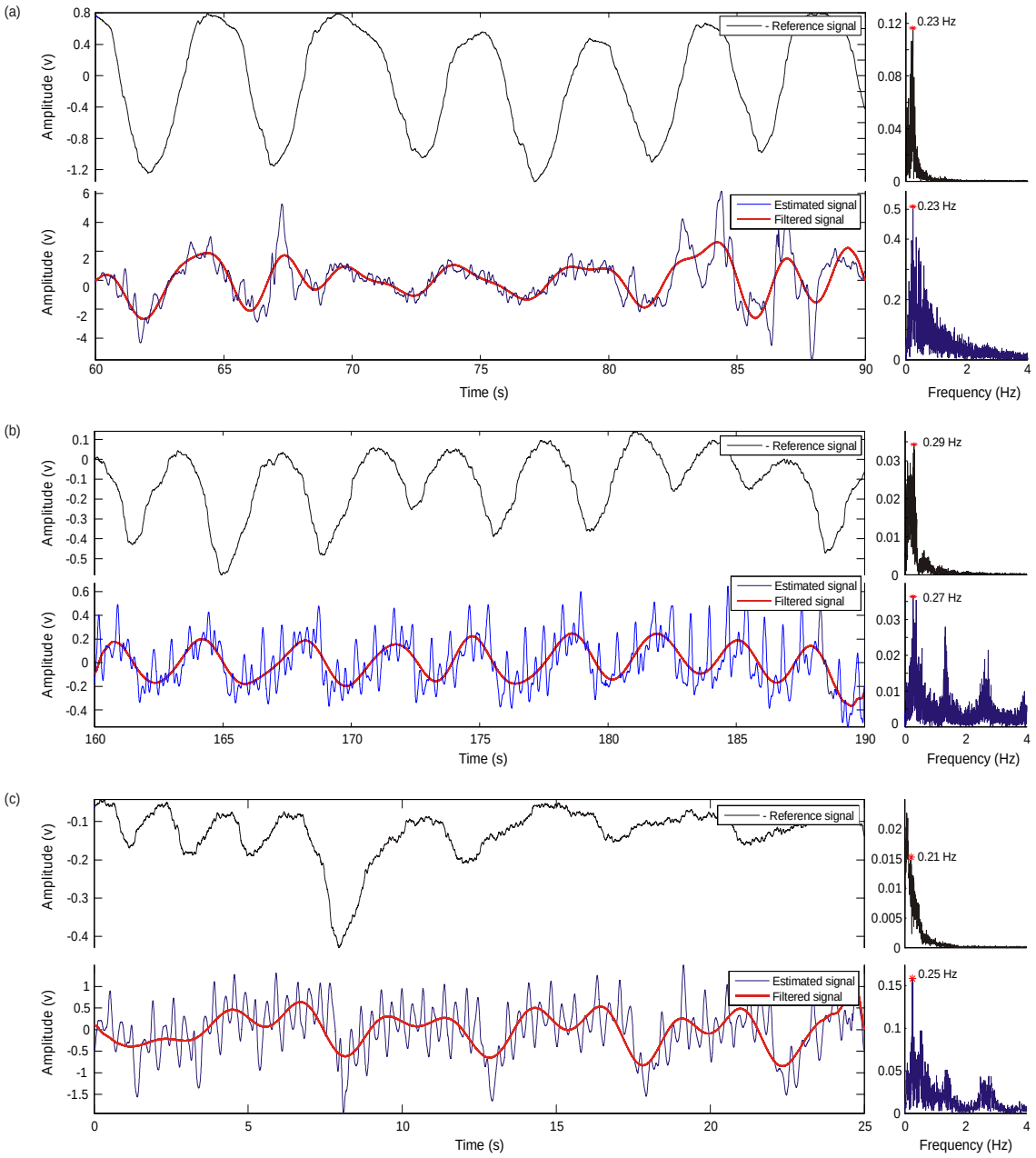

Figure 10.15. Segments of the maternal respirogram of (a) subject 1, (b) subject 2, and (c) subject 3. In each case three traces are presented: the black trace represents the reference signal recorded by a piezoelectric sensor (multiplied by minus one for visual comparison), the blue trace corresponds the time-series estimated in this work, and the red trace is a low-pass filtered version of such an estimated signal. On the right-hand side, the spectrum of the reference and estimated respirograms given by the FFT.

10.4.4. Towards the final analysis

Figure 10.16 summarises the temporal variations in the statistics of the FHR in those cases where the abdominal CTG is available (*i.e.* fifteen cases). In each case, the mean and standard deviation of the FHR by QRS (in black colour) and the filtered FHR by S1 (in red colour) are plotted in intervals of 30 s. The number on the left-hand side of each case represents the recording ID as in Table 10.3, whereas the number below every couple of bars corresponds to the average SNR in that interval.

As can be seen in all cases, the trend given by the reference signal is followed by the estimated FHR, *i.e.* whenever the reference FHR increases, the estimated FHR increases and vice versa. The variance, on the other hand, does not show such a nice and steady behaviour, in fact, as already stated, it may significantly change over time. In this study, the variance of the estimated FHR has been larger than the variance of the reference FHR, which is especially obvious in cases 6, 10, 14, 15, 23, and during the last minute in case 18. However, as noticed in case 7, it is possible for the estimated FHR to have less variance than the reference FHR. Regarding the signal to noise ratio in these cases, as observed, it is usually lower than 20 dB.

Table 10.3 summarises the gestational age, the SNR, and the mean values of the vital signs collected from the signals processed as described in this chapter, *i.e.* the estimated beat-to-beat FHR, the reference beat-to-beat FHR, the estimated beat-to-beat MHR, the reference beat-to-beat MHR, the estimated MBR, and the reference MBR.

In the foetal case, as can be seen in the fourth and fifth columns, the instantaneous FHR has been collected from 21 out of the 25 estimated foetal PCGs, but only 15 cases have been verified by a reference FHR (shown in *italics*). On the other hand, in the maternal case, as shown in the sixth and seventh columns, it has been possible to collect the MHR in 21 cases (from 18 estimated maternal PCGs and from the 15 available abdominal ECGs), but only 12 were validated by a reference MHR (shown in *italics*). Regarding the MBR, as seen in the eighth and ninth columns, it has been suitable to collect and confirm the overall information by using the maternal respirogram for all cases in the dataset (although in some cases the maternal respirogram might not have been properly recorded). Thus, amongst the 25 cases studied in this research, only eight (*i.e.* 2, 3, 5, 7, 10, 16, and 25) show small differences in the overall rates calculated from the estimated and the reference respirograms.

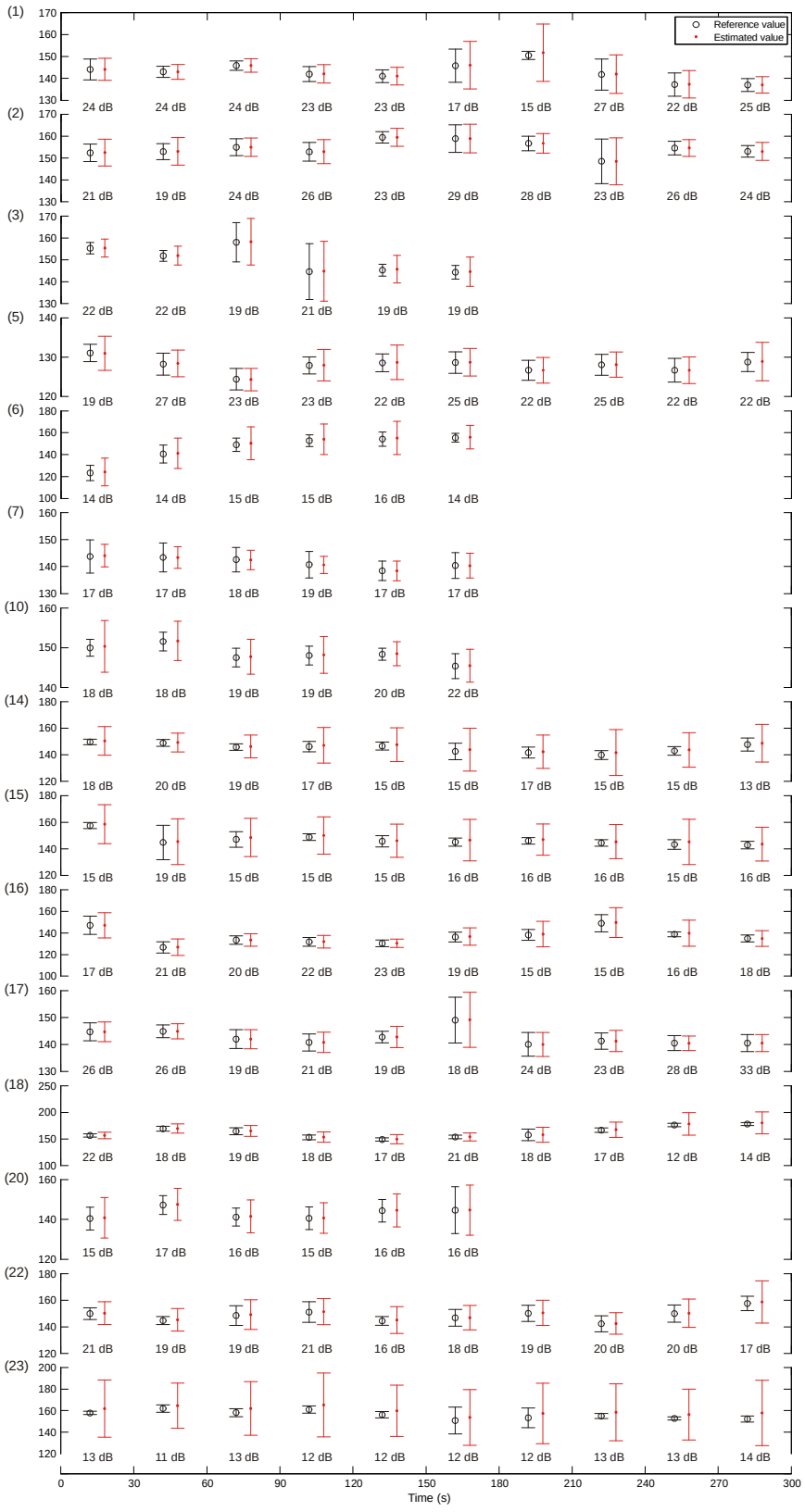

Figure 10.16. Mean and standard deviation of the FHR measured by the foetal QRS and by S1 in fifteen cases. Each bar represents the mean and standard deviation of the FHR within an interval of 30 s, black colour for the FHR by QRS and red colour for the FHR by S1. The number on the left-hand side of each case indicates the recording ID, whereas the number below each couple of bars indicates the average SNR in that interval.

Table 10.3. Mean values of the heart and breathing rates collected from the sources estimated by SCICA and some reference signals. The age is expressed in weeks, the SNR is expressed in dB, the heart rate is expressed in beats/min, and the breathing rate is expressed in breaths/min. The *italic values* in the FHR and MHR columns indicate those cases from where it was possible to collect heart rate values from both, the estimated signal and the reference signal.

ID	Age	Foetal			Maternal			
		SNR	Estimated FHR	Reference FHR	Estimated MHR	Reference MHR	Estimated MBR	Reference MBR
1	40	22	*142.66*	*142.67*	*78.27*	*78.26*	13.8	13.8
2	36	24	*154.22*	*154.23*	*80.40*	*80.38*	16.2	17.4
3	38	20	*149.71*	*149.70*	*80.64*	*80.61*	15.6	12.6
4	37	16	151.00	--	85.49	--	20.4	20.4*
5	36	23	*127.83*	*127.84*	*63.01*	*63.01*	16.2	13.8
6	36	15	*145.66*	*145.64*	*73.89*	*73.90*	16.2	16.2
7	36	17	*141.45*	*141.42*	*94.74*	*94.72*	13.8	12.6
8	36	16	119.08	--	89.07	--	22.2	22.2*
9	38	19	135.14	--	--	--	21.6	21.6*
10	36	19	*148.49*	*148.46*	*89.73*	*89.72*	16.2	13.8
11	38	18	133.96	--	--	--	21.6	21.6*
12	34	--	--	--	73.57	--	19.2	19.2
13	38	--	--	--	85.83	--	21.0	21.6*
14	40	16	*145.01*	*145.06*	--	79.55	14.4	14.4
15	40	16	*146.38*	*146.40*	--	79.34	14.4	14.4
16	36	18	*136.34*	*136.37*	*61.51*	*61.51*	16.8	13.8
17	36	23	*142.52*	*142.52*	--	77.08	16.2	16.2
18	33	17	*162.31*	*162.30*	*75.89*	*75.89*	27.6	27.6
19	36	--	--	--	93.01	--	27.6	27.6*
20	36	16	*142.74*	*142.76*	*83.81*	*83.81*	13.8	13.8
21	29	17	131.02	--	--	--	16.2	16.2*
22	33	19	*148.26*	*148.29*	*72.87*	*72.89*	25.8	25.8
23	34	13	*155.74*	*155.70*	*81.43*	*81.42*	12.6	12.6
24	37	19	152.77	--	83.58	--	20.4	20.4*
25	39	--	--	--	--	--	20.4	17.4*

-- Indicates that the datum is missing either because the abdominal ECG is unavailable or because the methodology described in this chapter did not manage to collect it from the estimated PCGs, * indicates that the signal presents quantisation problems.

Table 10.4 presents the statistical tests conducted on the FHR (for **N**= 15 cases), the MHR (for **N**= 12 cases), and the MBR (for **N**= 25 cases) values in Table 10.3. As can be seen, the paired *t*-tests show that there are not significant differences ($p > 0.05$) between the mean values obtained from the signals estimated by SCICA and the mean values obtained from the reference signals, *i.e.* the mean values of the parameters collected from the estimated signals are likely to be equivalent to the mean values obtained from the reference signals.

Table 10.4. Paired *t*-tests of the mean FHR, MHR, and MBR collected from the signals estimated by SCICA and the reference signals used in this research. The heart rate is expressed in beats/min, whereas the breathing rate is expressed in breaths/min.

	Foetal		**Maternal**			
	Estimated FHR	Reference FHR	Estimated MHR	Reference MHR	Estimated MBR	Reference MBR
Mean	145.95	145.96	78.02	78.01	18.41	16.13
Std	8.16	8.15	9.63	9.62	4.32	4.52
N	15		12		25	
p-value	p= 0.6946		p= 0.1708		p= 0.0544	

Finally, regarding the concern raised in Section 9.1.3 about the performance of the data-driven filters learnt by SCICA versus the performance of a "general" filter, Table 10.5 presents the mean FHR values collected from the reference signal (*i.e.* the abdominal ECG), the PCG estimated by SCICA, and the PCG obtained by filtering the abdominal phonogram using a "general" FIR filter (50-order band-pass filter with cut-off frequencies of 18.8 and 44.5 Hz, *i.e.* empirically filtered[6]). In addition, the table presents (1) the statistical test conducted on the mean FHR values collected from the empirical PCG (for **N**= 15 cases) and (2) the mean square error (MSE) values obtained when comparing the FHR collected from the reference signal with the FHR collected from the PCG estimated by the empirical filter and with the FHR collected from the PCG estimated by SCICA. As can be seen, the *t*-test shows that the mean FHR values collected from foetal PCGs extracted by a general filter (*i.e.* empirical) are significantly different ($p < 0.05$) to the mean FHR values obtained from the reference signal given by the abdominal ECG. In other words, when collected from empirically filtered PCGs as in this work, the mean values of FHR are unlikely to be equivalent to the mean values of FHR given by the

[6] The order of the filter has been chosen to match the order of the filters learnt by SCICA (m= 50) and the cut-off frequencies have been set according to the frequency interval used to validate foetal IC_ps in Chapter 8.

abdominal ECG. Regarding the MSE values, it can be seen that the error values obtained from the foetal PCG by SCICA are consistently lower than the values obtained from the empirical PCG, which means that the level of variations (*i.e.* noisiness) introduced when collecting the FHR from the PCG by SCICA is more likely to be lower than the level of variations introduced when collecting the FHR from an empirical PCG. Thus, when talking about measuring FHR, it must be taken into account that, even though the mean FHR values collected from the empirical PCG might seem as closer to the reference values as the mean values collected from the PCG by SCICA are, the FHR estimated from the empirical PCG is more likely to present larger errors than the FHR estimated by the PCG by SCICA.

Table 10.5. Mean and mean square error (MSE) values of the FHR collected from the reference signal (*i.e.* the abdominal ECG), the PCG estimated by SCICA, and the PCG obtained by applying a general filter to the abdominal phonogram (*i.e.* empirically filtered). Additionally, for the values collected from the empirical PCG, the paired *t*-test.

	Abdominal ECG (reference)	**Foetal PCG (empirically filtered)**		**Foetal PCG (by SCICA)**	
	Mean (beats/min)	Mean (beats/min)	MSE ($beats^2/min^2$)	Mean (beats/min)	MSE ($beats^2/min^2$)
	142.67	143.12	33.22	142.66	30.99
	154.23	154.52	15.04	154.22	13.73
	149.70	150.44	39.03	149.71	25.26
	127.84	128.00	17.54	127.83	11.38
	145.64	147.75	153.90	145.66	151.00
	141.42	141.64	45.02	141.45	35.09
	148.46	148.72	29.61	148.49	18.28
	145.06	146.44	196.35	145.01	153.31
	146.40	148.16	239.39	146.38	182.69
	136.37	137.37	75.51	136.34	59.51
	142.52	142.74	15.68	142.52	11.29
	162.30	164.47	264.58	162.31	155.75
	142.76	143.49	60.38	142.74	44.03
	148.29	149.21	96.61	148.26	74.70
	155.70	160.08	718.09	155.74	644.02
Mean	145.96	147.08			
Std	8.15	8.79			
N	15				
p-value	p= 0.0018				

10.5. Foetal surveillance: is SCICA a suitable approach?

This chapter considers the methodology used to collect information for well-being surveillance by means of the physiological sources retrieved by SCICA. For this purpose, three stages were implemented, first, the segmented sources retrieved by SCICA in Chapter 9 were concatenated to reconstruct the entire time-series underlying the abdominal phonogram, which have been identified as the foetal PCG, the maternal PCG/pressure-wave, the maternal respirogram, and noise. Second, the foetal PCGs were further analysed to collect information about foetal status in the form of beat-to-beat foetal heart rate and average morphology of the FHS. Third, the references signals (abdominal ECGs, maternal PCGs/pressure-waves, and maternal respirograms) were processed to calculate the foetal and maternal heart rate as well as the maternal breathing rate. The FHR was calculated for verification purposes by producing a reference signal, whereas the maternal rates were calculated for becoming familiar on the maternal status –by finding the beat-to-beat MHR and the breathing rate–, and their influence on the foetal condition (if any).

Results are promising, the entire time-series of the sources underlying the abdominal phonogram have been reconstructed and further processed to obtain information of interest, not only foetal, but also maternal. Moreover, as seen in Table 10.4, the analysis of such information has shown that the mean beat-to-beat FHR estimated from the foetal PCG, the mean beat-to-beat MHR estimated from the maternal PCG, and the overall breathing rate estimated from the maternal respirogram are likely to be equivalent to the values provided by the reference signals, which is especially significant since the signals have been retrieved from the noisy abdominal phonogram. Hence, as far as this preliminary study has gone, it seems that the signals retrieved by SCICA from the abdominal phonogram are likely to become a suitable alternative for antenatal well-being surveillance. The following sections discuss these results in more detail.

10.5.1. The scaling-concatenating procedure

In the first stage, results from 25 abdominal phonograms show entire time-series that are less dependent on the amplitude of the segmented traces used to reconstruct them. Consequently, the amplitude of the reconstructed signals is currently less likely to present abrupt variations over time, which means that the scaling-concatenating methodology used in this research is managing to correct the energy uncertainty produced by ICA, at least partially. This can be seen in Figure 10.4, Figure 10.5, and Figure 10.6 where, even though some sudden variations are still present in the scaled signals, their intensity and incidence are considerably lower than in the unscaled versions, which is a promising result for a first attempt.

The scaling-concatenating method is fast, although it still needs further development to decrease the side-effects that the scaling may have on the reconstructed time-series: overall

attenuation and spikes enlargement. The overall attenuation, as observed in Figure 10.5, reduces the amplitude of the scaled signal in comparison to the unscaled one. On the other hand, the spikes enlargement, as seen in the interval between 160 and 220 s in Figure 10.4, magnifies some "already large-amplitude" components in the signal. Even though the amplitude of the scaled signals is steadier than in the unscaled versions, there is a possibility for the reconstructed signals either to be fully attenuated or to present some significant spikes. Here, a closer analysis of these cases has shown that:

a) **The overall attenuation**, produced by scaling factors lower than one during the concatenation process, appears in those cases where the area of the first segment is lower than the area of the second segment and becomes a trivial issue that should be easily corrected by being certain that, at least for the first couple of segments, the scaling factor is larger than one. So far, this amplitude issue does not seem to harm the analysis currently performed, although further research is still necessary to evaluate the limitations, if any, of the scaling methodology used in this research.

b) **The spikes enlargement** is due to a scaling factor larger than one and is particularly magnified in those cases where the main characteristics of $s_{\beta'}$ can be described as (1) energy considerably lower than in s_{β} and (2) composed of some large-amplitude spikes. Thus, when the scaling factor is calculated, it becomes significantly larger than one because of (1) and, since it is equally applied to $s_{\beta'}$, the result is a scaled segment that, because of (2), presents enlarged spikes.

These side-effects have been seen in some reconstructed time-series and, at least in this preliminary study, their presence have not become a major problem at the time of collecting the heart rate, mainly because of the normalisation step in the procedure for peaks detection. Clearly, for more ambitious implementations, like automatic thresholding, such a normalisation might not be enough to deal with the spikes enlargement effect. Additionally, since the longest recording time in this study is 5 min, is it impossible to predict the performance of this scaling-concatenating methodology on long-recording conditions, which means that further research needs to be conducted on the matter of reconstructing entire time-series.

10.5.2. The estimates of the physiological time-series: a content overview

The scaling-concatenating methodology, in spite of its side-effects, allows one to reconstruct entire time-series from where information of interest has been collected, the next paragraphs will focus on discussing the potential of using such information for well-being surveillance purposes.

Let this section start by looking at Table 10.2, which provides a general characterisation of the reconstructed time-series by presenting their frequency content and rhythmicity. As can be seen, and expected due to the SCICA implementation, the main part of the energy and rhythm of the time-series recovered from the abdominal phonogram ranges in specific intervals depending on the physiological activity driving the time-series. Thus, as shown in the last seven columns, the maternal respirogram is the signal with the lowest frequencies (S_I = 2.0 Hz and R= 0.30 Hz), followed by the maternal PCG/pressure-wave (S_I = 2.0 Hz and R= 1.3 Hz), the foetal PCG (S_I = 30.5 Hz and R= 2.4 Hz), and the noise (S_I = 56.0 Hz).

The rhythms in these underlying signals, as discussed in Chapter 8, agree with well-known physiological intervals at pregnancy (Guijarro-Berdinas *et al.* 2002; Ogueh *et al.* 2009; van Leeuwen *et al.* 2009). Their frequency content, on the other hand, have not been intensively researched, at least for the signals recovered from the abdominal phonogram. Consequently, corroboration of the values of S_I in Table 10.2 becomes a difficult task that, in the case of the foetal information, was performed by looking at works where the *recorded* foetal PCG has been studied (Ruffo *et al.* 2010; Talbert *et al.* 1986; Zuckerwar *et al.* 1993). In such works, the authors reported peak values centred at 30 Hz for S1 and at 75-100 Hz for S2 (Talbert *et al.* 1986), at 23 Hz for S1 and at 19 Hz for S2 (Zuckerwar *et al.* 1993), and between 37 Hz to 54 Hz for S1 (Ruffo *et al.* 2010). Hence, since the frequency content of the foetal PCGs estimated in this research has been typically centred at about 30 Hz, it means that S1 is the most representative heart sound in the signals retrieved in this research, which corroborates the visual observations of the zoomed sections in Figure 10.4 (a), Figure 10.5 (a), and Figure 10.6 (a).

The fact that a single number like S_I has consistently shown typical values for cases where the foetal PCG is mainly composed of S1 seems promising, especially because it might quickly provide an idea of the main information enclosed in the signal (*i.e.* S1, S2 or noise). Ideally, if typical S_I values for dominant S1s and dominant S2s were identified, then the procedure for collecting information could be focused on the detection of the most representative heart sound in the signal, which would save processing time. Unfortunately, since for all the foetal PCGs in this work the dominant heart sound is S1, this idea will remain as a possibility, at least for the research described in this thesis.

10.5.3. The estimated foetal PCG as a source of specific information

As described in Section 10.2, the estimated foetal PCG was further analysed to obtain information in the form of the instantaneous heart rate and the average morphology:

a) The instantaneous FHR: Initially collected from to subjects 1, 2, and 3, showed that measuring the beat-to-beat FHR by using S1 (*i.e.* CTG by S1) and S2 (*i.e.* CTG by S2) was possible. The results, depicted in Figure 10.7 (a) and (c), Figure 10.8 (a) and (c), and Figure

10.9 (a) and (c), have shown that both estimates are more likely to present larger beat-to-beat variations than the reference CTG (*i.e.* CTG by QRS). Such variations, here referred to as noisiness, have been found to be larger and more frequent in the CTG by S2 than in the CTG by S1, which means that the SNR of the heart sounds is more likely to be an important factor for the purpose of measuring the beat-to-beat intervals.

To deal with the noisiness problem, and aiming to produce an estimated CTG more similar to the reference CTG, the CTGs by S1 and by S2 were low-pass filtered to obtain their trend (*i.e.* the long-term variations). The resulting signals, illustrated in Figure 10.10, are more alike to the trend of the reference CTG, which can be better seen in Figure 10.11 (a) and (c), Figure 10.12 (a) and (c), and Figure 10.13 (a) and (c). However, as can be noticed, the filtered CTG by S2 is still noisier than the filtered CTG by S1 and therefore noisier than the CTG by QRS. Moreover, the noisiness in the CTG by S2 has turn into slow oscillations that might be easily taken as normal variations and lead to wrong interpretations about foetal status, which is an inconvenient outcome. Based on these results, and knowing that lower SNR values of S2 were likely to persist in the others foetal PCGs, the calculation of the instantaneous FHR by means of S2 was excluded of this study (at least until a more robust CTG estimation becomes available).

b) The average morphologies of the FHS (avgS1 and avgS2): As seen in Figure 10.11 (b) and (d), Figure 10.12 (b) and (d), and Figure 10.13 (b) and (d), they present variations over time and amongst signals that make it difficult to talk about a consistent waveform (*i.e.* a characteristic acoustic signal). On the other hand, it has been consistently observed that (1) avgS2 changes a lot more than avgS1 over time and (2) that the number of sounds used to calculate avgS2 is considerable lower than the number of sounds used to calculate avgS1. This means that, according to the similarity criterion, S2 is significantly changing over time in the signals, probably due to its lower SNR, which makes it easily distorted by background noise and therefore unreliable for this study.

On the matter of S1, results herein might look promising since the waveform does not seem to change a lot over time. However, in those foetal PCGs where the SNR of S1 is lower, avgS1 shows the same behaviour of avgS2 (*i.e.* morphological variations over time and a significant reduction in the number of sounds used in the calculation), which makes it also unreliable for this study.

Now, although finding acoustic signatures related to the FHS would have been valuable for surveillance purposes (as it reveals the heart valves condition), it was impossible for this research to achieve such a goal. Certainly, since this study was based only on the observation of the temporal features of avgS, it probably missed some details, which means

that further research must be conducted on the study of the average morphology so that significant features can be found (*e.g.* in frequency domain or in time-frequency domain). This quest will be left as part of the future work and, from now on, the discussion will focus on the foetal information that has shown the most consistent behaviour, *i.e.* the CTG by S1.

Once the analysis of the information collected from the foetal PCG has pointed at the beat-to-beat FHR by S1 as the most consistent parameter in the dataset, it is time to proceed towards some quantitative analysis by using Figure 10.16 and Table 10.3. In Figure 10.16, it is possible to observe the statistics of the CTG by S1 over time for the fifteen cases whose abdominal ECG was available. In addition, the SNR of S1 is presented in the form of an average value. As can be seen, whilst the mean values between the reference and the CTG by S1 are similar over time, the standard deviation of the latter is larger[7] and, additionally, changes over time depending on the SNR of S1. Thus, according to this figure, the larger the SNR of S1, the closer the variance of the CTG by S1 to the variance of the reference signal and, most importantly, to a reliable observation of variations in the heart rate due to the foetal condition (*i.e.* foetal well-being). In particular, it has been observed that SNR values larger than 20 dB are good enough to produce estimates that are similar to the reference, although it needs to be tested on a larger dataset before the definition of the definitive value can be achieved.

Table 10.3 summarises the foetal and maternal vital signs collected in this study, which makes it suitable to (1) study the values finally obtained by means of the signals estimated by SCICA, (2) verify such values by using the reference signals, and (3) look for correlations between foetal and maternal status or between the SNR and the gestational age. Here, to make the analysis easier, it will be performed by focusing on two types of information in the table, the behaviour of the data in each column (*i.e.* the vital signs in the dataset) and the presence/absence of correlations/influences between columns.

a) The vital signs: As seen in the table, it was impossible to obtain the beat-to-beat heart rate for all cases, both foetal and maternal.

1. *The estimated FHR:* The SNR of the estimated PCGs in some cases was so low that the current methodology did not manage to detect the FHS, which reduced the number of cases to study in the fourth column from 25 to 21. Amongst these 21 cases, 15 were corroborated by means of the abdominal ECG, which has shown that (i) it is feasible

[7] Subject 7 could be thought as an exception of this statement, which makes it imperative to highlight that, in this particular case, the signal to noise ratio of the foetal QRS in the abdominal ECG was considerably lower than in the other cases. Consequently, although the CTG by S1 in this case is less noisy than the reference, the SNR of S1 is very low as well, which means that the standard deviation of this CTG is not reliable at all.

to use S1 for estimating the beat-to-beat FHR and (ii) the quality of the CTG depends on the SNR of S1.

Regarding the six unverified cases, three of them presented standard deviations larger than 30 beats/min, which indicates an important level of noise in their CTGs. Conversely, and important to highlight is case 24, which presented one of the lowest standard deviation in the whole dataset and resulted from a PCG processed without neither visual help by the QRS nor manual correction. In fact, this case is particularly promising for this research since shows the possibility for SCICA to take a noisy abdominal phonogram and truly estimate a foetal PCG that can be easily processed to measure the instantaneous FHR and thus, perform foetal surveillance. The question that raises now is how to increase the probability of cases with such a nice result, which points the attention at the recording setup, whose improvement would certainly enhance the final outcome.

2. *The maternal vital signs:* Collected to gain perspective on the maternal status, are shown in columns sixth, seventh, eighth, and ninth in the form of mean heart and breathing rates.

   As seen in the sixth and seventh columns, amongst the 25 cases in this study, the instantaneous MHR was obtained from 21 of them, fifteen by means of the abdominal ECG and 18 by means of the maternal PCG/pressure-wave estimated in this work, which indicates the possibility of using this latter signal to monitor the MHR, especially whenever the pressure wave is evident. Clearly, since the number of cases is this study might not be representative enough, further research on a larger dataset will have to be implemented on the matter of evaluating the use of this signal to estimate the instantaneous MHR.

   On the subject of the maternal breathing rate, columns eight and nine show that the FFT made it suitable to obtain the MBR from all the respirograms in the dataset, both the estimated and the reference signals. Moreover, it has been seen that the values calculated from the estimated signals are equivalent to the reference values, which is statistically shown in Table 10.4. However, since such MBR values were calculated as an overall index rather than a breath-to-breath one, further research is still needed to explain why some particular cases in Table 10.4 (*i.e.* 2, 3, 5, 7, 10, 16, and 25) gave different rates when collected from the estimated signals than when collected from the reference signals.

b) The influences/correlations: As formerly mentioned, the purpose of collecting additional parameters was to look for any influences on the estimated foetal CTG that would help

verify or perhaps understand its behaviour. Thus, three correlations were explored, the influence of the maternal status on the foetal CTG, the influence of the SNR on the foetal CTG, and finally, the influence of the gestational age on the foetal CTG. Thus

1. *In the maternal-foetal case*, current results do not make evident any sort of influence from the maternal activity on the foetal status, neither from the maternal cardiac nor from the maternal breathing activities. The values in the table do not show any correlation between the maternal rates with the foetal FHR.

2. *In the SNR-foetal case,* as previously discussed, the quality of the CTG by S1 is likely to depend on the SNR of S1.

3. *In the gestational age-foetal case* it was unsuitable to find any correlation, neither between the gestational age versus the SNR of S1 nor between the SNR of S1 versus the FHR. Hence, according to these results, the gestational age does not say anything about the possible SNR of S1 and therefore the CTG quality. In other words, and totally unexpected, larger gestational ages do not guarantee larger SNR of S1, which raises again the question of what to do in order to increase the number of recordings with outcomes similar to case 24.

Finally, after statistically testing the information collected in this chapter (Table 10.4), it can be said that the signals retrieved by SCICA from the abdominal phonogram are likely to be useful for antenatal surveillance purposes. In particular, as far as the study described in this chapter has gone, it has been observed that the mean values of the heart and breathing rates collected from the signals estimated by SCICA are statistically equivalent to the values given by the reference signals used in this work. Also, by using the mean beat-to-beat FHR values collected from the foetal PCGs retrieved by (1) SCICA and (2) an empirical filter (Table 10.5), it has been seen that the mean FHR collected from the signals retrieved by SCICA is statistically equivalent to the mean FHR collected from the abdominal ECG. Conversely, the FHR collected from the signals retrieved by the empirical filter has been statistically different to the FHR collected from the abdominal ECG. Thus, although further research on a larger dataset must be performed, the results achieved in this work show the feasibility of performing antenatal well-being surveillance by means of the single-channel independent component analysis approach studied in this research.

10.6. Summary

The work described in this chapter studied the possibility of collecting information for well-being surveillance from the physiological sources retrieved by SCICA. For this purpose, the segmented traces retrieved by SCICA were concatenated to reconstruct entire time-series

corresponding to the foetal PCG, the maternal PCC/pressure-wave, the maternal respirogram, and noise. Next, the signals were further processed to obtain the beat-to-beat FHR, the average morphology of the FHS, the beat-to-beat MHR, and the MBR. Statistical tests on 15 out of 25 cases showed that the foetal PCG retrieved by SCICA provide estimations of the mean beat-to-beat FHR values (by using S1) that are equivalent to the mean beat-to-beat FHR values given by the abdominal ECG. In addition, it was observed that the CTG by S1 becomes more similar to the CTG by QRS as long as the SNR of S1 is larger than 20 dB, behaviour that in the current dataset was independent on the gestational age. Regarding the maternal parameters, the MBR was successfully obtained in all 25 cases, whereas the instantaneous MHR was easily obtained from those maternal PCGs whose pressure-wave was evident. Thus, although further research needs to be done, it can be said that the signals recovered by SCICA from the abdominal phonogram are promising sources of information for antenatal well-being surveillance.

11 CONCLUSIONS AND FUTURE WORK

11.1. Conclusions

Today, it is generally accepted that current methods for biophysical antenatal surveillance do not facilitate a comprehensive and reliable assessment of foetal well-being. Alternatively, there is continuing development of existing technologies and research into new non-invasive methods that aim to improve antenatal monitoring procedures. These non-invasive methods rely on the detection of information regarding the cardiac function along with foetal activity, which is done by using passive transducers that sense electric, magnetic or vibration signals. Here, attention has been paid to the vibrations recorded by positioning an acoustic sensor on the maternal womb, *i.e.* the abdominal phonogram. The signal, recorded in a single-channel configuration, contains information about foetal activity, but hidden by maternal and environmental interferences whose characteristics turn the extraction of foetal information into a challenging task.

The research presented in this thesis studied, for the first time, Single-Channel Independent Component Analysis (SCICA) as an alternative signal processing approach to retrieve information for antenatal foetal surveillance from the single-channel abdominal phonogram.

The study, conducted through the development of three SCICA implementations, has produced a methodology that successfully exploits the time-structure in the abdominal phonogram for decomposition purposes (Jimenez-Gonzalez and James 2008b; Jiménez-González and James 2009; Jiménez-González and James 2010b). As a result, the methodology implemented in this work not only *retrieves estimates of the sources* underlying the noisy abdominal phonogram, but also *identifies their physiological origin*, which are essential contributions of this research (Jiménez-González and James 2010a; Jiménez-González and James 2010b). Indeed, as results from 25 noisy single-channel abdominal phonograms show, the current implementation of SCICA has consistently managed to retrieve estimates of the sources

related to *the foetal cardiac activity, the maternal cardiovascular activity, the maternal breathing activity, and the noise or noisy activity* (Jiménez-González and James 2010b).

In this outcome two facts were particularly remarkable. Firstly, that the cardiac information from maternal and foetal origins was consistently retrieved in separate traces by SCICA (as maternal cardiovascular and foetal cardiac). Secondly, that each trace was aligned with the maternal and foetal QRS complexes respectively. The former was a significant result in terms of separation performance, especially because the maternal cardiovascular activity may temporarily overlap the foetal cardiac activity (like the maternal QRS overlaps the foetal QRS in the abdominal ECG), and the most outstanding feature is that it was achieved by using a single-channel methodology. The latter was helpful in terms of physiological interpretation and made it possible to infer that (a) the maternal cardiovascular trace was more likely to represent the *maternal phonocardiogram* (PCG) and/or *the pressure wave*, whereas (b) the foetal trace was more likely to represent the *foetal PCG*, a signal where the main foetal heart sounds (FHS), S1 and/or S2, can be seen.

These results were promising in terms of decomposing the single-channel abdominal phonogram. Most importantly though, they showed that additional developments were still necessary in order to (1) improve the separation stage and (2) objectively identify the separate components in the grouping stage (Jimenez-Gonzalez and James 2008a; Jimenez-Gonzalez and James 2008b; Jiménez-González and James 2009). These are typical challenges for BSS methodologies and require further research on the signals of interest in order to find a suitable solution. Here, as already mentioned, the solution of both problems was achieved by exploiting the rich time-structure in the abdominal phonogram. In the separation stage, it was performed by using TDSEP, an implementation of ICA that in this work produces *a spectral decomposition of the abdominal phonogram* (Jimenez-Gonzalez and James 2008b). Next, for the grouping stage, a methodology was developed to disclose the rhythmic patterns in the ICs and thus, to automatically *identify the physiological processes underlying the separate components* (Jiménez-González and James 2010b).

Arriving to a solution that not only separates components, but also identifies their origin was one of the most important achievements in this research and, because of that, deserves further attention of the procedure followed and its outcome. In fact, the task was especially challenging since previous studies on the components underlying the abdominal phonogram were unavailable. As a solution, as soon as the separation stage was enhanced by TDSEP –in the second implementation of SCICA– so that the ICs were available, this work proceeded towards the most natural option, *i.e. an extensive study of the components* separated by TDSEP. Hence, four different methods for time-series analysis were incorporated to obtain meaningful features that, for the first time, *revealed valuable characteristics of the components separated*

from the abdominal phonogram by TDSEP: (1) the ICs are spectrally disjoint, (2) the ICs are sorted according to their frequency content, (3) the slowest ICs are more likely to present strong regular patterns, and (4) the regular patterns in the ICs are driven by well-known physiological processes, *i.e.* the maternal breathing rate, the maternal heart rate, and the foetal heart rate.

The implications of the findings from this research were immediately evident. First, since the ICs were sorted according to their frequency content –which in this work matched the physiological relevance–, it was clear that TDSEP was actually *removing the permutation ambiguity of ICA*. Moreover, because the components were spectrally disjoint and consistently arranged from higher to lower frequency, it was possible for this work to *learn the typical central frequencies of the physiological sources underlying the abdominal phonogram* (Jiménez-González and James 2010a). Second, since the strongest regular patterns were retrieved in the slowest ICs, it was clear that amongst the *m* components separated by TDSEP, only some were physiologically relevant and therefore suitable for recovering information of interest. Most importantly, because the rhythms of such patterns depended on the physiological process underlying the ICs, their quantification made it possible to *objectively establish whether an IC was foetal cardiac, maternal cardiovascular, maternal breathing or noise*.

In this way, the exploitation of the time-structure present in the abdominal phonogram led to an enhanced third implementation that, by combining the method of delays, TDSEP, and the rhythmicity-based analysis developed in this work, (1) successfully decomposes the single-channel signal into spectrally disjoint components, (2) objectively identifies their underlying physiological processes, (3) automatically finds similar components (*i.e.* forms physiological groups) and, finally, (4) consistently retrieves the estimates of the physiological sources underlying the single-channel abdominal phonogram, *i.e.* the foetal PCG, the maternal PCG/pressure-wave, the maternal breathing, and noise (Jiménez-González and James 2010b). The method, tested on segments of abdominal phonograms, showed that (5) the filters learnt by ICA are more likely to follow the variations in the abdominal phonogram –along time and from subject to subject– than a rigid empirical filter (Jiménez-González and James 2009), and (6) a classifier based on time-structure performs faster than a classifier based on entropy and, additionally, is more consistent than *K*-means (Jiménez-González and James 2010b).

Clearly, these results showed that the third implementation of SCICA was close to addressing the fundamental problem faced in this work, which was the extraction of information for foetal surveillance from the abdominal phonogram. In fact, being certain that SCICA decomposed the abdominal phonogram and, most importantly, that consistently retrieved four traces (corresponding to the foetal PCG, the maternal PCG/pressure-wave, the maternal breathing, and noise), made it easier to continue towards the next stage, *i.e.* reconstructing the entire time-series of the sources underlying the abdominal phonogram. Certainly, since the task

required solving the scaling ambiguity of ICA, it became the ultimate challenge for this research in terms of decomposing the abdominal phonogram. Here, following the idea by Corsini *et al.* (2006), the problem was solved by developing a scaling-concatenating methodology that managed to *reduce the energy uncertainty due to ICA.* As a result, it was possible to reconstruct entire time-series that were less dependent on the energy of the segmented traces used to build them up. Consequently, the amplitude of the reconstructed sources was less likely to present abrupt variations over time, and therefore, less likely to lead to wrong interpretations.

Finally, as soon as SCICA addressed the problem of decomposing the abdominal phonogram, and knowing that foetal information corresponding to the FHS (*i.e.* the foetal PCG) was consistently retrieved, this research explored the suitability of using such information for surveillance purposes. This need gave rise to *a preliminary study of the sources estimated by SCICA* that aimed to collect, and confirm (whenever possible), information about foetal status in the form of the beat-to-beat heart rate and the average morphology of the FHS. Results so far have been promising, the entire sources estimated by SCICA were further processed by relatively simple algorithms that managed to collect/verify valuable parameters, not only foetal but also maternal. More specific, preliminary analysis of such parameters has shown that *the beat-to-beat FHR obtained from the foetal PCG consistently follows the trend given by the reference FHR* calculated from the abdominal ECG, which is especially significant since the PCG comes from the noisy abdominal phonogram. Also, it has been seen that additional parameters such as the beat-to-beat MHR and the maternal breathing rate can be collected respectively from the maternal PCG/pressure-wave and the maternal respirogram. Therefore, as far as this study has gone, it can be said that the signals estimated by SCICA from the abdominal phonogram are promising sources of information for foetal well-being surveillance.

In summary, *this research has given rise to an implementation of SCICA that separates the single-channel abdominal phonogram into its underlying components. Such components, identified as the foetal PCG, the maternal PCG/pressure-wave, and the maternal respirogram, are promising sources of information for antenatal surveillance of foetal well-being. Future work should focus on enhancing the quality of the estimated signals, developing better algorithms for collecting meaningful parameters from such estimates, and increasing the dataset so that the suitability of using these estimates for foetal surveillance can be thoroughly tested.*

11.2. Future work

Antenatal detection of the hypoxemic foetus is a challenging task that so far remains as an unsolved problem. Certainly, since a number of stillbirths occur in the low-risk pregnancy group

(Gribbin and James 2004), it is obvious that the techniques currently used for screening and assessing foetal well-being have gaps that must be filled. This could be associated to human error, lack of a complete understanding of how the foetus adapts to prolonged hypoxemia, or perhaps lack of sensitivity in the screening tools currently available (Gribbin and James 2004). In any case, it is evident that there is a need of further research on methods that effectively identify foetuses at risk in apparently low-risk pregnancies (Gribbin and James 2004). Clearly, the study described in this thesis belongs to the research category that attempts to increase the screening sensitivity by *long-term monitoring* the foetal condition, an idea that aims to enlarge the possibilities of detecting hypoxemic events as soon as they appear. To this end, this research was focused on studying SCICA as a novel approach for recovering the foetal information immersed in the noisy abdominal phonogram. As a result, it has been possible to develop an implementation of SCICA that manages to recover useful information for foetal surveillance, which makes this signal processing approach promising for further and more ambitious stages, both physiological and technological.

11.2.1. Physiological challenges

These challenges refer to the *extraction of meaningful physiological information* from the abdominal phonogram so that foetal well-being assessment can be better performed. As the reader may recall, the foetal information in the abdominal phonogram is composed of the heart sounds and, sometimes, of the breathing movements and/or body movements, all significant for well-being surveillance. In this work, the task corresponding to the separation of the foetal PCG was addressed by SCICA, which means that further research could focus on the separation of the FBM and FMs. Also, although the methods in Chapter 10 did not manage to reliable collect the average morphology of the FHS and the instantaneous FHR by S2, their extraction from the estimated foetal PCG would be priceless for foetal surveillance. The morphology would be useful for studying the heart valves condition, whereas the FHR by S2 would give the possibility (1) of corroborating FHR measurements along time and, perhaps, of choosing the temporal event (S1 or S2) that provides the most reliable FHR estimation and (2) of estimating the systolic and diastolic intervals during the cardiac cycle.

Certainly, the research on the subject of using the abdominal phonogram for detecting the hypoxemic foetus is still plenty of challenges, not only on the separation of the physiological components (*i.e.* the foetal adaptations), but also on the recovery/interpretation of meaningful information. From the perspective of this research, there are four major challenges to work on: (1) further separation of the abdominal phonogram, either to obtain the FBM/FMs estimates or to enhance the current estimates (*e.g.* the foetal PCG), (2) better analysis of the separate signals for efficient detection of physiological events such as S1, S2, FBM, and FMs, (3) reliable collection of parameters such as the instantaneous FHR, the systolic and diastolic intervals, the

FHS/FBM/FMs patterns, and finally, (4) a thoroughly study in a large dataset of normal and abnormal subjects to accurately test the suitability of using SCICA for foetal surveillance purposes.

Clearly, none of these challenges will be easily undertaken and they will definitely require extensive studies to develop appropriate solutions. Some of them will probably require using other approaches to be solved, for example, automatic algorithms for detecting events (either periodic like the FHS or asynchronous like the FBM/FMs), or time-frequency analysis for studying/characterising the FHS/FBM/FMs patterns. Also, as seen in Chapter 10, although the current implementation of SCICA is recovering the FHS, there is a possibility of finding either some foetal cardiac information in the noise estimate or some maternal cardiovascular information in the maternal breathing estimate. Consequently, additional studies are still necessary to be certain that each physiological estimate contains the most of the corresponding activity with the minimum of noise. Then, assuming that an enhanced separation and better algorithms will ease the collection of meaningful information, it should be feasible to better understand the foetal adaptations to hypoxemia and then, to reliably perform foetal surveillance. Finally, the application of such an enhanced analysis to a larger dataset should make it possible to find out what makes some abdominal phonograms easier to decompose than others and, most importantly, whether the gestational age and the maternal status are involved.

At this time, it is impossible to provide specific details about the solutions for these problems. Alternatively, since these tasks do not have to be consecutively solved, the current availability of signals makes it suitable to start searching for and testing alternatives to recover information of interest.

11.2.2. Technological challenges

This research sees two core technological challenges in terms of foetal monitoring, improved recording of the abdominal phonogram and mobile implementation of SCICA for foetal surveillance.

a) Improved recording of the abdominal phonogram: So far, it has been seen that SCICA is suitable to address the problem of decomposing the abdominal phonogram, but with different degrees of separation amongst signals. As a result, the SNR in some estimates is so low that complicates the extraction of meaningful information for foetal surveillance. This situation has attracted attention towards the recording setup and thus, raised the question of whether it could be modified to help SCICA estimate better-quality foetal PCGs from the abdominal phonograms.

To this end, two approaches could be explored (1) keeping a single-channel configuration and using a more sensitive acoustic sensor, which would increase the financial cost of the

system, or (2) increasing the number of channels so that not only temporal, but also spatial information can be exploited during the separation stage, which would increase both the financial and computational costs. In any case, by testing these configurations in a large population, there should be possible to find the circumstances that make some phonograms easier to be decomposed by SCICA than others (*e.g.* the recording setup, the gestational age, or perhaps some physiological conditions that modify the spectra of the underlying components), and develop recording protocols that increase the possibilities of a good-quality separation.

In this context, it is important to recall that, currently, the recording protocol described in Chapter 5 uses US images to find a suitable position for the acoustic sensor on the maternal womb. This might be acceptable for a study like the one described in this thesis, where a signal processing methodology is being explored and validated. However, when thinking of future work and "trouble-free" implementations of a system for well-being monitoring, the need of the US in the recording protocol becomes a key issue. Thus, the technological challenges in this research also involve the development of alternatives that simplify the procedure for sensor positioning and eliminate the US from the recording protocol.

As a preliminary idea, taking into account that the SNR of the FHS seems to have an effect on the quality of the CTG, it has been considered that an SNR index could be useful to establish whether the sensor is close to the foetal heart or whether it has to be relocated. Also, in a more complete implementation that deals with the possibility of a foetus changing its position (and the resulting SNR reduction) without having to relocate the sensor, a set of sensors could be positioned all over the maternal womb. In this way, by monitoring the SNR in each single-channel, it should be feasible to find the most favourable channel for recording and automatically switch to it whenever the foetus moves and the SNR changes.

b) Mobile implementation of SCICA: This could be considered as the ultimate challenge in terms of foetal surveillance by means of the abdominal phonogram, developing a portable instrument that records the signal(s), performs the decomposition, retrieves the foetal sources, and collects/transmits parameters for assessing foetal well-being (*e.g.* the FHR).

Certainly, assuming that the separation issues have been overcome, one of the most important challenges for developing a portable instrument would be given by the on-line implementation of the algorithms for separation and collection of parameters of interest. Additionally, depending on the number of channels to record and the recording time, the memory of the system would be required to be large and fast enough to make it possible the recording, processing, storing, and transmission of data in a simultaneous way. Eventually,

in a more ambitious implementation for home-monitoring, the system could also be required to perform the analysis of the collected information by itself and thus, identify foetuses at risk.

Ideally, an instrument like this would increase the screening sensitivity by performing long-term monitoring, either in the hospital or at home. However, longer and more frequent screening also means more data for clinical interpretation. Moreover, if it is taken into account that several monitors will be working simultaneously, then the amount of data for clinical interpretation will considerably increase. This means that another challenge for a mobile implementation would be associated to appropriate storage media and data managing in the hospital that guarantees proper access to the information, either for clinical diagnosis or for research purposes.

Finally, assuming that such a foetal monitor could be developed, obstetricians would be able to perform foetal surveillance as often and longer as needed without exposing the foetus to US radiation. Additionally, the availability of more frequent and longer observations of the foetal adaptations to hypoxemia could lead to further understanding of them and, perhaps, give rise to tools for a more assertive evaluation of foetal risk.

APPENDIX **A**. COPYRIGHT CLEARANCES

SPRINGER LICENSE
TERMS AND CONDITIONS

Nov 25, 2010

This is a License Agreement between Aida Jimenez-Gonzalez ("You") and Springer ("Springer") provided by Copyright Clearance Center ("CCC"). The license consists of your order details, the terms and conditions provided by Springer, and the payment terms and conditions.

All payments must be made in full to CCC. For payment instructions, please see information listed at the bottom of this form.

License Number	2555860554630
License date	Nov 25, 2010
Licensed content publisher	Springer
Licensed content publication	Medical and Biological Engineering and Computing
Licensed content title	Extracting sources from noisy abdominal phonograms: a single-channel blind source separation method
Licensed content author	A. Jiménez-González
Licensed content date	Jan 1, 2009
Volume number	47
Issue number	6
Type of Use	Thesis/Dissertation
Portion	Full text
Number of copies	8
Author of this Springer article	Yes and you are a contributor of the new work
Order reference number	
Title of your thesis / dissertation	Antenatal foetal monitoring through abdominal phonogram recordings: A single-channel independent component analysis approach
Expected completion date	Jan 2011
Estimated size(pages)	200
Total	0.00 GBP
Terms and Conditions	

Introduction
The publisher for this copyrighted material is Springer Science + Business Media. By clicking "accept" in connection with completing this licensing transaction, you agree that the following terms and conditions apply to this transaction (along with the Billing and Payment terms and conditions established by Copyright Clearance Center, Inc. ("CCC"), at the time that you opened your Rightslink account and that are available at any time at http://myaccount.copyright.com).

Limited License
With reference to your request to reprint in your thesis material on which Springer Science and Business Media control the copyright, permission is granted, free of charge, for the use indicated in your enquiry. Licenses are for one-time use only with a maximum distribution

equal to the number that you identified in the licensing process.

This License includes use in an electronic form, provided it is password protected or on the university's intranet, destined to microfilming by UMI and University repository. For any other electronic use, please contact Springer at (permissions.dordrecht@springer.com or permissions.heidelberg@springer.com)

The material can only be used for the purpose of defending your thesis, and with a maximum of 100 extra copies in paper.

Although Springer holds copyright to the material and is entitled to negotiate on rights, this license is only valid, provided permission is also obtained from the (co) author (address is given with the article/chapter) and provided it concerns original material which does not carry references to other sources (if material in question appears with credit to another source, authorization from that source is required as well). Permission free of charge on this occasion does not prejudice any rights we might have to charge for reproduction of our copyrighted material in the future.

Altering/Modifying Material: Not Permitted
However figures and illustrations may be altered minimally to serve your work. Any other abbreviations, additions, deletions and/or any other alterations shall be made only with prior written authorization of the author(s) and/or Springer Science + Business Media. (Please contact Springer at permissions.dordrecht@springer.com or permissions.heidelberg@springer.com)

Reservation of Rights
Springer Science + Business Media reserves all rights not specifically granted in the combination of (i) the license details provided by you and accepted in the course of this licensing transaction, (ii) these terms and conditions and (iii) CCC's Billing and Payment terms and conditions.

Copyright Notice:
Please include the following copyright citation referencing the publication in which the material was originally published. Where wording is within brackets, please include verbatim.
"With kind permission from Springer Science+Business Media: <book/journal title, chapter/article title, volume, year of publication, page, name(s) of author(s), figure number (s), and any original (first) copyright notice displayed with material>."

Warranties: Springer Science + Business Media makes no representations or warranties with respect to the licensed material.

Indemnity
You hereby indemnify and agree to hold harmless Springer Science + Business Media and CCC, and their respective officers, directors, employees and agents, from and against any and all claims arising out of your use of the licensed material other than as specifically authorized pursuant to this license.

No Transfer of License
This license is personal to you and may not be sublicensed, assigned, or transferred by you to any other person without Springer Science + Business Media's written permission.

No Amendment Except in Writing

This license may not be amended except in a writing signed by both parties (or, in the case of Springer Science + Business Media, by CCC on Springer Science + Business Media's behalf).

Objection to Contrary Terms
Springer Science + Business Media hereby objects to any terms contained in any purchase order, acknowledgment, check endorsement or other writing prepared by you, which terms are inconsistent with these terms and conditions or CCC's Billing and Payment terms and conditions. These terms and conditions, together with CCC's Billing and Payment terms and conditions (which are incorporated herein), comprise the entire agreement between you and Springer Science + Business Media (and CCC) concerning this licensing transaction. In the event of any conflict between your obligations established by these terms and conditions and those established by CCC's Billing and Payment terms and conditions, these terms and conditions shall control.

Jurisdiction
All disputes that may arise in connection with this present License, or the breach thereof, shall be settled exclusively by the country's law in which the work was originally published.

Other terms and conditions:

v1.2

Gratis licenses (referencing $0 in the Total field) are free. Please retain this printable license for your reference. No payment is required.

If you would like to pay for this license now, please remit this license along with your payment made payable to "COPYRIGHT CLEARANCE CENTER" otherwise you will be invoiced within 48 hours of the license date. Payment should be in the form of a check or money order referencing your account number and this invoice number RLNK10889941.
Once you receive your invoice for this order, you may pay your invoice by credit card. Please follow instructions provided at that time.

Make Payment To:
Copyright Clearance Center
Dept 001
P.O. Box 843006
Boston, MA 02284-3006

If you find copyrighted material related to this license will not be used and wish to cancel, please contact us referencing this license number 2555860554630 and noting the reason for cancellation.

Questions? customercare@copyright.com or +1-877-622-5543 (toll free in the US) or +1-978-646-2777.

Jimenez Gonzalez A.

From: Mahfoudh, Samir (ELS-OXF) [S.Mahfoudh@elsevier.com]
Sent: 08 December 2010 15:56
To: Jimenez Gonzalez A.
Subject: RE: Obtain Permission

Elsevier

Dear Miss Jimenez-Gonzalez,
We hereby grant you permission to reprint the material detailed below at no charge **in your thesis** subject to the following conditions:
1. If any part of the material to be used (for example, figures) has appeared in our publication with credit or acknowledgement to another source, permission must also be sought from that source. If such permission is not obtained then that material may not be included in your publication/copies.
2. Suitable acknowledgment to the source must be made, either as a footnote or in a reference list at the end of your publication, as follows:
"This article was published in Publication title, Vol number, Author(s), Title of article, Page Nos, Copyright Elsevier (or appropriate Society name) (Year)."
3. Your thesis may be submitted to your institution in either print or electronic form.
4. Reproduction of this material is confined to the purpose for which permission is hereby given.
5. This permission is granted for non-exclusive world **English** rights only. For other languages please reapply separately for each one required. Permission excludes use in an electronic form. Should you have a specific electronic project in mind please reapply for permission.
6. Should your thesis be published commercially, please reapply for permission.
Kind regards,

Sam Mahfoudh

Sam Mahfoudh :: Rights Assistant :: Elsevier
T: +44 (0)1865 843715 :: F: +44 (0)1865 853333
E: s.mahfoudh@elsevier.com

-----Original Message-----
From: aj11v07@soton.ac.uk [mailto:aj11v07@soton.ac.uk]
Sent: 06 December 2010 19:54
To: Health Permissions (ELS-PHI)
Subject: Obtain Permission

This Email was sent from the Elsevier Corporate Web Site
and is related to Obtain Permission form:

Product: Customer Support
Component: Obtain Permission
Web server: http://www.elsevier.com
IP address: 152.78.241.56
Client: Mozilla/4.0 (compatible; MSIE 6.0; Windows NT 5.1; SV1; .NET CLR 1.1.4322; .NET CLR 2.0.50727; .NET CLR 3.0.4506.2152; .NET CLR 3.5.30729; InfoPath.1)
Invoked from: http://www.elsevier.com/wps/find/obtainpermissionform.cws_home?isSubmitted=yes&navigateXmlFileName=/store/scstargets/prd53/act/framework_support/obtainpermission.xml

Request From:
Miss Aida Jimenez-Gonzalez
University of Southampton, ISVR
University Road
SO17 1BJ
Southampton
United Kingdom

Contact Details:
Telephone: +44 (0)23 8059 2289
Fax: +44 (0)23 8059 3190
Email Address: aj11v07@soton.ac.uk

To use the following material:
ISSN/ISBN: ISBN 978-1-4160-2944-1
Title: Maternal, fetal, & neonatal physiology: a clinical
Author(s): Susan Tucker Blackburn
Volume: Third edition
Issue: Third edition
Year: 2007
Pages: 294 - 295
Article title: Chapter 9. Cardiovascular System

How much of the requested material is to be used:
figure 9-13 and figure 9-14

Are you the author: No
Author at institute: No

How/where will the requested material be used: In a thesis or dissertation

Details:

Additional Info: I wish to include figure 9-13 and figure 9-14 within the electronic version of my PhD thesis, which I am required to deposit in the University of SouthamptonÃ¢Â Â s online research repository (http://eprints.soton.ac.uk/). The repository is non-commercial and openly available to all.
Additionally, I would like to produce 8 hard-copy versions of my PhD thesis, which will be entitled as:

"Antenatal foetal monitoring through abdominal phonogram recordings: A single-channel independent component analysis approach"

I would be grateful if you could advise if this will be acceptable.

Yours faithfully,

Aida

Aida Jimenez-Gonzalez
Research Student
Signal Processing and Control Group
Institute of Sound and Vibration Research
University of Southampton, Southampton, UK

[acronym]
- end -

Jimenez Gonzalez A.

From: j.hansson@ieee.org
Sent: 12 December 2010 16:30
To: Jimenez Gonzalez A.
Subject: Re: Requesting copyright clearance

Comments/Response to Case ID: 00682732

ReplyTo: Pubs-Permissions@ieee.org

From: Jacqueline Hansson Date: 12/12/2010

Subject: Re: Requesting copyright clearance

Send To: "Jimenez Gonzalez A." <ajllv07@soton.ac.uk>

cc:

Dear Aida Jimenez-Gonzalez:

We are happy to grant you this permission to reprint this IEEE copyrighted paper in your thesis and, if you wish, have your thesis placed on your university's website. We have only two requirements that must be satisfied before we can consider this permission final:

(1) The following copyright/credit notice must appear prominently either on the first page of the reprinted material or prominently in the references of the reprinted paper, with the appropriate details filled in: © [year] IEEE. Reprinted, with permission, from [IEEE publication title, paper title, and author names].

(2) Additionally, if your thesis is to appear on the university's website, the following message should be displayed either at the beginning of the credits or in an appropriate and prominent place on the website: This material is posted here with permission of the IEEE. Such permission of the IEEE does not in any way imply IEEE endorsement of any of the University of Southampton's products or services. Internal or personal use of this material is permitted. However, permission to reprint/republish this material for advertising or promotional purposes or for creating new collective works for resale or redistribution must be obtained from the IEEE by writing to pubs-permissions@ieee.org.By choosing to view this material, you agree to all provisions of the copyright laws protecting it.

If applicable, University Microfilms, Inc. or ProQuest may supply single copies of the dissertation.

Sincerely,

Jacqueline Hansson

© © © © © © © © © © © © © © © © © © ©
IEEE Intellectual Property Rights Office
445 Hoes Lane
Piscataway, NJ 08855-1331 USA
+1 732 562 3966 (phone)
+1 732 562 1746 (fax)

IEEE-- Fostering technological innovation and excellence for the benefit of humanity.
© © © © © © © © © © © © © © © © © © ©

1

To whom it may concern,

My name is Aida Jimenez-Gonzalez, and I am one of the authors of the following work published by IEEE Transactions on Biomedical Engineering:

Jiménez-González, A.; James, C.J.; , "Time-Structure Based Reconstruction of Physiological Independent Sources Extracted From Noisy Abdominal Phonograms," Biomedical Engineering, IEEE Transactions on , vol.57, no.9, pp.2322-2330, Sept. 2010
doi: 10.1109/TBME.2010.2051226

I wish to include this entire work within the electronic version of my PhD thesis, which I am required to deposit in the University of Southampton's online research repository (http://eprints.soton.ac.uk/). The repository is non-commercial and openly available to all.
Additionally, I would like to produce 8 hard-copy versions of my PhD thesis, which will be entitled as:

"Antenatal foetal monitoring through abdominal phonogram recordings: A single-channel independent component analysis approach"

I would be grateful if you could advise if this will be acceptable.

Yours faithfully,

Aida

Aida Jimenez-Gonzalez
Research Student
Signal Processing and Control Group
Institute of Sound and Vibration Research
University of Southampton, Southampton, UK

2

References

Abramowicz, J. S., & Sheiner, E. (2008). Ultrasound of the placenta: a systematic approach. Part II: functional assessment (Doppler). *Placenta, 29*, 921-929.

ACOG. (2000). Antepartum fetal surveillance (ACOG practice bulletin). *International Journal of Gynecology & Obstetrics, 68*, 175-186.

Adam, D., & Shavit, D. (1990). Complete foetal ECG morphology recording by sincronised adaptive filtration. *Medical & Biological Engineering & Computing, 28*, 287-292.

Akay, M., & Szeto, H. (1995). Analyzing fetal breathing rates using matching pursuits. *IEEE Engineering Medical and Biological Magazine, 14*, 195-198.

Al-Zaben, A., & Al-Smadi, A. (2006). Extraction of foetal ECG by combination of singular value decomposition and neuro-fuzzy inference system. *Physics in Medicine and Biology, 51*, 137-143.

Alus, M., Okumus, H., Mete, S., & Guclu, S. (2007). The effects of different maternal positions on non-stress test: an experimental study. *Journal of Clinical Nursing, 16*, 562-568.

Ansourian, M. N., Dripps, J. H., Jordan, J. R., Beattie, G. J., & Boddy, K. (1993). A transducer for detecting foetal breathing movements using PVDF film. *Physiological Measurement, 14*, 365-372.

Assaleh, K. (2007). Extraction of fetal electrocardiogram using adaptive neuro-fuzzy inference systems. *IEEE Transactions on Biomedical Engineering, 54*(1), 59-68.

Azevedo, S., & Longini, R. (1980). Abdominal-lead fetal electrocardiographic R-wave enhancement for heart rate determination. *IEEE Transactions on Biomedical Engineering, 27*(5), 255-260.

Bahtiyar, M. O., & Copel, J. A. (2008). Cardiac changes in the intrauterine growth-restricted fetus. *Seminars in Perinatology, 32*, 190-193.

Banks, E. H., & Miller, D. A. (1999). Perinatal risks associated with borderline amniotic fluid index. *American Journal of Obstetrics & Gynecology, 180*(6), 1461-1463.

Barman, S. M., & Kenney, M. J. (2007). Methods of analysis and physiological relevance of rhythms in sympathetic nerve discharge. *Clinical and Experimental Pharmacology and Physiology, 34*, 350-355.

Barnett, S. B. (2001). Intracranial temperature elevation from diagnostic ultrasound. *Ultrasound in Medicine & Biology, 27*(7), 883-888.

Barsoom, M. J., Borgida, A. F., & Egan, J. F. X. (2001). Re-evaluation of the non-stress test. *Prenatal and Neonatal Medicine, 6*, 70-74.

Bassil, H. E., & Dripps, J. H. (1989). Real time processing and analysis of fetal phonocardiographic signal. *Clinical Physics and Physiological Measurements, 10*(SUPPL. B), 67-74.

Berbey, R., Manduley, A., & Vigil-De Gracia, P. (2001). Counting fetal movements as a universal test for fetal wellbeing. *International Journal of Gynecology & Obstetrics, 74*, 293-295.

Bergveld, P., Kolling, A. J., & Peuscher, J. H. J. (1986). Real-time fetal ECG recording. *IEEE Transactions on Biomedical Engineering, 33*(5), 505-509.

Bergveld, P., & Meijer, W. J. H. (1981). A New Technique for the Suppression of the MECG. *IEEE Transactions on Biomedical Engineering, 28*(4), 348-354.

Blaas, H.-G. K., & Eik-Nes, S. H. (2008). Sonographic development of the normal foetal thorax and abdomen across gestation. *Prenatal Diagnosis, 28*, 568-580.

Black, R. S., & Campbell, S. (1997). Cardiotocography versus Doppler. *Ultrasound in Obstetrics and Gynecology, 9*, 148-151.

Bocking, A. D. (2003). Assessment of fetal heart rate and fetal movements in detecting oxygen deprivation in-utero. *European Journal of Obstetrics & Gynecology and Reproductive Biology, 110*, S108-S112.

Broomhead, D. S., & King, G. P. (1986). Extracting qualitative dynamics from experimental data. *Physica D 20*, 217-236.

Callaerts, D., De Moor, B., Vandewalle, J., & Sansen, W. (1990). Comparison of SVD methods to extract the foetal electrocardiogram from cutaneous electrode signals. *Medical & Biological Engineering & Computing, 28*, 217-224.

Cardoso, J. F. (1998). Multidimensional independent component analysis. Paper presented at the *International Conference on Acoustics, Speech and Signal Processing, ICASSP'98*, 1941-1944.

Casey, M. A. (2000). Separation of mixed audio sources by independent subspace analysis. Paper presented at the *International Computer Music Conference*.

Castells, F., Mora, C., Millet, J., Rieta, J. J., Sanchez, C., & Sanchis, J. M. (2004). Multidimensional ICA for the separation of atrial and ventricular activities from single lead ECGs in paroxysmal atrial fibrillation episodes. *Lecture Notes in Computer Science, 3195*, 1229-1236.

Choi, S., & Jiang, Z. (2008). Comparison of envelope extraction algorithms for cardiac sound signal segmentation. *Expert Systems with Applications, 34*, 1056-1069.

Cito, G., Luisi, S., Mezzesimi, A., Cavicchioli, C., Calonaci, G., & Petraglia, F. (2005). Maternal position during non-stress test and fetal heart rate patterns. *Acta Obstetricia et Gynecologica Scandinavica, 84*, 335-338.

Clerici, G., Luzietti, R., & Di Renzo, G. C. (2001). Monitoring of antepartum and intrapartum fetal hypoxemia: pathophysiological basis and available techniques. *Biology of the Neonate, 79*, 246-253.

Coifman, R. R., & Donoho, D. L. (1995). Translation-invariant de-noising. In A. Antoniadis & G. Oppenheim (Eds.), *Lecture Notes in Statistics* (Vol. 103, pp. 126-150). Springer, New York, USA.

Colley, N., Talbert, D. G., & Southall, D. P. (1986). Biophysical profile in the fetus from a phonographic sensor. *European Journal of Obstetrics, Gynecology, and Reproductive Biology 23*, 261-266.

Comani, S., & Alleva, G. (2007). Fetal cardiac time intervals estimated on fetal magnetocardiograms: single cycle analysis versus average beat inspection. *Physiological Measurement, 28*, 49-60.

Comani, S., Liberati, M., Mantini, D., Merlino, B., Alleva, G., Gabriele, E., *et al.* (2005). Beat-to-beat estimate of fetal cardiac time intervals using magnetocardiography: longitudinal charts of normality ranges and individual trends. *Acta Obstetricia et Gynecologica Scandinavica, 84*, 1175-1180.

Comani, S., Mantini, D., Alleva, G., Di Luzio, S., & Romani, G. L. (2004). Fetal magnetocardiographic mapping using independent component analysis. *Physiological Measurement, 25*, 1459-1472.

Comani, S., Mantini, D., Alleva, G., Di Luzio, S., & Romani, G. L. (2005a). Automatic detection of cardiac waves on fetal magnetocardiographic signals. *Physiological Measurement, 26*, 459-475.

Comani, S., Mantini, D., Alleva, G., Di Luzio, S., & Romani, G. L. (2005b). Optimal filter design for shielded and unshielded ambient noise reduction in fetal magnetocardiography. *Physics in Medicine and Biology, 50*, 5509-5521.

Comani, S., Mantini, D., Lagatta, A., Esposito, F., Di Luzio, S., & Romani, G. L. (2004). Time course reconstruction of fetal cardiac signals from fMCG: independent component analysis versus adaptive maternal beat subtraction. *Physiological Measurement, 25*, 1305-1321.

Comani, S., Mantini, D., Pennesi, P., Lagatta, A., & Cancellieri, G. (2004). Independent component analysis: fetal signal reconstruction from magnetocardiographic recordings. *Computer Methods and Programs in Biomedicine, 75*, 163-177.

Comani, S., Srinivasan, V., Alleva, G., & Romani, G. L. (2007). Entropy-based automated classification of independent components separated from fMCG. *Physics in Medicine and Biology, 52*, N87-N97.

Cook, A. C., Yates, R. W., & Anderson, R. H. (2004). Normal and abnormal fetal cardiac anatomy. *Prenatal Diagnosis, 24*, 1032-1048.

Corsini, J., Shoker, L., Sanei, S., & Alarcon, G. (2006). Epileptic seizure predictability from scalp EEG incorporating constrained blind source separation. *IEEE Transactions on Biomedical Engineering, 53*(5), 790-799.

Cosmi, E. V., Anceschi, M. M., Cosmi, E., Piazze, J. J., & La Torre, R. (2003). Ultrasonographic patterns of fetal breathing movements in normal pregnancy. *International Journal of Gynecology and Obstetrics, 80*, 285-290.

Creasy, R. K., & Resnik, R. (2004). Maternal-fetal medicine: principles and practice (Fifth Edition). SAUNDERS Elsevier, Philadelphia, USA.

D'Urso, P., & Maharaj, E. A. (2009). Autocorrelation-based fuzzy clustering of time series. *Fuzzy Sets and Systems, 160*(24), 3565-3589.

Davies, G. (2000). Antenatal fetal assessment. *Journal SOGC, 90*, 1-7.

Davies, M. E., & James, C. J. (2007). Source separation using single channel ICA. *Signal Processing, 87*, 1819-1832.

Dawes, G. S., Moulden, M., Sheil, O., & Redman, C. W. G. (1992). Approximate entropy, a statistic of regularity, applied to fetal heart rate before and during labor. *Obstetrics & Gynecology, 80*, 763-768.

Devoe, L. D. (2008). Antenatal fetal assessment: contraction stress test, nonstress test, vibroacoustic stimulation, amniotic fluid volume, biophysical profile, and modified biophysical profile—an overview. *Seminars in Perinatology, 32*, 247-252.

Driscoll-Children's-Hospital. (2010). Fetal Circulation. Retrieved from http://www.persistent-pulmonary-hypertension-newborn.com/images/fetal_circulation.gif

Eke, A., Herman, P., Bassingthwaighte, J. B., Raymond, G. M., Percival, D. B., *et al.* (2000). Physiological time series: distinguishing fractal noises from motions. *European Journal of Physiology, 439*, 403-415.

Ferrara, E. R., & Widrow, B. (1982). Fetal electrocardiogram enhancement by time-sequenced adaptive filtering. *IEEE Transactions on Biomedical Engineering, 29*(6), 458-460.

Ferrario, M., Signorini, M. G., Magenes, G., & Cerruti, S. (2006). Comparison of entropy-based regularity estimators: application to the fetal heart rate signal for the identification of fetal distress. *IEEE Transactions on Biomedical Engineering, 53*(1), 119-125.

Frank, B., Pompe, B., Schneider, U., & Hoyer, D. (2006). Permutation entropy improves fetal behavioural state classification based on heart rate analysis from biomagnetic recordings in near term fetuses. *Medical & Biological Engineering & Computing, 44*, 179-187.

Giebultowicz, J. M. (2001). Peripheral clocks and their role in circadian timing: insights from insects. *Philosophical Transactions of The Royal Society of London Series B-Biological Sciences, 356*, 1791-1799.

Godinez, M., Jimenez, A., Ortiz, M. R., & Pena, M. A. (2003). On-line fetal heart rate monitoring by phonocardiography. Paper presented at the *25th Annual EMBS International Conference, EMBS'03*, 3141-3144.

Golyandina, N., Nekrutkin, V., & Zhigljavsky, A. (2001). Analysis of time series structure: SSA and related techniques (First Edition). Chapman & HALL/CRC, Florida, USA.

Goovaerts, H. G., Rompelman, O., & van Geijn, H. P. (1989a). A transducer for detection of fetal breathing movements. *IEEE Transactions on Biomedical Engineering, 36*(4), 471-478.

Goovaerts, H. G., Rompelman, O., & van Geijn, H. P. (1989b). A transducer for recording fetal movements and sounds based on an inductive principle. *Clinical Physics and Physiological Measurements, 10*(B), 61-65.

Govindan, R. B., Wilson, J. D., Murphy, P., Russel, W. A., & Lowery, C. L. (2007). Scaling analysis of paces of fetal breathing, gross-body and extremity movements. *Physica A, 386*, 231-239.

Gribbin, C., & James, D. (2004). Assessing fetal health. *Best Practice & Research Clinical Obstetrics and Gynaecology, 18*(3), 411-424.

Guijarro-Berdinas, B., Alonso-Betanzos, A., & Fontenla-Romero, O. (2002). Intelligent analysis and pattern recognition in cardiotocographic signals using tightly coupled hybrid system. *Artificial Intelligence, 136*, 1-27.

Guimaraes-Filho, H. A., Araujo-Junior, E., Machado-Nardozza, L. M., Dias da Costa, L. L., Fernandes-Moron, A., & Rosiane, M. (2008). Ultrasound assessment of the fetal biophysical profile: What does an radiologist need to know? *European Journal of Radiology, 66*, 122-126.

Hanson, M. A. (1997). Do we understand the control of the fetal circulation? *European Journal of Obstetrics & Gynecology and Reproductive Biology, 75*, 55-61.

Heazell, A. E. P., & Froen, J. F. (2008). Methods of fetal movement counting and the detection of fetal compromise. *Journal of Obstetrics and Gynaecology, 28*(2), 147-154.

Holburn, D. M., & Rowsell, T. D. (1989). Real time analysis of fetal phonography signals using the TMS320. Paper presented at the *IEE Colloquium on Biomedical Applications of Digital Signal Processing*, Digest No. 1989/144:7/1–7/12.

Hon, E. H. (1965). Fetal electrocardiography. *Anesthesiology, 26*(4), 477-486.

Horigome, H., Shiono, J., Shigemitsu, S., Asaka, M., Matsui, A., Kandori, A., *et al.* (2001). Detection of cardiac hypertrophy in the fetus by approximation of the current dipole using magnetocardiography. *Pediatric Research, 50*(2), 242-245.

Horner, S. L., Holls, W. M., & Crilly, P. B. (1995). A robust real-time algorithm for enhancing a noninvasive fetal electrocardiogram. *Digital Signal Processing, 5*, 194-194.

Huang, W.-X., Yu, Q., & Cohen, M. I. (2000). Fast (3 Hz and 10 Hz) and slow (respiratory) rhythms in cervical sympathetic nerve and unit discharges of the cat. *Journal of Physiology, 523*(2), 459-477.

Hyvarinen, A., Karhunen, J., & Oja, E. (2001). Independent Component Analysis (First Edition). John Wiley & Sons, Inc., New York, USA.

Hyvarinen, A., & Oja, E. (1997). A fast fixed-point algorithm for Independent Component Analysis. *Neural Computation, 9*, 1483-1492.

Hyvarinen, A., & Oja, E. (2000). Independent Component Analysis: algorithms and applications. *Neural Networks, 13*, 411-430.

James, C. J., Gibson, O., & Davies, M. (2006). On the analysis of single versus multiple channels of electromagnetic brain signals. *Artificial Intelligence in Medicine, 37*, 131-143.

James, C. J., & Hesse, C. W. (2005). Independent component analysis for biomedical signals. *Physiological Measurement, 26*, R15-R39.

James, C. J., & Lowe, D. (2000). Using dynamical embedding to isolate seizure components in the ictal EEG. Paper presented at the *IEE Proceedings of Science, Measurement and Technology, 147*, 315–320.

James, C. J., & Lowe, D. (2001). Single channel analysis of electromagnetic brain signals through a dynamical systems framework. Paper presented at the *23 Annual EMBS International Conference, EMBS'01*, 1974-1977.

James, C. J., & Lowe, D. (2003). Extracting multisource brain activity from a single electromagnetic channel. *Artificial Intelligence in Medicine, 28*, 89-104.

Jansen, A. H., & Chernick, V. (1991). Foetal breathing and development of control of breathing. *Journal of Applied Physiology, 70*(4), 1431-1446.

Jensen, A., Garnier, Y., & Berger, R. (1999). Dynamics of fetal circulatory responses to hypoxia and asphyxia. *European Journal of Obstetrics & Gynecology and Reproductive Biology, 84*, 155-172.

Jimenez-Gonzalez, A., & James, C. J. (2008a). Blind Source Separation to extract foetal heart sounds from noisy abdominal phonograms: a single channel method. Paper presented at the *4th IET International Conference on Advances in Medical, Signal and Information Processing MEDSIP'08*, Electrophysiology, 1.1.4.

Jimenez-Gonzalez, A., & James, C. J. (2008b). Source separation of foetal heart sounds and maternal activity from single-channel phonograms: a temporal independent component analysis approach. *Computers in Cardiology, 35*, 949-952.

Jiménez-González, A., & James, C. J. (2009a). Extracting sources from noisy abdominal phonograms: a single-channel blind source separation method. *Medical & Biological Engineering & Computing, 47*, 655-664.

Jiménez-González, A., & James, C. J. (2009b). On the analysis of foetal heart sound morphology after de-noising the abdominal phonogram. Paper presented at the *5th UKRI PG Conference in Biomedical Engineering and Medical Physics, PGBIOMED'09*, 7-8.

Jiménez-González, A., & James, C. J. (2010a). On the measurement of physiological similarity between independent components: time-structure versus frequency-based methods. *Computing in Cardiology (formerly Computers in Cardiology), 37*, 477-480.

Jiménez-González, A., & James, C. J. (2010b). Time-structure based reconstruction of physiological independent sources extracted from noisy abdominal phonograms. *IEEE Transactions on Biomedical Engineering, 57*(9), 2322-2330.

Jimenez, A., Ortiz, M. R., Pena, M. A., Charleston, S., & Aljama, A. T. (1999). The use of wavelet packets to improve the detection of cardiac sounds from the fetal phonocardiogram. *Computers in Cardiology, 26*, 463-466.

Jimenez, A., Ortiz, M. R., Pena, M. A., Charleston, S., Gonzalez, R., *et al.* (2001). Performance of a method to generate fetal cardiotachograms using fetal phonocardiography. *Computers in Cardiology, 28*, 453-456.

Kahler, C., Schleubner, E., Grimm, B., Schneider, U., Nowak, H., & Seewald, H. J. (2002). Fetal magnetocardiography: development of the fetal cardiac time intervals. *Prenatal Diagnosis, 22*, 408-414.

Keunen, H., van Wijngaarden, W. J., Sahota, D. S., & Hasaart, T. (1999). The PR interval-fetal heart rate relationship during repetitive umbilical cord occlusions in immature fetal sheep *European Journak of Obstetrics & Gynecology and Reproductive Biology, 89*, 69-74.

Khamene, A., & Negahdaripour, S. (2000). A New Method for the Extraction of Fetal ECG from the Composite Abdominal Signal. *IEEE Transactions on Biomedical Engineering, 47*(4), 507-516.

Klemm, M., Haueisen, J., & Ivanova, G. (2009). Independent component analysis: comparison of algorithms for the investigation of surface electrical brain activity. *Medical & Biological Engineering & Computing, 47*, 413-423.

Korszun, P., Dubiel, M., Kudla, M., & Gudmundsson, S. (2002). Doppler velocimetry for predicting outcome of pregnancies with decreased fetal movements. *Acta Obstetricia et Gynecologica Scandinavica, 81*, 926-930.

Kovacs, F., Torok, M., & Habermajer, I. (2000). A rule-based phonocardiographic method for long-term fetal heart rate monitoring. *IEEE Transactions on Biomedical Engineering, 47*, 124-130.

Kraskov, A., Stogbauer, H., Andrzejak, R. G., & Grassberger, P. (2005). Hierarchical clustering using mutual information. *Europhysics Letters, 70*(2), 278-284.

LAPACK. (2006). LAPACK -- Linear Algebra PACKage. Retrieved from http://www.netlib.org/lapack/

Levy, D. S., Zielinsky, P., Aramayo, A. M., Behle, I., Stein, N., & Dewes, L. (2005). Repeatability of the sonographic assessment of fetal sucking and swallowing movements. *Ultrasound in Obstetrics and Gynecology, 26*, 745-749.

Lewis, M. J. (2003). Review of electromagnetic source investigations of the fetal heart. *Medical Engineering & Physics, 25*, 801-810.

Lipsitz, L. A., Pincus, S. M., Morin, R. J., Tong, S., Eberle, L. P., & Gootman, P. M. (1997). Preliminary evidence for the evolution in complexity of heart rate dynamics during autonomic maturation in neonatal swine. *Journal of the Autonomic Nervous System, 64*, 1-9.

Lowery, C. L., Campbell, J. Q., Wilson, J. D., Murphy, P., Preissl, H., *et al.* (2003). Noninvasive antepartum recording of fetal S-T segment with a newly developed 151-channel magnetic sensor system. *American Journal of Obstetrics & Gynecology, 188*, 1491-1497.

Luchinger, A. B., Hadders-Algra, M., Van Kan, C. M., & De Vries, J. I. P. (2008). Fetal onset of general movements. *Pediatric Research, 63*(2), 191-195.

Macdonald, A. A., & Johnstone, M. (1995). Comparative anatomy of the cardiac foramen ovale in cats (felidae), dogs (canidae), bears (ursidae) and hyaenas (hyaenidae). *Journal of Anatomy, 186*, 235-243.

Magann, E. F., Chauhan, S. P., Kinsella, M. J., McNamara, M. F., Whitworth, N. S., & Morrison, J. C. (1999). Antenatal testing among 1001 patients at high risk: The role of ultrasonographic estimate of amniotic fluid volume. *American Journal of Obstetrics & Gynecology, 180*(6), 1330-1336.

Mangesi, L., & Hofmeyr, G. J. (2007). Fetal movement counting for assessment of fetal wellbeing. *Cochrane Database of Systematic Reviews*(1), 1-27.

Manning, F. A. (2002). Foetal biophysical profile: a critical appraisal. *Clinical Obstetrics and Gynecology, 45*(4), 975-985.

Mantini, D., Alleva, G., & Comani, S. (2005). A method for the automatic reconstruction of fetal cardiac signals from magnetocardiographic recordings. *Physics in Medicine and Biology, 50*, 4763-4781.

Mantini, D., Hild, K. E., Alleva, G., & Comani, S. (2006). Performance comparison of independent component analysis algorithms for fetal cardiac signal reconstruction: a study on synthetic fMCG data. *Physics in Medicine and Biology, 51*, 1033-1046.

Marieb, E. N. (2004). Human anatomy & physiology (Sixth Edition). PEARSON Benjamin Cummings, New Jersey, USA.

Martens, S. M. M., Rabotti, C., Mischi, M., & Sluijter, R. J. (2007). A robust fetal ECG detection method for abdominal recordings. *Physiological Measurements, 28*, 373-388.

Martin, C. B., Jr. (2008). Normal fetal physiology and behavior, and adaptive responses with hypoxemia. *Seminars in Perinatology, 32*, 239-242.

Matonia, A., Jezewsky, J., Kupta, T., Horoba, K., Wrobel, J., & Gacek, A. (2006). The influence of coincidence of fetal and maternal QRS complexes on fetal heart rate reliability. *Medical & Biological Engineering & Computing, 44*, 393-403.

McAuley, J. H., Rothwell, J. C., & Marsden, C. D. (1997). Frequency peaks of tremor, muscle vibration and electromyographic activity at 10 Hz, 20 Hz and 40 Hz during human finger muscle contraction may reflect rhythmicities of central neural firing. *Experimental Brain Research, 114*, 525-541.

Menihan, C. A., & Kopel, E. (2008). Electronic fetal monitoring: concepts and applications (Second Edition). Lippincott Williams & Wilkins, Philadelphia, USA.

Mielke, G., & Benda, N. (2001). Cardiac output and central distribution of blood flow in the human fetus. *Circulation, 103*, 1662-1668.

Moghavvemi, M., Tan, B. H., & Tan, S. Y. (2003). A non-invasive PC-based measurement of fetal phonocardiography. *Sensors and Actuators A, 107*, 96-103.

Mor, Y., & Lev-Tov, A. (2007). Analysis of rhythmic patterns produced by spinal neural networks. *Journal of Neurophysiology, 98*, 2807-2817.

Nabney, I. T. (2004). NETLAB: algorithms for pattern recognition (First Edition). Springer-Verlag, London, UK.

Najafabadi, F. S., Zahedi, E., & Ali, M. A. M. (2006). Fetal heart rate monitoring based on independent component analysis. *Computers in Biology and Medicine, 36*, 241-252.

Nelson, J. C., Rizwan-Uddin, Griffin, M. P., & Moorman, J. R. (1998). Probing the order within neonatal heart rate variability. *Physiological Research, 43*, 823-831.

Northrop, R. B. (2001). Noninvasive instrumentation and measurement in medical diagnosis (First Edition). CRC Press, Florida, USA.

Ogueh, O., Brookes, C., & Johnson, M. R. (2009). A longitudinal study of the maternal cardiovascular adaptation to spontaneous and assisted conception pregnancies. *Hypertension in Pregnancy, 28*(28), 273-289.

Oldenburg, J. T., & Macklin, M. (1977). Processing the Abdominal Fetal ECG. *IEEE Transactions on Biomedical Engineering, 24*(6), 501-507.

Olesen, A. G., & Svare, J. A. (2004). Decreased fetal movements: background, assessment, and clinical management. *Acta Obstetricia et Gynecologica Scandinavica, 83*, 818-826.

Ortiz-Pedroza, M. R. (2007). Foetal respiratory arrhythmia in pregnancy and its interaction with respiratory movements and foetal well-being (In Spanish). PhD Thesis, Universidad Autónoma Metropolitana-Iztapalapa, México City, México.

Parer, J. T., & King, T. (2000). Foetal heart rate monitoring: is it salvageable? *American Journal of Obstetrics & Gynecology, 182*, 982-987.

Pattison, N., & McCowan, L. (1999). Cardiotocography for antepartum fetal assessment. *Cochrane Database of Systematic Reviews*(1), 1-16.

Peters, C. H. L., ten Broeke, E. D. M., Andriessen, P., Vermeulen, B., Berendsen, R. C. M., Wijn, P. F. F., *et al.* (2004). Beat-to-beat detection of fetal heart rate: Doppler ultrasound cardiotocography compared to direct ECG cardiotocography in time and frequency domain. *Physiological Measurement, 25*, 585-593.

Pieri, J. F., Crowe, J. A., Hayes-Hill, B. R., Spencer, C. J., Bhogal, K., & James, D. K. (2001). Compact long-term recorder for the transabdominal foetal and maternal electrocardiogram. *Medical & Biological Engineering & Computing, 39*, 118-125.

Pincus, S. M., & Goldberger, A. L. (1994). Physiological time-series analysis: what does regularity quantify? *American Journal of Physiology - Heart and Circulatory Physiology, 266*, H1643-H1656.

Pinette, M. G., Blackstone, J., Wax, J. R., & Cartin, A. (2005). Using fetal acoustic stimulation to shorten the biophysical profile. *Journal of Clinical Ultrasound, 33*(5), 223-225.

Popescu, E. A., Popescu, M., Bennett, T. L., Lewine, J. D., Drake, W. B., & Gustafson, K. M. (2007). Magnetographic assessment of fetal hiccups and their effect on fetal heart rhythm. *Physiological Measurement, 28*, 665-676.

Popescu, E. A., Popescu, M., Wang, J., Barlow, S. M., & Gustafson, K. M. (2008). Non-nutritive sucking recorded in utero via fetal magnetography. *Physiological Measurement, 29*, 127-139.

Puthusserypady, S. (2007). Extraction of fetal electrocardiogram using H-infinity adaptive algorithms. *Medical & Biological Engineering & Computing, 45*, 927-937.

Rezek, I. A., & Roberts, S. J. (1998). Stochastic complexity measures for physiological signal analysis. *IEEE Transactions on Biomedical Engineering, 45*(9), 1186-1191.

Richman, J. S., & Moorman, J. R. (2000). Physiological time-series analysis using approximate entropy and sample entropy. *American Journal of Physiology - Heart and Circulatory Physiology, 278*, H2039-H2049.

Rolfe, P., F, S., & G, S. (2006). Biomedical instruments for fetal and neonatal surveillance. *Journal of Physics, 48*(Conference series), 1131-1136.

Rudolph, A. M., & Heymann, M. A. (1967). The circulation of the fetus in utero: methods for studying distribution of blood flow, cardiac output and organ blood flow. *Circulation Research, 21*, 163-184.

Ruffo, M., Cesarelli, M., Romano, M., Bifulco, P., & Fratini, A. (2010). An algorithm for FHR estimation from foetal phonocardiographic signals. *Biomedical Signal Processing and Control, 5*, 131-141.

Rychik, J. (2004). Fetal cardiovascular physiology. *Pediatric Cardiology, 25*, 201-209.

Salgado, D. R., & Alonso, F. J. (2006). Tool wear detection in turning operations using singular spectrum analysis. *Journal of Material Processing and Technology, 171*, 451-458.

Sato, M., Kimura, Y., Chida, S., TIto, T., Katayama, N., Okamura, K., *et al.* (2007). A novel extraction method of fetal electrocardiogram from the composite abdominal signal. *IEEE Transactions on Biomedical Engineering, 54*(1), 49-58.

Sauer, T., James, A. Y., & Casdagli, M. (1991). Embedology. *Journal of Statistical Physics, 65*, 579-616.

Sener, T., Ozalp, S., Hassa, H., & Yildirim, A. (1996). Doppler and B-mode ultrasonography in biophysical profile scoring. *International Journal of Gynecology & Obstetrics, 54*, 231-236.

Seyam, Y. S., Al-Mahmeid, M. S., & Al-Tamimi, H. K. (2002). Umbilical artery Doppler flow velocimetry in intrauterine growth restriction and its relation to perinatal outcome. *International Journal of Gynecology & Obstetrics, 77*, 131-137.

Siira, S., Ojala, T., Ekholm, E., Vahlberg, T., Blad, S., & Rosén, K. G. (2007). Change in heart rate varibility. *Journal of Obstetrics and Gynaecology, 114*, 819-823.

Sreeman, N., & Brockmeier, K. (2004). Fetal magnetocardiography: the clinician's viewpoint. *Neurology and Clinical Neurophysiology, 64*, 1-6.

Steer, P. J. (2008). Has electronic fetal heart rate monitoring made a difference? *Seminars in Fetal & Neonatal Medicine, 13*, 2-7.

Stinstra, J. G., Golbach, E., van Leeuwen, P., Lange, S., Menendez, T., *et al.* (2002). Multicentre study of fetal cardiac time intervals using magnetocardiography. *International Journal of Obstetrics and Gynecology, 109*, 1235-1243.

Stinstra, J. G., & Peters, M. J. (2002). The Influence of Fetoabdominal Tissues on Fetal ECGs and MCGs. *Archives of Physiology and Biochemistry, 110*, 165-176.

Stone, J. V. (2004). Component Analysis: A tutorial introduction (First Edition). MIT Press, London, UK.

Stumper, O. (2009). Circulation before birth. Retrieved from http://www.lhm.org.uk/info/circulation-before-birth-35.aspx

Takens, F. (1981). Dynamical systems and turbulence. In *Lecture Notes in Mathematics* (Vol. 898, pp. 366-381): Springer.

Talbert, D. G., Davies, W. L., Johnson, F., Abraham, N., Colley, N., & Southall, D. P. (1986). Wide bandwidth fetal phonography using a sensor matched to the compliance of the mother's abdominal wall. *IEEE Transactions on Biomedical Engineering, 33*, 175-181.

Tamas, P., Szilagyi, A., Jeges, S., Vizer, M., Csermely, T., IFI, Z., *et al.* (2007). Effects of maternal central hemodynamics on fetal heart rate patterns. *Acta Obstetricia et Gynecologica Scandinavica, 86*, 711-714.

Teixeira, A. R., Tome, A. M., Lang, E. W., Gruber, P., & Martins da Silva, A. (2006). Automatic removal of high-amplitude artefacts from single-channel electroencephalograms. *Computer Methods and Programs in Biomedicine, 83*, 125-138.

Teknomo, K. (2006). Similarity measurement. Retrieved from http://people.revoledu.com/kardi/tutorial/Similarity/

ten Hof, J., Nijhuis, I. J. M., Nijhuis, J. G., Narayan, H., Taylor, D. J., *et al.* (1999). Quantitative analysis of fetal general movements: methodological considerations. *Early Human Development, 59*, 57-73.

Tsukada, K., Haruta, Y., Adachi, A., Ogata, H., Komuro, T., Ito, T., *et al.* (1995). Multichannel SQUID system detecting tangential components of the cardiac magnetic field. *Review of Scientific Instruments, 66*(10), 5085-5091.

Tucker, S. (2007). Maternal, fetal, & neonatal physiology: a clinical perspective (Third Edition). SAUNDERS Elsevier, Missouri, USA.

Tufillaro, N. B. (1998). A dynamical systems approach to behavioral modelling (Technical report). Palo Alto, California: HP Labs.

Turan, S., Turan, O. M., Berg, C., Moyano, D., Bhide, A., Bower, S., *et al.* (2007). Computerized fetal heart rate analysis, Doppler ultrasound and biophysical profile score in the prediction of acid–base status of growth-restricted fetuses. *Ultrasound in Obstetrics and Gynecology, 30*, 750-756.

van Leeuwen, P. (2004). Fetal magnetocardiography: time intervals and heart rate variability. *Neurology and Clinical Neurophysiology, 46*, 1-7.

van Leeuwen, P., Geue, D., Thiel, M., Cysarz, D., Lange, S., Romano, M. C., *et al.* (2009). Influence of paced maternal breathing on fetal-maternal heart rate coordination. Paper presented at the Conference of The National Academy of Sciences of the United States of America, *PNAS-USA'98*, 13661-13666.

van Leeuwen, P., Hailler, B., Bader, W., Geissler, J., Trowitzsch, E., & Gronemeyer, D. H. W. (1999). Magnetocardiography in the diagnosis of fetal arrhythmia. *British Journal of Obstetrics and Gynecology, 106*, 1200-1208.

van Leeuwen, P., Lange, S., Klein, A., Geue, D., Zhang, Y., Krause, H. J., *et al.* (2004). Reproducibility and reliability of fetal cardiac time intervals using magnetocardiography. *Physiological Measurement, 25*, 539-552.

Vandenhouten, R., Lambertz, M., Langhorst, P., & Grebe, R. (2000). Nonstationary time-series analysis applied to investigation of brainstem system dynamics. *IEEE Transactions on Biomedical Engineering, 47*(6), 729-737.

Vanderschoot, J., Callaerts, D., Sansen, w., Vandewalle, J., Vantrappen, G., & Janssens, J. (1987). Two methods for optimal MECG elimination and FECG detection from skin electrode signals. *IEEE Transactions on Biomedical Engineering, 34*(3), 233-243.

Varady, P., Wildt, L., Benyo, Z., & Hein, A. (2003). An advanced method in fetal phonocardiography. *Computer Methods and Programs in Biomedicine, 71*, 283-296.

VuBovy, J. (1978). Introduction to biomedical electronics (First Edition). McGraw-Hill, Inc., USA.

Vullings, R., Peters, C. H. L., Sluijter, R. J., Mischi, M., Oei, S. G., & Bergmans, J. W. M. (2009). Dynamic segmentation and linear prediction for maternal ECG removal in antenatal abdominal recordings. *Physiological Measurement, 30*, 291-307.

Wallstrom, G. L., Kass, R. E., Miller, A., Cohn, J. F., & Fox, N. A. (2004). Automatic correction of ocular artifacts in the EEG: a comparison of regression-based and components-based methods. *International Journal of Psychophysiology, 53*, 105-119.

Westgate, J. A., Gunn, A. J., Bennet, L., Gunning, M. I., & de Haan, H. H. (1998). Do fetal electrocardiogram PR-RR changes reflect progressive asphyxia after repeated umbilical cord occlusion in fetal sheep? *Pediatric Research, 44*(3), 297-303.

Widrow, B., Glover, J. R., Jr., McCool, J. M., Kaunitz, J., Williams, C. S., Hearn, R. H., *et al.* (1975). Adaptive noise cancelling: principles and applications. *Proceedings of the IEEE, 63*(12), 1692-1716.

WIKIMEDIA-project. (2009). Electrocardiograma. Retrieved from http://es.wikipedia.org/wiki/Electrocardiograma

Woon, W. L., & Lowe, D. (2004). Can we learn anything from single-channel unaveraged MEG data? *Neural Computing & Applications, 13*, 360-368.

Wubbeler, G., Ziehe, A., Mackert, B. M., Muller, K. R., Trahms, L., & Curio, G. (2000). Independent component analysis of noninvasively recorded cortical magnetic DC-fields in humans. *IEEE Transactions on Biomedical Engineering, 47*(5), 594-599.

Xu, J., Durand, L.-G., & Pibarot, P. (2000). Aortic and pulmonary components of the second heart sound. *IEEE Transactions on Biomedical Engineering, 47*(7), 1328-1335.

Zarzoso, V., & Nandi, A. K. (2001). Noninvasive fetal electrocardiogram extraction: blind separation versus adaptive noise cancellation. *IEEE Transactions on Biomedical Engineering, 48*(1), 12-18.

Zhao, H., & Wakai, R. T. (2002). Simultaneity of foetal heart rate acceleration and foetal trunk movement determined by foetal magnetocardiogram actocardiography. *Physics in Medicine and Biology, 47*, 839-846.

Ziehe, A., & Muller, K. R. (1998). TDSEP-an efficient algorithm for blind separation using time structure. Paper presented at the *8th International Conference on Artificial Neural Networks, ICANN'98,* 675-680.

Ziehe, A., Muller, K. R., Nolte, G., Mackert, B. M., & Curio, G. (2000). Artifact reduction in magnetoneurography based on time-delayed second-order correlations. *IEEE Transactions on Biomedical Engineering, 47*(1), 75-87.

Zuckerwar, A. L., Pretlow, R. A., Stoughton, J. W., & Baker, D. A. (1993). Development of a piezopolymer pressure sensor for a portable fetal heart rate monitor. *IEEE Transactions on Biomedical Engineering, 40*(9), 963-969.